

University of Warwick institutional repository: <http://go.warwick.ac.uk/wrap>

A Thesis Submitted for the Degree of PhD at the University of Warwick

<http://go.warwick.ac.uk/wrap/4496>

This thesis is made available online and is protected by original copyright.

Please scroll down to view the document itself.

Please refer to the repository record for this item for information to help you to cite it. Our policy information is available from the repository home page.

**The New Flux Switching Motor –
A DC Motor without Brushes**

by

Mark Wallace

**A thesis submitted in partial fulfilment of the requirements for
the degree of Doctor of Philosophy in Electrical Engineering**

University of Warwick, School of Engineering

September 2000

CONTENTS

	Page
List of Figures	viii
List of Tables	xviii
Acknowledgements	xix
Declaration	xx
Summary	xxi
Dedication	xxii
CHAPTER 1 INTRODUCTION	1
1.1 Background	1
1.1.1 The need for low-cost drive-systems	1
1.1.2 The need for brushless drive-systems	3
1.2 Review of motor options	5
1.2.1 Universal brushed motor	5
1.2.2 Brushed DC-motor	6
1.2.3 Single-phase induction-motor	6
1.2.4 Brushless DC-motor	7
1.2.5 Switched-reluctance motor	7
1.3 Discussion of motor selection for the appliance market	8
1.4 The proposed new drive-system	10
1.5 Thesis layout	11

	Page
CHAPTER 2 EVOLUTION OF THE NEW FLUX-SWITCHING MOTOR	13
2.1 Introduction	13
2.2 Switched-reluctance motors	13
2.2.1 Introduction and history	13
2.2.2 Principle of operation	16
2.2.3 Torque production	18
2.2.4 Self-starting requirements of two-phase motors	23
2.2.5 Power-converters	28
2.3 Switched-reluctance motors with fully-pitched windings	30
2.3.1 Introduction and history to the use of fully-pitched windings	31
2.3.2 Principle of operation of switched-reluctance motors with additional fully-pitched windings	33
2.3.3 Power-converters for switched-reluctance motors with additional fully-pitched windings	39
2.3.4 Principle of operation of the three-phase fully-pitched switched-reluctance motor	40
2.3.5 Power-converters for the three-phase fully-pitched switched-reluctance motor	41
2.3.6 Principle of operation of the two-phase fully-pitched switched-reluctance motor	42
2.3.7 Torque production of the two-phase fully-pitched switched-reluctance motor	45

	Page
2.3.8 Power-converters for the two-phase fully-pitched switched-reluctance motor	46
2.4 The new flux-switching motor	49
2.4.1 A DC-motor	49
2.4.2 Similarities to other machines	52
2.5 Conclusions	53
CHAPTER 3 MATHEMATICAL MODEL AND SIMULATION	54
3.1 Introduction	54
3.2 Development of mathematical model	54
3.2.1 First principles model	54
3.2.2 Coupling-coefficient model	60
3.3 Motor simulation	69
3.3.1 Simulation objectives and model	69
3.3.2 Implementation using MATLAB SIMULINK	70
3.3.3 Results and chosen winding design	76
3.3.4 Further work required to simulation	78
3.4 Conclusions	82
CHAPTER 4 PROOF-OF-PRINCIPLE FLUX-SWITCHING MOTOR	84
4.1 Introduction	84
4.2 Motor and drive design	84

	Page
4.2.1 Lamination and winding design	84
4.2.2 New power-converter designs	86
4.2.3 Gate-drive and control circuit design	94
4.2.4 Component selection and drive-system manufacture	95
4.3 Testing and analysis	96
4.3.1 Static tests	96
4.3.2 Dynamic tests	103
4.4 Conclusions	107
CHAPTER 5 DESIGN OF THE NEW FLUX-SWITCHING MOTOR	108
5.1 Introduction	108
5.2 Motor design	108
5.2.1 Lamination design	108
5.2.2 Winding design	114
5.2.3 Manufacture	115
5.3 Drive design and manufacture	117
5.3.1 Power-converter design	117
5.3.2 Gate-drive and control circuit design	119
5.3.3 Drive-protection circuit	122
5.3.4 Component selection and drive manufacture	124
5.4 Control method design and implementation	128
5.4.1 Control method principles	128

	Page
5.4.2 Selection of an appropriate control method	129
5.4.3 Design and implementation of selected control method	131
5.5 Conclusions	133
CHAPTER 6 TESTING OF A NEW FLUX-SWITCHING MOTOR	134
6.1 Introduction	134
6.2 Test-rigs	134
6.3 Static tests	137
6.3.1 Winding resistance	137
6.3.2 Winding inductance and coupling-coefficient	139
6.4 Specification review	145
6.4.1 Performance	145
6.4.2 Starting	147
6.4.3 Braking	148
6.4.4 Other deliverables	148
6.5 Dynamic testing of a prototype motor	149
6.5.1 Initial operational tests	149
6.5.2 Power tests	155
6.5.3 High-speed power tests	169
6.5.4 Reserve torque tests	173
6.5.5 Start-up tests	178
6.5.6 Braking tests	184

6.6	Conclusions	186
CHAPTER 7 FURTHER TESTING AND DEVELOPMENT OF FLUX-SWITCHING MOTORS		189
7.1	Introduction	189
7.2	Dynamic testing of the second prototype motor	190
7.2.1	Power tests	190
7.2.2	Reserve torque tests	190
7.2.3	Continuous power tests	202
7.2.4	Start-up tests	204
7.2.5	Testing conclusions	216
7.3	Dynamic testing of the third prototype motor	217
7.3.1	Power tests	217
7.3.2	Testing conclusions	218
7.4	Dynamic testing of the fourth prototype motor	223
7.4.1	Power tests	223
7.4.2	Additional power delivery	240
7.4.3	Testing conclusions	246
7.5	Conclusions	249
CHAPTER 8 ANALYSIS OF THE NEW FLUX-SWITCHING MOTOR		251
8.1	Introduction	251

	Page
8.2 Validating the torque equation	251
8.2.1 Further tests	251
8.2.2 Back-EMF tests	252
8.2.3 Field and armature current data	259
8.2.4 Analysis of instantaneous data	259
8.3 Conclusions	262
 CHAPTER 9 CONCLUSIONS	 265
9.1 General conclusions	265
9.2 Author's contribution to knowledge	268
9.3 Further work	269
References	270
Appendix I: Performance Specification	279

Figure Number		Page
2.14	Ideal lamination profile for a two-phase fully-pitched switched-reluctance motor	47
2.15	Standard H-bridge inverter circuit	48
2.16	Series-field split-capacitor supply	50
2.17	Ideal flux waveforms for a two-phase fully-pitched switched-reluctance motor	51

CHAPTER 3 MATHEMATICAL MODEL AND SIMULATION

3.1	Back-EMF and armature-current waveforms	55
3.2	(a) A generalised machine, (b)The idealised flux-switching motor	61
3.3	A simple magnetic circuit with two coils	65
3.4	The top level of the MATLAB SIMULINK model	72
3.5	The model heart of the MATLAB SIMULINK model	73
3.6	The speed-block in the MATLAB SIMULINK model	74
3.7	The back-EMF block-in the MATLAB SIMULINK model	75
3.8	The voltage-block in the MATLAB SIMULINK model	77
3.9	The winding-block in the MATLAB SIMULINK model	77
3.10	Instantaneous and average torque waveforms at a speed of 9000 rpm	79
3.11	The instantaneous and average combined armature current	79
3.12	The armature voltage and back-EMF waveforms generated	80

Figure Number		Page
3.13	A simulated torque-speed curve	81

CHAPTER 4 PROOF OF PRINCIPLE FLUX SWITCHING MOTOR

4.1	The 4/2 switched-reluctance motor rewound with fully-pitched windings	85
4.2	(a) Normal armature-winding, (b) Bifilar armature-winding	88
4.3	Half-bridge voltage-source inverter	90
4.4	Half-bridge current-source inverter circuit	92
4.5	Variation in phase flux-linkage with rotor position at different currents for one half of the bifilar armature-winding	97
4.6	Flux linking the shunt-field-winding due to current in one half of the bifilar armature-winding	99
4.7	Back-EMF generated across one half of the bifilar armature-winding	100
4.8	Average back-EMF against shunt-field-winding volts	102
4.9	Current waveforms for the field and one half of the bifilar armature-windings	104
4.10	Torque-speed curve and output-power characteristic	106

Figure Number		Page
CHAPTER 5 DESIGN OF THE NEW FLUX SWITCHING MOTOR		
5.1	Chosen 8/4 lamination profile	110
5.2	Winding location and flux patterns	112
5.3	Stator with windings in place	116
5.4	Component parts of the motor	118
5.5	Power circuit for shunt-motor	120
5.6	Power circuit for series-motor	120
5.7	Power circuit for series motor with additional diode	121
5.8	Gate-drive and control circuit	121
5.9	Drive-protection circuit	123
5.10	Initial combined armature-current spike	125
5.11	Drive and protection circuit	127
CHAPTER 6 TESTING OF A NEW FLUX SWITCHING MOTOR		
6.1	Dynamic test-rig set up	135
6.2	Electrical representation of the motor shown as a transformer with a movable iron core	140
6.3	Phasor diagram of the electrical circuit given in Figure 6.2	140
6.4	Comparison of the measured coupling-coefficient and that predicted using Finite Element Analysis	143
6.5	The rate-of-change of coupling-coefficient with respect to position, the differential of Figure 6.4	146

Figure Number		Page
6.6	Power Test V no-load speed waveforms	151
6.7	Power Test VI no-load speed waveforms	152
6.8	Back-EMF waveform generated across one half of the bifilar armature-winding	156
6.9	Power Test XIII, 3/4 duty-cycle current-waveforms	158
6.10	Power Test 14, 7/8 duty-cycle current waveforms	159
6.11	Power Tests XIII and XIV, Torque – speed curves comparing 3/4 duty-cycle with 7/8 duty-cycle using an advance-angle of 8° (mechanical)	160
6.12	Power Tests X, XI, XII and XIII, Torque – speed curves comparing advance-angles of 5°, 6°, 7° and 8° respectively using the same PIC micro-controller program	162
6.13	Power Tests X, XI, XII and XIII, Torque – efficiency curves comparing advance-angles of 5°, 6°, 7° and 8° respectively using the same PIC micro-controller program	163
6.14	Power Test XX, Torque – speed curve using an advance-angle of 12° (demonstrates the sudden drop in torque-output)	165
6.15	Power Test XX, current waveforms for the final four measurements of this test	166
6.16	Current waveforms just prior to a stall	168
6.17	Power Tests XXXIII, XXXIV, XXXV and XXXVI, Torque – speed curves at an advance-angle of 10° (mechanical)	171

Figure Number		Page
6.18	Current waveforms for the end test points shown	172
6.19	Power Tests XXXIV, XXXVI, XXXVII, XXXVIII and XLI, Torque – speed curves at an advance-angle of 10° (mechanical) at armature-voltages of 240 V and 280 V	174
6.20	Power Tests XXXVII, XXXVIII, XLI and XLII, Torque – speed curves at an advance-angle of 10° (mechanical)	176
6.21	Power Tests XXXVII, XXXVIII, XLI and XLII, Torque – power out curves at an advance-angle of 10° (mechanical)	177
6.22	Power Tests XXXVII, XXXVIII, XLI and XLII, Torque – power in curves at an advance-angle of 10° (mechanical)	179
6.23	Power Tests XXXVII, XXXVIII, XLI and XLII, Torque – efficiency curves at an advance-angle of 10° (mechanical)	180
6.24	A complete start-up sequence using the first prototype motor	182
6.25	Braking performance waveforms	185

CHAPTER 7 FURTHER TESTING AND DEVELOPMENT OF FLUX SWITCHING MOTORS

7.1	Power Tests XLII (First Prototype) and ZI (Second Prototype) Torque – speed curves	191
7.2	Characteristics of PIC micro-controller program “Warp II Speed”	193

Figure Number		Page
7.3	Further characteristics of PIC micro-controller program “Warp II Speed”	194
7.4	Power Tests ZI, ZVIII, ZXI, and ZXII, Torque – speed curves	195
7.5	Characteristics of PIC micro-controller programs “Warp II (Speed)”, “Warp ZIII”, “Warp ZIV”, and “Warp ZV”	197
7.6	Power Tests ZXXXI and ZXXXII, Torque – speed curves	198
7.7	Power Tests ZXXXI and ZXXXII, Torque – power-out curves	199
7.8	Power Tests ZXXXI and ZXXXII, Torque – power-in curves	200
7.9	Power Tests ZXXXI and ZXXXII, Torque – efficiency curves	201
7.10	Comparison of temperature-rise in the windings of the first and second prototypes	203
7.11	Position sensor showing the effects of the advance-angle	206
7.12	Normal starting operation with rotor positioned three degrees prior to commutation, sufficient momentum is accumulated to overcome the negative torque region	207
7.13	Oscillation of motor at starting around a position-sensor edge with rotor positioned one degree prior to commutation; insufficient momentum is accumulated to overcome the negative torque region, (Each high and low position-sensor edge consists of forward and backward motion, which shouldn’t be confused with rotation)	209

Figure Number		Page
7.14	Starting operation with 15ms delay with rotor positioned in low state just prior to commutation. In the low state the motor starts in the correct direction of rotation with no negative torque, on the 4 th edge normal operation resumes and the motor continues to rotate	210
7.15	Starting operation with 15ms delay with rotor positioned in high state just prior to commutation. In the high state the motor starts in the reverse direction of rotation due to negative torque. Rotation continues in reverse passing a position sensor and so initialising the delay. Commutation occurs after the duration of the delay allowing the rotor to turn back in the correct direction and continue to rotate. On the 4 th edge normal operation resumes	211
7.16	Final starting routine shown with selected waveforms with time from start indicated	212
7.17	Acceleration ramp of second prototype motor	215
7.18	Power Test NI, Torque – speed curve of third prototype motor (without gearbox)	219
7.19	Power Test NI, Torque – power out curve of third prototype motor (without gearbox)	220
7.20	Power Test NI, Torque – power in curve of third prototype motor (without gearbox)	221

Figure Number		Page
7.21	Power Test NI, Torque – efficiency curve of third prototype motor (without gearbox)	222
7.22	Power Test QVIII and QIX, Torque – speed curves of fourth prototype series-motor	225
7.23	Power Test QVIII and QIX, Torque – power out curves of fourth prototype series-motor	226
7.24	Power Test QVIII and QIX, Torque – power in curves of fourth prototype series-motor	227
7.25	Power Test QVIII and QIX, Torque – efficiency curves of fourth prototype series-motor	228
7.26	Comparison of current waveforms recorded at 1.6 Nm, (a) Power Test NI, third prototype shunt-motor, (b) Power Test QVIII, fourth prototype series-motor	229
7.27	Power Test NI, QVIII and QXXIII, Torque - speed curves	231
7.28	Armature-current regeneration recorded at 0.9 Nm	232
7.29	Power Test QVIII and QXXIII, Torque - DC Armature Voltage curves	233
7.30	Power Test QVIII, QXII and QXXIII, Torque - speed curves comparing capacitor sizes	234
7.31	Current waveforms and armature-capacitor voltage with a capacitance C2 of 30 μ F	236
7.32	Torque – speed curve comparison	237

Figure Number		Page
7.33	Comparison of current and voltage waveforms at a torque of 1.4 Nm	238
7.34	Power Test QXXVII, Torque - speed curve	241
7.35	Power Test Q27, Torque – power out curve, over twice rated power-out	242
7.36	Power Test QXXVII, Torque – power in curve	243
7.37	Power Test QXXVII, Torque - efficiency curve	244
7.38	Power Test QXXVII, Torque – DC supply voltage curve	245
7.39	Current waveforms for Power Test QXXVII	248

CHAPTER 8 ANALYSIS OF THE NEW FLUX SWITCHING MOTOR

8.1	RMS back-EMF induced in armature winding against Field-MMF	254
8.2	RMS back-EMF induced in armature-winding against speed	255
8.3	RMS back-EMF induced in armature-winding against field-MMF with 1 st and 2 nd order polynomial curve fits	257
8.4	RMS back-EMF induced in armature-winding against field-MMF with 1 st and 2 nd order polynomial curve fits (zoomed out)	258
8.5	Comparison of four differential of coupling-coefficients	263

List of tables

Table Number		Page
CHAPTER 6 TESTING OF A NEW FLUX SWITCHING MOTOR		
6.1	Winding resistances and specification for the four prototype motors	138
6.2	Measurements and calculations for coupling-coefficient k , self-inductance and mutual-inductance. Negative angle owing to gearbox	144
CHAPTER 7 FURTHER TESTING AND DEVELOPMENT OF FLUX SWITCHING MOTORS		
7.1	Performance figures for Power Test QXXVII	247
CHAPTER 8 ANALYSIS OF THE NEW FLUX SWITCHING MOTOR		
8.1	A summary of the results of the analysis showing a comparison between the calculated and measured torques	261

Acknowledgements

I would like to thank Professor Charles Pollock for the opportunity to carry out this research, and, the ongoing support of Professor David Hutchins in his supervisory role, the members of the power electronics and drives research group, and the assistance of Black and Decker Ltd, for which this research was supported.

I would also like to thank my friends and family for their continued support and patience throughout my studies.

This research was made possible by my sponsorship from the Engineering and Physical Sciences Research Council.

Declaration

One piece of published work has so far resulted from the work done during research for this thesis, and is included as reference [47]. Material in Chapter 4 uses some of this published work.

This thesis has not been submitted for a degree at another university.

Summary

This thesis is principally concerned with the theoretical modelling, design, manufacture, performance testing, and development of a new type of low-cost electronically-commutated doubly-salient wound-field brushless DC-motor, named the flux-switching motor. The drive-system that was designed, and developed, was specifically intended to be used in a low-power application (2.5 horsepower, less than 2 kW output-power), according to a given specification. Extensive testing using four prototype motors has been carried out in attempting to satisfy the specification. From this testing empirical modelling techniques have been demonstrated to be of use in the design of such motors. The motor is showing excellent promise for the future, when it should become a realistic alternative to currently available motors on the market.

Dedication

In memory of my Father

CHAPTER 1 INTRODUCTION

1.1 Background

1.1.1 The need for low-cost drive-systems

Cost is more often than not a dominant factor when it comes to selecting any system, provided the system chosen is able to satisfy the design specification. Limiting cost determines drive-system choice in the appliance market, where the emphasis is placed on finding the cheapest solution possible. The market for these low-cost drive-systems is huge as such systems power the majority of household appliances, from lawnmowers to food mixers to hairdryers; the list goes on and on. Without these appliances, which we take for granted, our lives would be very different. There is no question then about the need for these drive-systems, and any possibility of reducing cost, owing to a design change, usually results in that change being made.

The complexity of a low-cost drive-system is generally reflected in its operating requirements. The motor, within the drive-system for a typical appliance, would usually need to rotate in one direction only and perform a very straightforward operation, thus requiring a very simple control method. The rated output-power of a motor used in such an appliance does not usually exceed 2 kW.

In order to compete with existing, well developed, drive systems already in the market place, new products must be priced accordingly, unless of course additional features warrant a higher price. Thus a trade off is involved. With

cost in mind, three main criteria must be satisfied in drive-system selection, simplicity, mass production and a multi-product market.

Simplicity

Cost is related directly to the complexity of the drive-system and therefore the number of components of which it consists. Not only is it the material cost of the components in the motor and the drive that needs to be considered, but also the cost of manufacturing the system.

Mass produced

Production costs depend on how simply the drive can be made, which of course reflects in the price the consumer pays. For cost effectiveness the system normally needs to be designed to be mass-produced in the shortest time possible, preferably with existing machinery.

Multi-product market

Costs can be further reduced by the ability of the drive-system to be incorporated into a number of different products. For example, the same motor type might be used in two different products, the only difference between them is that the motors may have different operating conditions. This could require a different control scheme or some slight alteration to the winding design.

The need for low-cost drive-systems has been, therefore, identified, along with the market they refer to, and the criteria used for selecting one of them.

1.1.2 The need for brushless drive-systems

Most appliances that need a variable speed drive-system currently incorporate a universal motor. The universal motor is an almost ideal choice as it satisfies all of the criteria in the previous section, and it is also a very versatile motor.

This motor is identical in construction to a brushed DC-motor; the only difference between them is that the universal motor operates from a single-phase AC supply. To operate, mechanical commutation is needed, and this is achieved with the combination of the brushes and the commutator. Current is delivered to the armature windings via the brushes and the commutator at the correct time, torque being created by the interaction of the armature-current with the field-flux.

Mechanical commutation results in a number of undesirable characteristics exhibited by the universal motor. The brushes and commutator suffer from mechanical wear due to friction, which eventually leads to motor failure. This friction results in additional losses, thereby reducing efficiency. Another feature of mechanical commutation is that the imperfect contact between the brushes and the commutator, during operation, results in sparking. This type of motor is therefore unsuitable for use in certain dangerous environments owing to, for example, the possibility of igniting flammable substances. Mechanical commutation is also inherently noisy, in both the electrical and acoustic sense.

All of these problems, referred to above, can be overcome by using a brushless drive-system that incorporates an electronic commutation method. In such motors there are fewer mechanical parts to fail, and, as a result, it has superior mechanical robustness. There is also no noise from the commutation process, thus giving quieter operation. The motor construction is simplified to the extent that there are no windings on the rotor. The implications of this are firstly that production time and costs are generally lowered, owing to the reduced complexity of the motor, and, secondly, since the rotor is not supporting any windings it has a lower mass giving improved power-to-weight ratio. Reduced power-to-weight ratio is necessary for hand-held appliances, and very desirable in other portable appliances. Also, brushless motors can be used in dangerous environments without any problems.

There are of course disadvantages of using brushless motors. Because commutation is electronic, the drive-system has to incorporate additional electronics and have a more complex control scheme, to operate properly. This adds to the cost of the drive. The brushless drive-system is more mechanically robust implying a longer working life. This is of course in the interests of the consumer, but not of the manufacturers who want to sell as many of their products as possible. Thus a programme of planned obsolescence is adopted in that, with most products, a limited life span is usually designed into them. This is but one demonstration of the numerous considerations that need to be made when selecting a product design for the market.

The universal motor has been around for longer than one-hundred years. The technology to manufacture them is well established, and they are still the current choice for most household appliances. However, if a brushless drive-system could be manufactured at a lower cost it would undoubtedly replace the universal motor as its advantages outweigh its disadvantages. As with all developing technologies, extensive and on-going testing is needed to develop the expertise in achieving the best performance from these motors at a competitive cost.

1.2 Review of motor options

When selecting a drive-system to be used in an appliance there are a number of different motors to choose from. These range from established designs to emerging technologies that could be exploited in the future.

1.2.1 Universal brushed motor

The operation of a universal brushed motor and some of its features were described in the previous section. It is the common choice of motor for most domestic appliances where variable speed, simple control and versatility are required. These motors operate at relatively high speeds and have the benefits of being lightweight and mechanically robust. The universal motor is powered from the single-phase mains supply using just a few additional passive components. Where an electronic controller is used it is usually very simple. It

does have disadvantages as described, due mainly to the mechanical commutation needed.

1.2.2 Brushed DC-motor

The brushed DC-motor is identical in construction to the brushed universal motor. The only difference is that it is supplied with direct rather than alternating current. Where an alternating current supply is used additional components are required for rectification purposes. The instantaneous torque profile is smoother than that of the universal motor resulting in quieter operation. Either permanent magnets or field-windings can supply the field excitation. Larger machines use field-windings, as large permanent magnets can be expensive. Hand-held cordless appliances use the permanent magnet DC-motor exclusively, as the batteries have a longer operating time because the field does not need an electrical supply.

1.2.3 Single-phase induction motor

Where a fixed speed is required the single-phase squirrel cage induction motor is the best choice. This motor has the benefits that it is brushless and can be directly connected to the mains supply. Like the universal motor the torque produced varies at twice the supply frequency, and this causes a 'humming' noise to be generated, even so it is quieter in operation than the brushed motors. The single-phase induction motor does not develop any net torque at standstill, and, therefore, it requires an auxiliary starting method. There are a number of starting methods that can be employed; the selection depends upon

the starting requirements of the load. It is possible to obtain variable speed from this motor with the use of an inverter to vary the frequency of excitation. The inverter drive, however, would add significantly to the cost of the overall drive-system.

1.2.4 Brushless DC-motor

The brushless DC-motor can be described as an inverted permanent magnet brushed DC-motor. The rotor carries the field flux producing permanent magnets whilst the stator holds the normally rotating armature windings stationary. Electronic commutation is required for rotation, which is achieved by exciting the appropriate armature winding at the correct time. To do this, firstly the rotor position is established, via Hall-effect transistors mounted on the stator being activated by the permanent magnets on the rotor. Secondly the signal triggers the appropriate power transistor to excite the corresponding winding. These motors, as well as being brushless, can be operated at variable speed. If they could be made cheaply enough, they would replace the brushed motor.

1.2.5 Switched-reluctance motor

The switched-reluctance motor is another type of brushless electronically commutated DC-motor. However, unlike the brushless DC-motor there is only one source of excitation as opposed to two. Both the rotor and stator are constructed with salient laminations with the stator carrying the exciting windings. Torque production, and hence, rotation, is achieved by using the

changing reluctance between the stator and rotor, as a result of the changing airgap in different relative positions. This motor offers a number of benefits over existing motor topologies. The construction of the switched-reluctance motor is the simplest of any motor, which also means that it is cheap to manufacture. There are no permanent magnets or rotor windings, and the stator windings are concentrated rather than distributed, thereby simplifying the manufacture further. Since the phases of the motor are excited individually with unipolar current, the drive is also simpler in design than those used with the brushless DC and AC motors. The operation of the switched-reluctance motor is essentially determined by the physical profile of the laminations. As different profiles can be used to satisfy certain operating requirements desired by the product there are numerous possible motor configurations. One problem that is inherent to the construction and operation of the switched-reluctance motor is that it can be acoustically noisy in operation, owing to the instantaneous torque pulsations produced by the phases. This can be largely overcome by carefully designing the lamination profiles and, to some extent, electronically.

1.3 Discussion of motor selection for the appliance market

Due to the competitiveness of the appliance market the selection of all the components that make up the product is largely driven by cost, drive-systems are no exception to this rule, as mentioned previously in this chapter. Where manufacturing is concerned the cost can be broken down into two areas, material cost and manufacturing cost, although the two are closely related, and

affect each other. To keep material cost to a minimum the aim is to, use as little material as possible, use standard components, as opposed to specialist ones that need a special manufacturing requirement, and use readily available materials. Using mass production, simple designs with a minimum number of components, and multi-product, shared components can reduce manufacturing costs.

Although cost is the prime selection criteria there are other considerations to take into account, that are largely dependent upon the application itself, and the conditions in which it is designed to operate. For example, out-and-out performance may be required in terms of achieving a maximum efficiency. The power-to-weight ratio may be very important, when, for example, the device is used in a hand-held appliance. The level of acoustic noise that the motor develops may have to be considered, in a fan application, for example. Other criteria could be environmental survival, weight, size, reliability etc. Another very important motor requirement could be that the application has a set of operating conditions, that need a specifically shaped torque-speed curve, that the motor needs to match.

Drive-system selection is determined by finding a system that can satisfy the design specification whilst being the most economical. The universal motor is the first choice in most cases for the following reasons, it can be manufactured relatively cheaply, it can be operated with only a few additional components, it is an established well-understood motor technology, and, it can deliver the

performance required. The switched-reluctance motor could be an attractive and viable option to manufacturers if the conditions were right. The manufacturing and material costs would possibly be the lowest of any drive-system. The only hindrance is that the power electronics used in the drive are still not cheap enough for the drive-system to be competitive. The price of power electronics is beginning to fall, which means that drive-systems employing the minimum number of components possible can start to challenge the more conventional choice of motor. In conclusion, the adoption of new technology depends on whether it can show clear advantages over existing technology for the right price.

1.4 The proposed new drive-system

The main aim of the proposed design for a new drive-system was to develop an alternative low-cost variable speed system utilising a switched-reluctance motor. To achieve this goal the design had to demonstrate that it could be a low-cost solution. That is, if the fundamental concept of the drive proved it had potential then some aspects of the design could be relaxed for optimisation at a later date. To put this project into context the drive-system had to be capable of satisfying the given industrial specification, with the cheapest solution possible.

An idea for a solution had been put forward. This idea was twofold, firstly, it was discovered that a regular switched-reluctance motor stator could be wound with two fully-pitched windings occupying the available slot area. Secondly, if

these windings could be controlled in the appropriate manner motoring operation would result. On further consideration of the operation of the motor a very simple, and therefore a cheap drive, with few components looked very promising. It was hoped that performance would not be compromised within this low-cost proposed solution.

The flux-switching motor, as it has been named, has shown considerable promise as a result of the extensive testing carried out in a range of desirable operating conditions. The main aim has been satisfied and the performance obtained from the drive-system has demonstrated its potential for the future. Once the rated power-out had been achieved, following a new winding design, and a change in the speed at which the power was delivered, the torque-speed curve was shaped to deliver reserve torque. Start-up and braking tests were also performed producing satisfactory results.

1.5 Thesis layout

This chapter has so far highlighted the nature of the requirements of drive-systems used within the appliance market, and, in particular, the importance of finding low-cost solutions. The benefits of using brushless drive-systems have been discussed in conjunction with the criteria that are currently holding back their widespread use throughout the appliance market. The present choice of motor options has been reviewed and the selection of a drive-system has been discussed. In conclusion it was found that for a new drive-system to become adopted it had to be able to demonstrate that its performance was comparable

to existing drive-systems whilst being competitive in cost. A new drive-system has been proposed that incorporates a switched-reluctance motor with two-fully pitched windings. The unique operation of the motor, named the flux-switching motor, required the use of a new drive design. Although this new drive was capable of operating with the minimum number of components, performance was never compromised. The flux-switching drive-system demonstrated that a doubly-salient motor could be operated with a very low-cost drive, and even though not cost effective at present, with the falling cost of power electronics this drive could be one of the first to be exploited commercially in the future.

Chapter 2 explores the evolution of the new flux-switching motor. Beginning with the operating principles behind the switched-reluctance motor the chapter, develops the use of fully-pitched windings in these motors. The new flux switching motor is then introduced and its own particular characteristics are discussed. In Chapter 3 the mathematical model and simulation of the operation of the motor are presented. Chapter 4 describes the design and performance of a proof-of-principle motor, designed to do what the name suggests. Chapter 5 looks at all aspects of the design of the new flux-switching motor based on a given industrial specification contained in Appendix I. Testing of prototype motors and their drives are detailed in Chapters 6 and 7. Chapter 8 presents an additional set of tests carried out solely for the purpose of validating the theory. Conclusions are then presented in Chapter 9 along with proposals for further work.

CHAPTER 2 EVOLUTION OF THE NEW FLUX-SWITCHING MOTOR

2.1 Introduction

The evolution of the new flux-switching motor is described. The Chapter begins with a brief introduction to switched-reluctance motor technology describing the principles behind its operation, how torque is developed, self-starting requirements and some of the power-converters used to operate the motor. The use of fully-pitched windings in switched-reluctance motors is explored in detail. The two-phase fully-pitched 4/2 switched-reluctance motor is discussed further as it helps to illustrate the concept behind the new flux-switching motor. The characteristics that the motor exhibits are identified and similarities are shown with those of the conventional DC motor. Other electrical machines with comparable qualities to the new flux-switching motor are also discussed.

2.2 Switched-reluctance motors

2.2.1 Introduction and history

The switched-reluctance motor is a brushless electronically-commutated DC motor. Both the rotor and stator are constructed from salient laminations with the stator carrying the source of electrical excitation, that is the concentrated phase windings. A cross-sectional view of a three-phase 6/4 switched-reluctance motor is shown in figure 2.1. It is so called because it has four rotor poles, six stator poles and three phases, with each phase consisting of two diametrically opposed windings connected in either series or parallel. This

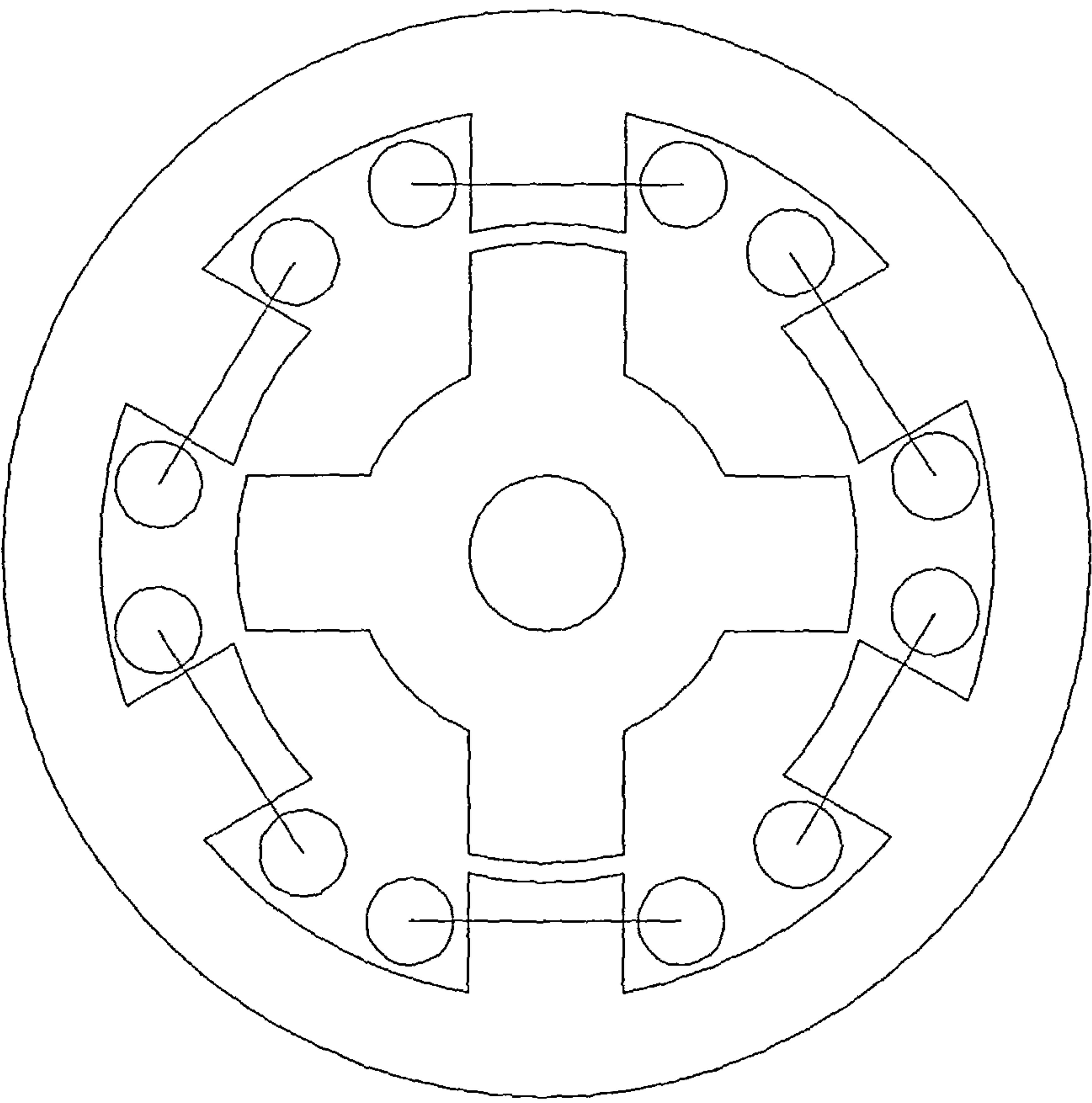


Figure 2.1 Three-phase 6/4 switched-reluctance motor

motor has a single pair of stator poles per phase, and it is said to be regular because the lamination profile is symmetrical. The changing reluctance, due to the changing airgap between the stator and rotor, with different relative positions is exploited to develop torque.

The switched-reluctance motor was originally invented in the form of an electromagnetic engine in 1840 by Taylor [1]. The engine was of a very simple construction and the electromagnets it used were switched with the use of a mechanical commutator arrangement that was also used as a position sensor. Owing to the earlier invention of the DC commutator machine by Jacobi in 1838 [2], and its subsequent rise in popularity, the switched-reluctance motor appeared to be consigned to history and no further development at that time took place. With the invention of high power semiconductor devices in the late 1960's the switched-reluctance motor made a return, as the mechanical commutator could be replaced with an electronic version that was more reliable. The first modern switched-reluctance motors were proposed by Byrne [3], [4], Unnewehr [5], Nassar [6], and Bedford [7], [8]. Rapid development followed with numerous experimental machines being constructed and tested by various groups. The "classic", or most notable, methodology for the design of switched-reluctance motor was proposed by Lawrenson [9].

The potential for these motors became more apparent particularly for use in high power applications [10], [11], but, even today, they are slow to be adopted because of the existence of more well established drive systems. However the

switched-reluctance motor offers a number of benefits over existing motor topologies. They have the simplest construction of any electric motor, with no permanent magnets or rotor windings and concentrated stator windings, which means that they are cheap to manufacture and also very reliable. The drive is also simpler in design than those used with the brushless DC and AC motors because the phases of the motor are excited individually with unipolar current. They can produce high starting-torque and also have a high efficiency.

2.2.2 Principle of operation

The operation of the switched-reluctance motor is based upon the principle of minimising reluctance within a magnetic circuit. This can be illustrated with the use of figure 2.2, which shows a cross sectional view of a regular three-phase 6/4 motor in a series of sequential positions. In position A-A the rotor is said to be in the aligned position with the stator poles of phase A. With phase A excited this becomes a position of minimum reluctance, as the airgap is at its *smallest and the path for the flux is shortest*. If however phase B was to be excited, not being in a minimum reluctance position, the rotor would tend to rotate in a clockwise direction until the quadrature poles of the rotor were in the next fully aligned position B-B. Similarly if phase C had been excited, instead of phase B, rotation would have been in an anticlockwise direction. Assuming that the rotor has rotated clockwise to position B-B it can be seen that, by commutating the phases so that phase B becomes de-energised and phase C is excited at the appropriate time, clockwise rotation can be maintained as depicted in figure 2.2d.

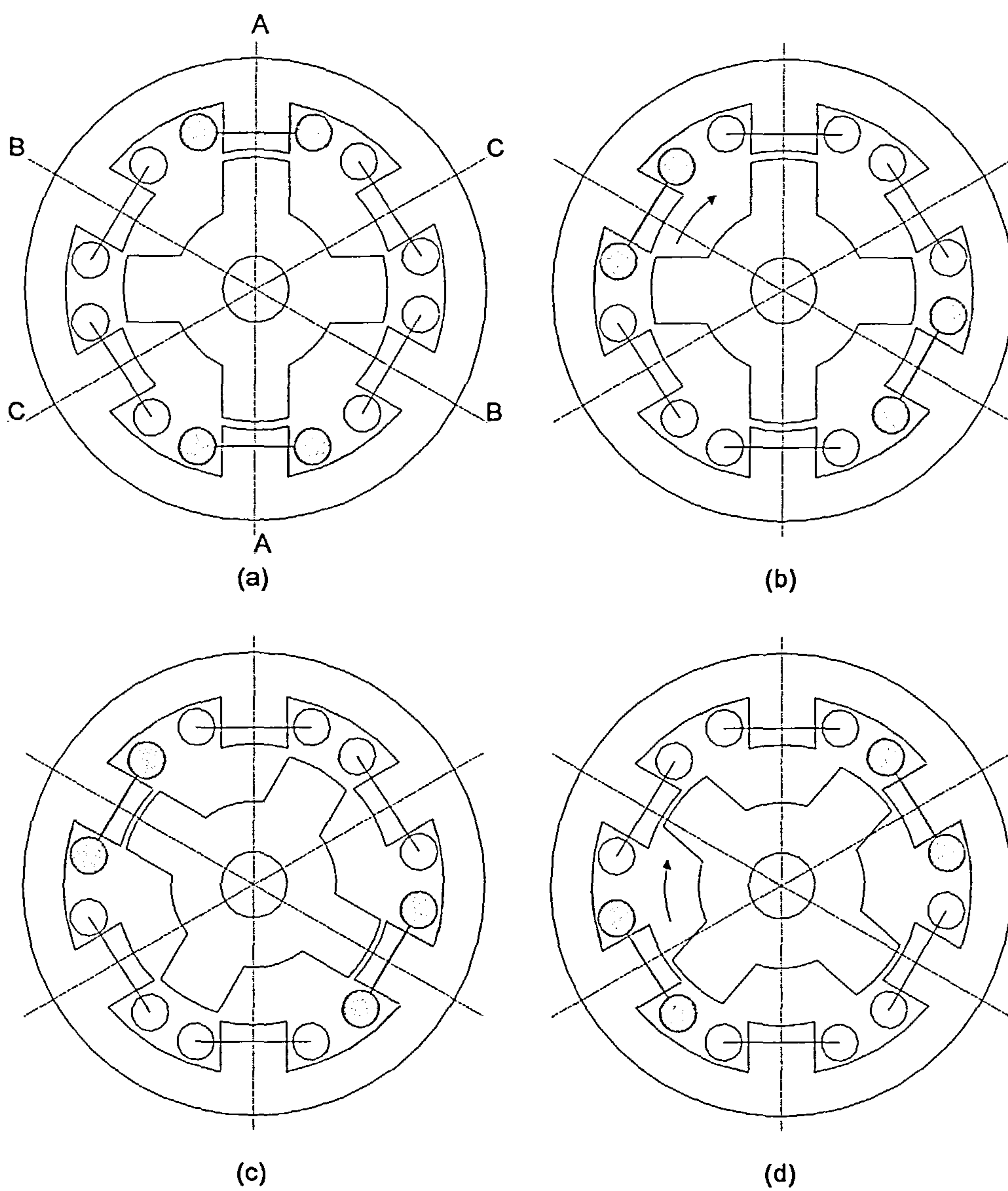


Figure 2.2 Three-phase 6/4 switched-reluctance motor in sequential positions

To summarise, the switched-reluctance motor operates by ensuring that the motor always tends to turn into a position of minimum reluctance, that is the nearest aligned position, which is achieved by the appropriate excitation of the phases. A repetitive sequence of pulse excitations of the phases results in continued rotation. Reversing the sequence causes rotation in the opposite direction.

2.2.3 Torque production

From the previous section it follows that torque is developed when the inductance, which is inversely proportional to reluctance, of an excited winding is increasing with respect to a change in position. Conversely negative torque is produced with a decreasing change in inductance. Consider the set of linear inductance profiles for each phase of the three-phase motor in figure 2.3. This shows that it is always possible to be in a range of increasing inductance at any rotor position. These linear profiles, applicable to an ideal motor, would only occur if the effects of magnetic saturation and fringing could be neglected.

For each rotor position there is a corresponding magnetisation (flux-linkage) curve that describes the magnetic characteristics of the lamination at different levels of applied phase current. An example of these curves is given in figure 2.4. The uppermost curve corresponds to the aligned position. At low current levels the curve rises linearly until a 'knee' is reached. At this point the iron begins to saturate with magnetic flux such that reluctance increases restricting

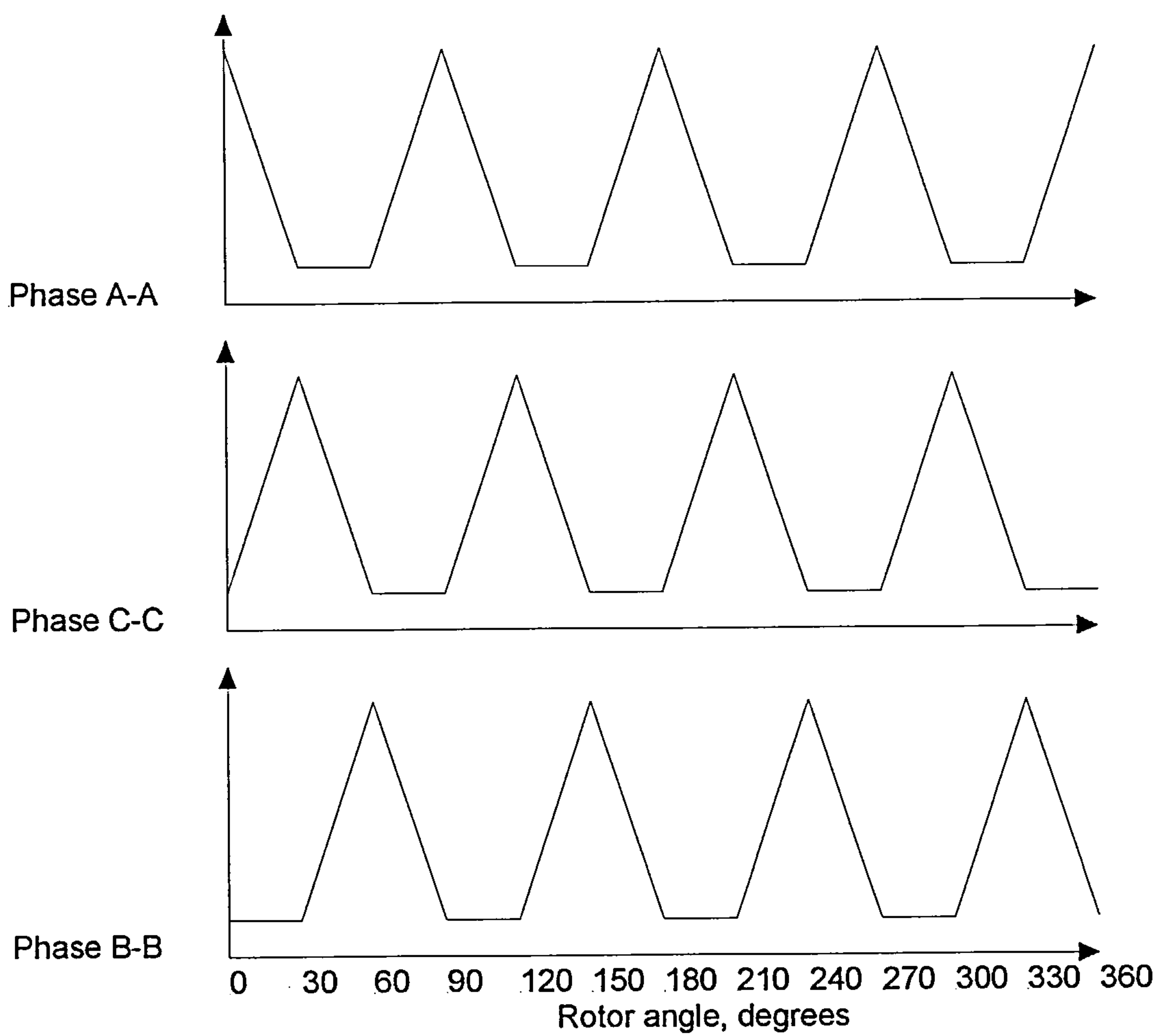


Figure 2.3 Linear inductance profiles for a three-phase 6/4 switched-reluctance motor

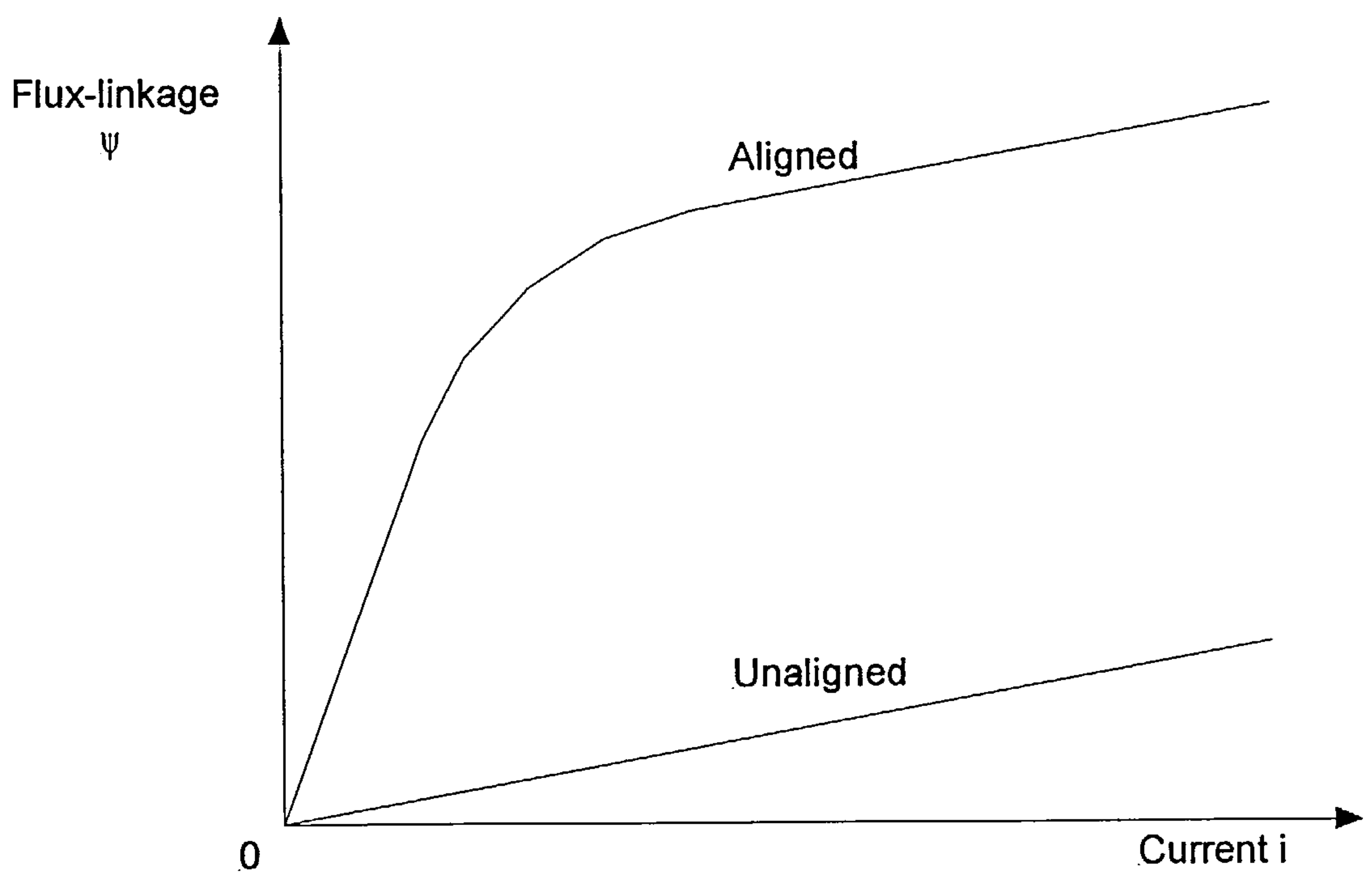


Figure 2.4 Aligned and unaligned magnetisation curves

the flow of flux. This continues until a point is reached where no more flux can be produced with further increase in the current level. The lower curve applies to the unaligned position, which possesses the greatest reluctance due to the largest possible airgap. Saturation effects would not be noticed at this position with the same current levels as for the aligned position. In this case the relative size of the reluctance of the airgap restricts the flow of flux.

The fundamentals of electromagnetic energy, with respect to the switched-reluctance motor, are presented as an overview. Numerous texts cover these aspects in further detail [12] - [14]. The torque produced by a single phase, at any moment in time, is equal to the rate of change of the energy converted to a mechanical form, or coenergy, with respect to rotor position.

$$T = \left[\frac{\partial W'}{\partial \theta} \right]_{i=const.} \quad (2.1).$$

The coenergy W' is the area beneath the magnetisation curve at a given position that is given by.

$$W' = \int_0^{i_1} \psi \, di \quad (2.2).$$

This is illustrated in figure 2.5. The stored magnetic-field energy W_f is the corresponding area above the magnetisation curve. In an ideal motor, one that exhibits a linear set of flux-linkage curves, the coenergy equals the stored magnetic field energy.

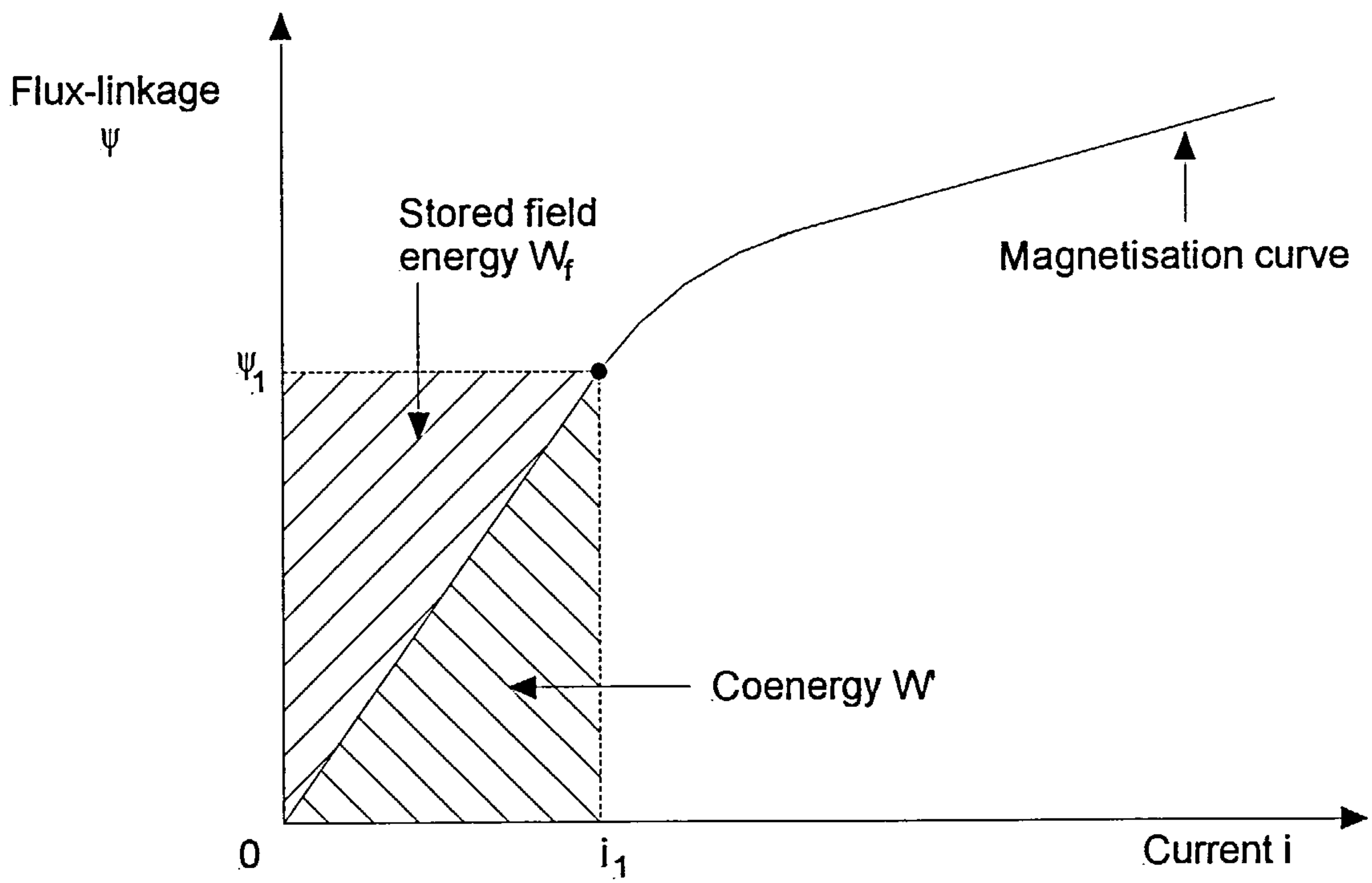


Figure 2.5 Definition of stored magnetic field energy W_f and coenergy W'

$$W_f = W' = \frac{1}{2} Li^2 \quad (2.3).$$

Thus the instantaneous torque is a function of the rate-of-change of inductance with respect to position.

$$T = \frac{1}{2} i^2 \frac{dL}{d\theta} \quad (2.4).$$

To maximise the torque output the rate-of-change of inductance, with respect to position, needs to be as large as possible for a given phase current. This implies that the airgap is as small as possible in the aligned position and a maximum in the unaligned position.

2.2.4 Self-starting requirements of two-phase motors

Referring back to the set of linear-inductance profiles in figure 2.3, for each phase of the three-phase motor, in any rotor position, it is always possible to be in a range of increasing inductance such that positive torque can be developed. The position of the rotor needs to be known at start-up to get the desired direction of rotation, and it also subsequently needs to be known to correctly commutate the phases.

Now consider the corresponding inductance profiles of the phases of a regular two-phase 4/2 switched-reluctance motor shown in figure 2.6. The overlapping of the profiles, this time, shows that it is not sufficient to guarantee that the motor would be able to start in all positions, because there results flat regions

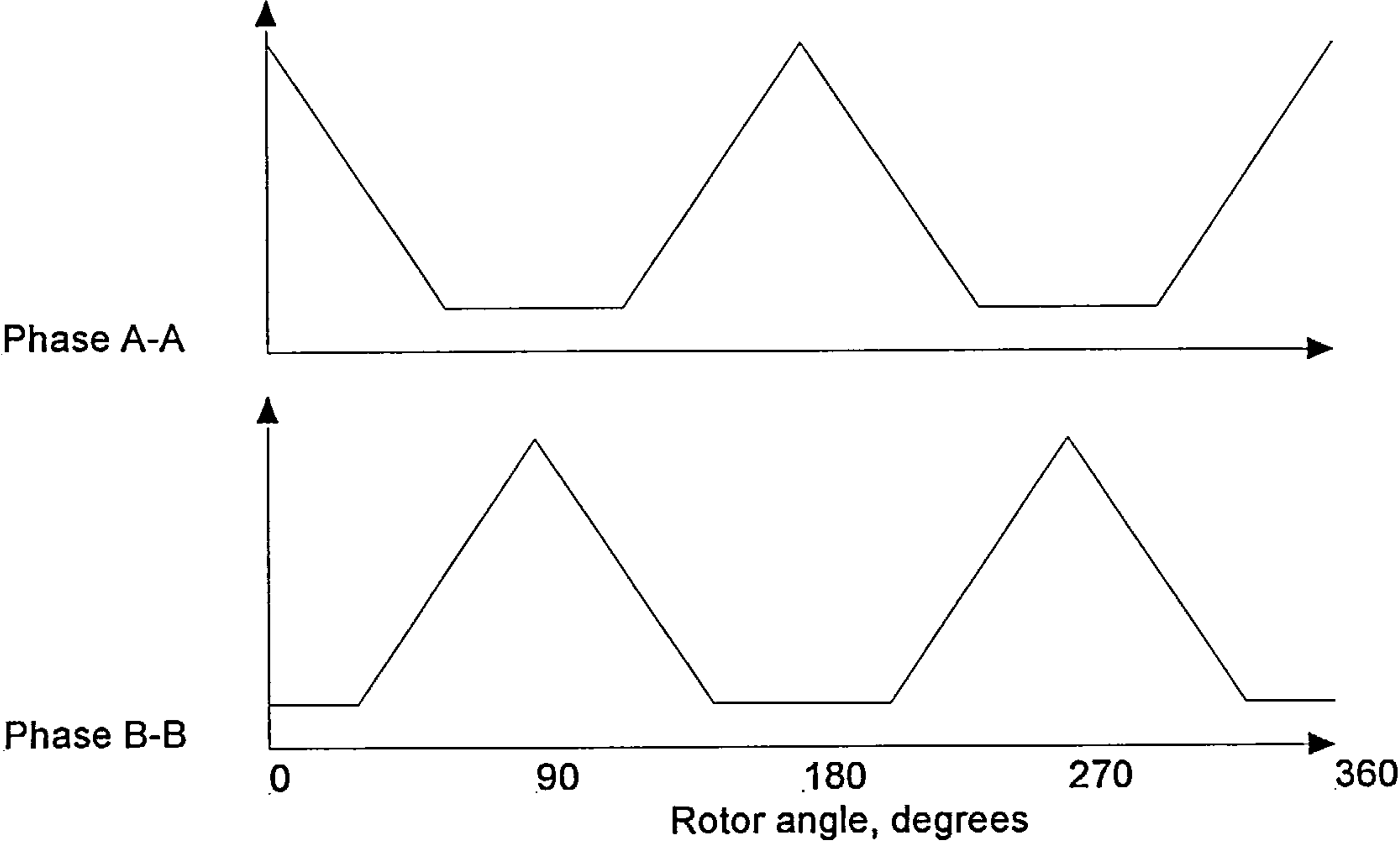


Figure 2.6 Linear inductance profiles for a two-phase 4/2 switched-reluctance motor

in the profile, where inductance does not change do not match up for each phase. These positions, where such a difficulty would be encountered, relate to one phase being exactly in the aligned position with the other exactly in the unaligned position. These positions are also known as torque-equilibrium positions. The aligned position is a position of stable torque-equilibrium whilst the unaligned position is a position of unstable torque-equilibrium. Given the rotor in the unaligned position if it could be displaced by a small amount, enough to get through the flat region of the inductance profile, it would be able to rotate to the next aligned position.

All two-phase switched-reluctance motors experience this torque-equilibrium problem with self-starting. This is analogous to that experienced by the single-phase squirrel cage induction motor. Just as the starting problem can be successfully overcome for the induction motor with the use of shaded poles, it can be solved, with various design changes, for the switched-reluctance motor. However, also like the induction motor, there is a price to be paid for the self-starting solution. Performance is compromised by the restriction of rotation to one direction only and by the non-ideal running characteristics caused by the need for self-starting.

The methods to facilitate self-starting in single and two-phase switched-reluctance motor include starting using a parking-magnet [15], [16], controlled saturation [17], pole shaping [18], and a stepped [19], and graded airgap [20]. A parking-magnet is held in between a pair of adjacent stator poles so that the

next position of the rotor is off centre. As the rotor comes to rest, the flux created by the magnet is sufficient enough to overcome the frictional torque of the load and thus park the rotor next to the magnet. When the motor is next excited the rotor is in a position of rising inductance allowing starting to take place easily. To be successful this method is dependent upon the friction of the load being low. Use of magnets that are too large would result in excessive eddy-currents being induced at high speeds. The other starting methods share the same principle of operation, that is the modification of the inductance profile. The flat regions are eliminated and replaced by an asymmetric sloping profile that creates an unbalance in the magnetic forces that leads to rotation. These other methods are the most common and cheapest to implement, for a simple change to the lamination design is all that is required. Figure 2.7 shows some common examples to achieve this.

It is feasible to design a single-phase motor [16], [21], [22]. However, considering a single-phase, see figure 2.6, this shows that positive motoring torque occurs in less than half the possible rotor positions. Therefore after being started the motor would experience a large torque ripple due to the large gaps between successive excitations of the single-phase. The general rule is the more phases there are the smoother the torque profile becomes.

So why consider using a two-phase motor if it has problems starting and, inevitably, has a poorer torque-profile than a motor with more phases? This question was answered in Chapter 1. The cost of the motor is low in

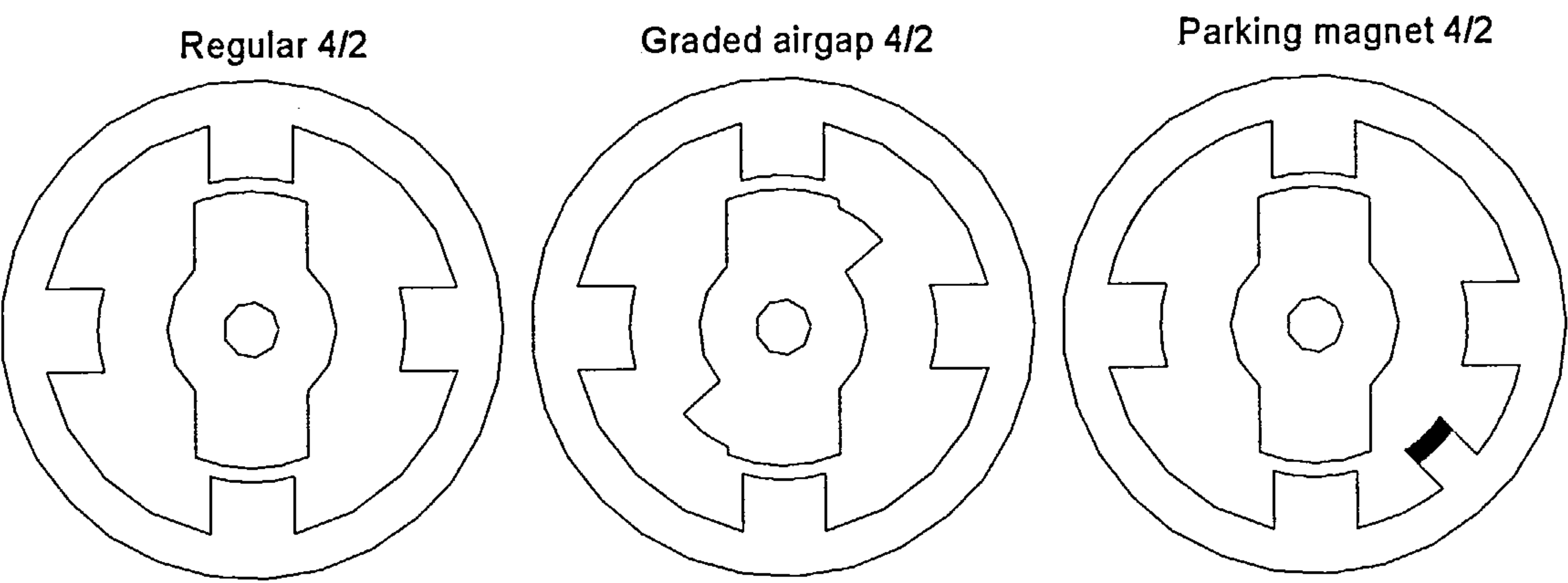


Figure 2.7 Two-phase 4/2 switched-reluctance motor lamination profiles

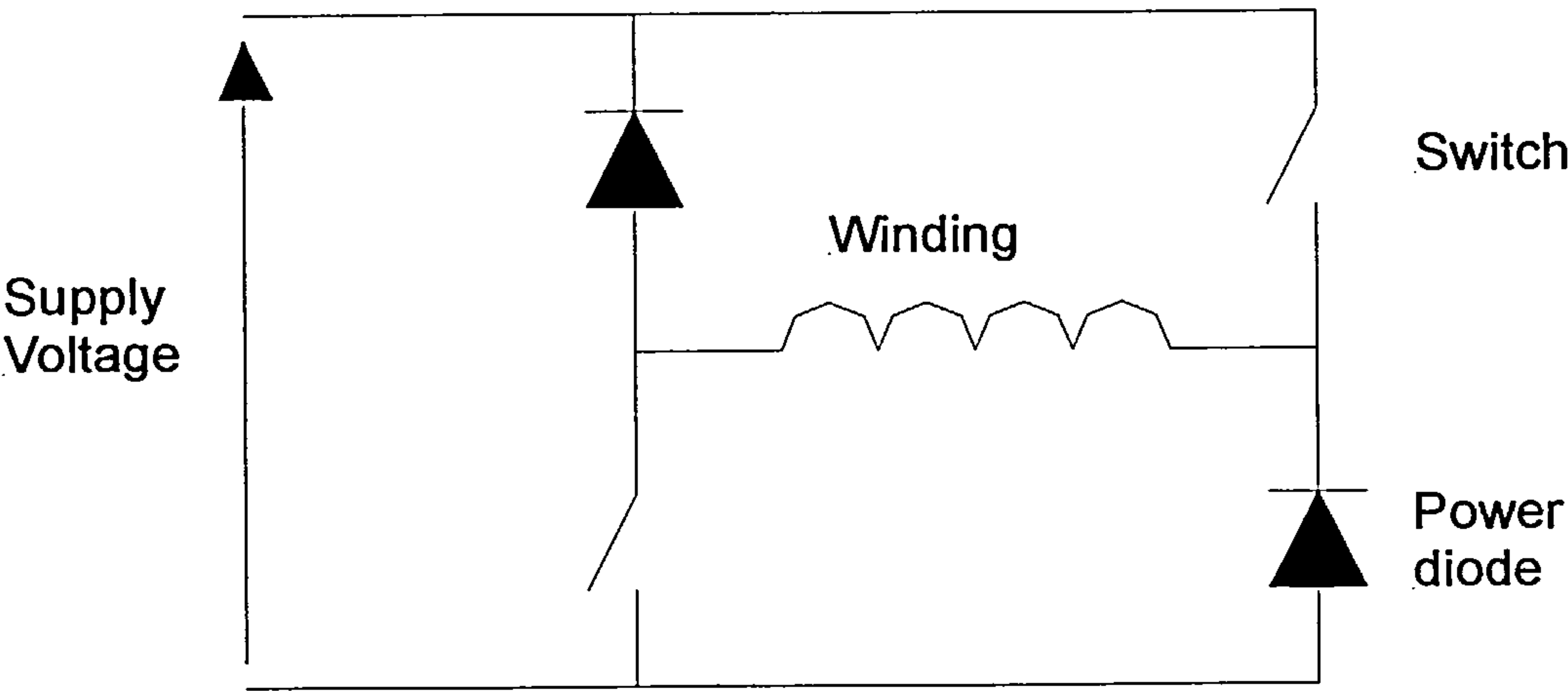


Figure 2.8 Asymmetric half-bridge

comparison to the cost of the electronics used in the drive, therefore to produce a low-cost drive-system the amount of electronics employed must be kept to a minimum [23], [24]. Generally speaking, a two-phase drive will have two-thirds the electronics used in a three-phase drive. The two-phase motor can, however, be used with applications that require rotation in one direction only because of the need for self-starting.

2.2.5 Power-converters

A switched-reluctance drive-system consists of a motor and a drive. The drive is the interface between the motor and the power supply, and the motor is the interface between the drive and the mechanical system. The power-converter is a component of the drive, which is responsible for delivering the required pulses of current to the windings of the motor. Other drive components include the motion controller, which controls the motor output often using direct feedback signals from the motor, and the gate-drive, which amplifies logic signals from the motion controller to drive the power-switches. Numerous different designs of drive have been proposed and detailed descriptions of their operation can be found in the literature, [25] – [28].

Torque can be developed irrespective of phase-current direction as implied by equation (2.4). This greatly simplifies the design of the power-converter as unipolar input current can be used.

During each motoring stroke, that is the time in which phase-inductance is increasing, it is necessary to build-up the phase-current from zero, and then before the end of the stroke, return it to zero. These transitions should be done as rapidly as possible so as to maximise the time spent at full available current excitation, and thus maximise torque-production and work-output. To build-up current rapidly in the winding the full-supply voltage needs to be available, which implies that the generated opposing back-EMF must be a minimum, this can be achieved by firstly ensuring that the inductance of the winding is as low as possible and secondly by exciting the winding when the inductance is either not changing, or changing very slowly. To avoid negative torque production the current in the winding needs to be zero before or at the aligned position.

The most common power-converter used for each phase of the switched-reluctance motor is the asymmetric half-bridge. This consists of two power-switches and two power-diodes arranged as shown in figure 2.8. It has three operating modes, a positive-voltage loop, a zero-voltage loop and a negative-voltage loop. The positive-voltage loop is used to energise initially the phase-winding with current by switching both switches on. To control the level of the current effectively in the phase winding, it is preferable to alternate between the positive-voltage loop mode and the zero-voltage loop mode. The zero-voltage loop is used to let the phase-current decay slowly, the bottom switch is left on and the top switch is switched-off. To de-energise the phase winding at the end of the operating cycle the negative-voltage loop is used. Both switches are

switched-off placing a negative voltage across the winding, which returns the energy to the supply.

The asymmetric half-bridge offers the best control of the switched-reluctance motor although it does have some inherent disadvantages. To operate a two-phase switched-reluctance motor a total of eight power-devices are needed, comprising four switches and four diodes. These are expensive components. Also there are the additional gate-drive components that have to be considered. Furthermore, the top switches of the asymmetric half-bridge require isolated, or floating, gate drives that require even more components. In order to overcome this problem, and reduce the complexity of the power-converter numerous types of shared-switched converters have been proposed [26], [29]. Use of such circuits has enabled the power-device count to be reduced by as much as half, however a compromise in performance usually results.

2.3 Switched-reluctance motors with fully-pitched windings

Previously the emphasis in the design of switched-reluctance motors has been to attempt to optimise their performance by improving their control. More recently though this area of research has become less fruitful and the focus has shifted more to changing the fundamental machine design in order to solve some of the remaining problems that these motors experience. Concentrated short-pitched windings have predominantly been used in switched-reluctance motors since their inception. It has been realised, lately, that other winding-

configurations can be used, and interest has returned to this area of design [30], [31].

2.3.1 Introduction and history to the use of fully-pitched windings

The switched-reluctance motor, as previously mentioned, is not a new concept, and neither is the use of fully-pitched windings in electrical machines. They have been used in various types of machine for example the induction-motor, the synchronous-machine, and the inductor-alternator. The operation of the inductor-alternator is particularly relevant to the flux-switching motor, and it is described in more detail later in this Chapter.

Recent research has demonstrated that fully-pitched windings can be applied to switched-reluctance motors. Originally conceived for use in three-phase motors [31], it has since been demonstrated that the motor worked perfectly well with the use of such windings solely, completely replacing the more conventional concentrated short-pitched windings. Also the use of an additional, or auxiliary, fully-pitched winding, to complement the operation of the short-pitched windings, has been researched [32]-[34]. The purpose of the extra winding was for it to operate in a complementary manner to help to overcome some of the inherent problems experienced with the function of the switched-reluctance motor.

Unlike a short-pitched winding that spans only one stator pole, a fully-pitched winding spans the same number of stator poles, as there are phases in the

motor. Of course fully-pitched windings are longer than their short-pitched counterparts, although the active portion of the winding remains the same, the extra length is taken up by the end-windings. As a result the winding inductance and the copper losses are higher. The copper losses can be kept to a minimum by using more poles per phase. For example, the fully-pitched winding in a two-phase motor would span two stator poles. Referring to figure 2.9, if two poles per phase were used to give a four-pole stator, the end-windings would span the whole width of the stator with the main active part of the winding located in opposing stator slots. The end-windings would have to describe an arc the same radius as the stator slots to avoid interfering with the rotor. In figure 2.9 they are distributed equally around both sides of the stator to balance the magnetic leakage and fringing effects. Increasing the number of poles per phase to four, so that the stator now has eight poles and four fully-pitched windings to a phase, allows each end-winding to be halved to only span a quarter of the stator as shown in figure 2.10. The total end-winding length remains the same as in the two poles per phase motor, but the ratio of active length to end-winding length is doubled such that the copper losses incurred, as a result of the end-windings, will be approximately halved. This ratio improves with the number of poles per phase added, however doubling the number of poles per phase also doubles the number of electrical cycles per revolution, thus increasing the switching losses in the power switches and also the iron losses incurred. As with many design changes a compromise is necessary.

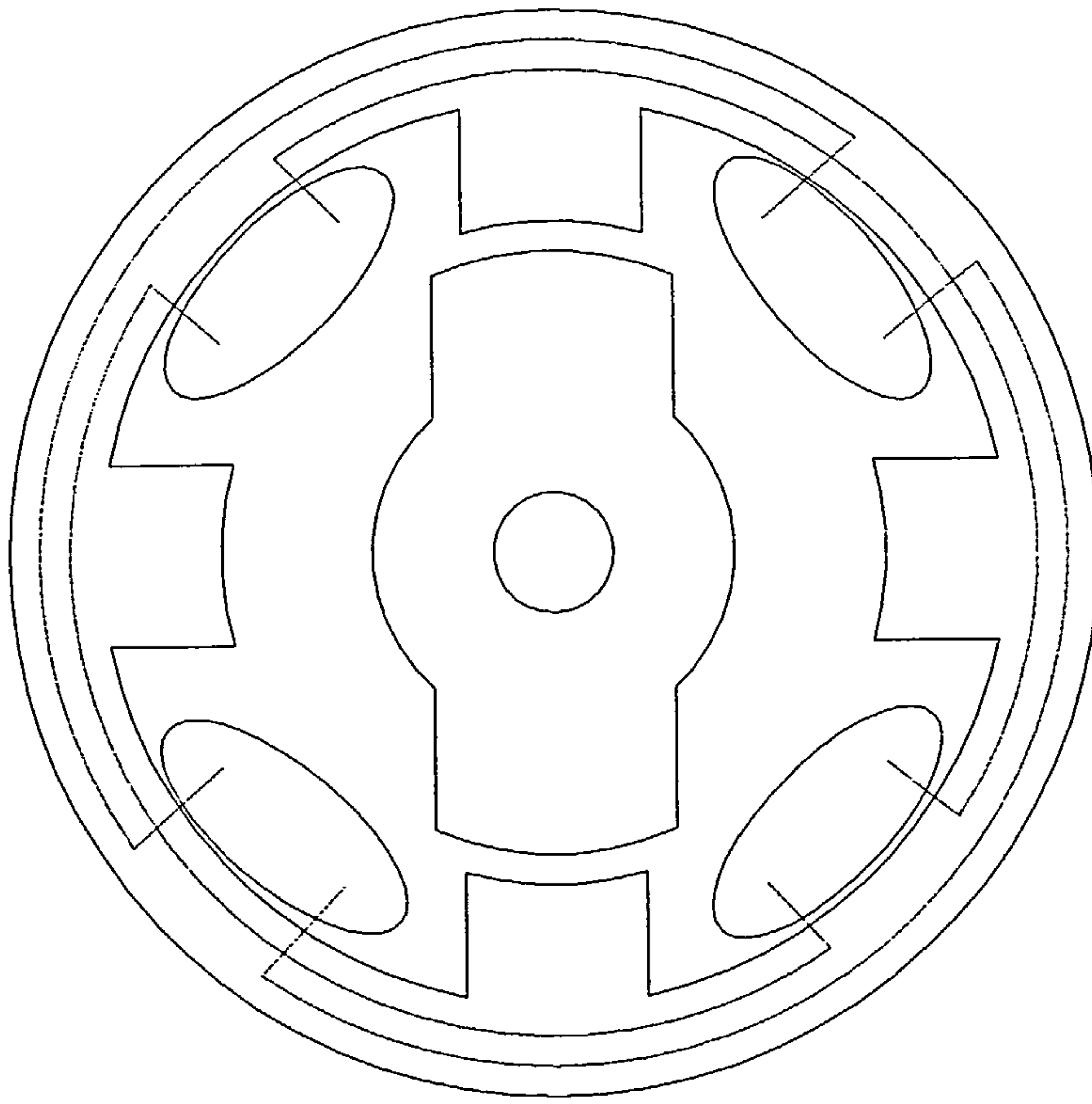


Figure 2.9 Fully-pitched 4/2 switched-reluctance motor

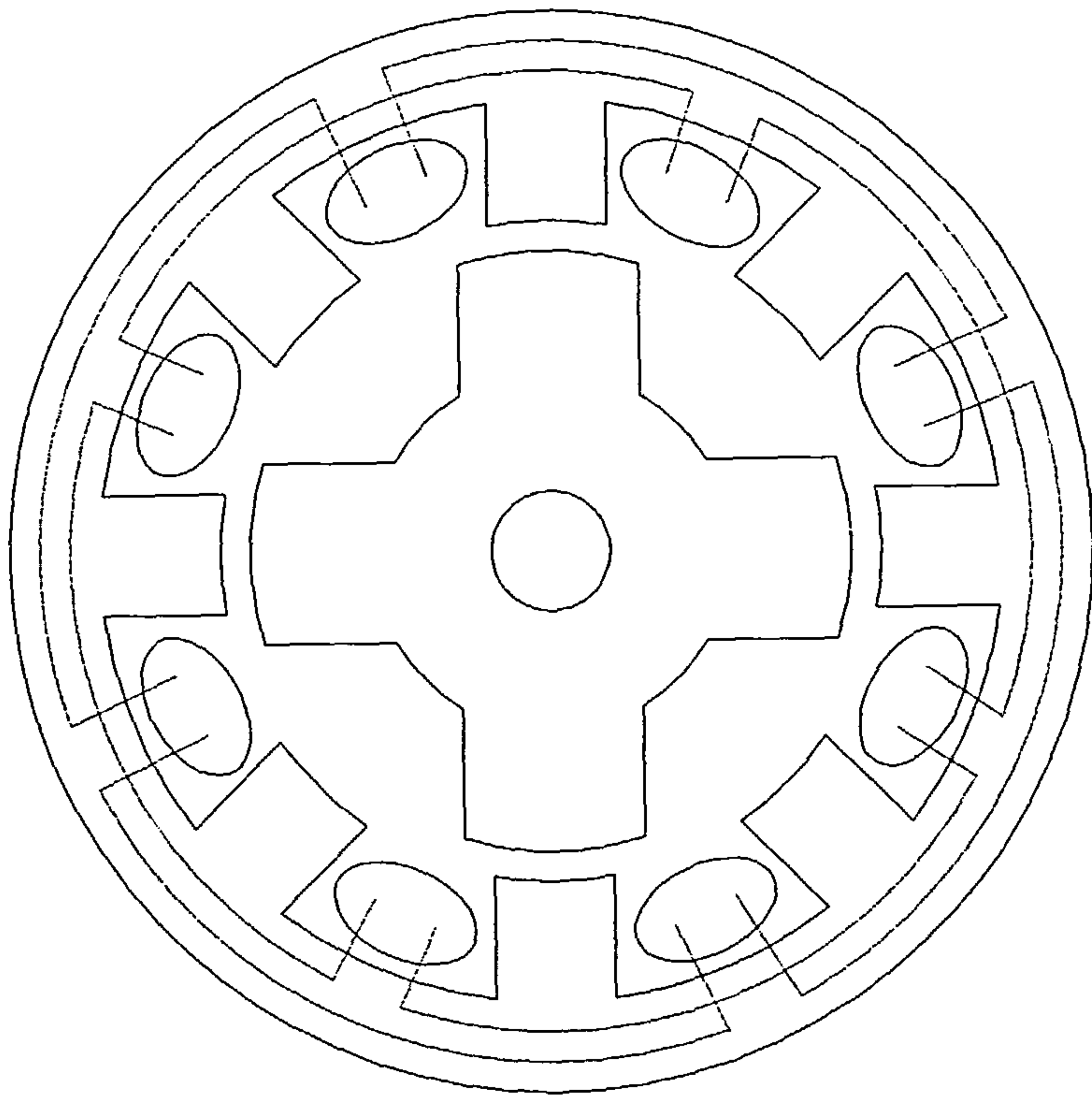


Figure 2.10 Fully pitched 8/4 switched-reluctance motor

2.3.2 Principle of operation of switched-reluctance motors with additional fully-pitched windings

The addition of a fully-pitched DC excited winding into the structure of a conventional three-phase short-pitched motor has been presented, the fully-pitched winding being referred to as an “Auxiliary DC winding” [34] and an “Auxiliary commutation winding” [33]. Figure 2.11 depicts the three-phase switched-reluctance motor with the additional fully-pitched winding located in the gaps between the short pitched windings. It is important to note at this point that the motor can still operate, without this fully-pitched winding being actively used, in the normal manner. The purpose of the extra winding is that it is to work in a complementary manner, to help to overcome some of the inherent, poor current commutation and poor energy circulation problems experienced with the function of the switched-reluctance motor. For switched-reluctance motors to achieve the best utilisation of their torque producing capacity it is important that the phase currents are increased and decreased as quickly as possible before and after commutation. However, instantaneous change is physically impossible and the worst-case scenario occurs at the ideal commutation point, the aligned position. Therefore it is usually necessary to commutate early to allow adequate current build-up, thus reducing the output torque and power. Throughout the operation of the switched-reluctance motor the electrical energy circulates between the power supply and the motor, in such a way that not all of this electrical energy is converted to useful mechanical energy. This is commonly known as the “excitation penalty” [9], [11], [12], [35], [36]. Figure 2.12 is a flux-linkage diagram that shows the

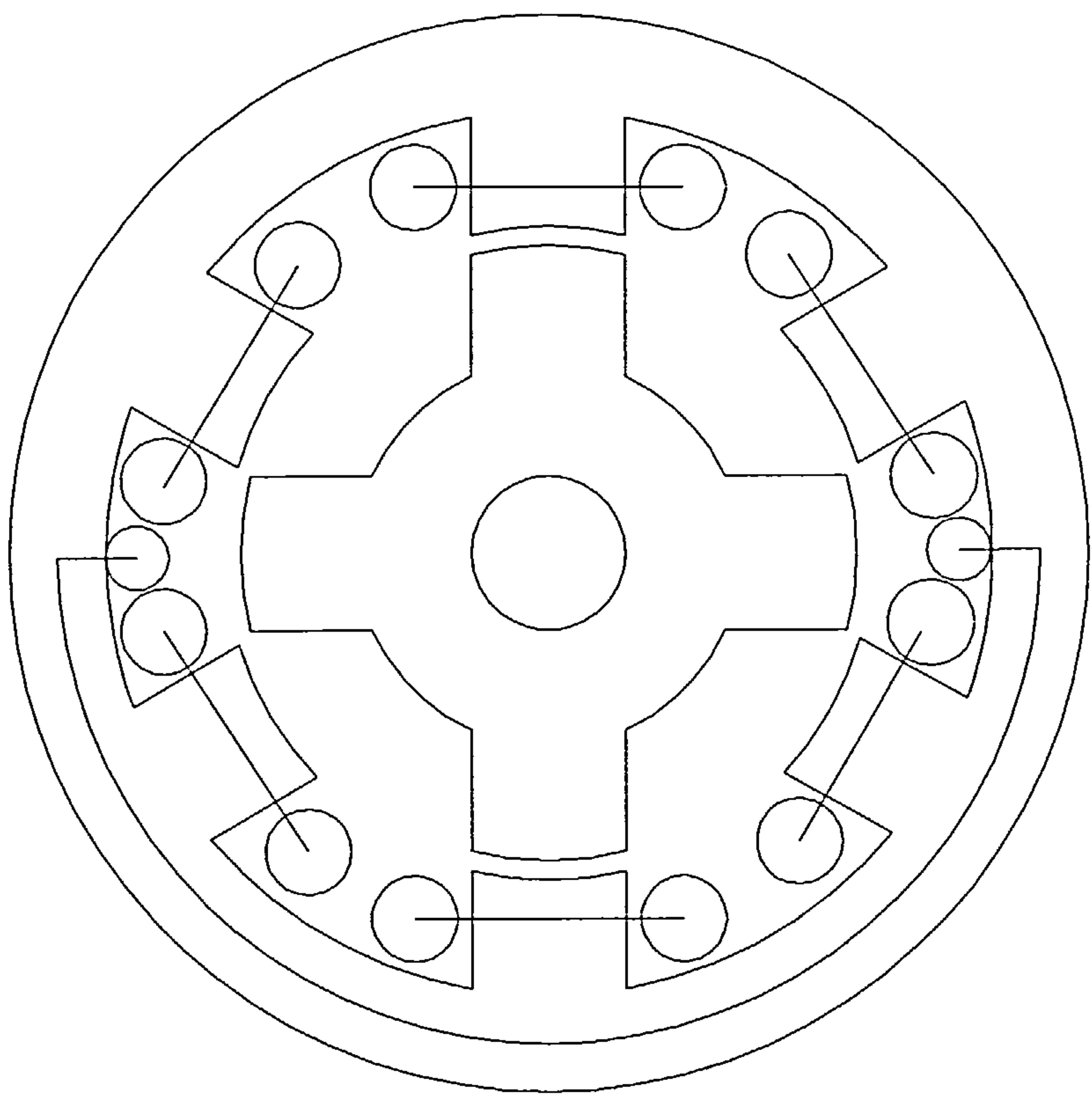


Figure 2.11 Three-phase 6/4 switched-reluctance motor with an additional fully-pitched winding

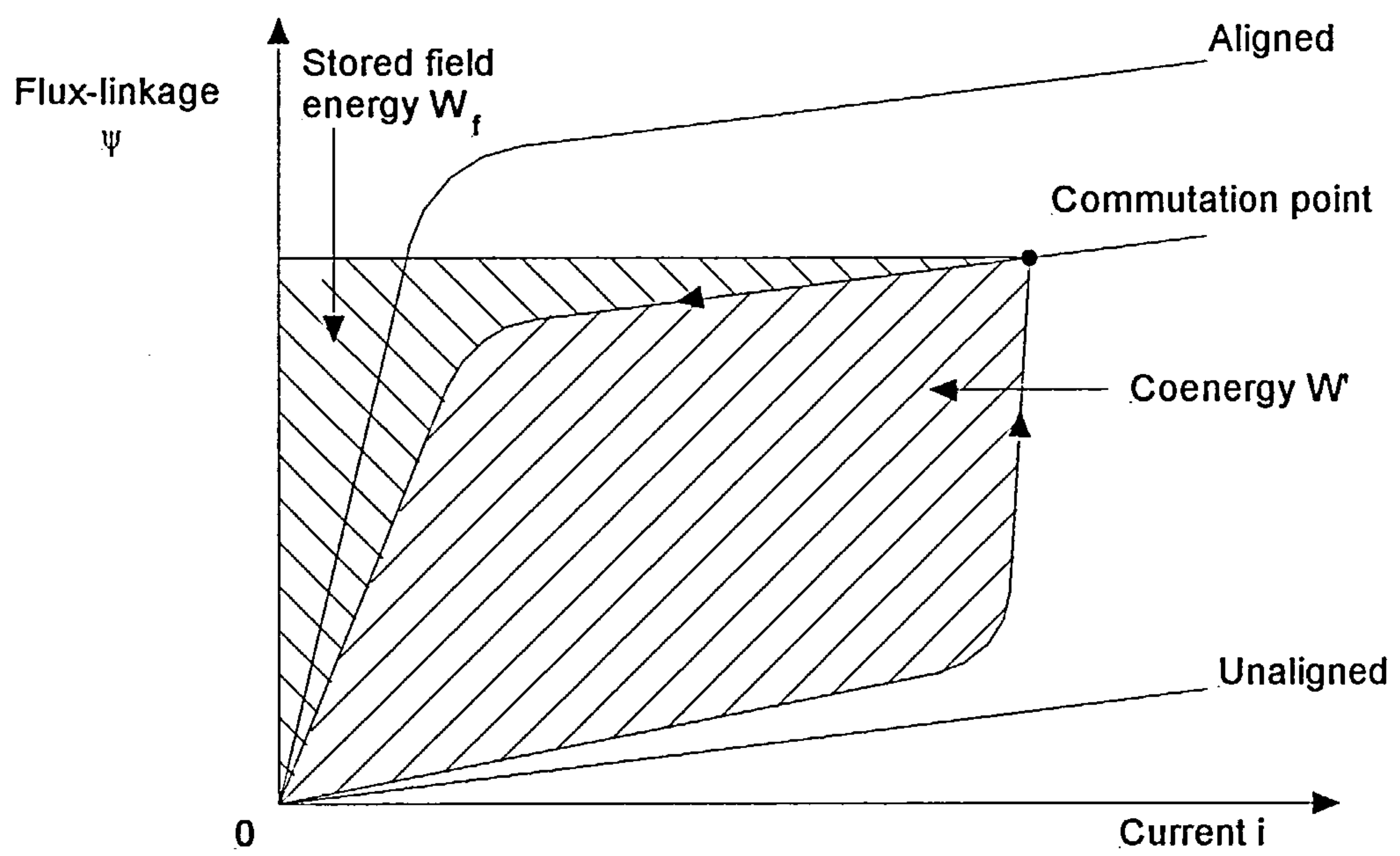


Figure 2.12 Flux-linkage diagram showing the energy converted per stroke in a switched-reluctance motor

energy converted per stroke (complete phase-excitation) in a switched-reluctance motor. The total input energy is the sum of the stored magnetic-field energy W_f and the energy converted to a mechanical form, the coenergy W' . The stored magnetic-field energy W_f is returned to the supply at the end of each stroke.

Both of these problems have a single cause, which is that the stored energy is not used efficiently. The fully-pitched winding serves the purpose of retaining the field energy at commutation, thus overcoming the problems. During commutation the energy associated with the short pitched winding being turned off, is transferred to the fully-pitched winding. A proportion of this stored energy is then transferred to the field of the next excited short-pitched winding, whilst the remainder is converted to mechanical energy. To ensure the efficient transferral of energy there needs to be good coupling between the two types of winding. The same magnetic path is shared so therefore the only energy lost is from leakage effects. The fully-pitched winding also has no detrimental effect on torque production, as the self-inductance of the winding is independent of the rotor position.

In conclusion a motor employing an additional fully-pitched winding has been shown [33] to develop higher output power with the same converter rating, which also translates into improved efficiency. The only disadvantages that

arise with this new design are that more copper is required and a higher torque ripple is incurred.

A DC-flux, that remains in constant use, can also be realised with the inclusion of permanent magnets into the stator back-iron [37] - [39]. The addition of permanent magnets into the motor structure is a more costly solution than an extra winding, as well as being more difficult to manufacture.

2.3.3 Power-converters for switched-reluctance motors with additional fully-pitched windings

Essentially the fully-pitched winding can be considered to be an additional phase of the motor [33], [34]. Therefore the power electronics for this phase are no different to any other. An asymmetrical half bridge can be used to provide full control over the fully-pitched phase. Whilst this method does allow the best means of control, it is not an inexpensive solution. For a more cost-effective answer it is possible to simply short the two ends of the fully-pitched winding together, via a diode, thereby removing the supply completely. The disadvantage of doing this is that the performance is not as great as it was before, but the advantage is clear in terms of component count and cost of electronics.

2.3.4 Principle of operation of the three-phase fully-pitched switched-reluctance motor

In terms of switched-reluctance motor history as stated previously fully-pitched windings first appeared in three-phase motors [31]. The reason for them being adopted was that with this simple winding change, the utilisation of the magnetic and electrical circuits within the switched-reluctance motor were shown to be significantly improved. Consider the operation of a normal short pitched concentrated wound motor. Each phase has to be excited in turn to provide positive torque. It is not possible to excite more than one phase at a time and the maximum duration a phase can produce positive torque is equal to one half the time of a revolution of the motor. In electrical terms only half of the copper within the motor is being used at any one time. This copper takes up space in the magnetic circuit within the slot area. This inefficient use of copper translates to the restricted use of the magnetic circuit.

It was realised that the flux patterns experienced within a three phase short pitched switched-reluctance motor with a single-phase excited, and hence an opposing pair of excited stator teeth, could be reproduced by simultaneously exciting two fully-pitched windings located either side of the same stator teeth. Where previously half of the stator slot area, either side of a tooth is used for an excited short-pitched winding, the fully-pitched winding is able to use the whole slot area, thus doubling the copper utilisation. With a third fully-pitched winding in the remaining slots, the windings could be excited in pairs in such a way as to operate the motor. It was found that most of the torque was

developed from the change in mutual-inductance between the phases, as the variation in the self-inductance of a phase was practically negligible with rotor position. Different excitation methods of the three phases were explored, [31], [40] - [42], higher efficiencies and a greater torque-per-unit-volume were measured relative to a short-pitched, equivalent sized, three-phase motor.

2.3.5 Power-converters for the three-phase fully-pitched switched-reluctance motor

The emphasis of the majority of research into three-phase fully-pitched switched-reluctance motors has been on the performance of the motor and its comparison to the conventional switched-reluctance motor with concentrated windings [31], [43]. The design of the power-converter has largely remained unchanged with the use of a standard asymmetrical half bridge for each of the three phases. The asymmetrical half-bridge incurs nearly double the losses of the conventional switched-reluctance motor because each phase conducts for double the time. Therefore, in addition to the need to reduce the component count for financial reasons, the losses must also be reduced to ensure that the fully-pitched motor is a viable alternative. A number of different designs of power-converter have been proposed to solve this problem [43], [44].

2.3.6 Principle of operation of the two-phase fully-pitched switched-reluctance motor

The simplest example of the construction of the two-phase fully-pitched switched-reluctance motor was shown in figure 2.9. For motors with two poles per phase a fully-pitched winding spans the whole width of the stator so that the main active part of the winding is located in opposing stator slots. In general, where fully-pitched windings are used, they span the same number of stator poles, as there are phases in the motor. With the aid of figure 2.13 the principle of operation can be explained. Conventional dot and cross notation is used to denote the direction of current-flow in the windings, whilst the path travelled by the magnetic-flux is indicated by dashed lines. Two cross-sectional views of the motor, with the rotor in each of the two possible aligned positions are given. The flux-patterns shown are identical to those that are experienced in a two-phase short-pitched switched-reluctance motor, with each of the phases excited. The difference between the two motors is the method by which this flux-pattern is created. The fully-pitched motor uses the interaction between the two magnetic-fields produced by the currents in each of the two-phase windings. The combined resultant flux, created by this interaction can then be directed along one of the two orthogonal axes centred through the stator poles. The axis selected is dependent upon the direction of the current in both of the windings.

Considering figure 2.13 (a), winding A-A creates a flux in the north-westerly direction, whilst winding B-B creates a flux in the north-easterly direction. The

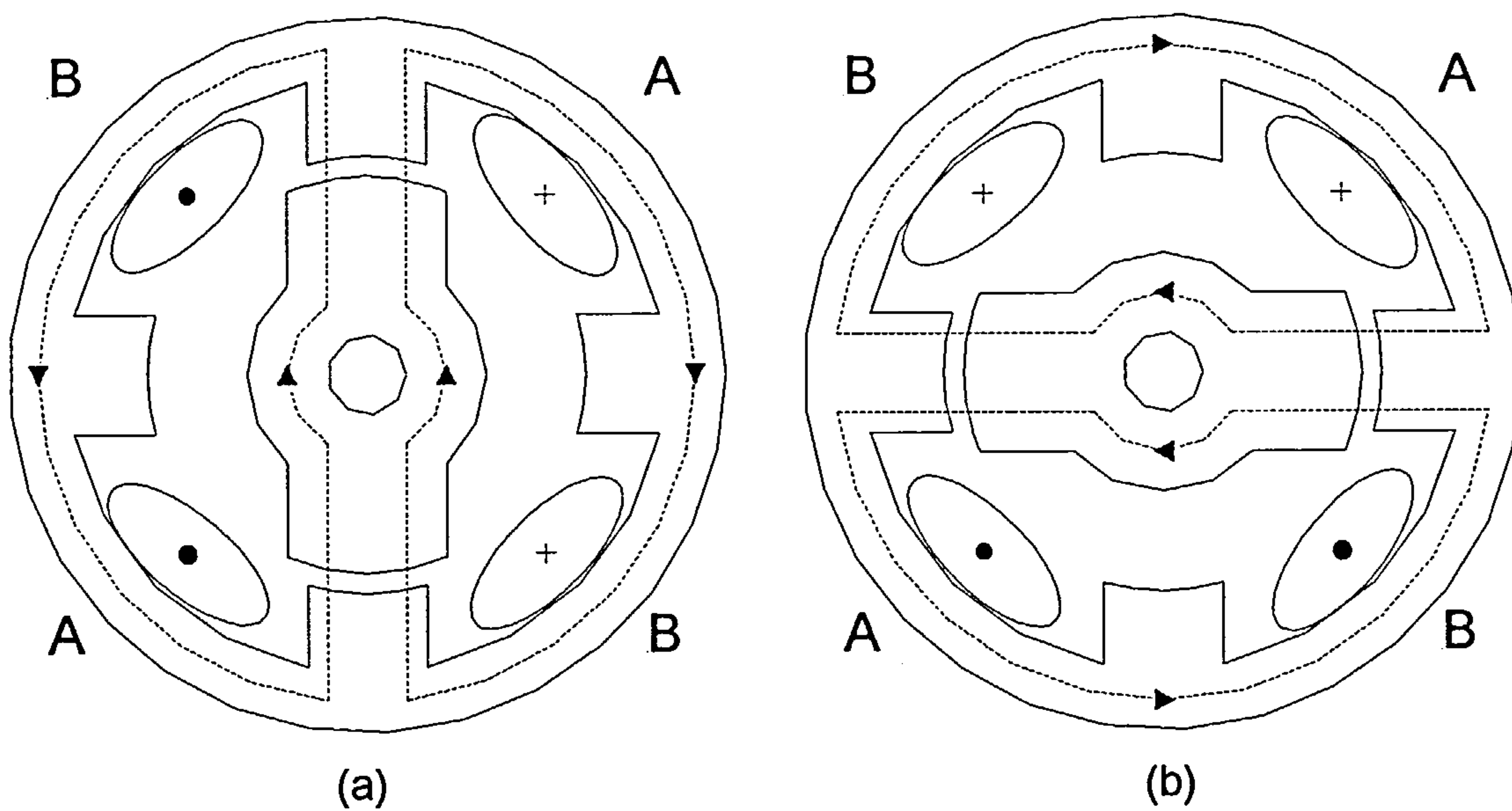


Figure 2.13 Principle of operation of a two-phase fully-pitched switched-reluctance motor

combined resultant flux, produced by both windings, travels in the northerly vertical direction, which subsequently causes the rotor to align itself with the vertical pair of stator poles. In figure 2.13 (b) winding A-A remains constantly excited in the same direction as before such that the flux continues to be in the north-westerly direction. The current in the winding B-B is reversed, thus causing a 180° shift in the direction of the flux to south-westerly. The combined resultant flux now travels in the westerly direction through the horizontal stator poles so that the rotor tends to align with them. Each reversal of current direction in winding B-B causes the resultant stator flux to switch between the horizontal and vertical axes in the manner described. The resultant stator flux does not rotate. Rotation is maintained by the sequential commutation of winding B-B at the correct time with respect to the position of the rotor.

The two-phase fully-pitched switched-reluctance motor has three distinctive features that distinguishes its operational characteristics from those of the conventional two-phase short-pitched switched-reluctance motor and other fully-pitched motors. Firstly, in a two-phase fully-pitched switched-reluctance motor, excitation-current is supplied to both windings constantly throughout the duration of its operation for both rotor alignment positions. Secondly, winding A-A is excited continuously with unipolar direct-current that does not require switching. Thirdly, the switching of the current direction in winding B-B controls the direction of the resultant stator flux and, therefore, to which stator poles the rotor is attracted.

Unlike the two-phase fully-pitched switched-reluctance motor the phases of the fully-pitched three phase switched-reluctance motor [31] are all switched. All of the required power-switching devices for the two-phase fully-pitched switched-reluctance motor are dedicated to winding B-B alone, to provide the necessary bipolar current. Winding A-A does not need any power-switching devices.

Each of the windings of a two-phase short-pitched switched-reluctance motor can potentially be energised for a maximum of one half the time per revolution, if useful torque is to be produced. Utilisation of the available copper is therefore a maximum of 50 %. Neglecting the switching time during current reversal in winding B-B, the two-phase fully-pitched switched-reluctance motor can achieve close to 100 % copper utilisation.

2.3.7 Torque production of the two-phase fully-pitched switched-reluctance motor

As for all motors with a doubly salient construction, the two-phase fully-pitched switched-reluctance motor develops torque by the tendency of the rotor to arrange itself into a position of maximum inductance with the stator when the phase windings are excited. The two-phase fully-pitched switched-reluctance motor only produces a resultant flux directed through opposite stator poles when both windings are excited. Therefore torque-production is dependent upon the flux produced by the currents in both windings. Rather than a change in self-inductance of the individual phases to produce torque, the two-phase fully-pitched switched-reluctance motor requires a change in mutual inductance

between phases. The production of torque by this means is similar to that employed in the Laws Relay limited motion actuator and other rotary actuators [45].

Figure 2.14 shows an ideal lamination profile for a two-phase fully-pitched switched-reluctance motor. The reluctance of the magnetic circuit remains constant with changing rotor position due to the constant overlap between the stator and rotor poles. The self-inductance of the two windings therefore does not change, so there is no torque developed from this quarter. The changing mutual-inductance is optimised with this lamination profile.

2.3.8 Power-converters for the two-phase fully-pitched switched-reluctance motor

The two-phase fully-pitched switched-reluctance motor has very different power-converter requirements from those of a conventional two-phase short-pitched switched-reluctance motor because of the different requirement for exciting the windings. Referring to figure 2.13, it has already been established that winding A-A is a permanently-excited DC-winding that needs no switches to operate, whilst winding B-B has to be excited with bipolar current to obtain the necessary bipolar flux. The standard H-bridge inverter circuit, shown in figure 2.15, offers the best control of the bipolar current in winding B-B, although the active component count is high, thus making this an expensive solution. Other power-converters have been proposed [46] that use fewer active components, namely the series-field split-capacitor supply shown in

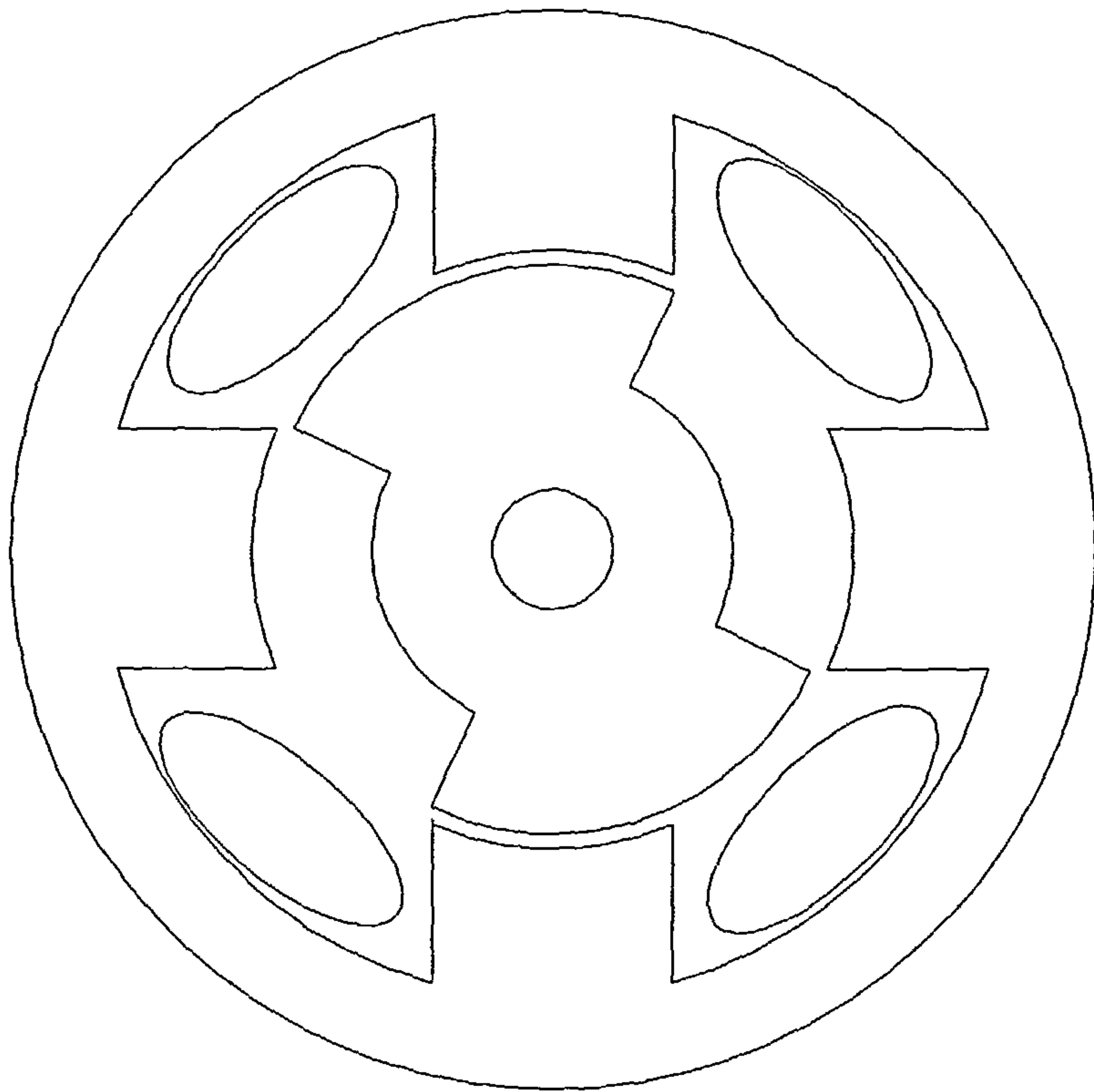


Figure 2.14 Ideal lamination profile for a two-phase fully-pitched switched-reluctance motor

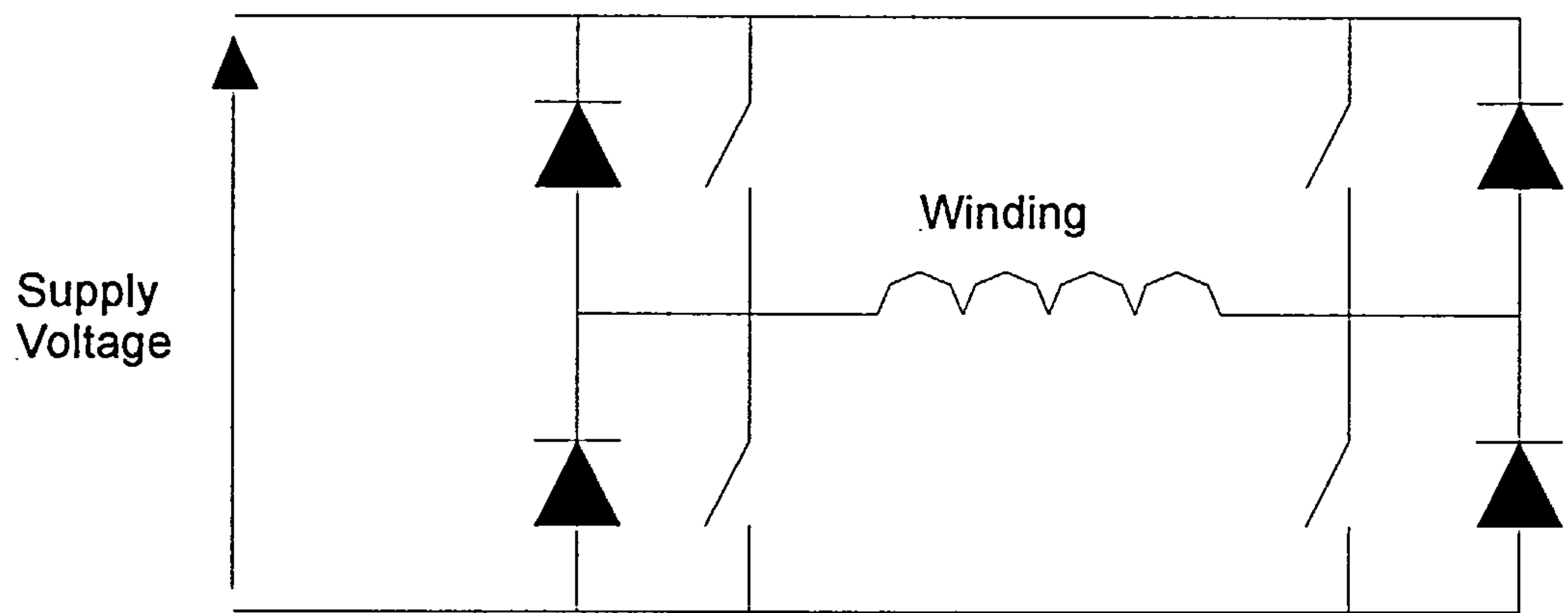


Figure 2.15 Standard H-bridge inverter circuit

figure 2.16. The two capacitors form the DC link allowing the bridge-supply voltage to be divided into two.

2.4 The new flux-switching motor

2.4.1 A DC motor

Figure 2.17 shows idealised waveforms for the flux created by the DC winding A-A and the induced flux in the winding B-B, for the ideal two-phase fully-pitched switched-reluctance motor given in figure 2.14. As the rotor rotates the flux in the DC winding, linking unexcited winding B-B, is bipolar. It changes from a maximum to a minimum value every 90° (mechanical), ideally varying linearly with position giving a triangularly shaped flux waveform. The coupling between the two windings is assumed to be ideal in this case, and the flux in the DC winding A-A is assumed to be constant because the reluctance of the magnetic path is constant with rotor position.

Considering the flux-waveforms in figure 2.17, the characteristics they exhibit are similar to those of a conventional four-pole stator DC motor. The flux created by the field winding in a DC machine is constant, and the flux induced in a single armature winding is bipolar. In Chapter 3 the mathematical equations are developed from first principles effectively using DC-motor theory. The two fully-pitched windings are now referred to as the field and armature windings.

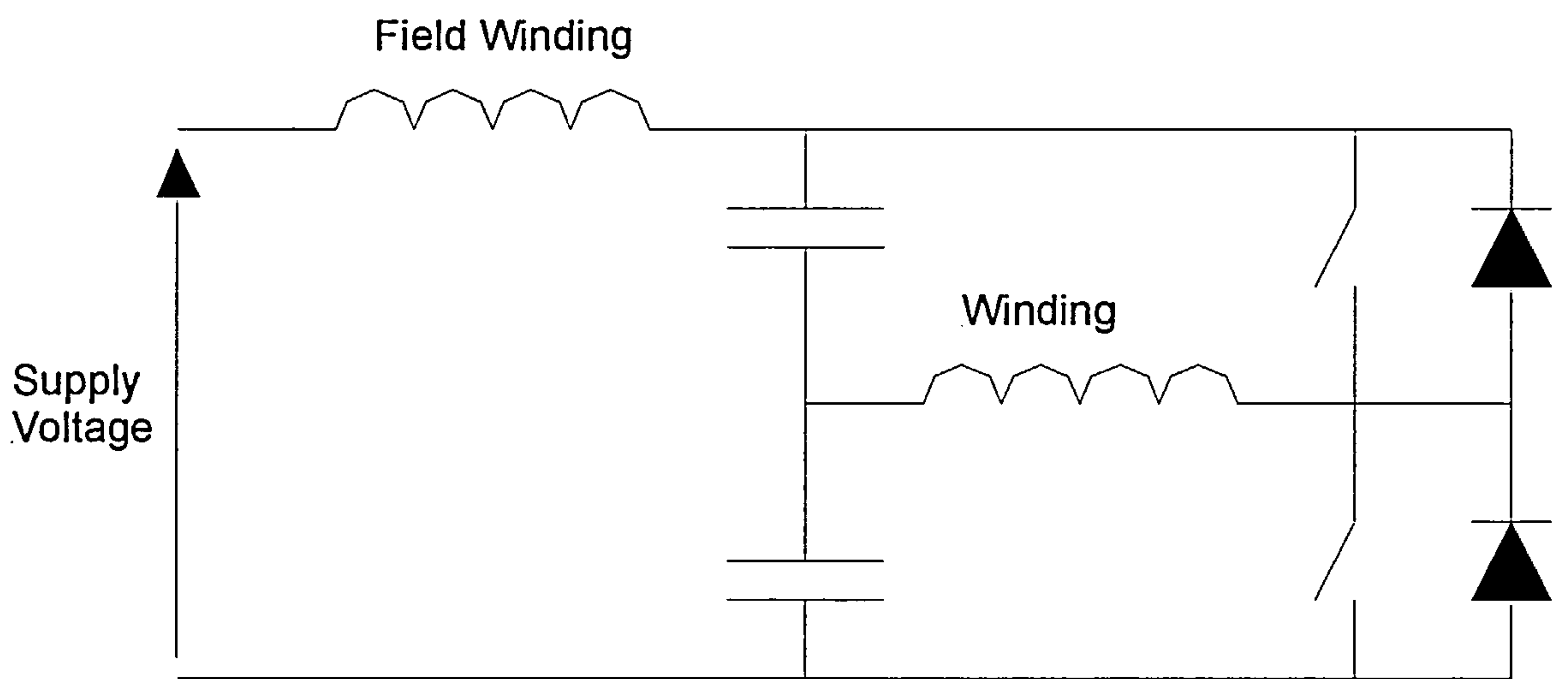


Figure 2.16 Series-field split-capacitor supply

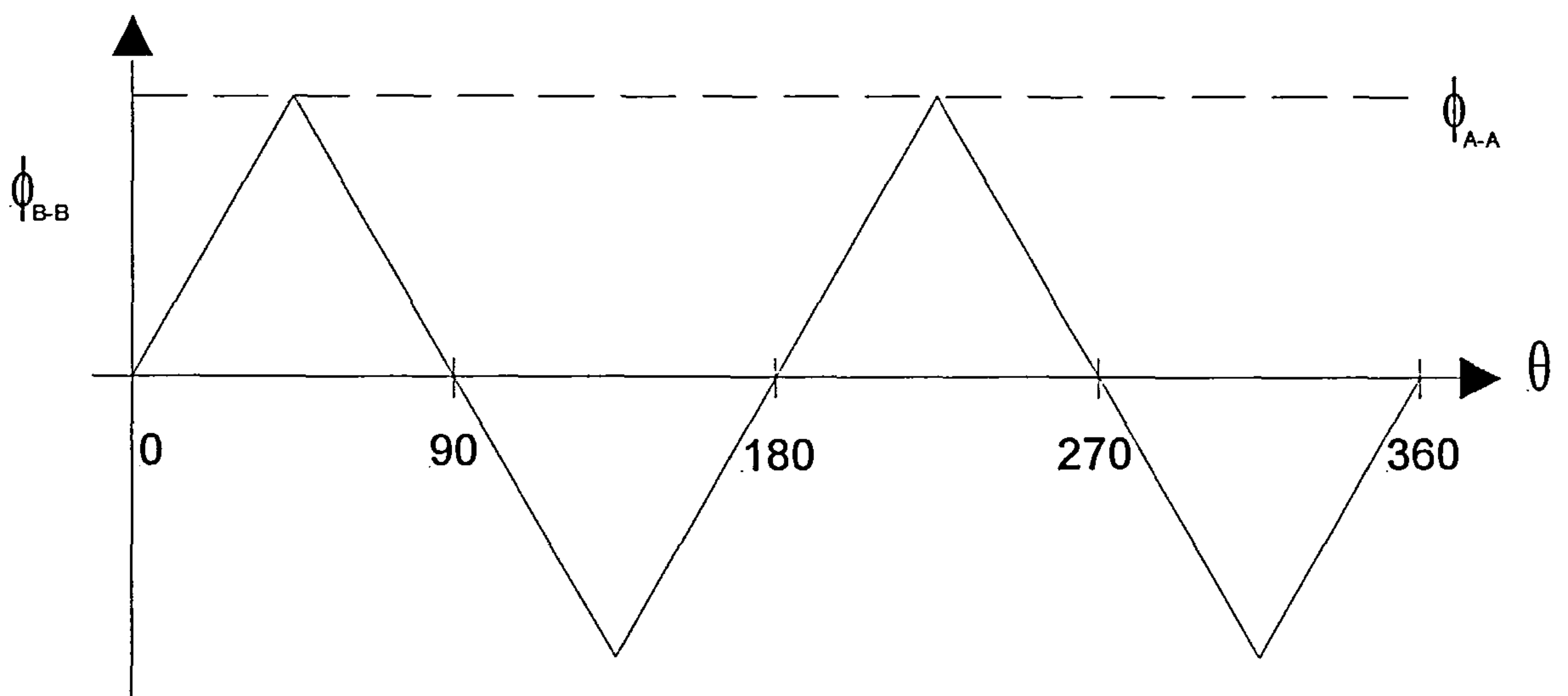


Figure 2.17 Ideal flux waveforms for a two-phase fully-pitched switched-reluctance motor

The new motor was given the name flux-switching motor [47] because the resultant flux switches direction within the machine. It could also have been called a wound-field brushless DC motor, although it was thought that this would have been confusing.

2.4.2 Similarities to other machines

The flux-switching motor shares similarities in its operation and the use of fully-pitched windings to a number of other machines [48] – [55]. The inductor-alternator was first patented in 1901 by Guy [48] and has been reported more recently in [49] – [52]. This was a machine that essentially consisted of a salient stator and rotor with numerous teeth on both, with the stator divided into poles by gaps in the stator surface. Fully-pitched windings were placed in the gaps in the stator. One of the fully-pitched windings, termed an “inductor winding”, was constantly excited with direct current such that when the rotor was turned by a prime mover an alternating, approximately sinusoidal voltage was induced across the terminals of one, or more, of the fully-pitched “induced windings”. The frequency of the voltage generated was proportional to the number of teeth present. If the flux-switching motor is used as a generator exactly the same principles apply.

Another more-recent machine, to operate in a similar manner to the flux-switching motor, is the flux-reversal machine [51]. The flux-reversal machine is a brushless doubly-salient permanent-magnet machine that has two magnets of opposite polarity mounted on the face of the stator poles. Wrapped around the

stator poles are concentrated windings. The permanent magnets produce the field flux, which is directed along different paths within the machine depending upon the relative position of the rotor. The changing flux in the stator and rotor, as a result of the rotor being turned, induces a bipolar flux in the windings. Again the same applies to the flux-switching motor except that the field flux is derived from permanent magnets as opposed to excited windings.

2.5 Conclusions

This Chapter has described the evolution of the new flux-switching motor and has provided background and historical information on the design, operation and torque production of switched-reluctance motors. Other electrical machines with fully-pitched windings have been presented and their relative merits have been discussed. The characteristics that the flux-switching motor exhibits were identified and comparisons were drawn with the operation of the conventional DC motor. Chapter 3 deals with the development of a mathematical model and produces further similarities to the DC machine.

CHAPTER 3 MATHEMATICAL MODEL AND SIMULATION

3.1 Introduction

Chapter 2 described the evolution of the new flux-switching motor and concluded that it behaved as a DC motor as demonstrated by the idealised flux-waveforms presented in figure 2.17. This Chapter takes the study forward with the development of a mathematical model. The mathematical equations derived are used in a time-stepping simulation, from which the winding-design for the motor was calculated.

3.2 Development of mathematical model

3.2.1 First principles model

The idealised flux-waveforms experienced in the field and armature windings of the new flux-switching motor at increasing rotor angles are given in figure 2.17. These showed that the characteristics exhibited by the motor are very similar to those experienced by the windings in a DC motor. Having established these similarities a mathematical model was developed from first principles.

The induced-EMF, or the back-EMF, which is the rate of change of armature flux in the armature windings, is shown in figure 3.1. The equation to describe the back-EMF for a motor with p stator poles and $p/2$ rotor poles can be established as

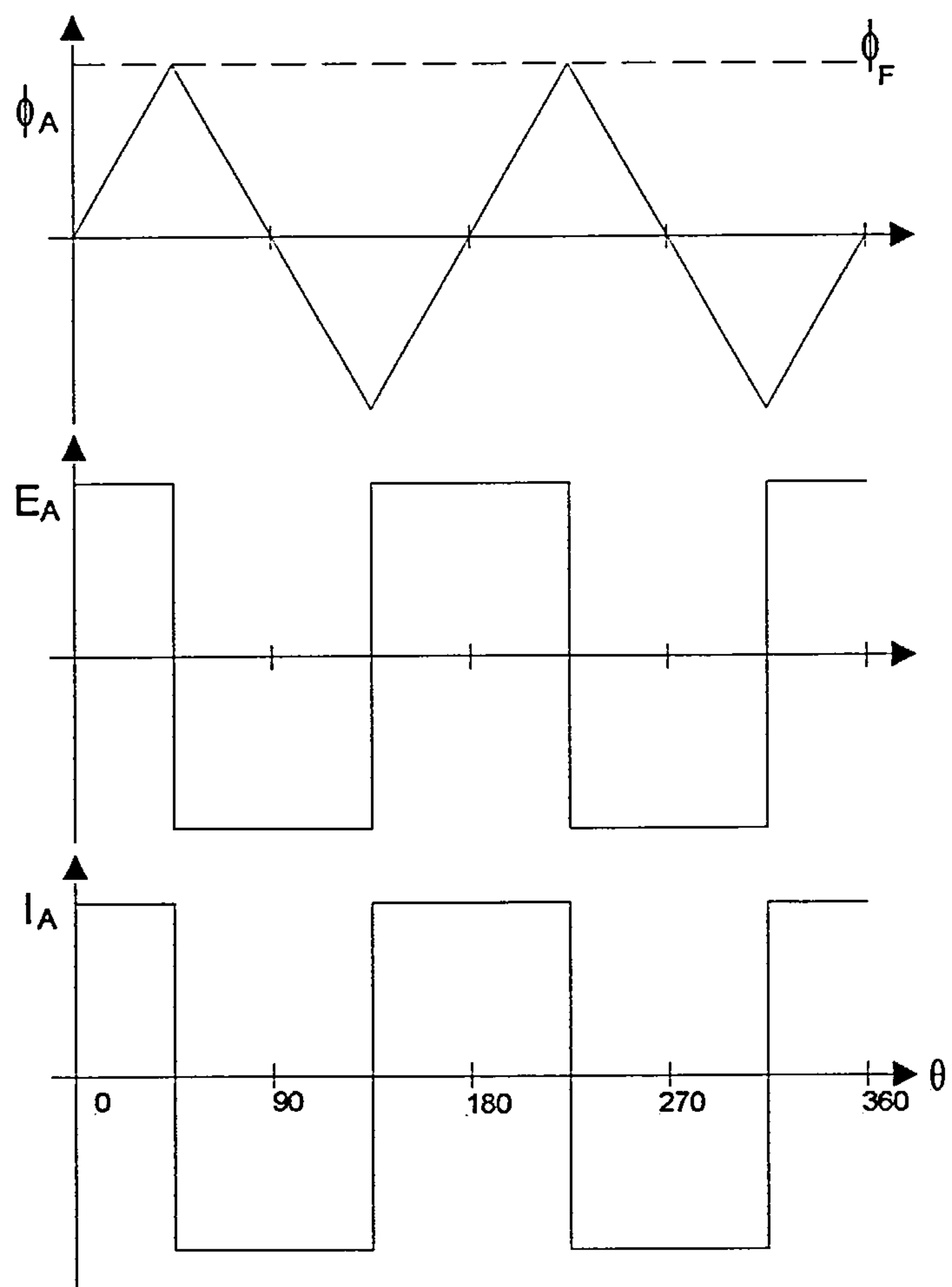


Figure 3.1 Back-EMF and armature-current waveforms

$$E_a = \frac{pK N_a}{\pi} \phi_f \omega \quad (3.1).$$

Where N_a is the number of armature turns, ω is the speed, ϕ_f is the field-flux and K is the fraction of field-flux linking the armature winding. Substituting for field-flux with,

$$\phi_f = \frac{N_f I_f}{\mathfrak{R}} \quad (3.2),$$

the back-EMF becomes

$$E_a = \frac{pK}{\pi \mathfrak{R}} N_a N_f I_f \omega \quad (3.3).$$

Where N_f is the number of field-turns, I_f is the field-current and \mathfrak{R} is the reluctance of the magnetic circuit. To produce the greatest output power the armature-current waveform is synchronised with the induced-EMF waveform as shown in figure 3.1, this is assumed to be a square-wave with a maximum value of $+I_a$ and a minimum value of $-I_a$. Equating the electromagnetic power with the mechanical-power developed, and rearranging, gives the general expression for torque T as,

$$T = \frac{E_a I_a}{\omega} \quad (3.4).$$

Substituting for the back-EMF E_a with equation (3.1), gives the torque as

$$T = \frac{pKN_a}{\pi} \phi_f I_a \quad (3.5).$$

Substituting for the field-flux ϕ_f with equation (3.2), gives the torque as

$$T = \frac{pK}{\pi \mathfrak{R}} N_f I_f N_a I_a \quad (3.6).$$

The general torque equation for a DC machine is

$$T = K_a \phi_f I_a \quad (3.7).$$

The constant K_a is given by

$$K_a = \frac{Zp}{2\pi\alpha} \quad (3.8),$$

where α is the number of parallel-paths in the electrical circuit, formed by the armature windings, and their connection with the brushes via the commutator. The number of stator poles is p , and the total number of conductors Z in the armature-winding is equal to twice the number of armature-turns N_a . If, in an ideal flux-switching motor, the fraction of the field-flux K can be assumed to be 100 %, and the number of parallel paths α is equal to 1, then equation (3.5) is equivalent to equation (3.7). This was a further demonstration that the flux-switching motor behaved like a conventional DC motor, at least in theory. The major assumption made in developing this first-principles model is that the field flux ϕ_f was constant owing to the reluctance of the magnetic path being

constant with rotor position. This is explained in Chapter 2 by the ideal flux-switching motor given in figure 2.13. With a constant reluctance, and therefore self-inductance, no torque could have been generated from field, or armature excitation alone. Constant reluctance also meant that the field-MMF, and therefore the field-current, used to drive the field-flux through the magnetic circuit was also constant. The other assumptions are that the magnetic leakage and the magnetic-fringing effects are constant with rotor position and are captured by K , the fraction of field-flux linking the armature-winding.

This first-principles model is rearranged, substituted into the voltage equation for a DC motor, and applied to generate a winding specification for the proof-of-principle motor based upon a number of input criteria. This is achieved as follows for a motor with four stator-poles. Using the voltage equation for a DC motor

$$V_a = E_a + I_a R_a \quad (3.9),$$

the back-EMF is substituted for, by equation (3.3), to give

$$V_a = \frac{pK}{\pi \mathfrak{R}} N_a N_f I_f \omega + I_a R_a \quad (3.10).$$

The resistance of the armature winding is then determined as a function of the available armature-slot area A_s , the turn length l_t , the number of armature turns N_a , the packing factor f_p and the resistivity of copper ρ_c as,

$$R_a = \frac{2\rho_c N_a^2 l_t}{A_s f_p} \quad (3.11).$$

Assuming that the field and armature MMFs are equal ($N_a I_a = N_f I_f$), substituting equation (3.11) into equation (3.10) gives,

$$V_a = N_a^2 I_a \left(\frac{pK}{\pi \mathfrak{R}} \omega + \frac{2\rho_c l_t}{A_s f_p} \right) \quad (3.12).$$

Using the same assumption, and rearranging equation (3.6) to produce $N_a I_a$ there results,

$$N_a I_a = \sqrt{\frac{T\pi \mathfrak{R}}{pK}} \quad (3.13).$$

Finally, substituting equation (3.13) into equation (3.12) gives the number of armature-turns N_a as

$$N_a = \frac{V_a}{\sqrt{\frac{T\pi \mathfrak{R}}{pK}} \left(\frac{pK}{\pi \mathfrak{R}} \omega + \frac{2\rho_c l_t}{A_s f_p} \right)} \quad (3.14).$$

With the number of armature turns known the wire diameter of the armature windings d_a can be calculated using

$$d_a = \sqrt{\frac{2A_s f_p}{N_a \pi}} \quad (3.15).$$

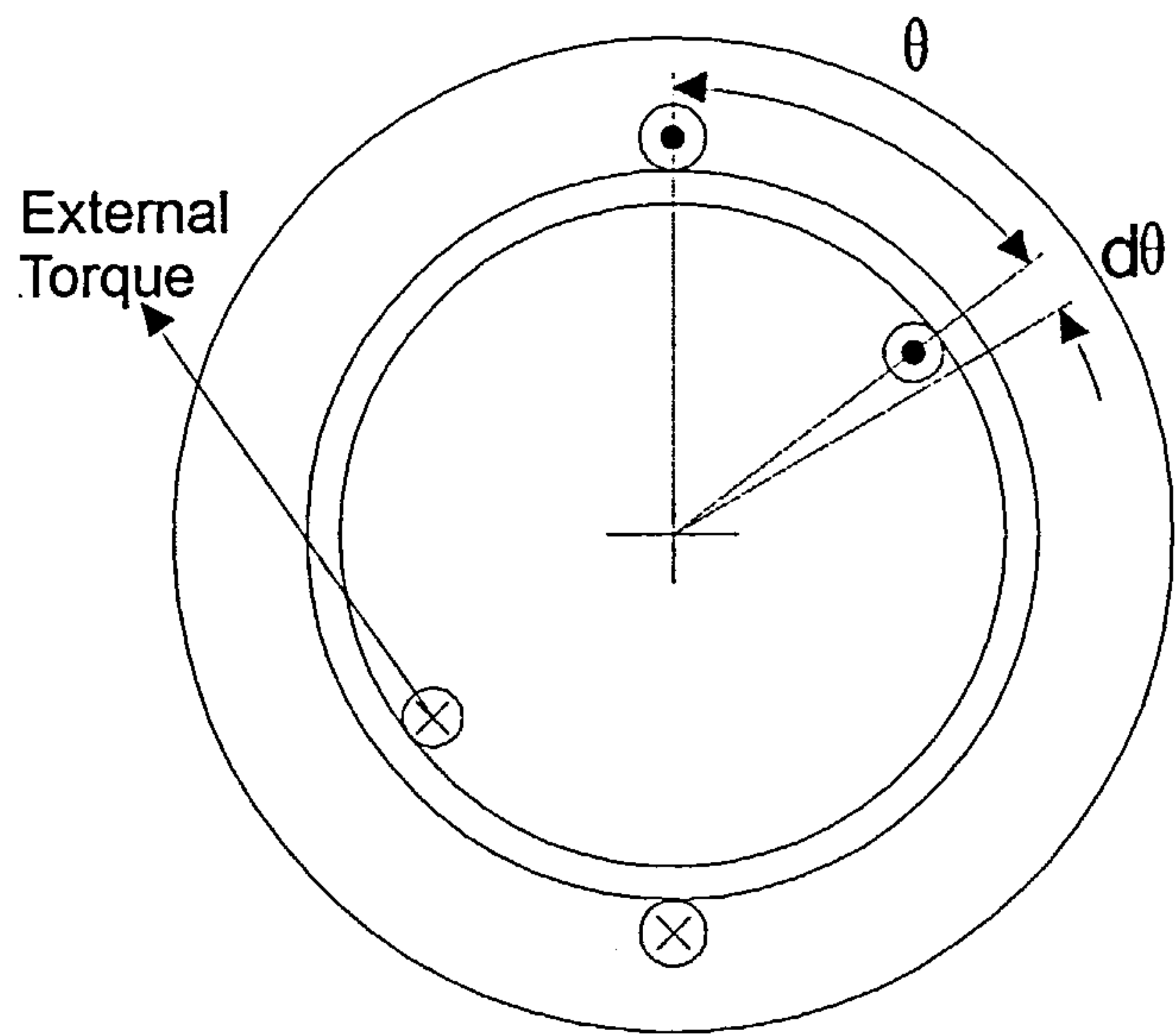
The number of field-turns and the diameter of the field-windings may be calculated in a similar manner to complete the winding specification for the proof-of-principle motor.

3.2.2 Coupling coefficient model

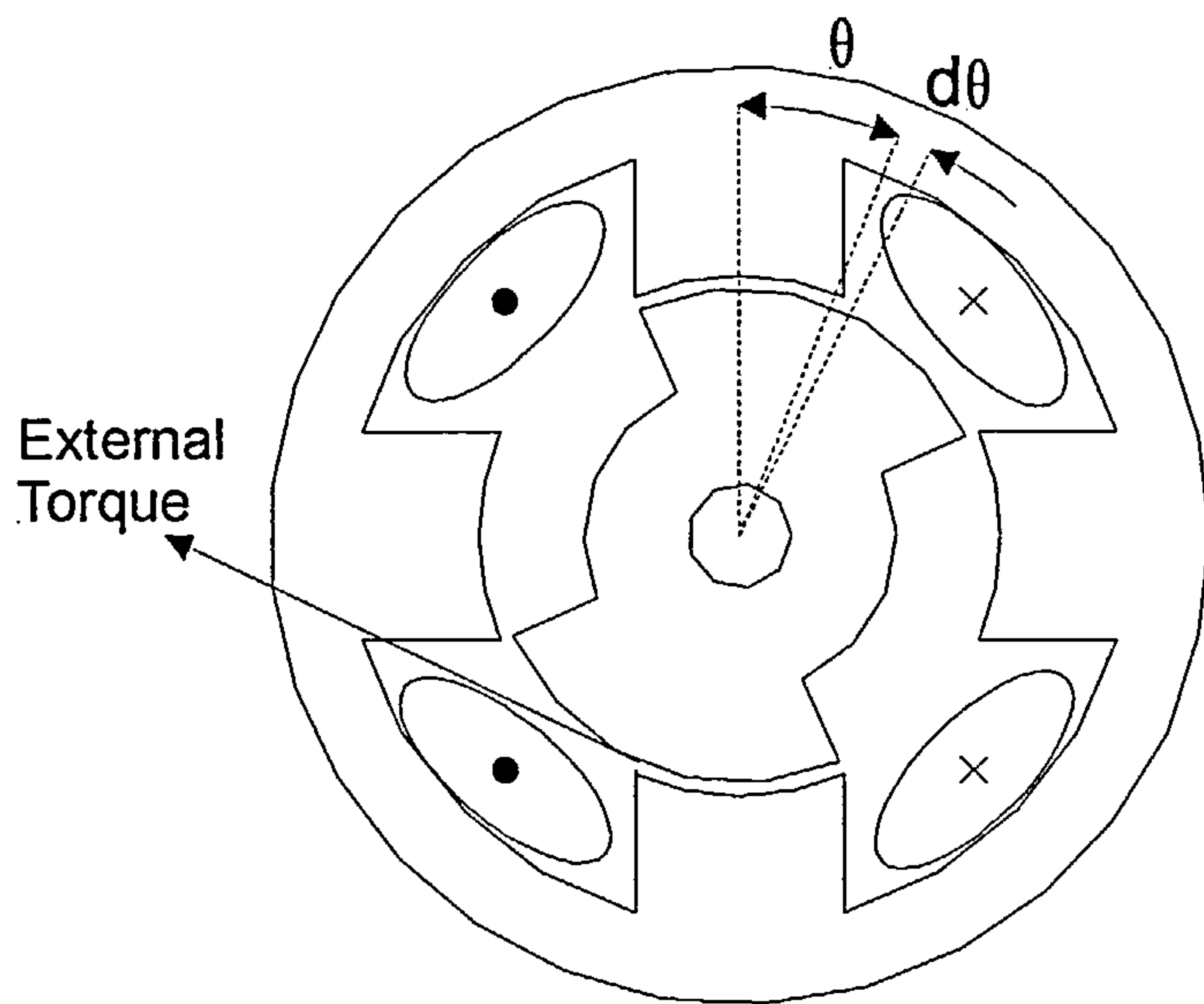
In addition to modelling the flux-switching motor directly using DC motor equations, it can also be modelled using the generalised theory of electrical machines [56] to verify the original method of calculation. In order to make a direct comparison between the generalised machine and the flux-switching motor the mathematical model is developed in parallel for both machines.

Figure 3.2 (a) shows a generalised machine having two windings with cylindrical stator and rotor cores separated by an airgap. The field-winding is mounted on the stator and the armature-winding is mounted on the rotor. The windings are displaced by an angle θ . Figure 3.2 (b) shows the idealised flux-switching motor with a field and armature-winding both mounted on the stator. The rotor is displaced from the stator by the same angle θ . It is important to note that per revolution the flux-switching motor goes through two electrical-cycles as opposed to the one by the generalised machine.

The flux-patterns created in both machines, as a result of both windings being excited as shown, are such that a torque is created in an anticlockwise direction. If an equal, external, clockwise torque is applied to the rotor, turning it through a small angle $d\theta$ as shown in figure 3.2, and assuming that there is negligible friction, the mechanical work done is,



(a)



(b)

Figure 3.2 (a) A generalised machine, (b) The idealised flux-switching motor

$$dW_m = T d\theta \quad (3.16).$$

The total energy-stored in the magnetic field is

$$W_f = \frac{1}{2} L_a i_a^2 + \frac{1}{2} L_f i_f^2 + M i_a i_f \quad (3.17).$$

The self-inductances of the field and the armature windings are independent of rotor position and they are, therefore, constant. If dM is the change of mutual inductance as a result of the change in position of the rotor $d\theta$ with respect to the stator, and the field and armature-currents remain constant, during the change in position, then the change in energy-stored in the magnetic field is

$$dW_f = i_a i_f dM \quad (3.18).$$

The energy-stored in the magnetic-field has decreased as a result of the reduction in mutual-inductance, which was, in turn, due to the increase of angle the rotor turned through. The flux-linkage between the windings decreases and an EMF is induced in each of them. If dt is the corresponding time taken for the rotor to turn through the angle $d\theta$ then the EMFs induced in the windings are given by,

$$E_a = -i_f \frac{dM}{dt} \quad (3.19),$$

$$E_f = -i_a \frac{dM}{dt} \quad (3.20).$$

According to Lenz's Law the EMF induced in the field-winding opposes the reduction of the flux-linkage caused by the increase of angle the rotor turned through. Thus, the direction of the induced-EMF is the same as that of the armature-current. Therefore, the voltage applied to the field-winding must be reduced by $i_a \frac{dM}{dt}$ to keep the current in the field winding at i_f for the time dt .

The respective energies supplied in each winding due to the induced-EMF are given by

$$dW_f = i_a \left(i_f \frac{dM}{dt} \right) dt \quad (3.21),$$

$$dW_a = i_f \left(i_a \frac{dM}{dt} \right) dt \quad (3.22).$$

The total electrical-energy supplied is,

$$dW_e = 2 i_f i_a dM \quad (3.23).$$

The electrical-energy supplied is equal to the decrease of energy stored in the magnetic-field, and the mechanical-work done in turning the rotor through the angle $d\theta$. That is

$$dW_e = dW_f + dW_m \quad (3.24).$$

Substituting in equations (3.16), (3.18) and (3.23) gives,

$$2 i_f i_a dM = i_f i_a dM + T d\theta \quad (3.25).$$

Rearranging this equation gives the torque developed for the generalised machine and the flux-switching motor as,

$$T = i_a i_f \frac{dM}{d\theta} \quad (3.26).$$

The mutual-inductance term in equation (3.26) can be expressed as a function of the field and armature winding self-inductances. The method by which this is achieved can be explained with the aid of the simple magnetic circuit shown in figure 3.3. This consists of two coils wound, as closely together as possible, on a non-ferromagnetic core so that all of the flux produced by the current in one coil is linked to all of the turns of the other coil. The self-inductances of the two coils are,

$$L_1 = \frac{N_1 \phi_1}{I_1} = \frac{N_1^2}{\mathfrak{R}} \quad (3.27),$$

$$L_2 = \frac{N_2 \phi_2}{I_2} = \frac{N_2^2}{\mathfrak{R}} \quad (3.28),$$

where, \mathfrak{R} is the reluctance of the magnetic circuit. If the whole of the flux ϕ_1 created due to current I_1 linked with coil 2, then,

$$M = \frac{N_2 \phi_1}{I_1} = \frac{N_1 N_2}{\mathfrak{R}} \quad (3.29).$$

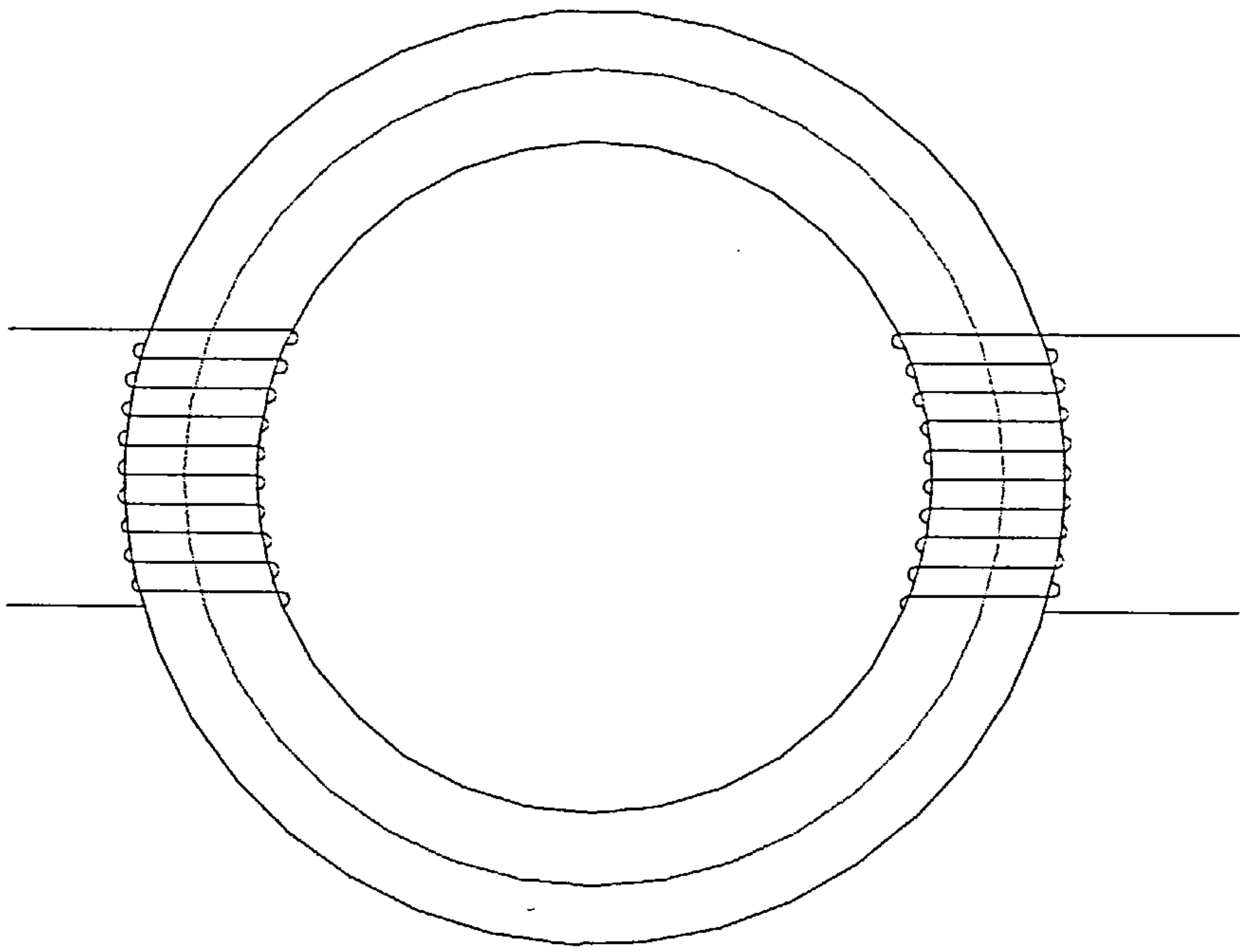


Figure 3.3 A simple magnetic circuit with two coils

Substituting into equation (3.29) with equation (3.27) and (3.28) for N_1 and N_2 respectively gives,

$$M = \sqrt{L_1 L_2} \quad (3.30).$$

Equation (3.30) only applies when the reluctance of the magnetic circuit is constant and the magnetic leakage is zero, that is perfect coupling. However, this expression is also approximately correct for a ferromagnetic circuit with one, or more, air-gaps. Where there is magnetic leakage, equation (3.30) is modified to become,

$$M = k\sqrt{L_1 L_2} \quad (3.31),$$

or,

$$M = k \frac{N_1 N_2}{\mathfrak{R}} \quad (3.32).$$

where, k is the coupling-coefficient between coils 1 and 2.

Applying equation (3.32) to the generalised machine and the flux-switching motor, where the two coils are the field and armature-windings, the only value changing with rotor position is the coupling coefficient as the reluctance of the magnetic circuit is constant. Substituting equation (3.32) into equation (3.26) allows the instantaneous torque at any electrical angle θ of the generalised machine and the flux-switching motor to be expressed as,

$$T = \frac{N_a i_a N_f i_f}{\mathfrak{R}} \frac{dk}{d\theta} \quad (3.33).$$

Using equation (3.4) allows the back-EMF to be expressed as,

$$e_a = \frac{N_a N_f i_f}{\mathfrak{R}} \frac{dk}{d\theta} \omega \quad (3.34).$$

For an idealised motor the coupling-coefficient is sinusoidal such that,

$$k = K \sin \theta \quad (3.35),$$

hence,

$$\frac{dk}{d\theta} = K_m \cos \theta \quad (3.36),$$

and the armature current is cosinal to produce the maximum torque then,

$$i_a = I_{am} \cos \theta \quad (3.37).$$

The rms value of the rate of change of coupling coefficient and armature current are given by,

$$K = \frac{K_m}{\sqrt{2}} \quad (3.38),$$

and,

$$I_a = \frac{I_{am}}{\sqrt{2}} \quad (3.39),$$

Substituting into equation (3.33) with equations (3.36) and (3.37) with an ideal constant field-current I_f and the flux distributed as $\frac{p}{\pi}$ gives

$$T = \frac{pK_m}{\pi\mathfrak{R}} N_f I_f N_a I_{am} \cos^2 \theta \quad (3.40),$$

or,

$$T = \frac{pK_m}{2\pi\mathfrak{R}} N_f I_f N_a I_{am} (1 + \cos 2\theta) \quad (3.41).$$

The average-torque developed is,

$$T = \frac{pK_m}{2\pi\mathfrak{R}} N_f I_f N_a I_{am} \quad (3.42).$$

On using equations (3.38) and (3.39), equation (3.42) becomes,

$$T = \frac{pK}{\pi\mathfrak{R}} N_f I_f N_a I_a \quad (3.43),$$

which is identical to equation (3.6).

The assumptions applied for the idealised motor are not generally applicable for a number of reasons. Under normal operating conditions magnetic-leakage, saturation effects and changing reluctance would all be present. Also, in addition, secondary effects would be experienced as a result of non-ideal

conditions. The most noticeable effect would be that the rate of change of coupling coefficient and the armature current would not be sinusoidally distributed.

3.3 Motor simulation

3.3.1 Simulation objectives and model

The primary objective of the simulation of the motor was to produce a winding specification for the flux-switching motor. In producing a specification based upon the output of the simulation, the aim was to observe some of the operational characteristics as well, in order to better understand how the motor worked. The secondary more long-term objective of the simulation was to develop it into a tool to enable rapid, prototyping from specification to winding-design, without the prolonged use of computationally-intensive finite-element analysis (FEA). The aim was to produce a generic, scalable lamination-design, using FEA, with a set of magnetic data that would remain constant. Then, using the simulation to process the magnetic data and the other electrical-information inputted, a winding design could be produced according to the desired specification. Others have modelled mutually coupled switched-reluctance motors [57], [58], although the process at arriving at a solution was far more complex than that described here. Further work is required to achieve an optimum lamination design for this type of motor.

In order to produce a lamination-design the instantaneous-torque equation of the motor needs to be considered. Referring to equation (3.33), to maximise the torque-produced the reluctance needs to be kept to a minimum whilst the rate of change of coupling-coefficient with position needs to be a maximum.

The minimal amount of FEA data taken, and used, in the simulation to represent the magnetic-effects present in the motor were, an average value of reluctance and a vector of values for the rate-of-change of coupling coefficient, with respect to electrical angle, at 5 ° intervals, over one complete cycle.

3.3.2 Implementation using MATLAB SIMULINK

The mathematical equations used to model the motor were combined with the FEA data in a MATLAB SIMULINK model as follows. The complete voltage equations for the armature and field windings are given by

$$v_a = e_a + i_a R_a + L \frac{di_a}{dt} + M \frac{di_f}{dt} \quad (3.44)$$

and

$$v_f = i_f R_f + L \frac{di_f}{dt} + M \frac{di_a}{dt} \quad (3.45).$$

The field-current was assumed to remain constant such that equation (3.44) became,

$$v_a = e_a + i_a R_a + L \frac{di_a}{dt} \quad (3.46).$$

Also since the mutual-inductance term was smaller in comparison to the other components of the equation the field-voltage equation was reduced to,

$$V_f = I_f R_f \quad (3.47).$$

The objective now was to solve these two voltage equations for armature and field-currents, respectively. The armature current could be found by integrating equation (3.46) to give,

$$i_{a_1} = \int \frac{v_a - e_a - i_{a_0} R_a}{L} dt_{1-0} \quad (3.48)$$

where i_{a_0} is the previous armature-current value and, i_{a_1} is the present armature-current value, separated by the time dt_{1-0} .

Equation (3.48) was solved within SIMULINK by using a simple time-stepping model. Figure 3.4 shows the top-level model with all of the fixed values entered in on the left-hand side, the model heart-block in the centre, which processed the fixed values and the equations, and the output of the equations on the right-hand side. The model heart-block contained a speed-block, a back-EMF-block, a voltage-block and a winding-block as shown in figure 3.5. The purpose of the speed-block, given in figure 3.6, was to create a motor-speed profile. This consisted of two parts, an initial linear acceleration followed by a constant maximum speed that switched-over automatically once the model had accelerated to the maximum speed. Figure 3.7 shows the back-EMF-block, that was used to generate a synchronised, periodic, back-EMF waveform

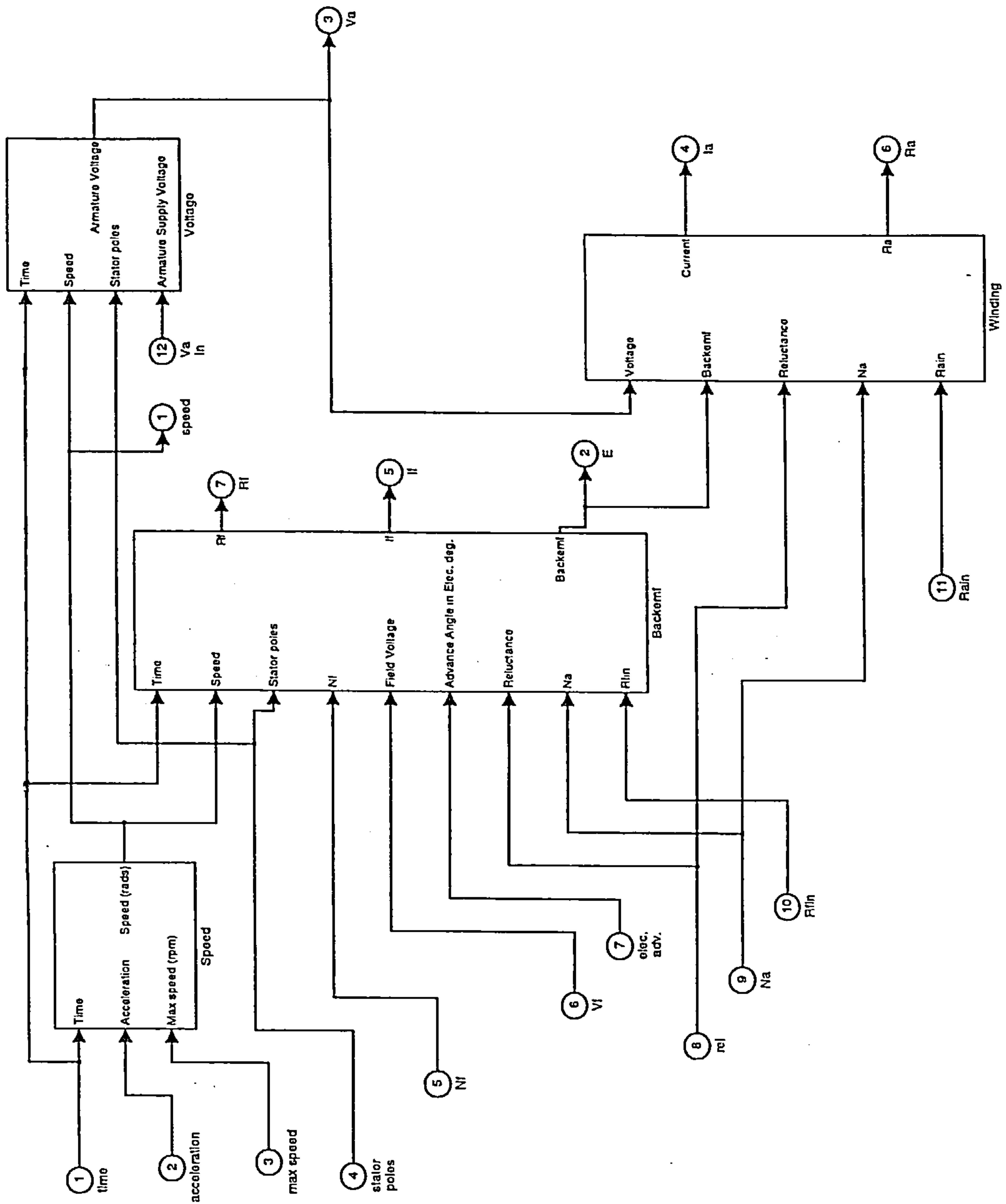


Figure 3.5 The model heart of the MATLAB SIMULINK model

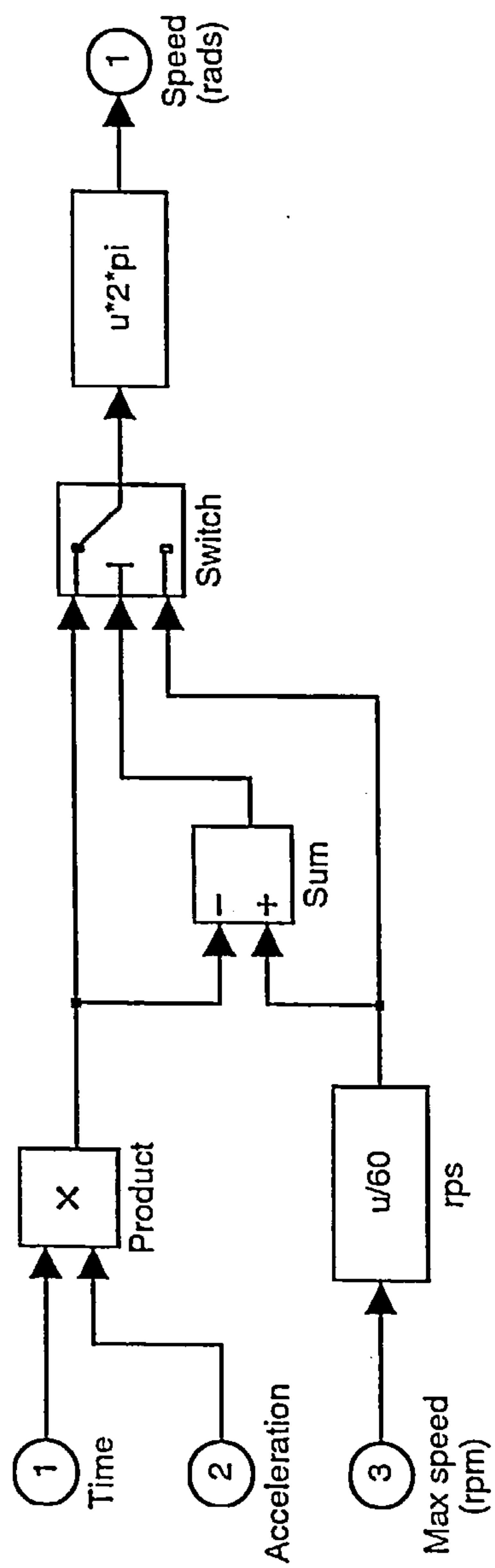


Figure 3.6 The speed-block in the MATLAB SIMULINK model

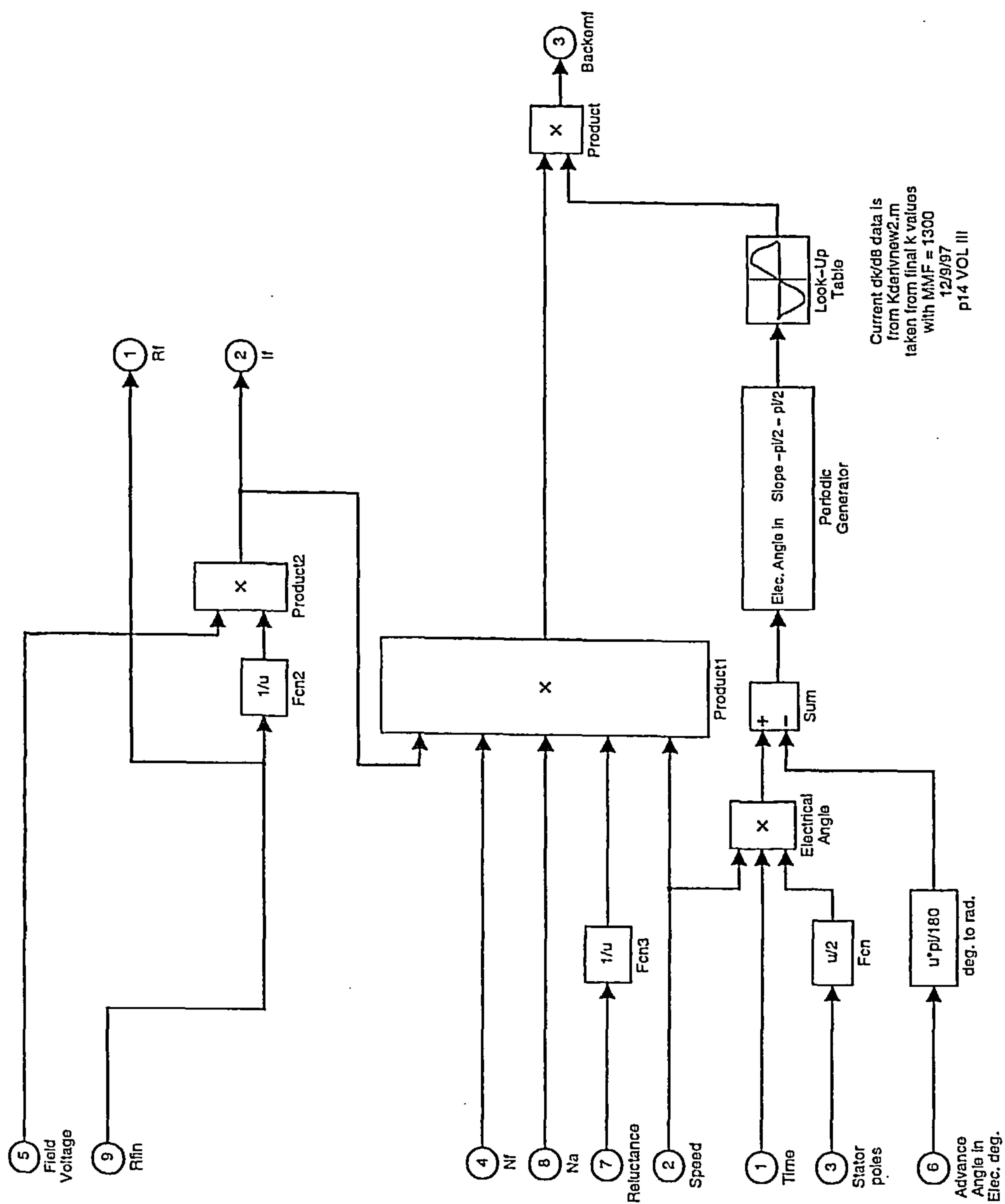


Figure 3.7 The back-EMF block-in the MATLAB SIMULINK model

based upon the vector of rate of change of coupling-coefficient values stored in a look-up table. The back-EMF waveform was calculated by using equation (3.34). Field-current was also calculated in the back-EMF-block using equation (3.47). An armature-voltage waveform was created as a square-wave using the voltage-block shown in figure 3.8. The armature-current equation (3.48) was solved in the winding-block shown in figure 3.9.

Having generated a set of waveforms for back-EMF and armature-current in conjunction with a speed-profile, instantaneous-torque was calculated using equation (3.4). Instantaneous values for torque, back-EMF, armature-voltage, armature-current, power-in, power-out and efficiency were outputted to a MATLAB data file for further processing. The output-power was factored by 90 % to take into account an estimate for the iron losses.

3.3.3 Results and chosen winding design

A simple MATLAB program was written to process the data outputted from the simulation to calculate a set of average values and present it in a graphical format. The simulation was used to produce a winding-specification for the flux-switching motor, which is discussed in detail in Chapter 5. An iterative approach was used in arriving at the chosen winding-design specification by changing the inputs to the model such that the specified-torque was produced. Figure 3.10 shows the instantaneous and average-torque waveforms at a rotor-speed of 9000 rpm. The instantaneous torque-fluctuates over a 7 Nm torque range and, in some places, is negative. This was due to the combined effects

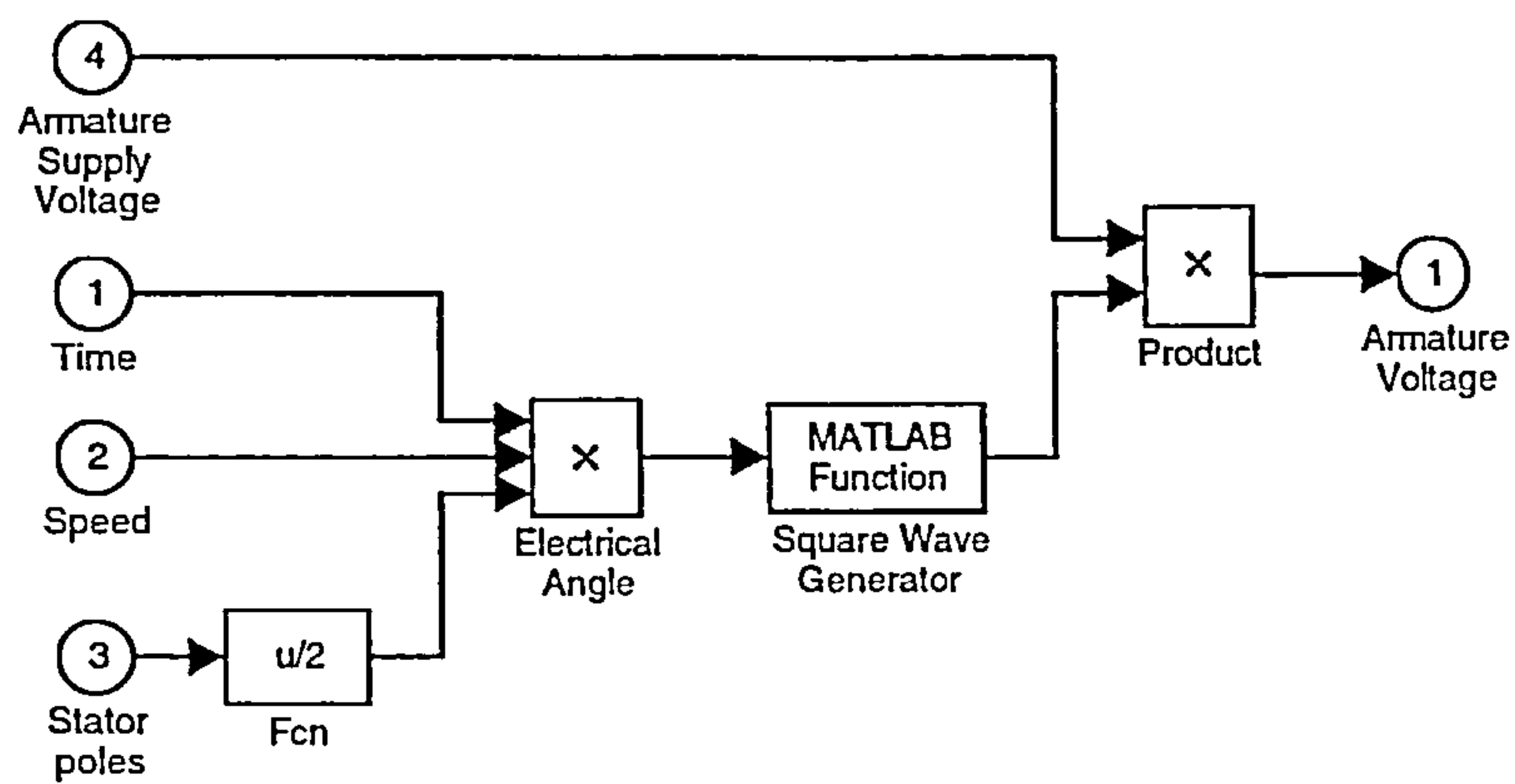


Figure 3.8 The voltage-block in the MATLAB SIMULINK model

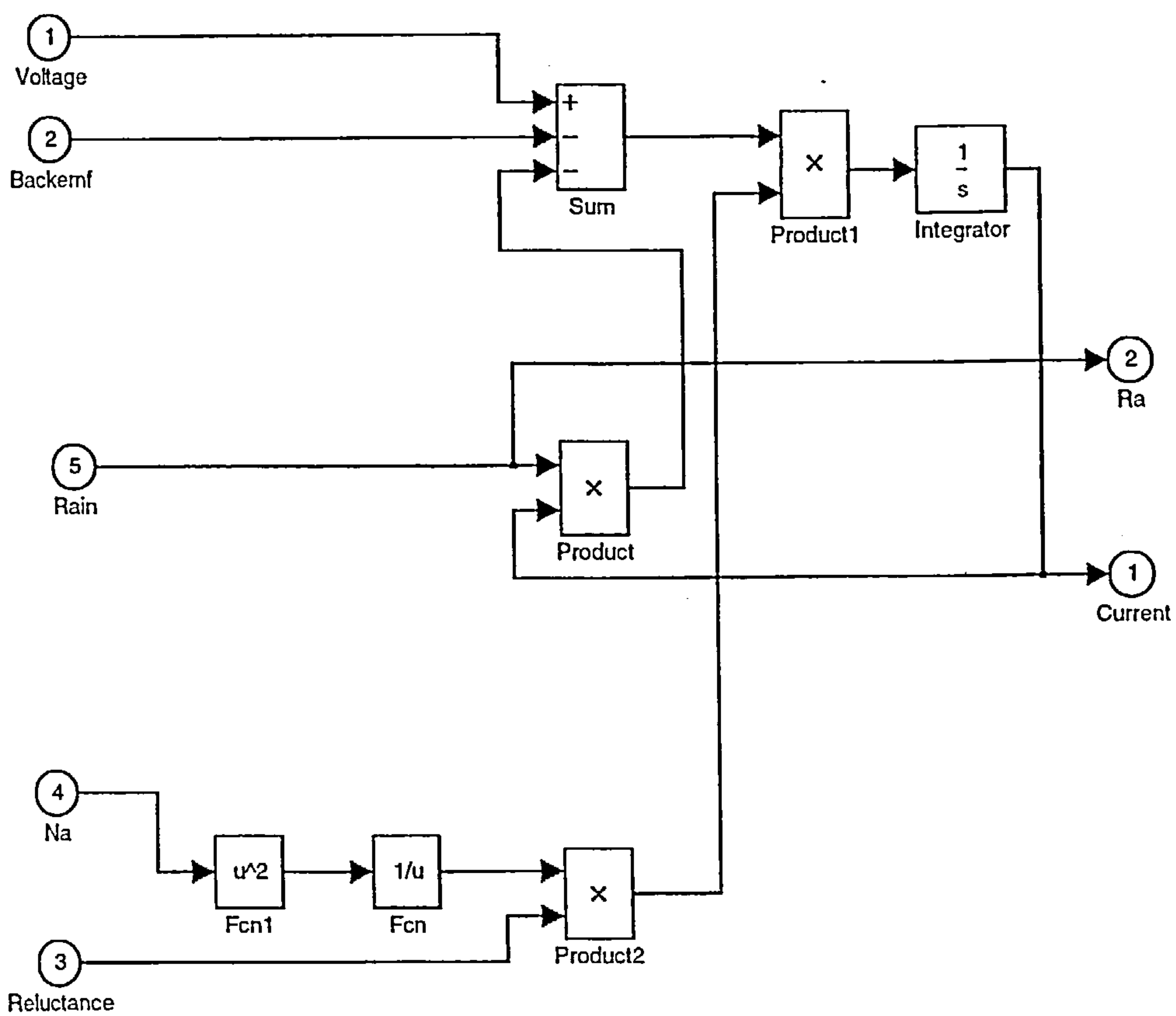


Figure 3.9 The winding-block in the MATLAB SIMULINK model

of a slight drift in the simulation and, also, the chosen advance-angle, which was optimised to produce the greatest positive-torque from the current available and the back-EMF generated. The average-torque produced by the simulation was 2.2 Nm. The instantaneous and RMS armature current is shown in figure 3.11, the offset in the instantaneous current is again due to the slight drift in the simulation. The drift in the simulation was not a major cause of concern as both a small-positive and small-negative swing was experienced. This averaged in time, thus cancelling each other. Figure 3.12 shows the armature voltage and back-EMF waveforms generated. The ideal-voltage waveform can be seen to be advanced by 90° (electrical) in front of the back-EMF waveform, this was found to be the optimum theoretical advance angle. A simulated torque-speed curve is shown in figure 3.13, changing the input speed to the simulation allowed the curve to be generated.

3.3.4 Further work required to simulation

The simulation was by no means comprehensive in its representation of a real flux-switching motor due to the assumptions made in the mathematical model. Further work is required on the simulation to make it more accurate, and true-to-life. The simulation was a mathematical model of an ideal linear flux-switching motor based upon a vector of magnetic data taken from FEA. Thus the effects of saturation and magnetic-leakage were not modelled. This part of the simulation could be improved by incorporating a three-dimensional look-up table of rate-of-change of coupling-coefficient values taken from FEA when the

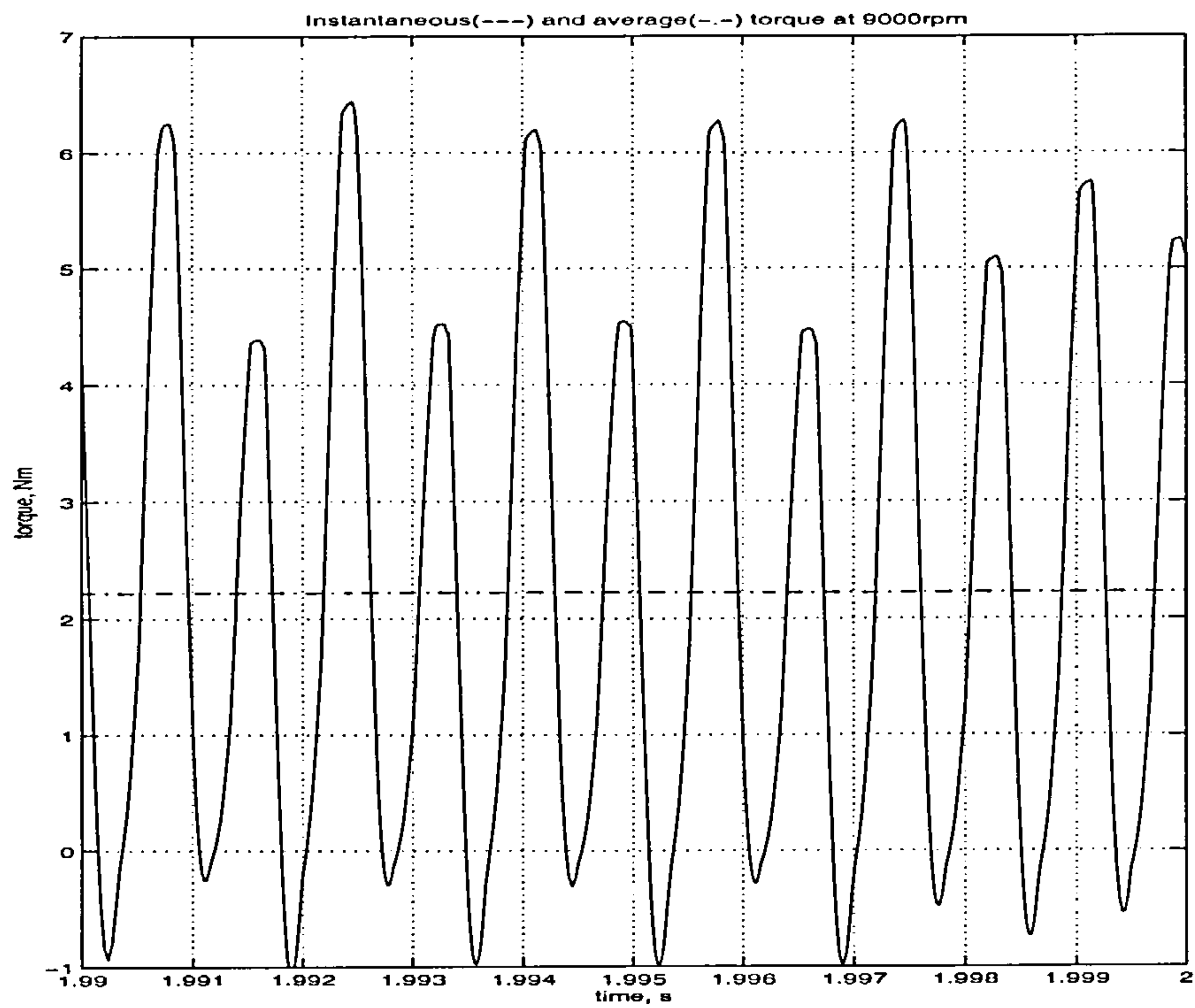


Figure 3.10 Instantaneous and average torque waveforms at a speed of 9000 rpm

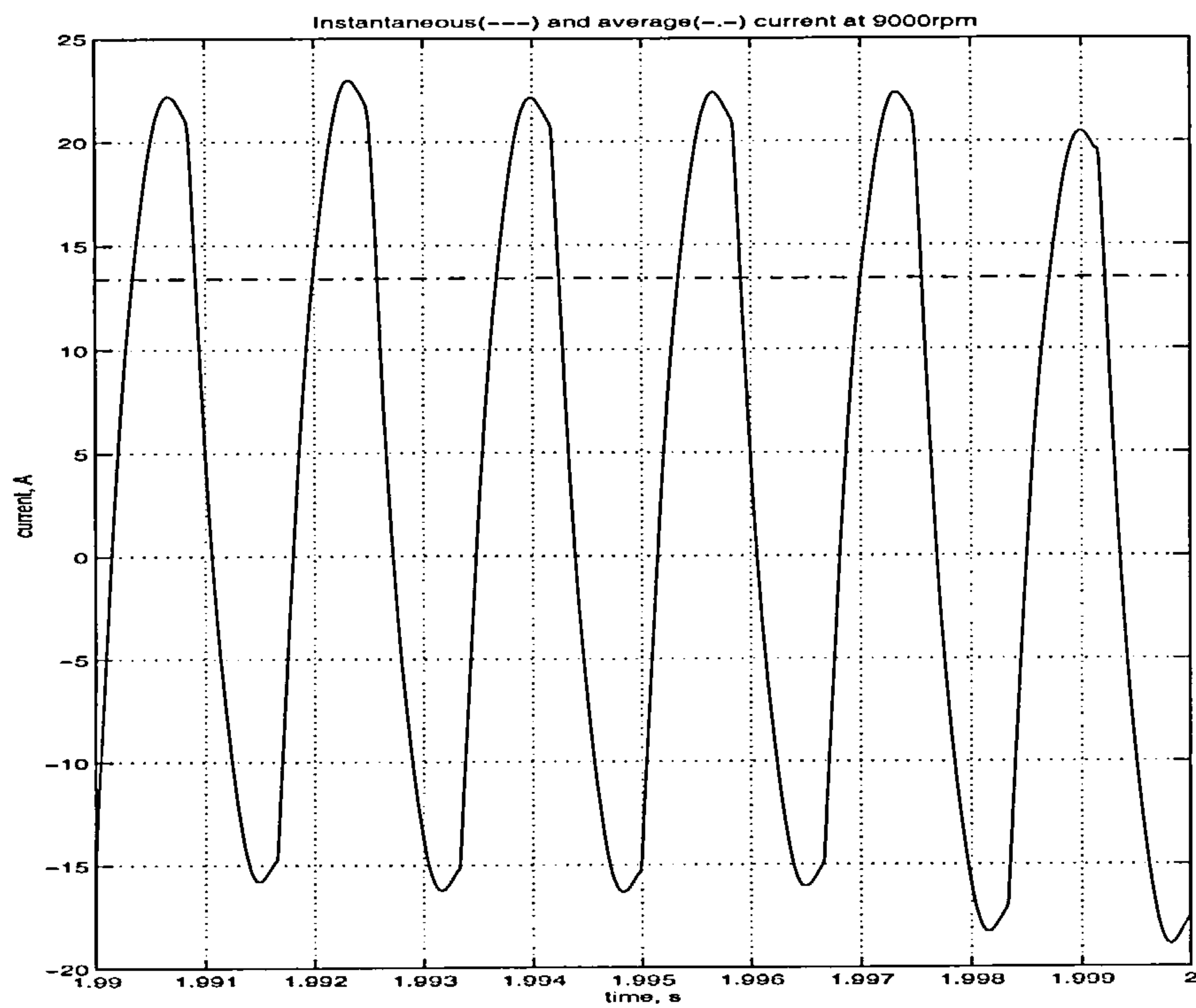


Figure 3.11 The instantaneous and RMS armature current

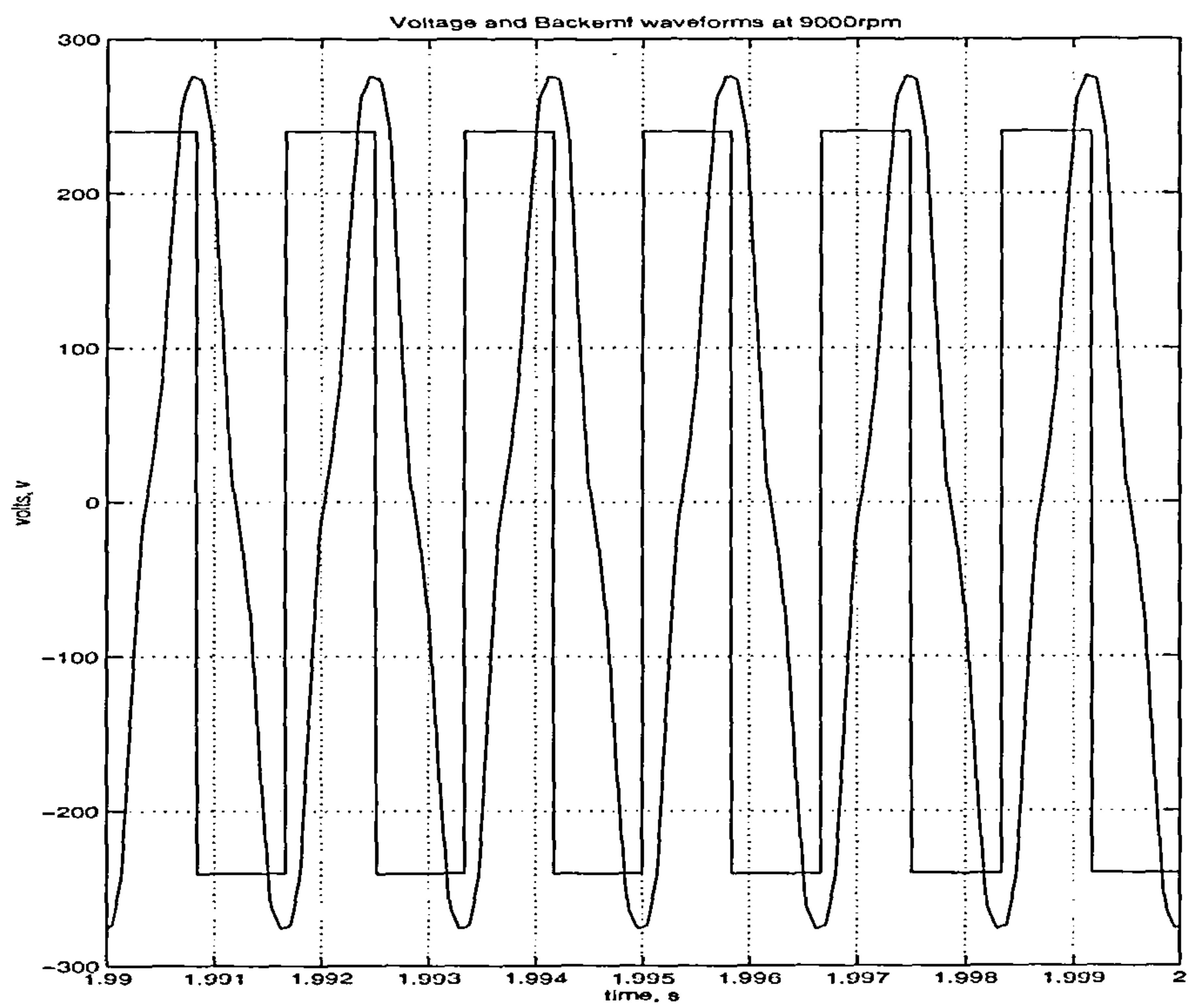


Figure 3.12 The square-wave armature voltage and back-EMF waveforms generated

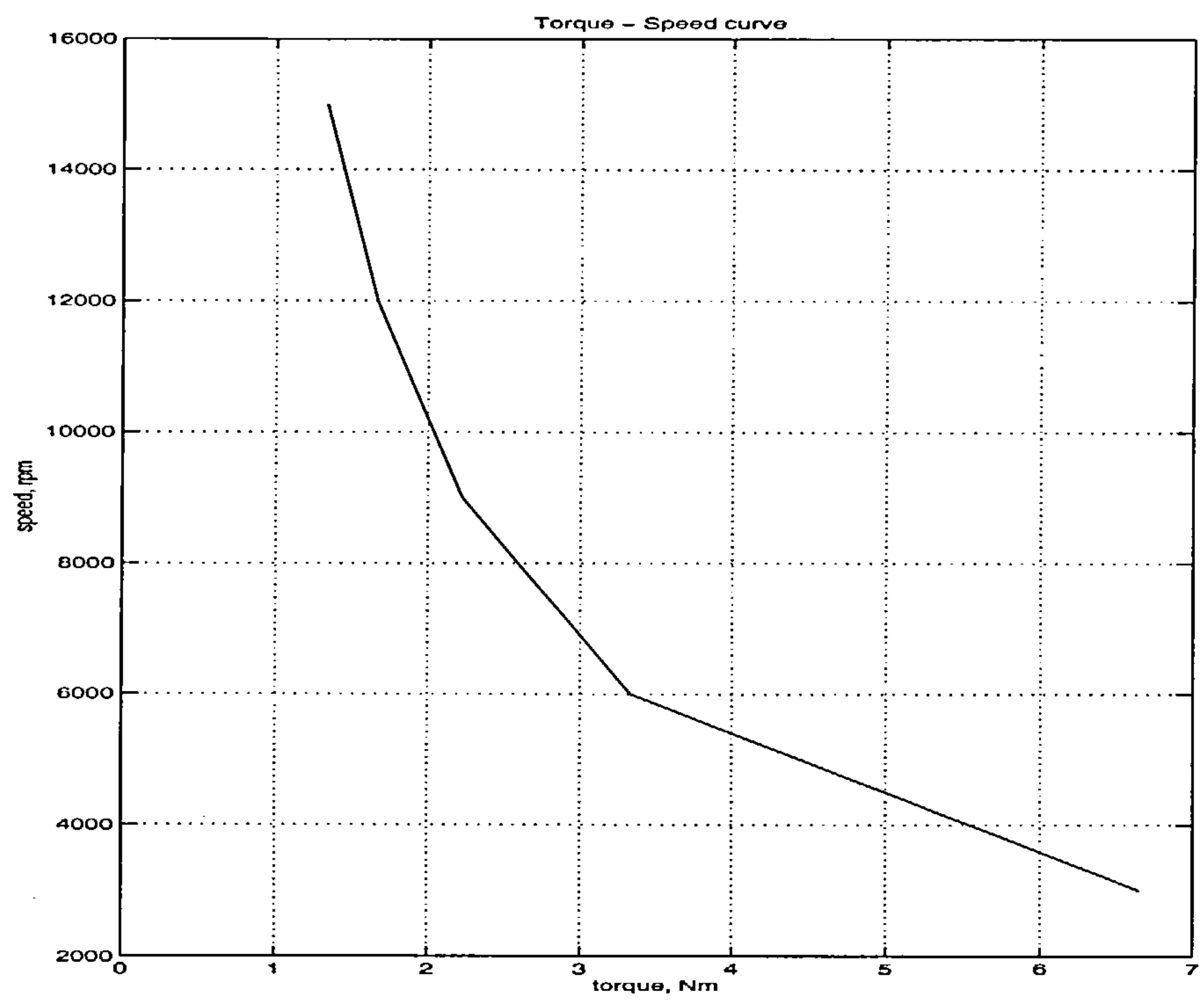


Figure 3.13 A simulated torque-speed curve

motor is operating at different flux-levels. This data could also be used to produce a more-meaningful figure for the iron-losses in the motor.

The major assumption made in the mathematical model, and hence the simulation, was that the field-flux, and therefore field-current, was constant due to constant field-reluctance. This represents an ideal model, but, owing to the non-linear magnetic characteristics of a doubly-salient motor operating with high-frequency pulsed magnetic-fields this was going to achieve an approximation at best. Also the braking requirements of the motor lead to a lamination design without a constant field-reluctance as discussed in Chapter 5. The result of a changing field-current is that the mutual-inductance term in equations (3.44) and (3.45) has a value that should be considered in the simulation.

With the incorporation of these additional terms, in the mathematical equation, and the use of a larger range of non-linear magnetic data the simulation could be improved. The ultimate aim is for the simulation to be good enough to be used as a tool to design flux-switching motors.

3.4 Conclusions

This Chapter has presented the development of the mathematical equations used to model the flux-switching motor, from the initial first-principles model to the improved coupling-coefficient model. Having derived the equations they were incorporated into a MATLAB SIMULINK time-stepping model, that was

used to produce a winding-specification for the flux-switching motor. The simulation gave a fair indication of the real motor characteristics. However, it became apparent, whilst testing, that the simulation should be developed to include the mutual effects that were present. Having identified the shortcomings of the simulation model, it must be remembered that it was, in fact, used to produce a winding-design procedure that proved to be successful when testing the prototype motors.

CHAPTER 4 PROOF- OF- PRINCIPLE FLUX-SWITCHING MOTOR

4.1 Introduction

The proof-of-principle machine was used purely to demonstrate that the concept for this type of motor worked. Existing laminations from a switched-reluctance motor incorporating fully-pitched windings, were used for the design, which was itself derived from the mathematical equations appearing in Chapter 3. The motor was tested with the intention of the results validating the mathematical equations, and thereby demonstrating that it was sensible to continue with the design and manufacture of purpose-built prototype motors. These would be used for further more detailed evaluation.

4.2 Motor and drive design

This section details the design of the motor, in terms of the laminations and windings, and, also, the drive with respect to the power-converter and gate-drive arrangements. The construction of the complete drive-system is described in conjunction with the operation of the drive.

4.2.1 Lamination and winding design

The design of an entirely new lamination profile for the flux-switching motor could not be justified, at this stage, for the purpose of investigating whether, or not, the motor would work. Therefore an existing 4-pole stator lamination, originally wound as a conventional short pitched $4/2$ switched-reluctance motor, was rewound with fully-pitched windings as shown in figure 4.1. Using a non-

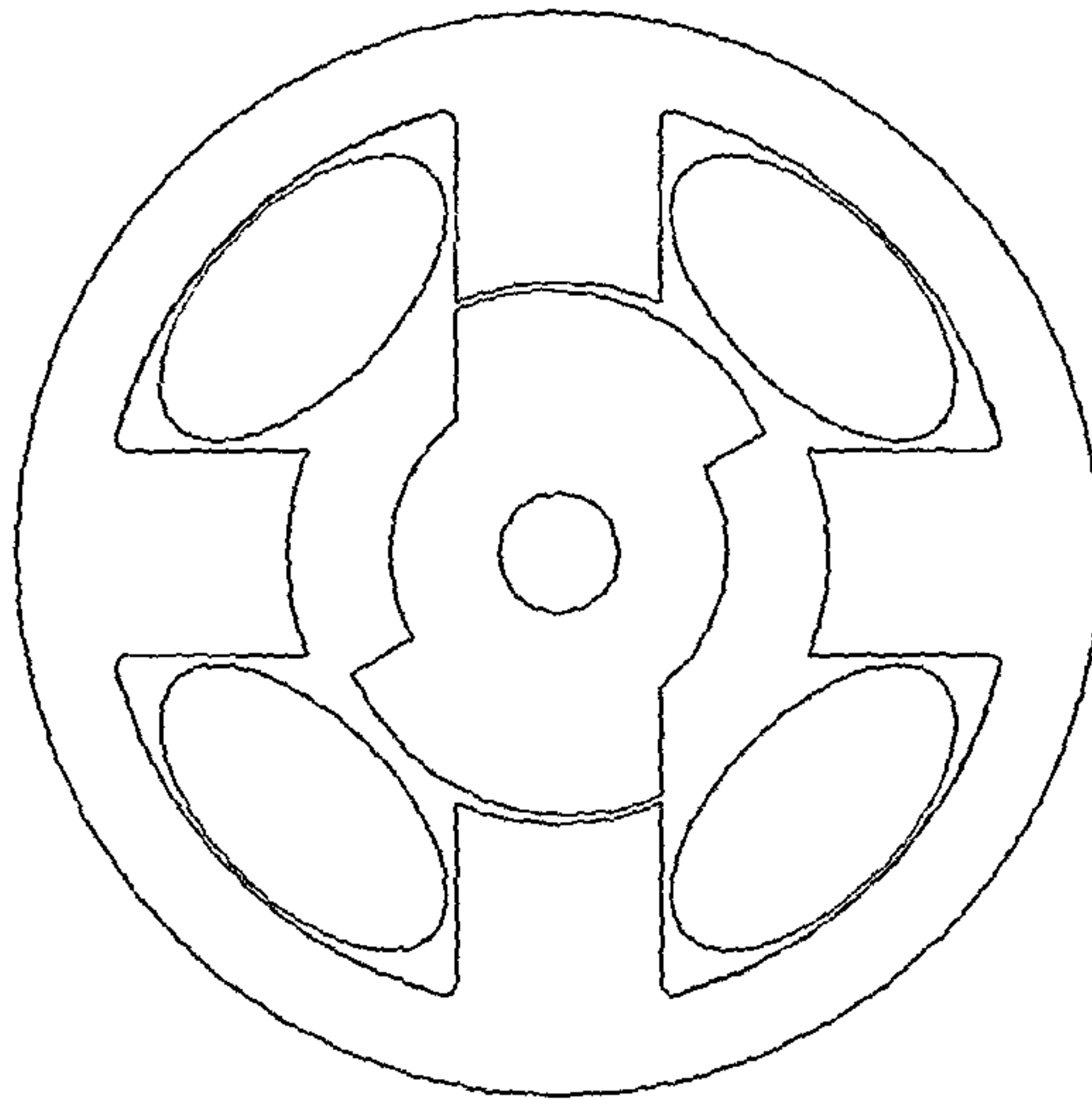


Figure 4.1 The 4/2 switched-reluctance motor rewound with fully-pitched windings

optimised lamination design was expected to degrade the operating characteristics of the motor. In particular, it was evident from the design that, in addition to the required change in mutual-inductance, there was also a change in the self-inductance of the windings. This was owing to the angle-of-overlap between the rotor and two adjacent stator poles not being constant with changing rotor position. This was largely due to the extent of the graded airgap used for starting the motor. Despite the lamination design not being ideal for the operation as a flux-switching motor, because of the change in mutual-inductance it was expected that the motor would still be able to demonstrate the principle of operation.

The winding specification was calculated using the magnetic data obtained from the switched-reluctance motor in conjunction with the first mathematical model presented in Chapter 3. On inputting the criteria requested, the output was given as the number of turns, and the diameter of wire needed, for both the field and armature-windings.

4.2.2 New power-converter designs

The original aim of the drive-system, as given in Chapter 1, was “to design and develop an alternative low-cost variable-speed drive-system that exploited the use of two fully-pitched windings in a doubly-salient structure. It had to be capable of satisfying the given industrial specification, with the cheapest solution possible”. In conjunction with the very-cheap motor design, emphasis was placed on designing a correspondingly cheap drive, as this, is more often

than not, the most expensive part of the drive-system. As cost is related directly to the complexity of the drive, reducing the component-count to a minimum was the prime objective in achieving a cheap drive. However, reducing the component-count should not result in unacceptable drive-system performance. A compromise was therefore necessary to achieve the optimum solution.

In Chapter 2 it was established that the operation of the new flux-switching motor was very different to a switched-reluctance motor. This dictated the use of a novel power-converter not normally associated with brushless doubly-salient motors. The continuously-excited DC field-winding required no form of electronic control, whereas the armature-winding had to be supplied with bipolar-current to generate the bipolar-flux distribution needed in the armature slots of the stator. Previous designs of a suitable power-converter had been based on this presumption that the armature-winding had to be supplied with a bipolar-current, derived from an inverter, with a high component-count, to achieve the necessary bipolar-flux distribution. However, a bipolar-flux distribution can also be derived from a bifilar-winding. Each half of the bifilar-winding is excited from opposite ends, alternately, with unipolar-current, to give unipolar-flux. The opposite winding polarity means that the two alternate unipolar-fluxes created are in opposing directions, so that when combined a resultant bipolar-flux distribution is produced. This can be clearly seen in figure 4.2.

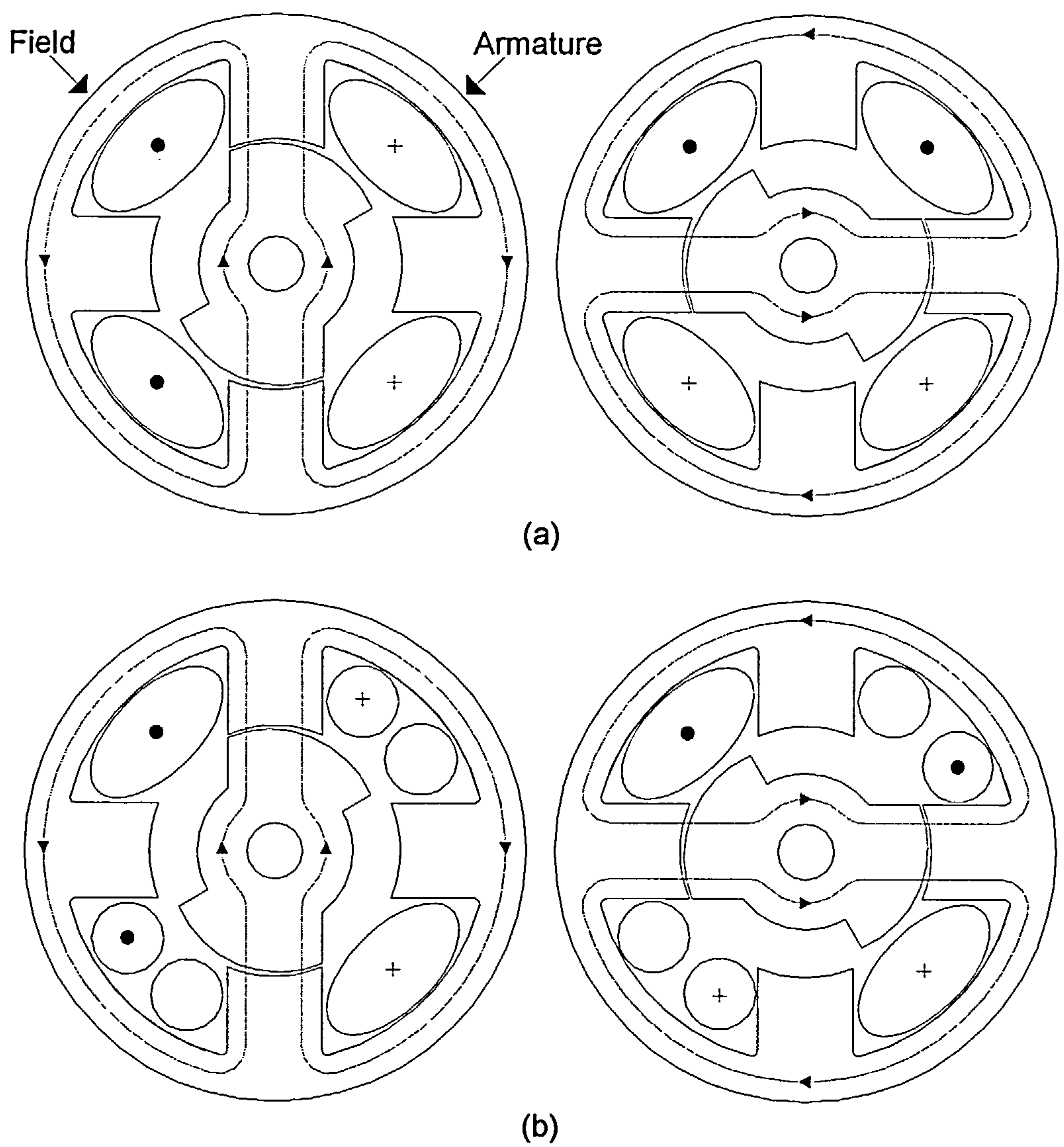


Figure 4.2 (a) Normal armature-winding, (b) Bifilar armature-winding

The main advantage of using a bifilar armature-winding was that it enabled a simplified power-converter, with only two power switches and two associated power diodes, to be used, as shown in figure 4.3. The reduction in the number of switches was made possible by the efficient use of the properties of the circuit. Additional components were needed in the R-C snubber circuit, which was used to capture and dissipate the leakage energy associated with the uncoupled flux between the armature-windings during commutation. The main disadvantage of using the bifilar armature-winding was the reduction of the copper-utilisation factor, for the armature-slot area to a maximum of 50 %. With this power-converter the new motor can achieve close to 75 % copper utilisation. This compromise was deemed to be valid in offering a more cost-effective solution.

The operation of the half-bridge voltage-source inverter-circuit in figure 4.3 can be explained as follows:

The first IGBT is switched-on allowing current from the supply to flow through the corresponding armature-winding. The rotor turns to align itself with the energised stator-poles as a consequence of the resultant combined flux that is produced by both the armature and field-windings. As rotation continues the position-sensor detects the point at which turn-on of the second IGBT is required. The first switch can be turned-off prior to, or at the same time as the second turns on. At first the stored magnetic-energy transfers to the second armature-winding. Recalling that this is wound in the opposite direction to the

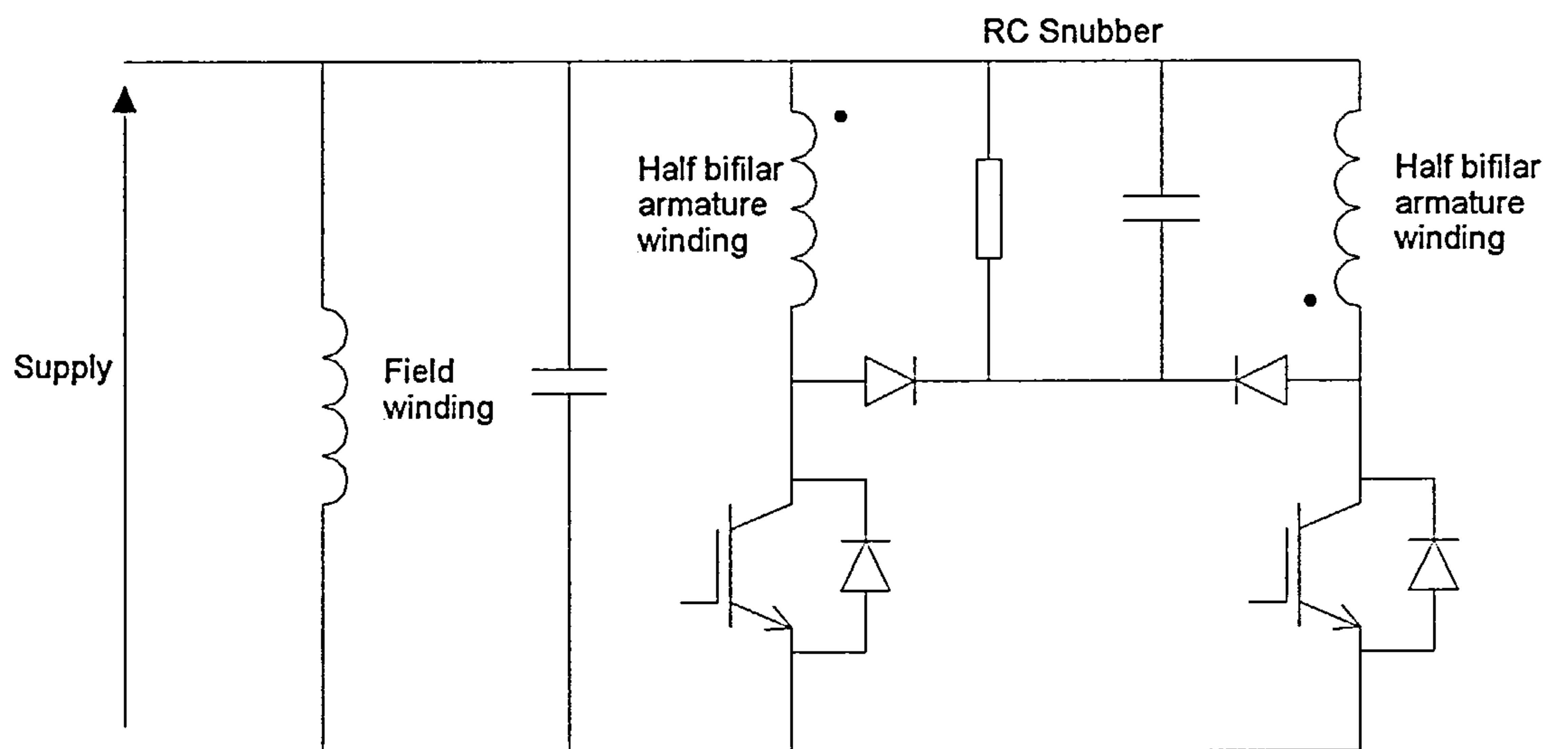


Figure 4.3 Half-bridge voltage-source inverter

first armature-winding, the current now flowing in this winding is negative and it tends to zero as energy is returned to the supply via the fast-recovery freewheel diode. When the second IGBT is turned-on, current, in the second half of the armature-winding, provides the reverse MMF that allows the motor to continue to rotate. This commutation process continues in synchronism with the rotation.

Instead of using IGBTs as the switching devices it is also possible to use thyristors in a half-bridge current-source inverter-circuit as shown in figure 4.4. Due to the thyristors needing to be force-commutated, a capacitor is required in place of the snubber circuit. The operation of the circuit can be explained as follows:

When one thyristor is turned-on current flows from the supply, through the appropriate armature-winding via the series field-winding, and the commutation capacitor is charged. As before, the rotor turns to align itself with the energised stator-poles, and the position-sensor detects the point at which to commutate the armature phases. Unlike the IGBT circuit the first switch of this circuit has to be turned-off at the same time as the second one turns-on. The second thyristor turns-on and the current, that was flowing through the first armature-winding, now flows through the capacitor, and on through the second thyristor, allowing the first thyristor to turn-off. The voltage across the capacitor reverses, ready for the next commutation. Whilst the current in the first armature-winding is decaying, the current in the second armature-winding is

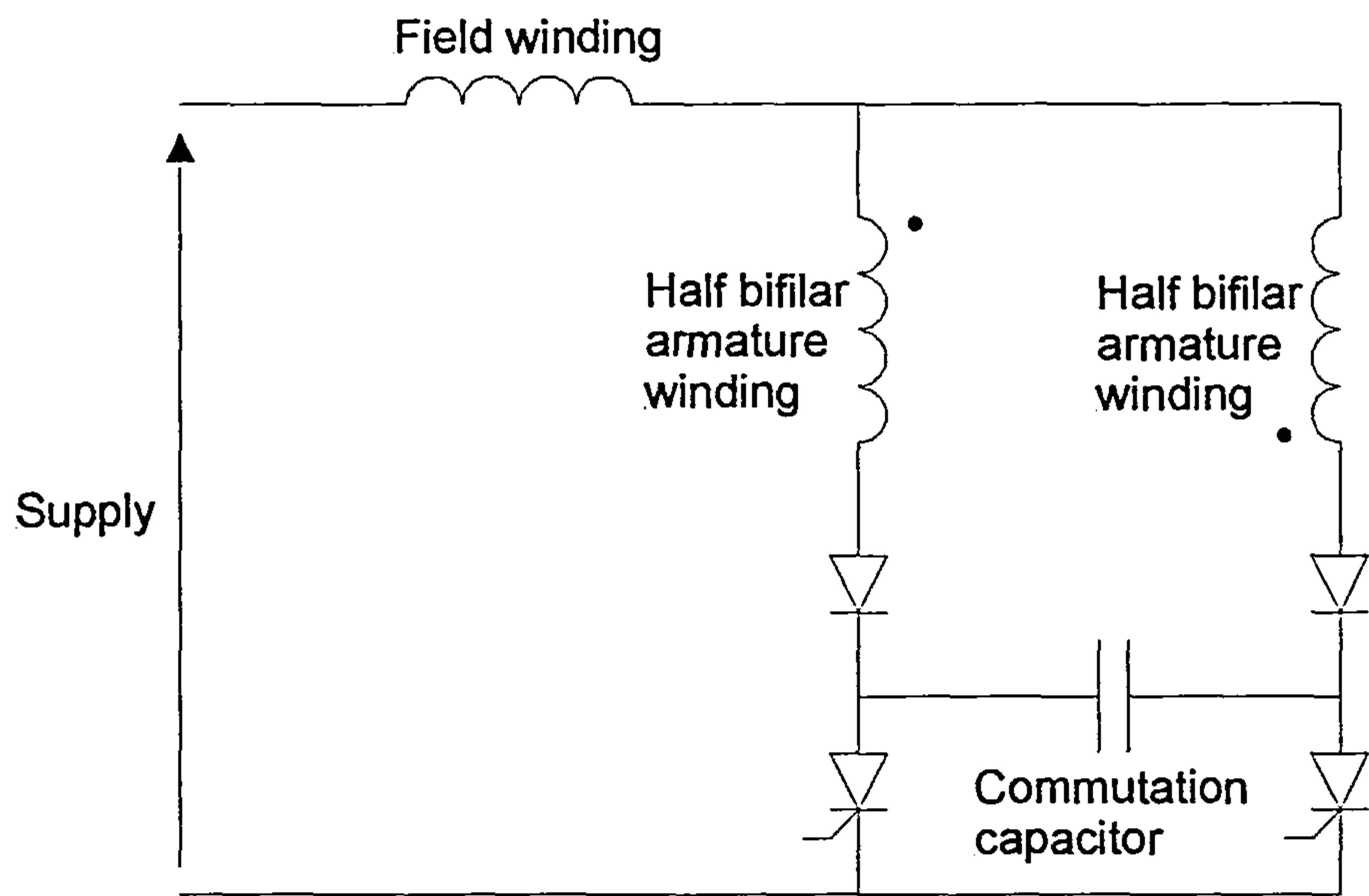


Figure 4.4 Half-bridge current-source inverter circuit

building-up, thereby, reversing the armature MMF. As before this commutation process continues in synchronism with the rotation.

Having identified two designs of power-converter, a choice had to be made as to which of them to use. The choice had to be cheap but also capable of satisfying the specification proposed. Both circuits had advantages and disadvantages. When the motor was first started it was expected that a large current-peak would occur. Comparing similar-sized devices the thyristors had an advantage over the IGBTs because they could withstand much-higher peak-currents and the associated voltages. Although the R-C snubber circuit was not needed, the half-bridge current-source inverter had an immediate disadvantage in that it required a very-large commutation-capacitor to operate, which was also relatively expensive. Also, because the thyristors had to be commutated at the same time, this restricted the degree of control over the motor, which for this application was very important, owing to the number of different operating modes required. Another quite important disadvantage, that the half-bridge current-source inverter circuit possessed, was that the field-winding had to be series-connected. This obviously restricted testing in determining what was the optimum winding-configuration. The half-bridge voltage-source inverter had no such problems. The field-winding could be separately-excited, series-connected, or shunt-connected, just as in a normal DC-wound motor. The only other disadvantage of using the half-bridge voltage-source inverter was that the snubber-voltage had to be at least twice

the supply-voltage. The half-bridge voltage-source inverter was selected because it offered more flexibility in terms of control and winding connections.

Both these power-converters offer an advantage, in kVA per kW rating, over a power-converter needed to operate a normal two-phase switched-reluctance motor [59]. The power-converter, for the flux-switching motor, does not control the energy in the field-winding (one-phase of the motor). The kVA per kW rating of the flux-switching motor is comparable to that of a DC brushed-motor. The flux-switching motor can rotate in either direction without redesigning the power-converter. Therefore, because each switch carries the rated armature-current for half the time at twice the supply-voltage, the power-converter has the same rating as a drive for a two-quadrant DC brushed-motor.

4.2.3 Gate-drive and control-circuit design

The power-converter essentially consisted of two identical power-switches, that had to be driven and controlled in order to operate the motor. Both of the IGBT power-switches were referenced to ground, therefore reducing the complexity of the required gate-drive circuit even further, so that only the minimum number of components were needed to implement a solution. For the purposes of actually operating the motor and not, at this stage, optimising the gate-drive circuit, a gate-drive chip was used. Obviously this was not the cheapest solution.

The gate-drive chip amplified the logic signals from the motion-controller to necessary suitable levels to drive the IGBTs. The complexity of the motion-controller reflected the stage of development of the motor, that is it was used in its simplest-possible state. The logic signal from the optical position-sensor was passed directly to one IGBT, via a channel in the gate-drive chip, and the other IGBT was controlled with an inverted position-sensor signal. Both IGBTs were on for the maximum length of time only, that is there were no PWM schemes implemented, or reduced duty-cycles imposed. The complete drive-system is one of the simplest, and hence cheapest, to implement for a brushless-motor.

4.2.4 Component selection and drive-system manufacture

To prove the principle-of-operation of the motor, both the motor and the drive had to be manufactured such that they were robust, whilst at the same time, also allowing for simple modifications and easy replacement of the main components. Optimisation of the components, in terms of rating and cost, followed later. For example more-expensive gate-drive chips were used for simplicity of implementation and robustness, and the other significant components were overrated during development. This enabled robust testing without unnecessarily damaging the drive-system.

The stator was constructed from an existing stack of laminations, from a switched-reluctance motor, which was encased with a nylon sleeve to allow it to fit into a pair of aluminium-cast end-bells obtained from another motor. Each

end-bell was then push-fitted with a steel reduction bush that enclosed a standard ball-race bearing that held the motor-shaft at each end. The motor-shaft was already fitted with the matching rotor-laminations taken from the switched-reluctance motor. The end-bells were sufficiently large to accommodate the additional end-winding length of the fully-pitched windings. The drive-circuit was constructed on a single piece of Veroboard apart from the IGBTs that were mounted on a separate heat-sink. An optical position-sensor, used in conjunction with a shaft mounted slotted disk, was attached to one of the end-bells and used to feedback the relative position of the rotor to the stator.

4.3 Testing and Analysis

This section gives the results of the tests carried out and their subsequent analysis. It is broken down into static and dynamic-tests. Tests were carried out with the help of Mr Jason Lewis.

4.3.1 Static-tests

The static-tests were performed to examine the waveforms of flux-linkage, flux and back-EMF. The shape of these waveforms was important in determining to what degree DC-motor theory would apply. Figure 4.5 shows the variation in phase flux-linkage with rotor position, at different currents, for one half of the bifilar armature-windings. It can be seen that the phase flux-linkage does not vary substantially with rotor-position. This is in contrast to a conventional

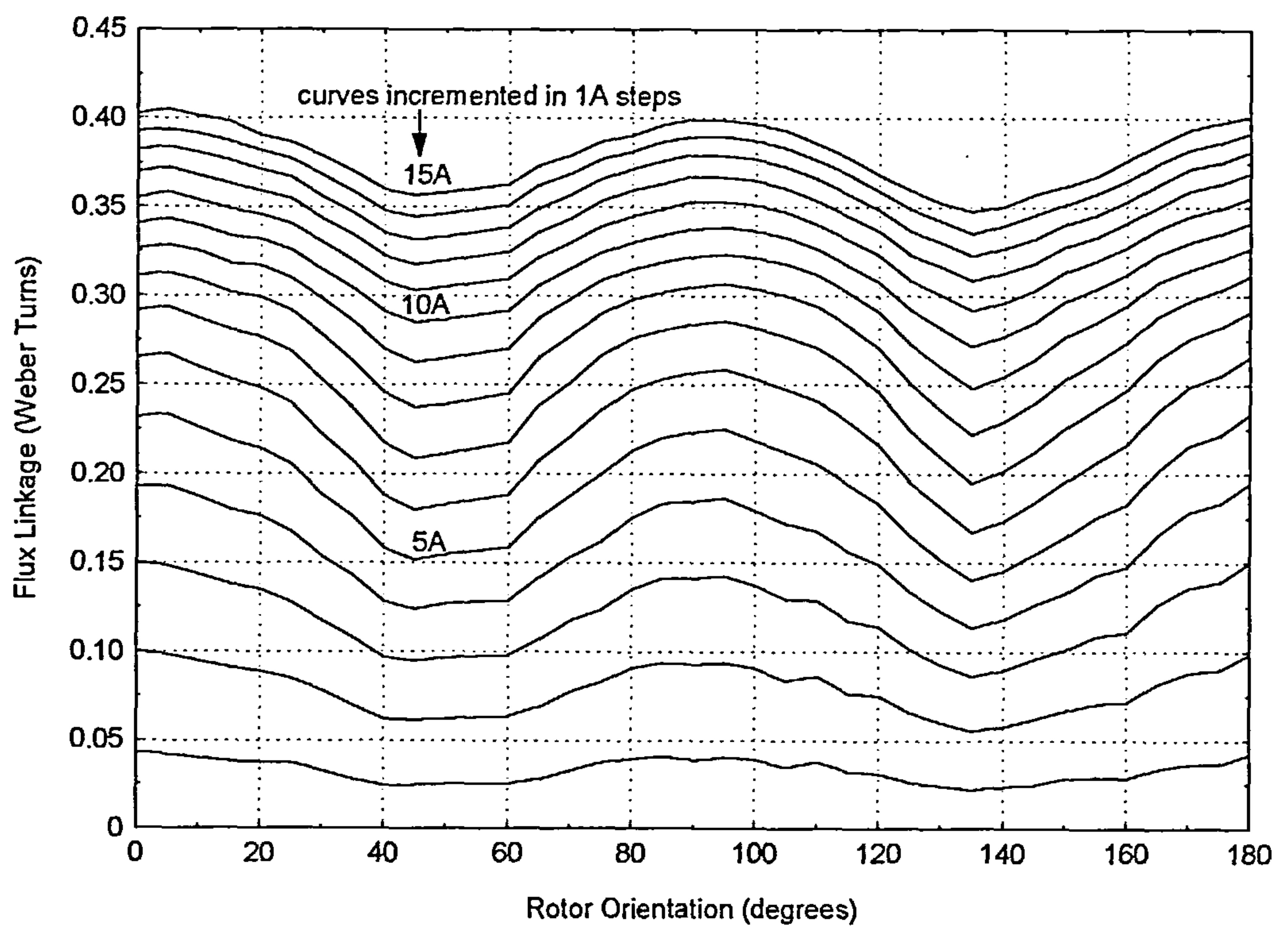


Figure 4.5 Variation in phase flux-linkage with rotor position at different currents for one half of the bifilar armature-winding

short-pitched phase winding. This property was desirable since the theory assumed that the reluctance would be constant for all rotor positions.

A field-winding was energised, with a pulsed-shaped voltage, whilst taking readings of the induced-EMF, in one of the armature-windings, at sequential rotor-positions, as depicted in figure 4.6. At the two half-aligned positions none of the flux, from the field-winding, actually links the armature-winding. At the two aligned-positions the flux linking the armature-winding reaches a maximum value having the same magnitude as the field-flux (the different sign is due to the orientation change of the rotor). An induced-EMF in the armature-windings is caused by this variation in flux-linkage with position. Shown in figure 4.7 is the back-EMF induced in one of the armature-windings. This was taken when the motor was rotated and with the field-windings excited.

In the mathematical model the flux waveform was assumed to vary linearly as a triangular wave, so that, upon differentiation the back-EMF waveform would be trapezoidal with an average value e_a . However, the experimental flux waveform obtained appears to be more consistent with that associated with a “flat-topped” sinusoid, which gave a back-EMF waveform with a high peak-to-average ratio. The maximum value of the back-EMF is therefore higher than the desired e_a , as the maximum rate-of-change of flux arises at the zero-crossing of the flux.

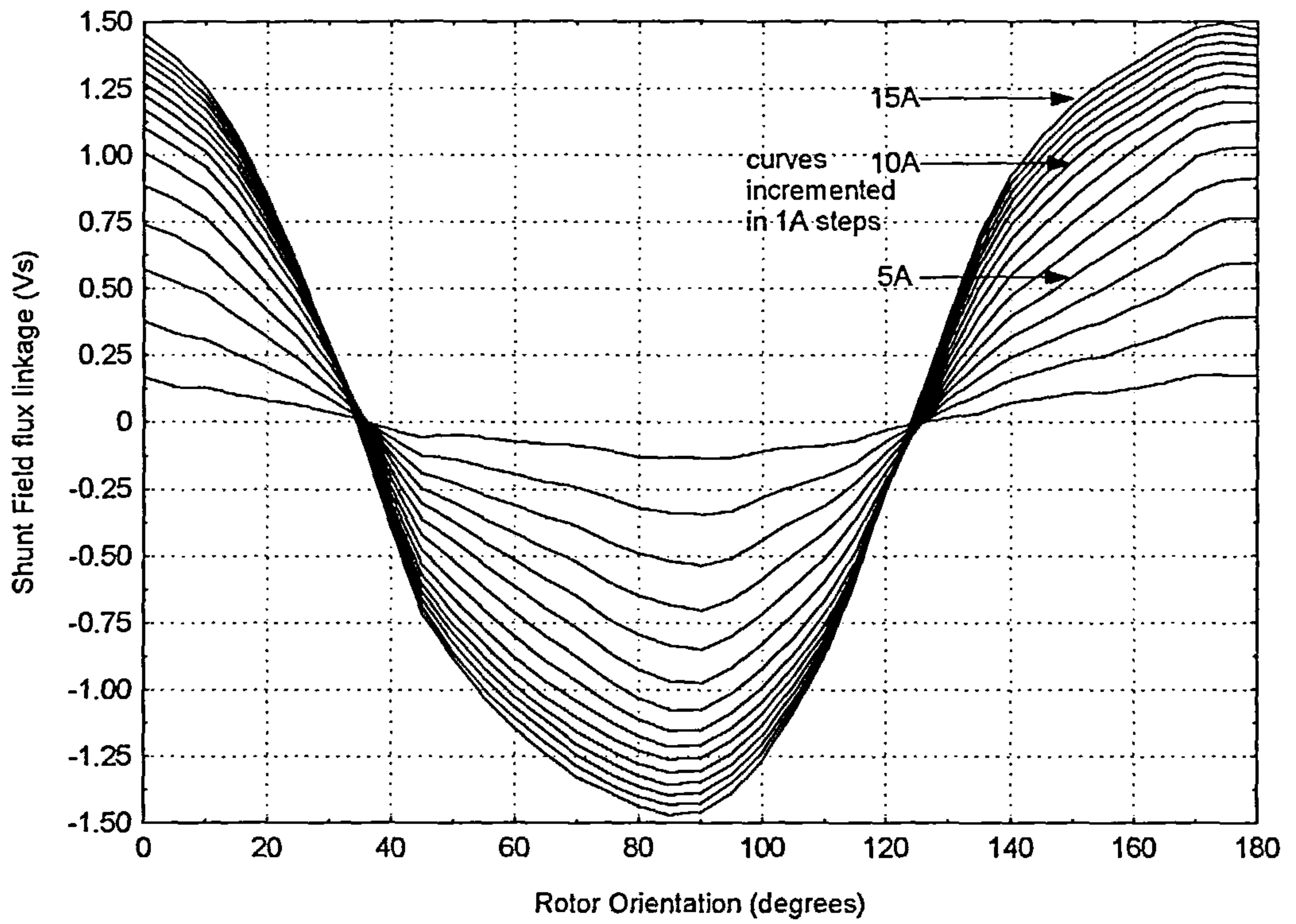


Figure 4.6 Flux linking the shunt-field-winding due to current in one half of the bifilar armature-winding

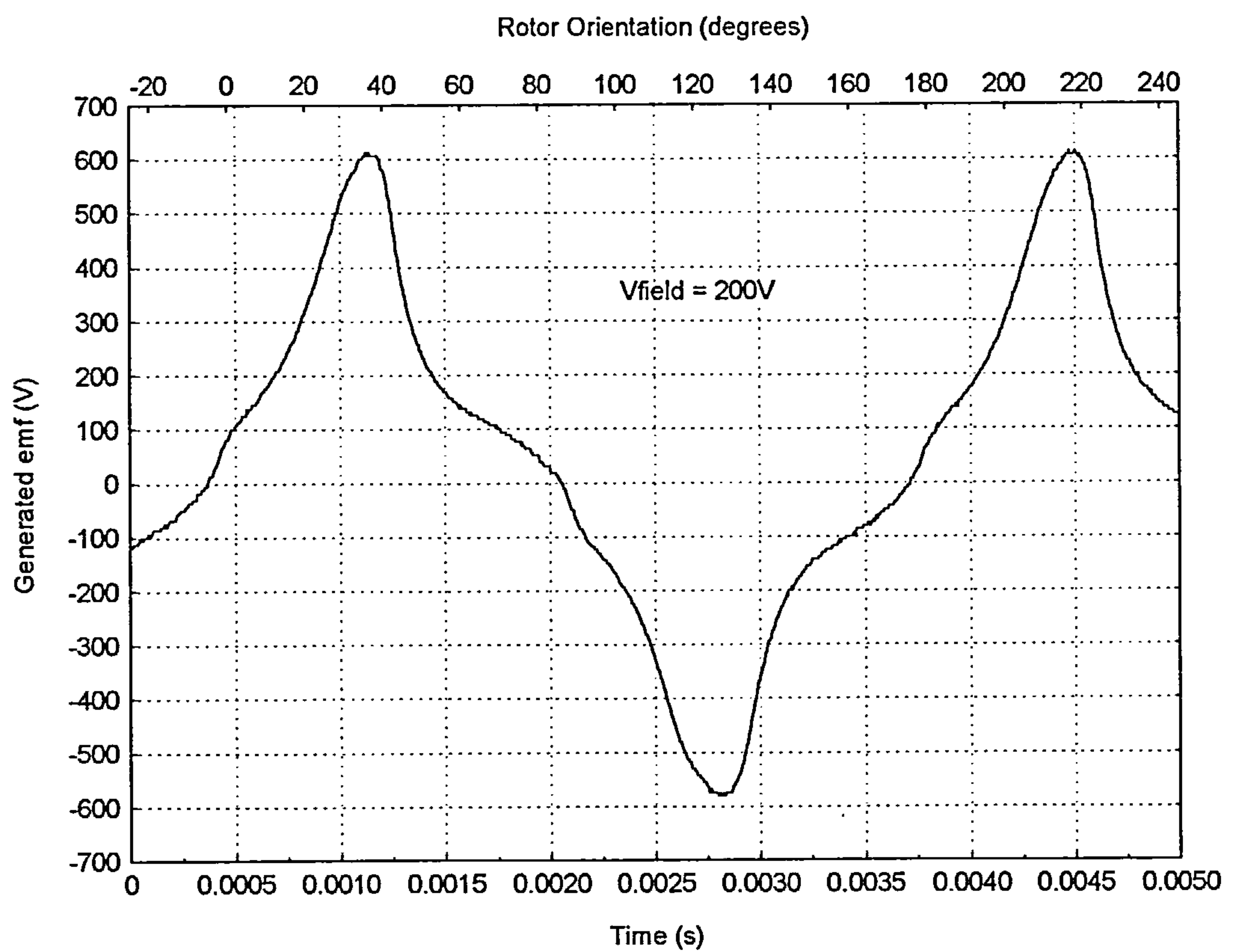


Figure 4.7 Back-EMF generated across one half of the bifilar armature-winding

The back-EMF waveforms for different speeds and applied field-voltages were averaged using an integration method. Graphs showing these data are collectively shown in figure 4.8. When the measured value of average back-EMF is compared with the predicted value, from the theory, there is inconsistency between the two values. The explanation for this was that not all of the flux, developed from the field-winding, linked with the armature-winding. This was expected and it was taken into account in equation (3.1) (in Chapter 3) as the fraction of field-flux K . This effectively reduces the theoretical value to that of the measured value. The average value of K was determined to be in the region of 0.6. See the linear portion of figure 4.8.

These static-tests have shown that a back-EMF is developed across the armature-windings when the field-winding is excited constantly, just as in a DC motor. However, the back-EMF waveform is not ideally shaped because it has a high peak-to-average ratio. It does not exhibit the same average back-EMF as that predicted by the model. This can be explained by the shape of the rotor. To achieve a linear change in flux and a back-EMF waveform that is more trapezoidal in nature, a constant value of reluctance, which does not change with position, is required. The rotor-poles need to have a constant overlap with the two adjacent stator-poles and the airgap of the overlapping regions must be uniform. These characteristics would give a smoother reversal of flux-linkage in the armature-winding and an optimised coupling between the field and armature-windings. This would increase the magnitude of the fraction of field-flux K . The rotor used in the experimental motor is therefore far from

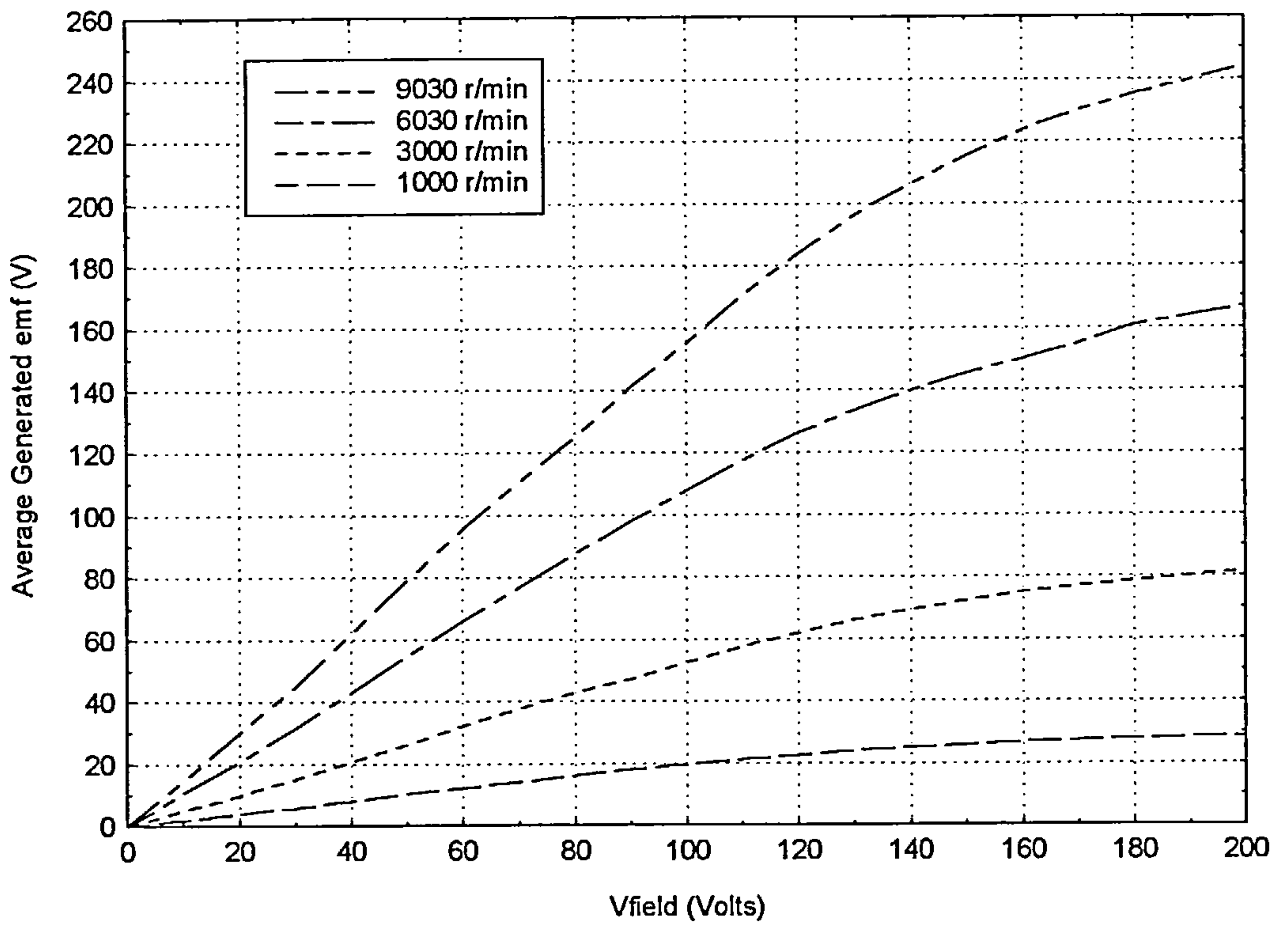


Figure 4.8 Average back-EMF against shunt-field-winding volts

perfect. The rotor-poles do not overlap constantly with the adjacent stator-poles, and the graded-airgap, used for self-starting purposes, results in non-uniform reluctance.

4.3.2 Dynamic tests

The objective of these tests was to observe the motor's behaviour, whilst under load, in order to obtain the performance characteristics, that is torque-speed curve, power capabilities and efficiency. Determination of the shape of the current waveforms would also be important for analysing the operation of the motor.

Shown in figure 4.9 are the current-waveforms for one half of the armature-winding and the field-winding. The controlled IGBT switches commute simultaneously and in a complementary manner. When commutation occurs the initial current flowing in the armature-winding, that has just been excited, is negative. The reason for this is that the stored magnetic-energy, in the first bifilar armature-winding, transfers directly to the second winding. Since this is wound in the opposite direction, the current must at first return to the supply via the freewheel diode. Once the supply is complete the current reverses, flowing back from the supply. Further testing found that by advancing the commutation-angle of the IGBTs, effectively shifting the current relative to the back-EMF, allowed the shape of the armature current-waveform to be improved. It is important to note that the motion controller was limited only to position-detection, no current-feedback was used.

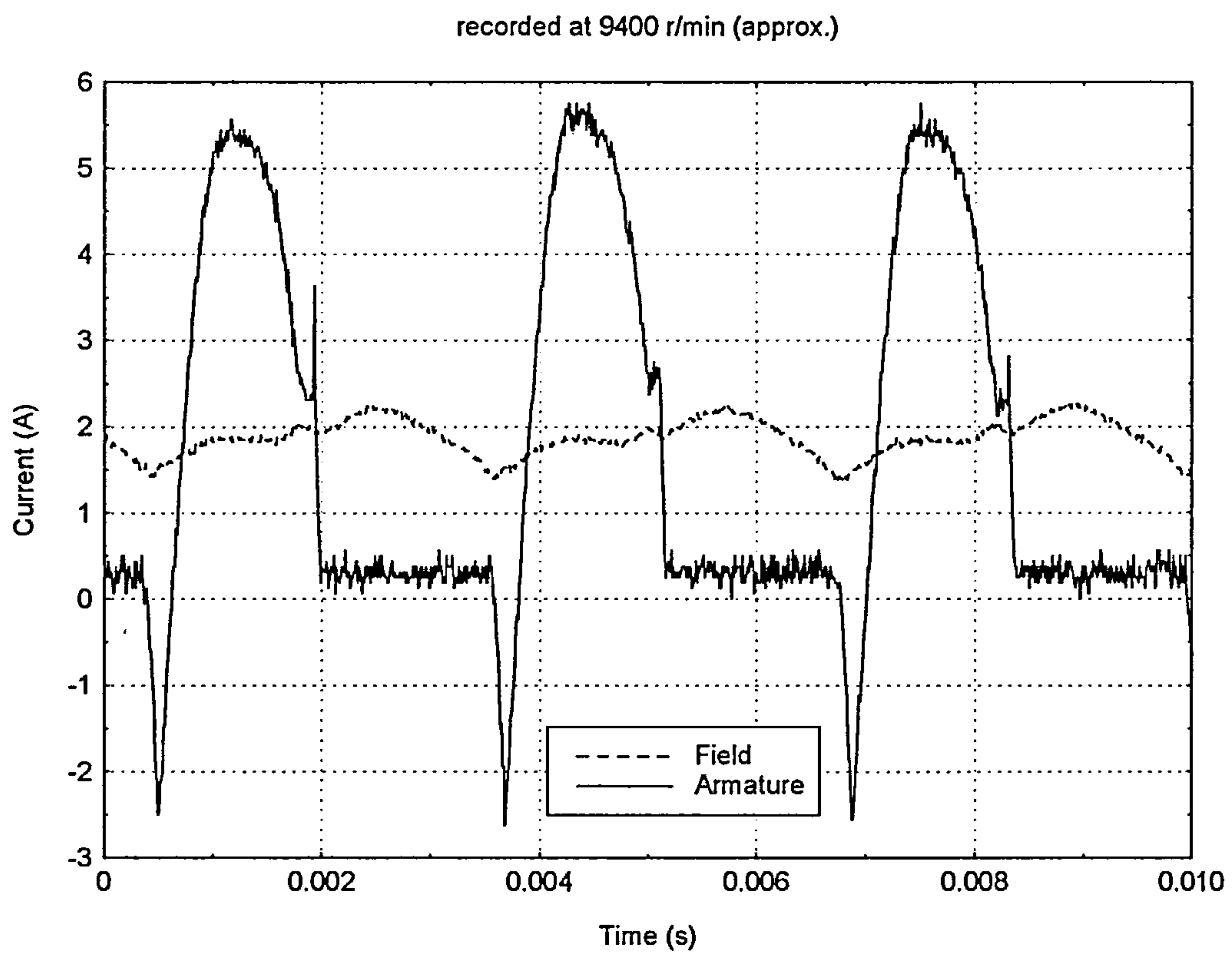


Figure 4.9 Current waveforms for the field and one half of the bifilar armature-windings

Figure 4.10 shows the torque and power output capabilities of the motor. The field-winding was separately excited and the commutation-angle of the IGBTs was advanced to achieve optimum performance from the motor. The motor developed a torque of just under 1.2 Nm at a speed of 9500 r/min. The design torque was 2 Nm at 9000 r/min. If the data is extrapolated to this latter speed the motor was only able to realise approximately 65 % of the specified torque. Furthermore the motor was expected to have a no-load speed of 12000 r/min according to the theory, which would have given a relatively-steep torque-speed characteristic (as for a DC motor with a shunt-field winding), in practice however the design speed was surpassed.

Peak efficiency of the complete drive was measured at just below 50 %, which was lower than anticipated. An efficiency of near 60 % had been previously recorded from an earlier experiment with the motor in a short-pitched configuration. The fully-pitched motor had promised an improvement in efficiency due to the better utilisation of the available copper at 75 %, as opposed to 50 % in a conventional short-pitched switched-reluctance motor. However, because the magnetic design of the laminations was in no way optimal for the operation of this motor, this was not the case.

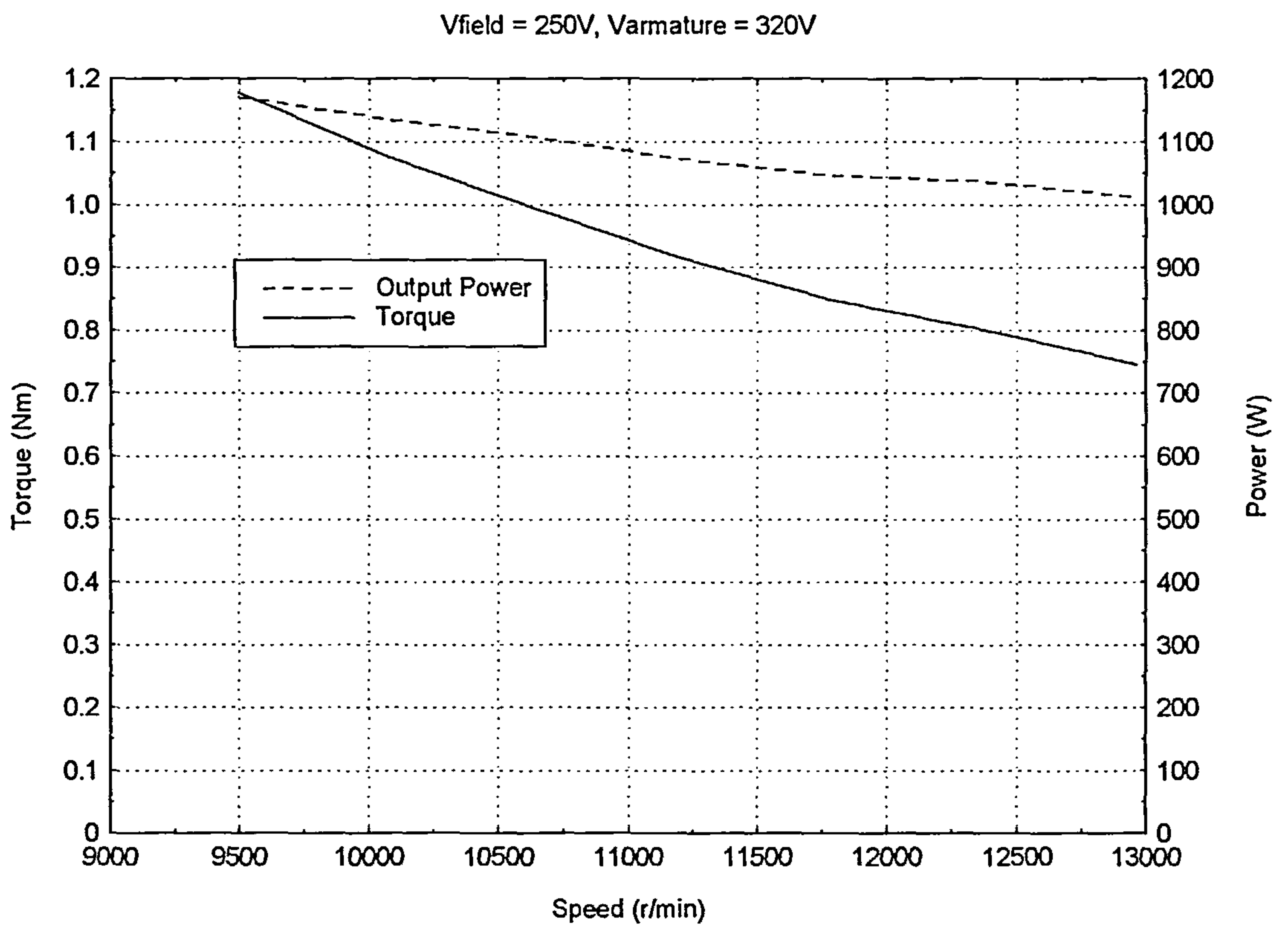


Figure 4.10 Torque-speed curve and output-power characteristic

4.4 Conclusions

The testing of the proof-of-principle flux-switching motor demonstrated it worked in principle. Tests also showed that the motor shared similar operating characteristics to the DC motor as expected, with the generation of a back-EMF induced across the armature-windings by the rotation of the rotor within a field flux. The performance capabilities of the motor were lower than hoped, owing to the use of the non-optimal lamination profiles.

The most important outcome demonstrated was that the drive-system had good potential for further development. The combination of a very-simple drive and motor showed that performance desired should be achievable from a brushless doubly-salient motor at competitive cost. The following Chapters detail the design and testing of a purpose-built prototype motor used to fully investigate the operation and performance of a flux-switching motor.

CHAPTER 5 DESIGN OF THE NEW FLUX-SWITCHING MOTOR

5.1 Introduction

The work on the proof-of-principle motor established the concept and also indicated good potential for developing a durable, useful motor. In order to ascertain the real capabilities of the motor it was necessary to test a purpose-built prototype against a commercially, desirable performance specification. This Chapter details the design of the new flux-switching motor, taking the mathematical model, the simulation and the results from the testing of the proof-of-principle motor to create a prototype ready for testing. Testing of the motor is the subject of the next Chapter in addition to further development of it as a result of the testing.

5.2 Motor design

The design of the laminations and the windings, and the manufacture of them, along with a casing to form a motor, are presented in this section. Professor Charles Pollock was responsible for the lamination design with input from Mr Richard Walter, of Black and Decker Ltd, and myself.

5.2.1 Lamination design

The first step in designing a motor is to establish the physical size of the motor required to deliver the power [60], which is achieved by using the Output Equation, (5.1) below. This is given in terms of power-density, that is the power-per-unit-volume needed, as

$$\text{Power Density} = \frac{T\omega}{\frac{\pi}{4}D^2L} \quad (5.1).$$

Where T is the torque, ω is the speed, D is the outside diameter of the stator and L is the length of the stator. In the specification in Appendix 1 it was stated “to achieve the power-density objectives, the D^2L product must not exceed 554470 mm³ (for example an 89 mm outside diameter and 70 mm stack-length could be used). Performing the calculation according to equation (5.1) with an output power of 2.5 HP (1864 W) this gave a power-density requirement of 4280 kW/m³.

Having found the dimensions of the motor the next step in the design was to decide upon a lamination profile. The chosen profile was of an 8/4 configuration as shown in figure 5.1. The main reason for doubling the number of stator and rotor-poles from the previous 4/2 configuration was to reduce the length of the end-windings. The windings in the 4/2 motor had to span the width of the stator to pass through opposing slots, whilst also avoiding the rotor, which meant that the end-windings had to be placed along the periphery of the stator. With the same stator dimensions this resulted in the length of the end-windings being greater than that of the active part of the winding. To overcome this problem the 8/4 configuration was used. Instead of the windings spanning the width of the stator they now only had to span 90° such that the number of stator-poles spanned still equalled two. The end-winding length was reduced by a factor of two approximately for the same active part of the

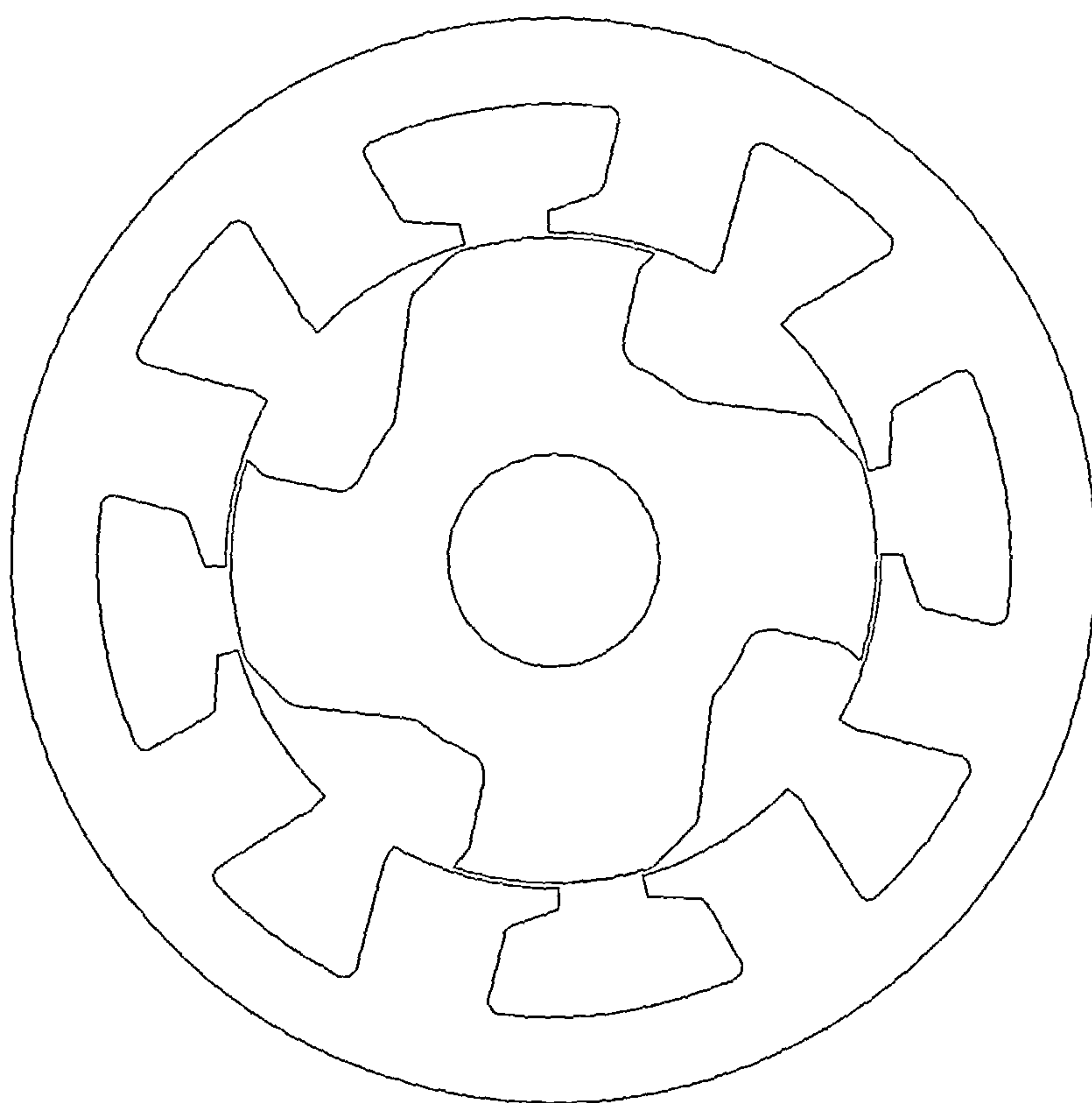


Figure 5.1 Chosen 8/4 lamination profile

winding. Therefore it was to be expected that for the same phase-currents the end-winding losses would also half.

In addition to the shorter end-windings another benefit of using an 8/4 configuration was that the manufacture of the windings was simplified in terms of positioning them within the motor.

There were a number of other implications in moving to an 8/4 configuration. Firstly, the magnetic-field distribution became four-pole whereas before it was two-pole distribution. This meant that per revolution the switching-frequency would double, switching-losses per revolution would therefore be expected to double. Also, as there were now four electrical-cycles per revolution, as opposed to two previously with the 4/2 configuration, the resolution of the electrical advance, and hence the mechanical advance-angle, was halved (for example, 1° mechanical = 4° electrical with the 8/4 configuration, whereas 1° mechanical = 2° electrical with the 4/2 configuration). Therefore any error in setting the advance-angle would have twice the effect than before.

Referring again to figure 5.1 it is clear that there are two different stator-slot designs, whereas in the 4/2 motor, all of the slots were identical. The most noticeable differences are the shape and cross-sectional area of the slots. The field-windings were located in the deeper straight-sided slots whilst the bifilar armature-windings were located in the shallow wide slots with the overhanging teeth, as indicated in figure 5.2. The field-winding slot area was less than that

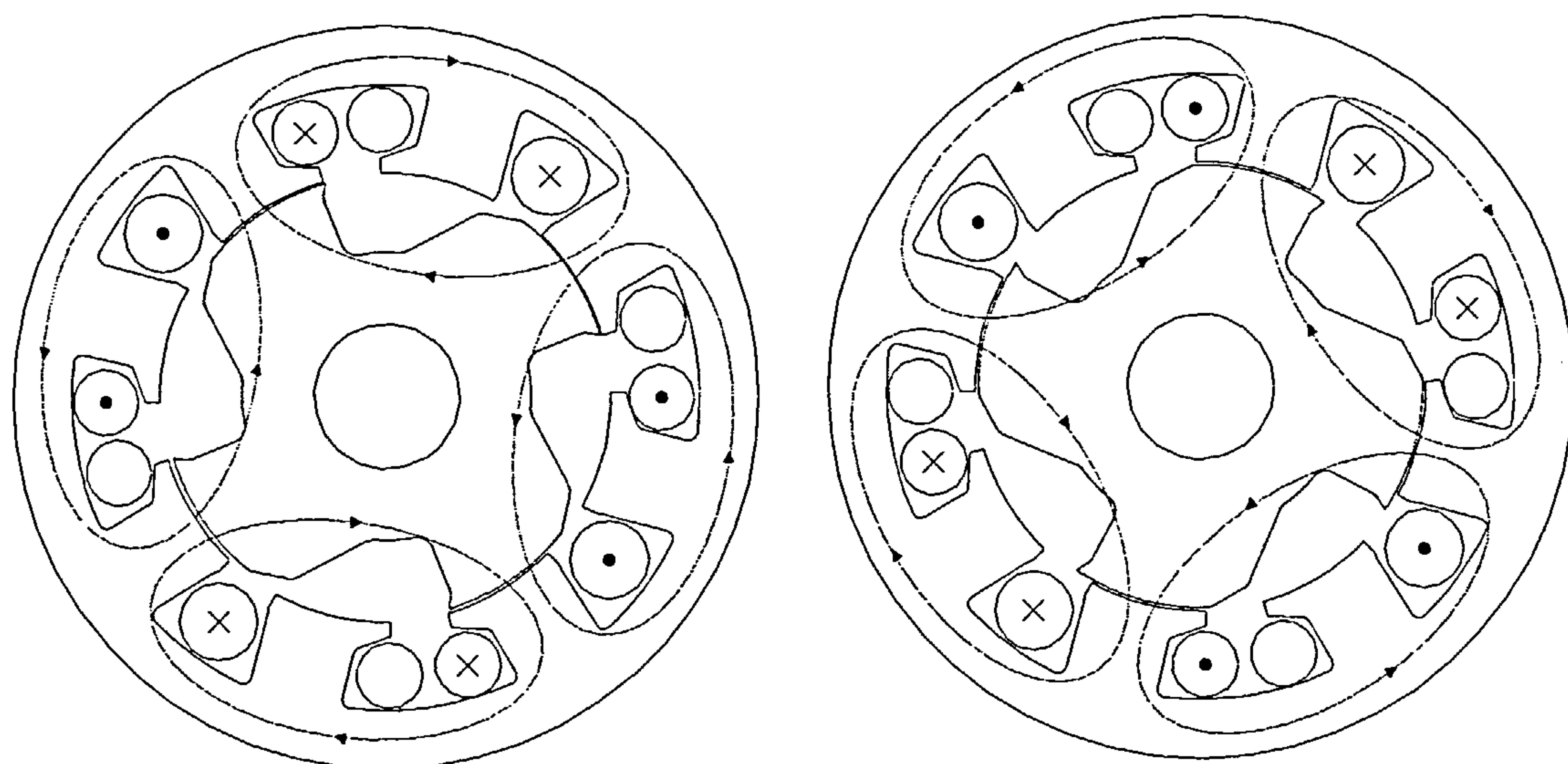


Figure 5.2 Winding location and flux patterns

of the armature because all of it was utilised to energise the field-winding. Whereas, only half the armature-winding slot area was used at any one time because each half of the bifilar-winding was being energised 50 % of the time.

Another important feature of the stator lamination was the different back-iron widths behind the field and armature slots. Considering the flux plots for the two aligned positions, shown in figure 5.2, it can be seen that there are regions of unipolar and bipolar flux. The back-iron behind the field slot always has unipolar flux flowing through it as a result of the combination of the fluxes created by both the field and armature-windings. The back-iron behind the armature slots also carries both fluxes, but when the armature is commutated this combined flux reverses in direction. Both of these sections of back-iron are carrying the same net flux, but the armature back-iron has a rapidly changing reversing flux in it, hence the reason for the armature back-iron being thicker.

The rotor was asymmetrical in design for the purpose of enabling self-starting, which is a feature required in all two-phase machines as discussed in Chapter 2. The rotor shape was optimised in conjunction with the stator, using finite-element analysis (FEA), to give the required starting-torque and to maximise the change in coupling-coefficient between the field and armature-windings. The stator teeth were regularly spaced towards the centre of the stator, with respect to the rotor, to give an equal pole-arc length, such that the change in coupling-coefficient was consistent in pattern with rotation.

In order to maximise the torque production of the motor it was important that the torque generated as a result of the change in mutual-inductance was not adversely affected by any torque resulting from a change in self-inductance of either the field or armature-windings. Minimising the torque due to the changing self-inductance limited the options to fulfil the braking requirement of the motor. It was envisaged that with some change in self-inductance the motor could be braked by leaving one phase permanently excited. As this was the simplest braking method available a compromise was chosen allowing a small change in self-inductance to be permitted.

5.2.2 Winding design

Following on from the proof-of-principle motor the initial winding design was again based upon a motor with a shunt connected field-winding, although it was anticipated that a series-connected field-winding would also have to be investigated to ascertain the full capabilities of the motor. A winding specification was established using the magnetic data derived from FEA with the mathematical model in a time-stepping simulation model, as described in Chapter 3. The input to the simulation in terms of the winding design was given as the number of turns and the diameter of wire needed for both the field and armature-windings. The output was then given as the torque developed by the motor at the rated-speed given the input of additional data. An optimum winding design was found using an iterative approach thus ensuring that the correct torque should be developed.

5.2.3 Manufacture

Figure 5.3 shows the stator lamination-stack with the field and armature-windings in place. The end-windings were equally distributed around the periphery of the stator to minimise the magnetic-leakage effects and to ensure that any energy-leakage was consistent. The motor was constructed as a possible direct replacement for a series-universal motor already in the intended application. The stator-laminations were housed in a nylon sleeve that was supported at each end by two machined-aluminium end-bells. The end-bell at the drive-end formed the motor-casing that facilitated the connection to the application. It also contained the speed-reduction gearbox, which consisted of two-helical cut gears that had a ratio of 4.7:1. The end-bell at the non-drive end held the optical-sensor that made up one-half of the position-sensor. This end-bell was allowed to rotate through approximately 50° (mechanical) relative to the stator to enable the advance-angle to be set. The rotor-laminations were held on a nylon-sleeve-insulated steel-shaft that ran centrally through the motor. The shaft was held in the aluminium end-bells via two ball-race bearings. Also mounted on the shaft was, a fan that was used to cool the windings, and the slotted disk, which formed the other component completing the position-sensor.

Once testing began, as described in Chapter 6, it became noticeable that, at the higher torques, mechanical problems associated with the breakdown of the air-gap between the stator and the rotor were occurring. After a number of attempts to resume testing with the same design a replacement casing was



Figure 5.3 Stator with windings in place

designed. This eliminated all associated mechanical problems allowing testing to be performed unhindered. The gearbox was removed from the replacement design to permit proper testing of the motor, that is the removal of the unquantifiable gearbox-losses. The existing cooling arrangement was also altered to allow heat to be removed from the windings more efficiently by permitting air to flow across the outside of the stator. Figure 5.4 shows the main component parts of the motor. Figure 6.1 in Chapter 6 shows the fully-assembled motor located on the test rig.

5.3 Drive design and manufacture

This section details the design and manufacture of the drive and control circuits. In addition the design for a drive-protection circuit is presented.

5.3.1 Power-converter design

The design of the power-converter circuit essentially remained the same as that for the proof-of-principle motor described in Chapter 4. The only differences were the addition of a single-phase bridge-rectifier, the incorporation of field-control for the shunt motor, and a modification that enabled the series field-winding to be used. The proof-of-principle motor had shown that the available DC-supply was reaching the limit of its capabilities in terms of power-output. To overcome this problem with the new motor, a Variac was used in conjunction with a bridge-rectifier. To smooth the supply from the bridge-rectifier a 2 mH inductor was included in the power-circuit, and it was placed in line with the positive supply-rail so that it connected with the top end of the DC-

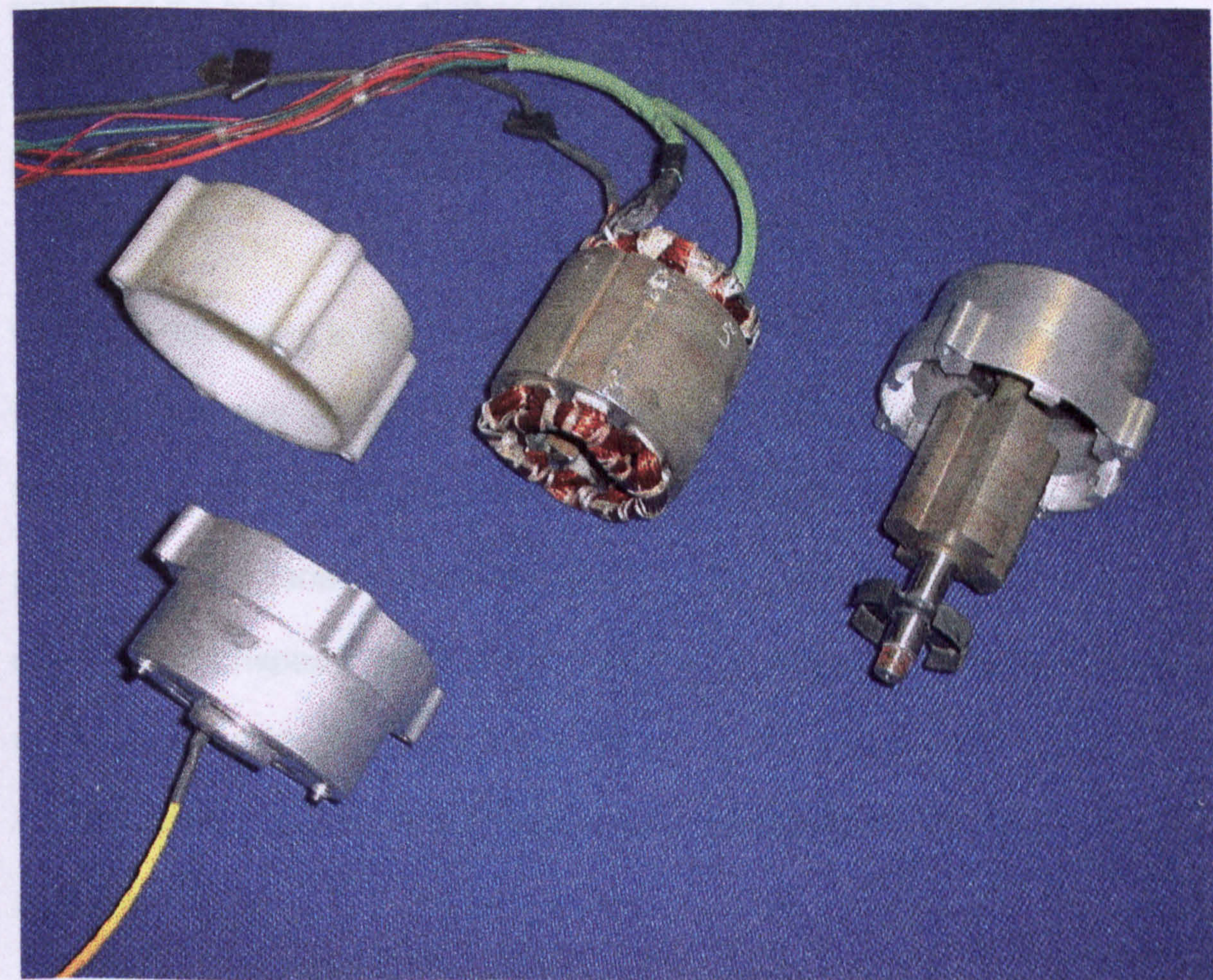


Figure 5.4 Component parts of the motor

link capacitor. It also became necessary to control the field to enable better control of the motor under starting conditions. This meant the addition of another electronic switch that was chosen to be a MOSFET. Figure 5.5 shows these modifications to the power-circuit.

Changes necessary in the power-converter design when moving to a series field-winding were minimal. Figures 5.6 and 5.7 show the two circuits used in this testing. The difference between them is simply the use of an extra diode placed after the series-winding in figure 5.7. The reason for doing this is explained in Chapter 7 where the series-motor testing is discussed. With the use of a series field-winding it was no longer necessary, or possible, to control the field without affecting the armature, such that the MOSFET was no longer needed.

5.3.2 Gate-drive and control circuit design

As with the proof-of-principle motor gate-drive chips were again used to drive the IGBTs and also the additional field MOSFET. However, the motion-controller was far more complex in design as it used an 8-bit 16F84 PIC micro-controller. The very simple, one IGBT on and the other IGBT off, control-method was no longer appropriate to meet the needs of the operation of the motor as specified. Hence the need for a more powerful means of control that allowed PWM schemes and reduced duty-cycles to be implemented relatively easily. Figure 5.8 shows the complete gate-drive and control-circuit, the extra components shown were needed for the PIC micro-controller.

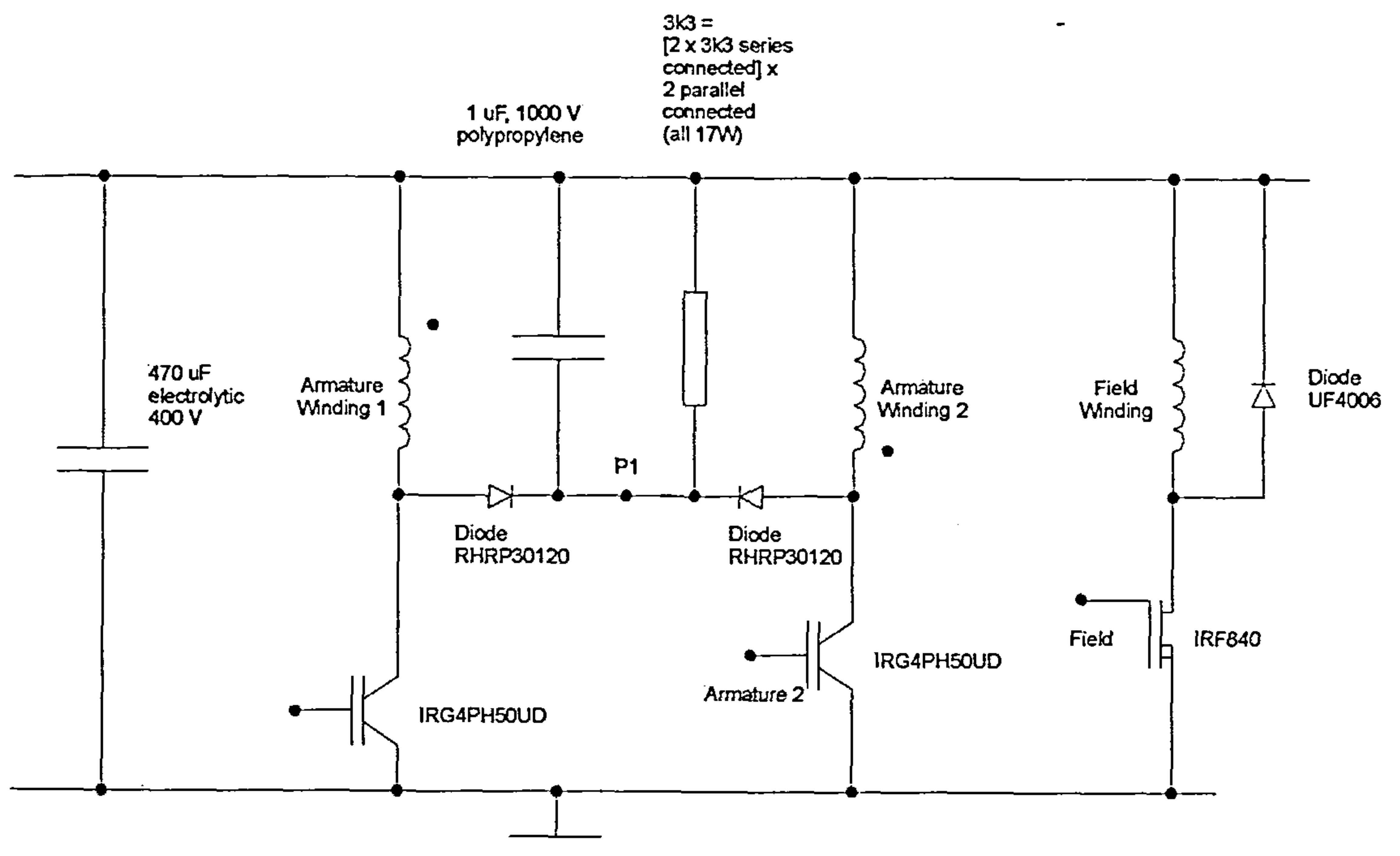


Figure 5.5 Power circuit for shunt-motor

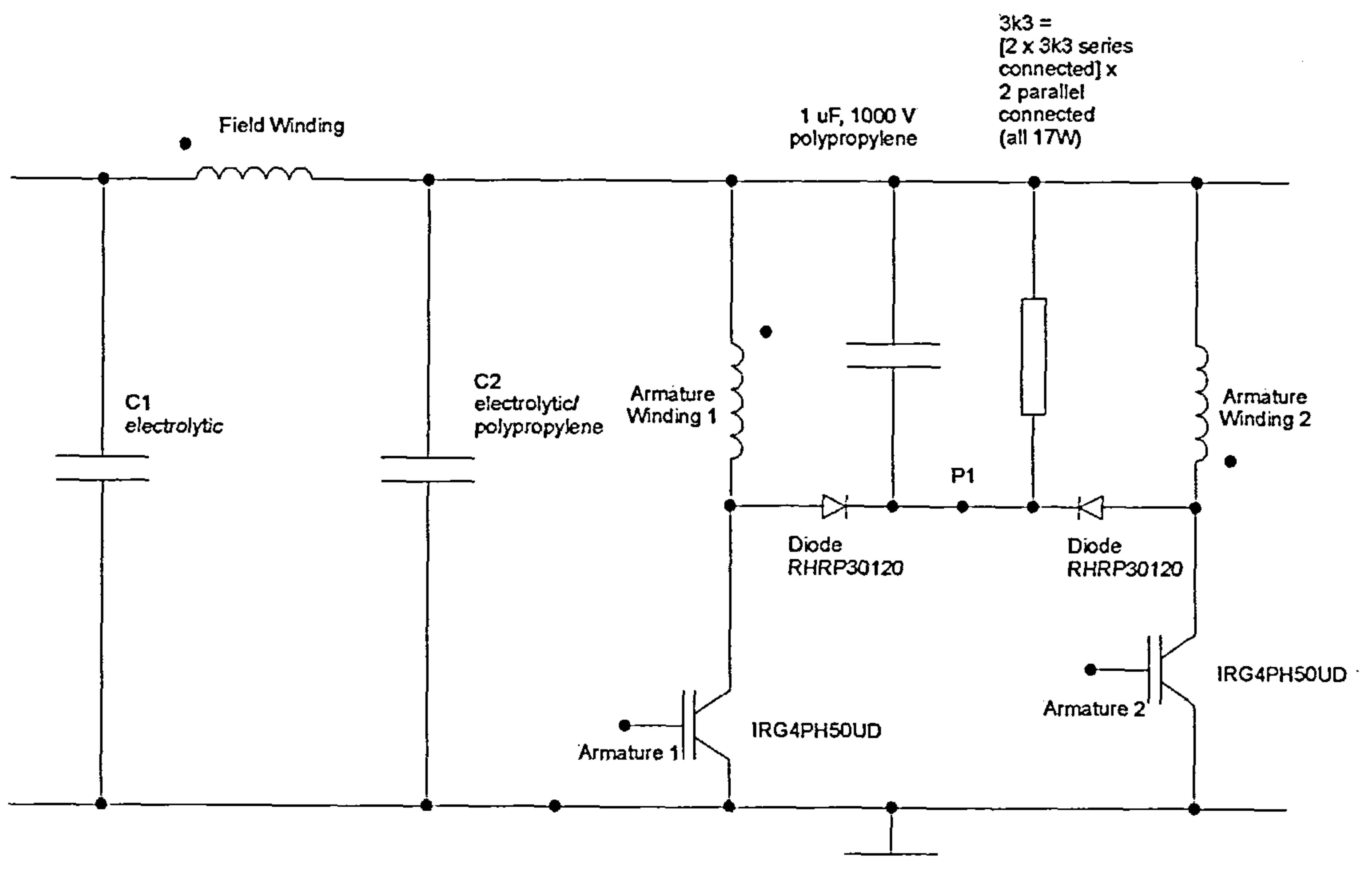


Figure 5.6 Power circuit for series-motor

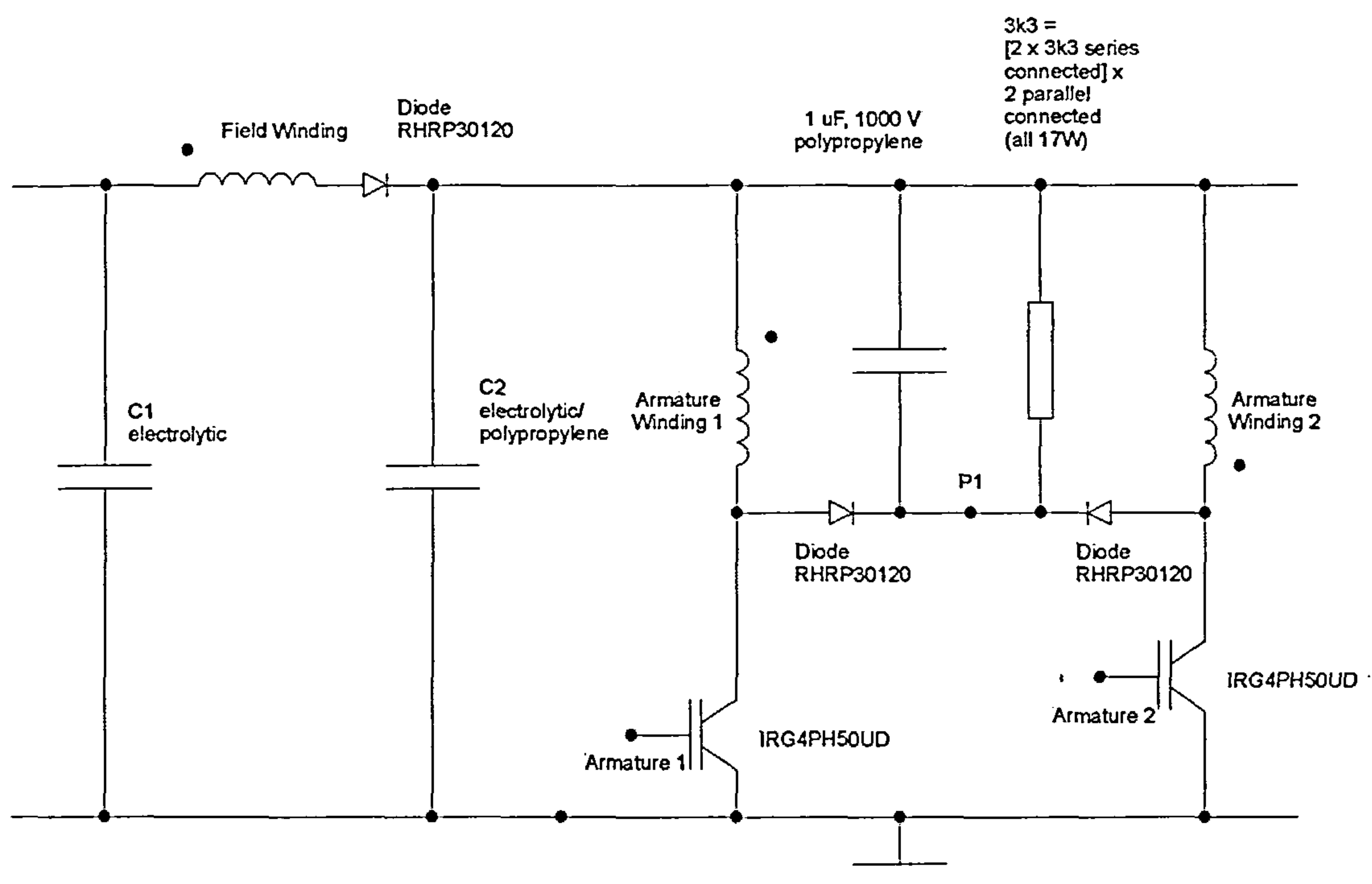


Figure 5.7 Power circuit for series motor with additional diode

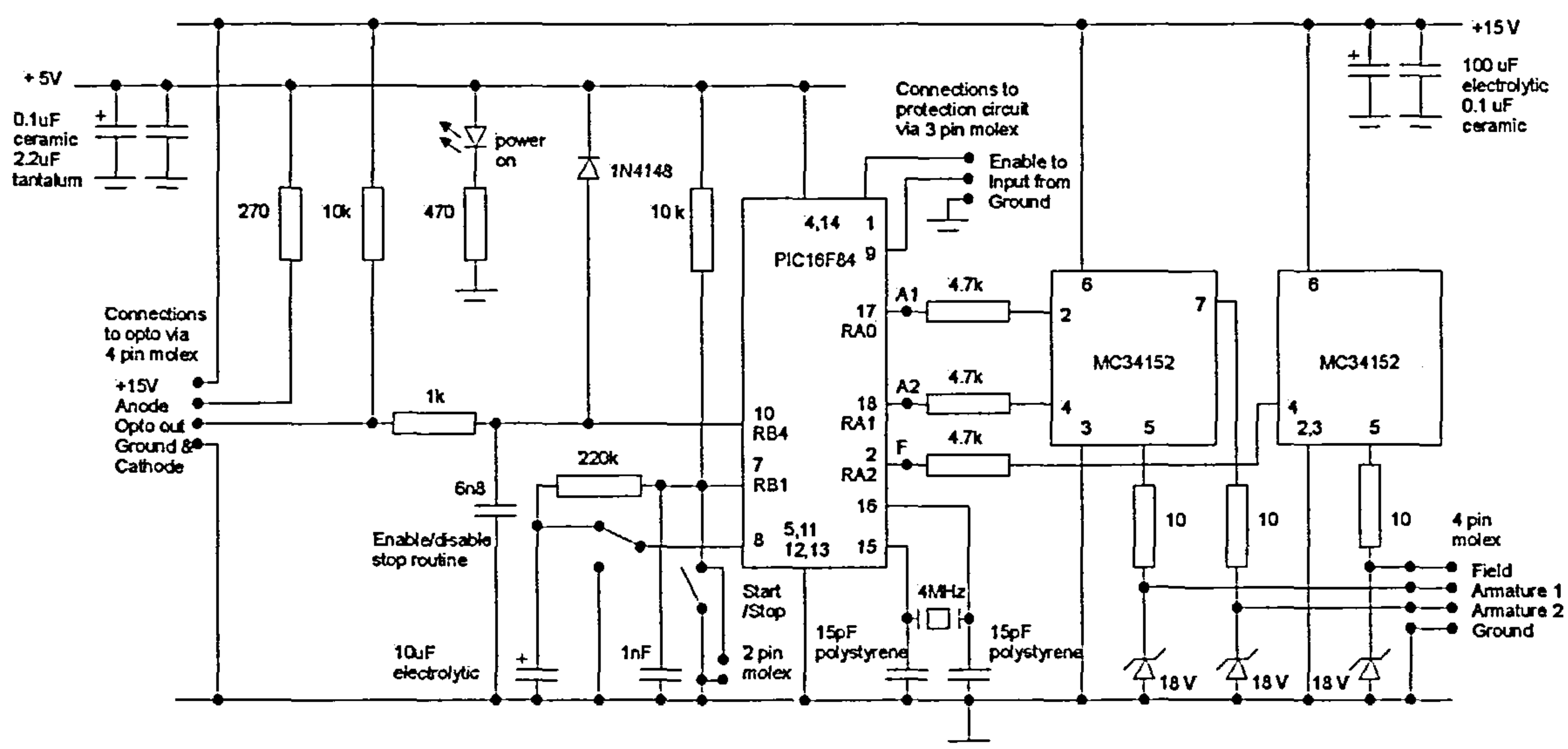


Figure 5.8 Gate-drive and control circuit

5.3.3 Drive-protection circuit

The drive-protection circuit was conceived as a development tool that was used to protect the drive from unnecessary failure, and, hence, avoid lengthy repairs. However, it also became useful in the analysis of fault-conditions to see just what could have caused such a failure. It must be stressed that the circuit was used for protection only, any detection of a fault-condition resulted in immediate shutdown of the drive by turning off all of the active power-devices. The drive was never switched-off momentarily by the drive-protection circuit and then allowed to switch-back-on, as this could have been interpreted as a form of current-feedback control, which this drive was not allowed to include.

The IGBTs and the power-diodes in the snubber circuit needed protection from excessive current and, also, periods of excessive voltage caused by the rapid change of current. The power-diodes were current-rated highly enough to not need any protection, the IGBTs had a peak-current limit of 90 A, and a continuous rating of 45 A. Both the IGBTs and the power-diodes had voltage limits of 1200 V. To detect excessive values and implement a shutdown required an appropriately-calibrated sensor, a comparator, to compare the measured value from the sensor with a threshold value, and some simple combinational logic to process the signals. Current was measured with a Hall-effect device whilst voltage was scaled with a potential-divider arrangement. The circuit is shown in figure 5.9.

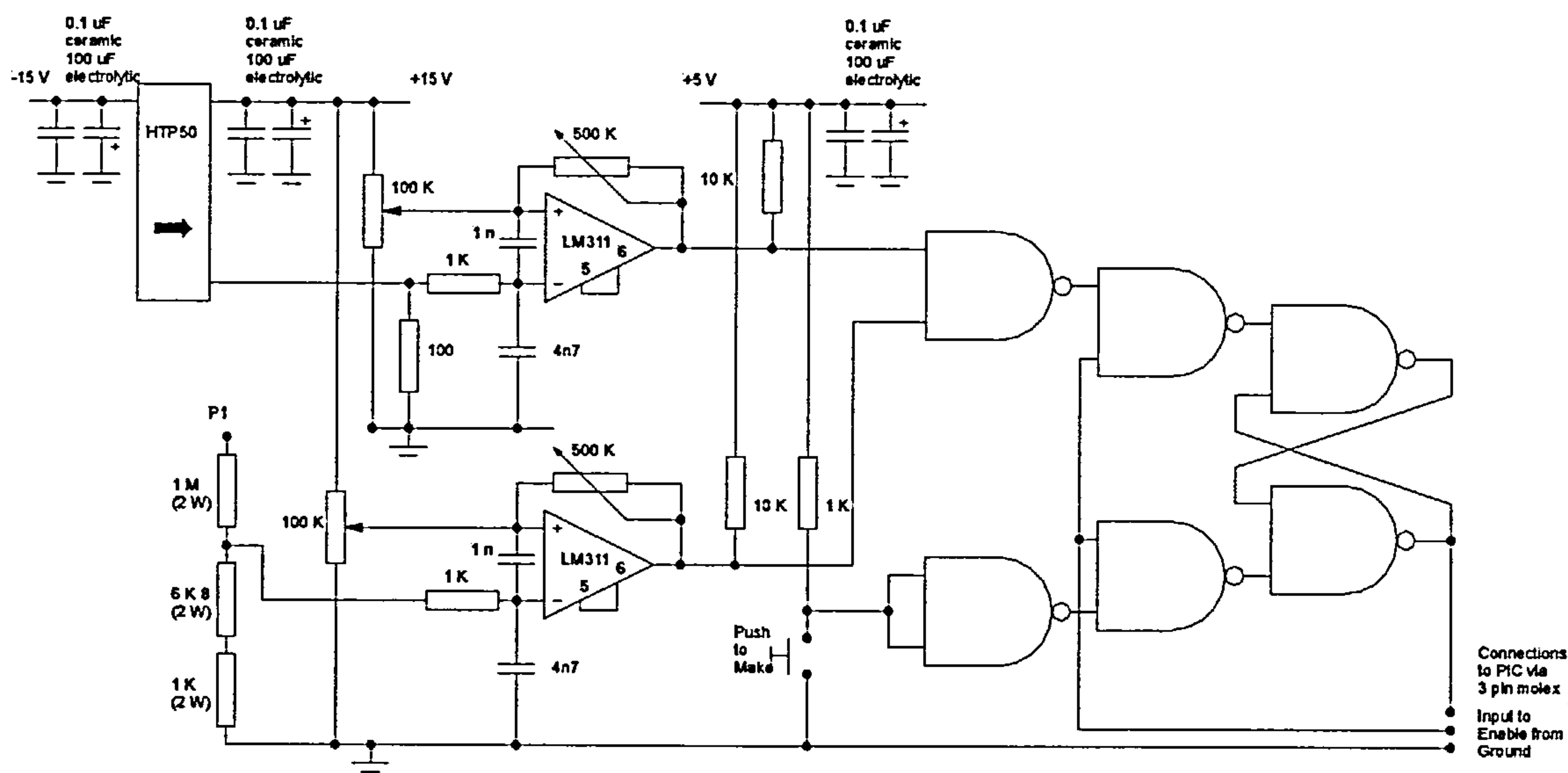


Figure 5.9 Drive-protection circuit

Owing to the unique operation of the new drive-circuit it was necessary to modify the combinational-logic processing the comparator signals. When initially switching on an IGBT a large current spike was detected in both armature-windings. This occurred because the other non-excited IGBT was switched on as a result of the large change in voltage, with respect to time, causing its winding to act like a short-circuited secondary-winding of a transformer. Although this current was not large enough to cause failure, because of the short period of time in which it was present, it did trip the drive-protection circuit. This problem was solved by means of an “enabled” flip-flop such that the comparator signals were ignored for a length of time that was long enough to exceed that of the current-spike. This period of time was found to be approximately 30 μs by analysing the armature current-waveforms at start-up as shown in figure 5.10. A time of 50 μs was programmed into the PIC micro-controller, such that after this time had been exceeded the flip-flop was “enabled”. This permitted the shutdown signals from the drive-protection circuit to be processed by the PIC micro-controller, and, ultimately shutdown the drive by turning off all of the active power-devices.

5.3.4 Component selection and drive manufacture

With regard to component selection the majority of components were unchanged from those used in the proof-of-principle motor. The only further main component was the shunt field-winding MOSFET. As the current drawn through the field-winding was less than 1 A, a relatively small device was required and an IRF840 was selected. In the series-motor the selection of

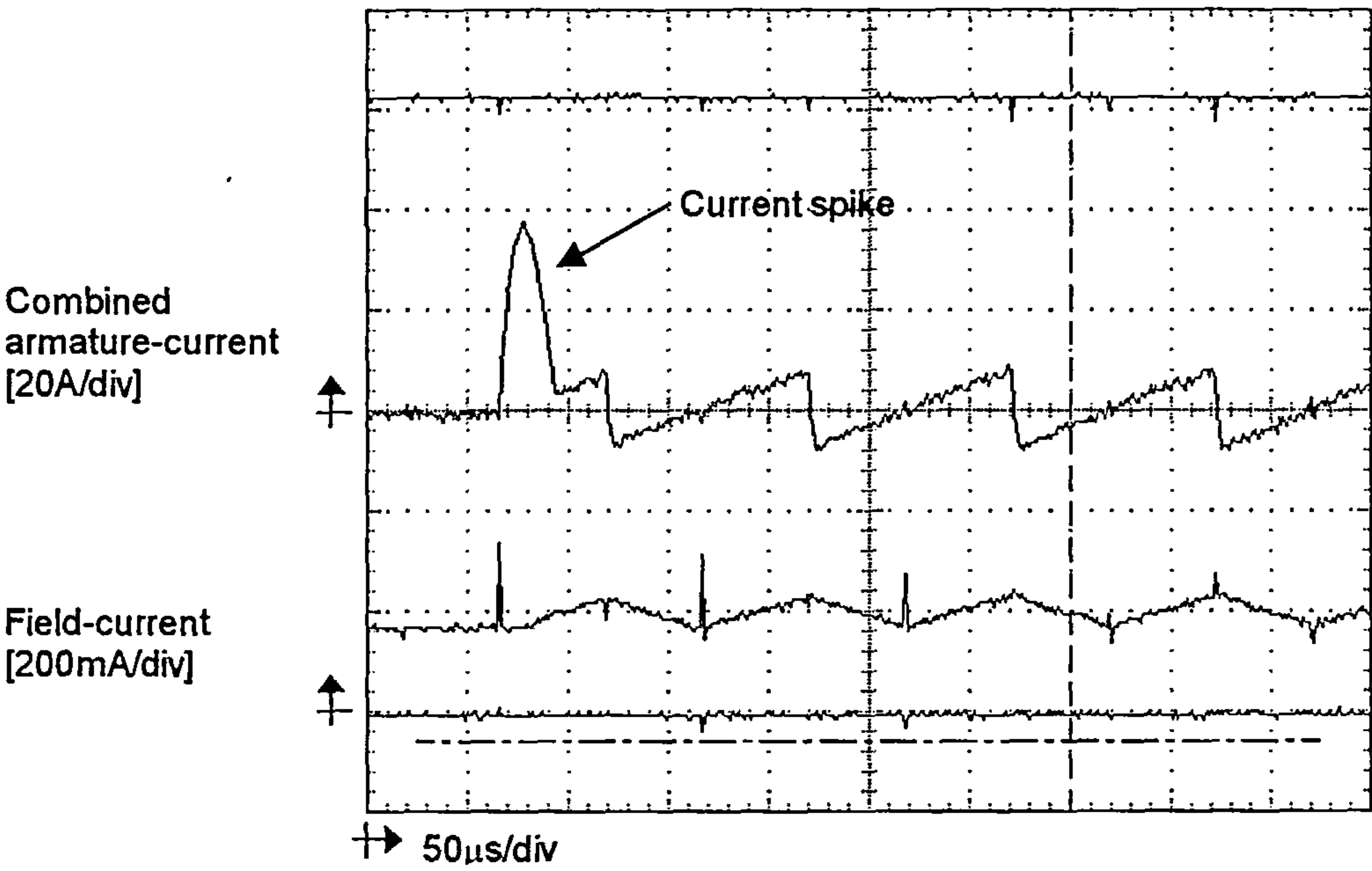


Figure 5.10 Initial combined amature-current spike

capacitors was very important in optimising the operation of the drive-circuit with the motor-performance. This is discussed, in detail, in Chapter 7.

From the proof-of-principle machine it was evident that the layout of all of the electronic components in the control and drive depended upon a number of factors. These were the electronic noise due to switching, the dissipation of heat from the power-devices and the snubber-circuit, and the ease of replacement of the components. In order to satisfy all of these problems a modular approach was used to give a practical drive-design as shown in the photograph in figure 5.11. The main control-board can be seen in the centre of the figure mounted vertically in an open-fronted metal box. This was used to overcome the potential for electronic-noise problems. On the main control-board the PIC micro-controller is to the left of the centre, whilst the gate-drive chips appear on the right. All integrated-circuits were plugged into sockets for ease of replacement, and all fly-leads were molex-connected to simplify connection. The main control-board was attached to the side of a heatsink that was deliberately oversized to accommodate all of the power-devices and the snubber-circuit components on top, as well. The temperature-coefficient of the heatsink was not optimised, although none of the devices ever exceeded 50 °C during the operation of the circuit. The power-devices were interconnected via the connection-block that can be seen to allow easy replacement of any that were damaged during the course of testing. The drive-protection circuit is shown in the foreground of figure 5.11, which was separate from the main control-board.

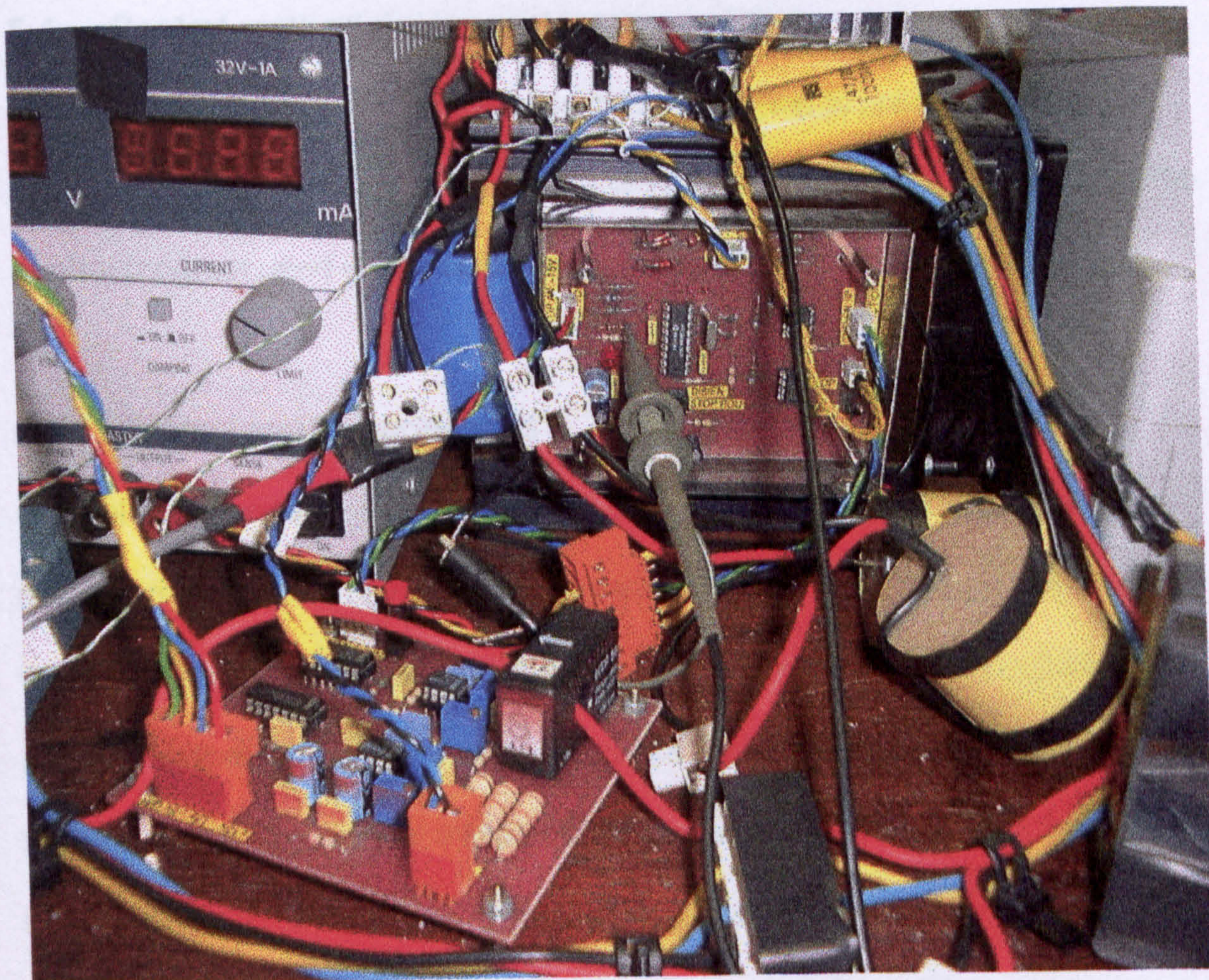


Figure 5.11 Drive and protection circuit

5.4 Control-method design and implementation

The design and implementation of the control-method is presented in this section. Dr Helen Pollock was responsible for implementing and designing the control program used with input from Professor Charles Pollock and myself.

5.4.1 Control-method principles

Control of any system is based upon the detection and processing of internal and external stimuli. The level of sophistication of control is dependent upon the number of inputs detected, via sensors, and the amount of conditioning and processing that can take place, so as to use these inputs productively. Owing to the limitation, by cost, of all selected components, the only available source of information to control the motor was the single-bit digital optical-sensor, which was used to sense the position of the rotor. No form of current-sensing device was used for the purposes of current-feedback control. In general, more sophisticated controllers include some form of current-sensing to implement current-chopping controlled-schemes. It could be argued that some form of current-sensing is essential to operation as there is the potential for over-current failure under certain operating conditions. Careful development of the control algorithms showed otherwise.

The optical-sensor was mounted on the non-drive-end stator end-bell and an evenly-spaced slotted disk was mounted on the rotor, as shown in figure 5.4, to form the position sensor. As the rotor turned an alternate-logic signal pulse

was produced, according to a tooth or a slot being present, such that the position of the rotor was given at a resolution of 90° (electrical) per digital state. The changing pulse-lengths gave the rate-of-change of position (speed). However, because the optical-sensor was only single-bit, the signal generated was a scalar quantity, and therefore information on rotational direction was unobtainable.

5.4.2 Selection of an appropriate control-method

Having established that the position-sensor could provide information to control the motor, an appropriate control-method, to satisfy each part of the specification, had to be selected prior to implementation. The specification could be broken down in terms of control into, on-line starting, delivery of load-torque, and braking.

On-line starting of the new flux-switching motor was not as straightforward an operation as it is for a universal-motor because of the susceptibility of the power-devices to high current-spikes. The amount of current flowing in the universal-motor, under starting, is not usually a problem for two reasons. Firstly, the armature-windings, commutator and brushes are usually capable of sustaining relatively-large inrush-currents without being damaged, and, secondly, the rapidly increasing back-EMF, due to speed, naturally suppresses the large inrush-current. The power-devices used in the power-converter of the new flux-switching motor were rated according to the continuous operation of the motor, and not to a current-level above the inrush-current. Rating the

devices based upon the complete range of operating conditions would have resulted in using large expensive devices.

The size of the inrush-current was dependent upon the resistance and inductance of the armature-windings, and the size of the inertia of the load that needed to be accelerated in the time specified. With a typical armature-winding resistance of $0.5\ \Omega$, to limit the mains-supply-voltage, the inrush-current easily exceeded the peak 90 A limit of the IGBTs. This current would have destroyed the devices and potentially the rest of the drive. Pulse-width modulation of the current was therefore necessary at start-up to limit current. As current was not being sensed the PWM scheme could only be implemented by using a closed-loop speed-control system rather than a closed-loop current-control system. An increase in speed corresponded to an increase of back-EMF, which naturally suppressed the current, allowing the duty-cycle of the PWM to rise accordingly. This increased the current, which increased the speed and then the back-EMF, thus repeating the cycle.

Testing the proof-of-principle motor had shown that the torque speed curve could be manipulated by controlling the current in the windings as expected. The most effective method to do this was found to be the reduction of the duty-cycle of the pulses applied to the IGBTs by cutting back the end of the pulse. A method for braking the motor was mentioned earlier in the Chapter whereby because the self-inductance of the windings was not designed to be exactly

constant with changing rotor-position, the motor could be braked by leaving one phase permanently-excited.

5.4.3 Design and implementation of selected control-method

With the range of operating conditions experienced by the motor it became apparent that a micro-controller had to be used. A relatively large amount of information had to be processed, and done rapidly enough to deliver accurate pulses of current to the armature-windings. This was beyond the capabilities of the previous simple combinational-logic controller. As with all of the other components, the selection of the controller was based on cost. The cheapest, and therefore simplest, controller was the 8-bit PIC micro-controller. The PIC had numerous useful features and it was also simple to use and program. The actual values of PWM frequency and duty-cycle were found using an iterative approach whilst testing. To avoid unnecessary drive-failure during testing the drive-protection circuit, integrated with the PIC control-scheme, was used.

The objective of the start-up routine was uncomplicated, the motor had to be accelerated in the shortest time possible to no-load speed without the failure of any power-devices or other components. Furthermore, start-up had to be reliable from any rotor position and in the correct direction of rotation. In terms of the actual routine this meant getting the duty-cycle of the PWM from its initial safe start-up value to one-hundred percent without allowing specified current-levels to be exceeded at any time. With the PIC micro-controller being used the simplest solution was to fix the PWM operating-frequency and change the

duty-cycle. The operating-frequency and duty-cycle were found experimentally as discussed in the following Chapter.

Having successfully started the motor the no-load speed had to be controlled. Testing of the proof-of-principle motor had demonstrated that the specified no-load speed was reached with less than half the supply-voltage applied. The no-load speed was limited by reducing the duty-cycle of the applied pulse to both IGBTs. More specifically the leading-edge of the pulse remained unchanged whilst the trailing-edge was moved. To control the motor when torque was applied to it the appropriate duty-cycle had to be used. The principle was simple such that as the torque was increased the speed decreased and it became necessary to increase the duty-cycle to maintain the torque, again the necessary values were found experimentally.

The operating conditions of the motor also lead to unwanted characteristics that had to, ideally, be removed to improve performance. The shape of the armature current-waveform determined the torque and also the losses induced in the snubber-circuit. Large tail-end armature-currents were undesirable as they caused regions of negative torque and excessive losses in the snubber owing to the large current at turn-off. Also the combined armature-current could not be allowed to become continuous, for there had to be sufficient time for the individual armature-currents to decay prior to commutation of the armature-windings. These problems were solved together by one solution, reducing the duty-cycle by moving the trailing edge of the applied pulse.

Delivering the desired torque whilst also avoiding the unwanted characteristics was a compromise in selecting the correct duty-cycle to apply to the IGBTs.

5.5 Conclusions

Following on from the testing of the proof-of-principle motor, this Chapter has detailed the design principles of the new flux-switching motor and its drive.

Information was taken from the specification, the mathematical model, and the simulation to produce a prototype ready for testing. Particular emphasis was placed on the development of the drive and its control. It was shown that the motor was capable of being controlled with a closed-loop speed-control system that interpreted current in proportion to speed under the different operating conditions without the need for current-feedback. The incorporation of the drive-protection circuit as a development-tool enabled testing and development-time to be significantly reduced.

Chapter 6 describes the testing of a new flux-switching motor in conjunction with the development of the control routines.

CHAPTER 6 TESTING OF A NEW FLUX-SWITCHING MOTOR

6.1 Introduction

The purpose of this Chapter is to describe the development of the new flux-switching motor and to measure the performance of the motor against the specification given in Appendix 1. This was achieved by obtaining results from a series of laboratory tests with a prototype motor using both static and dynamic tests. These tests are explained, in detail, in the following sections together with the results obtained and a subsequent analysis of the data. From these it was found that this first prototype motor needed to be developed and tested further, and subsequent prototypes were produced and work with these are described, in detail, in Chapter 7.

6.2 Test-rigs

The dynamic test-rig, shown in the photograph in figure 6.1, was designed for use with a range of motors by using interchangeable brackets that could be positioned along a fixed test-bed. Placed centrally on the test-bed was a water-cooled dynamometer capable of absorbing 12 kW. This was well in excess of the power of the 2 kW motor. The 12 kW specified on the dynamometer could be absorbed up to a maximum speed of 20,000 rpm and a maximum torque of 10 Nm, but not simultaneously, as this would give a power of nearly 21 kW. This dynamometer was chosen for two reasons, firstly, because the linear power envelope of the smaller dynamometer model below the one chosen was such that the high operational speed of the motor (15,000

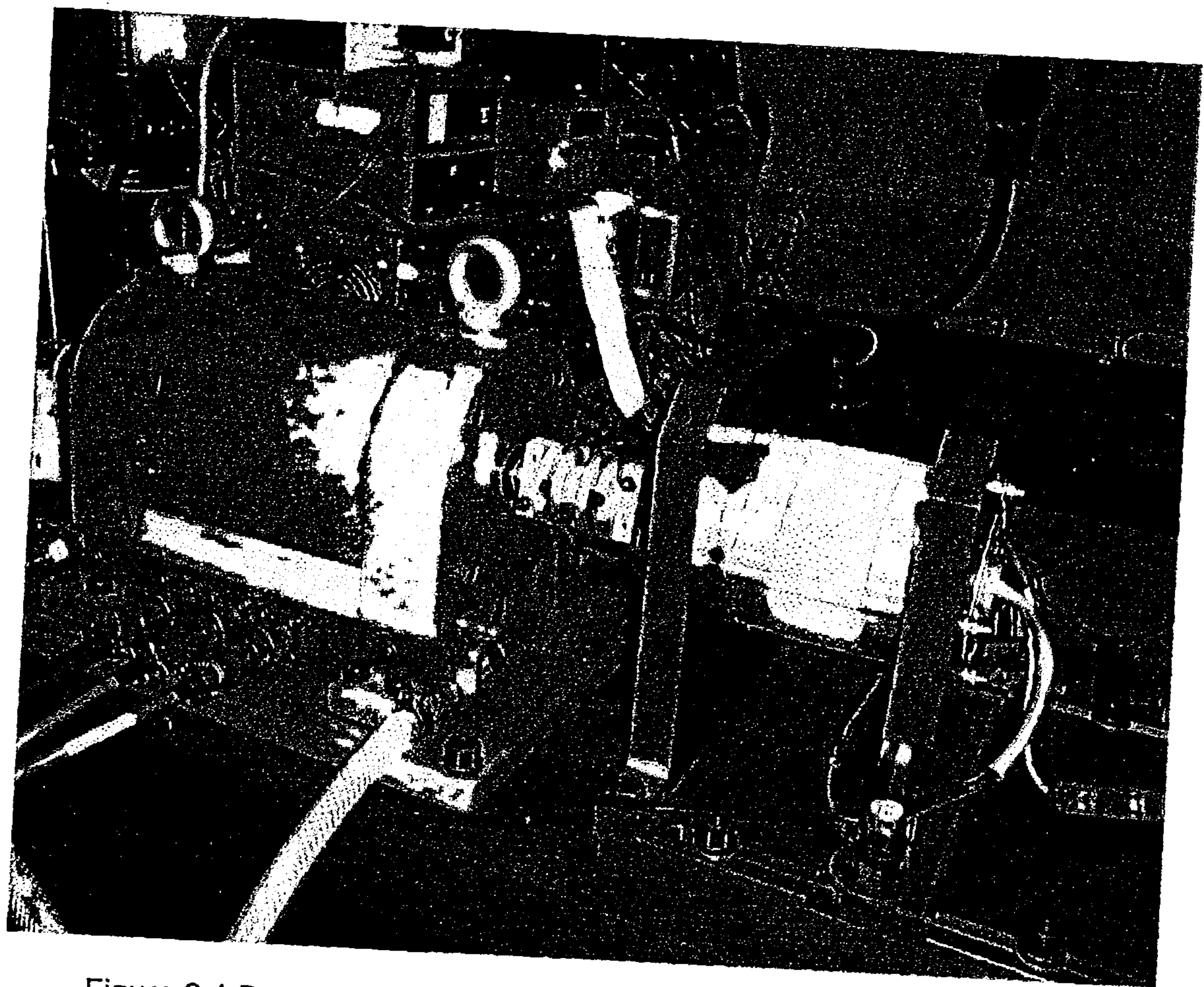


Figure 6.1 Dynamic test-rig set up

rpm) exceeded the maximum-speed that the smaller dynamometer model could withstand. Secondly, the larger dynamometer was chosen for the more practical reason of using the test-rig with other motors. At each end of the test-bed was a flat horizontal plate upon which a vertical plate could be bolted to form a bracket. The horizontal plates were a permanent part of the test-bed, whilst the vertical plates were interchangeable and specific to each motor tested. Alignment was maintained along the length of the test-bed by the use of a datum bar mounted on it. The dynamometer and brackets were retained with T-bolts that could slide within recesses along the length of the test-bed. One bracket was used to hold the motor under test, and another was used to hold an additional motor, that could be used to back-drive the motor under test enabling back-EMF tests to be carried out. The dynamometer had a shaft running through it allowing connection at either end. Connections to the motors were made via flexible couplings. During testing the controls for the dynamometer were manually operated. The torque output was interpreted as a voltage and read from a calibrated voltage-meter.

Additional equipment used to collect data included a four-channel digital-storage oscilloscope, a pair of current-probes, an isolated voltage-probe, a power-analyser and a pair of thermocouples.

Static tests were performed using a static test-rig that was of a similar design to the dynamic version. The test-rig consisted of a small test-bed with a dividing-head mounted at one end, and a horizontal plate, of the same design as in the

dynamic test-rig at the other. The vertical plate, with the motor attached, could then be mounted and connected securely to the dividing-head. The dividing head was used to rotate the rotor through precise angles such that the magnetic characteristics of the motor could be determined when the windings were excited.

6.3 Static tests

Static measurements of the motor’s characteristics were essential in assessing the degree of agreement between the experimental values and the predicted values used in the simulation. The following were measured using the method described.

6.3.1 Winding resistance

A measurement for winding resistance was required for two reasons, firstly to confirm the designed values, and, secondly, to enable the calculation of the copper losses incurred. Furthermore these losses needed to be split between the active part of the winding and the end turns. Each winding was thus measured with a four-probe low ohmmeter that used a Wheatstone bridge arrangement. All values recorded for the four prototype motors are shown collectively in Table 6.1 with details of the copper windings.

Motor	Winding	Resistance Ω	Turns	Wire Diameter mm
1 st Prototype Shunt motor with gearbox	Armature (each)	0.621	80	0.9
	Field	355.3	2520	0.2
2 nd Prototype Shunt motor with gearbox & revised armature	Armature (each)	0.425	68	1
	Field	343.5	2520	0.2
3 rd Prototype Shunt motor no gearbox	Armature (each)	0.453	68	1
	Field	344.6	2520	0.2
4 th Prototype Series motor same armature	Armature (each)	0.409	68	1
	Field	1.006	128	0.85

Table 6.1 Winding resistances and specification for the four prototype motors

The differences between the winding measurements for the motors can be explained. Each armature on the second prototype had a lower resistance than that of the first prototype because it had less turns and an increased wire-diameter. The wire-diameter was increased to fill the available slot area. The field-winding on the second prototype has a lower resistance simply because the process of winding the motor had been improved with the turns being tighter. Corresponding windings on the second and third prototypes should have been the same resistance, the slight difference was owing to the windings difference in tightness. The armature-winding on the fourth prototype has a lower value than that of the third prototype, because it was not separated into two coils as the other three prototypes had been. All measurements were

recorded at room temperature, minor differences might have occurred owing to fluctuations of room temperature.

6.3.2 Winding inductances and coupling-coefficient

Measurements of winding inductances and, more importantly, coupling-coefficient were required as these formed the basis of the mathematical model. By demonstrating that coupling-coefficient could be accurately and quickly predicted, using Finite Element Analysis, as described in Chapter 5, this new motor design could be rapidly prototyped. A single set of tests was carried out as the lamination design, and hence the magnetic characteristics of the motor, would essentially remain the same for it and future prototypes.

The magnetic-circuit of the motor, formed by the two fully-pitched field and armature-windings and the stator and rotor, can be represented as a transformer with a movable iron-core. The electrical-circuit diagram of such an arrangement is shown in figure 6.2 with an open-circuit test being performed. The primary winding is excited with an alternating current while the induced voltage, across the secondary winding, is measured. As explained previously in Chapter 3, the flux linking the armature-winding from the excited field-winding will be governed by the relative angle of the rotor within the stator. In the aligned and the unaligned positions the flux-linkage is a maximum and minimum value respectively. In the midway position between the aligned and the unaligned positions the flux-linkage is zero. Relating this back to the transformer, the amount of flux linking the secondary winding from the excited

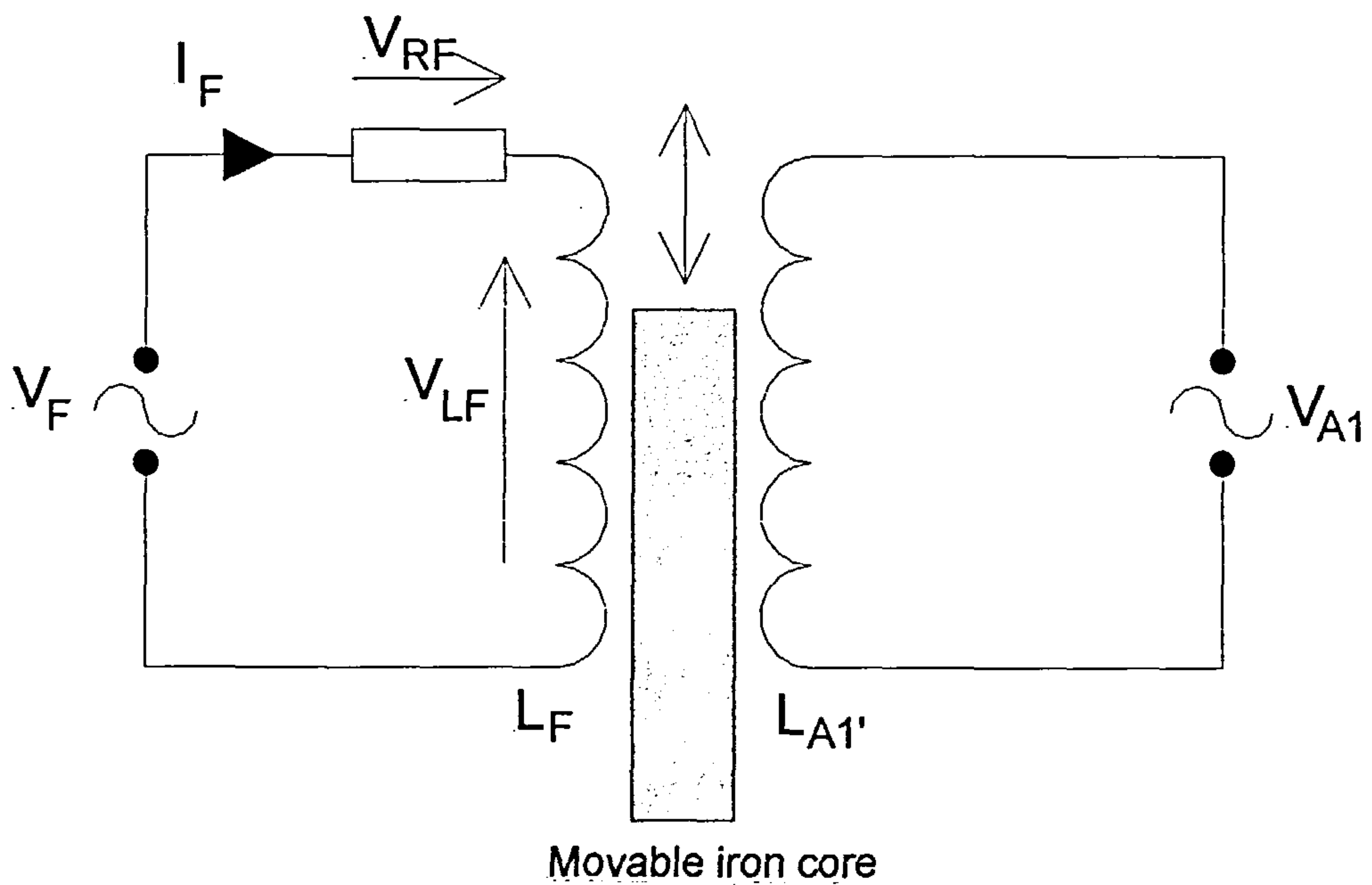


Figure 6.2 Electrical representation of the motor shown as a transformer with a movable iron core

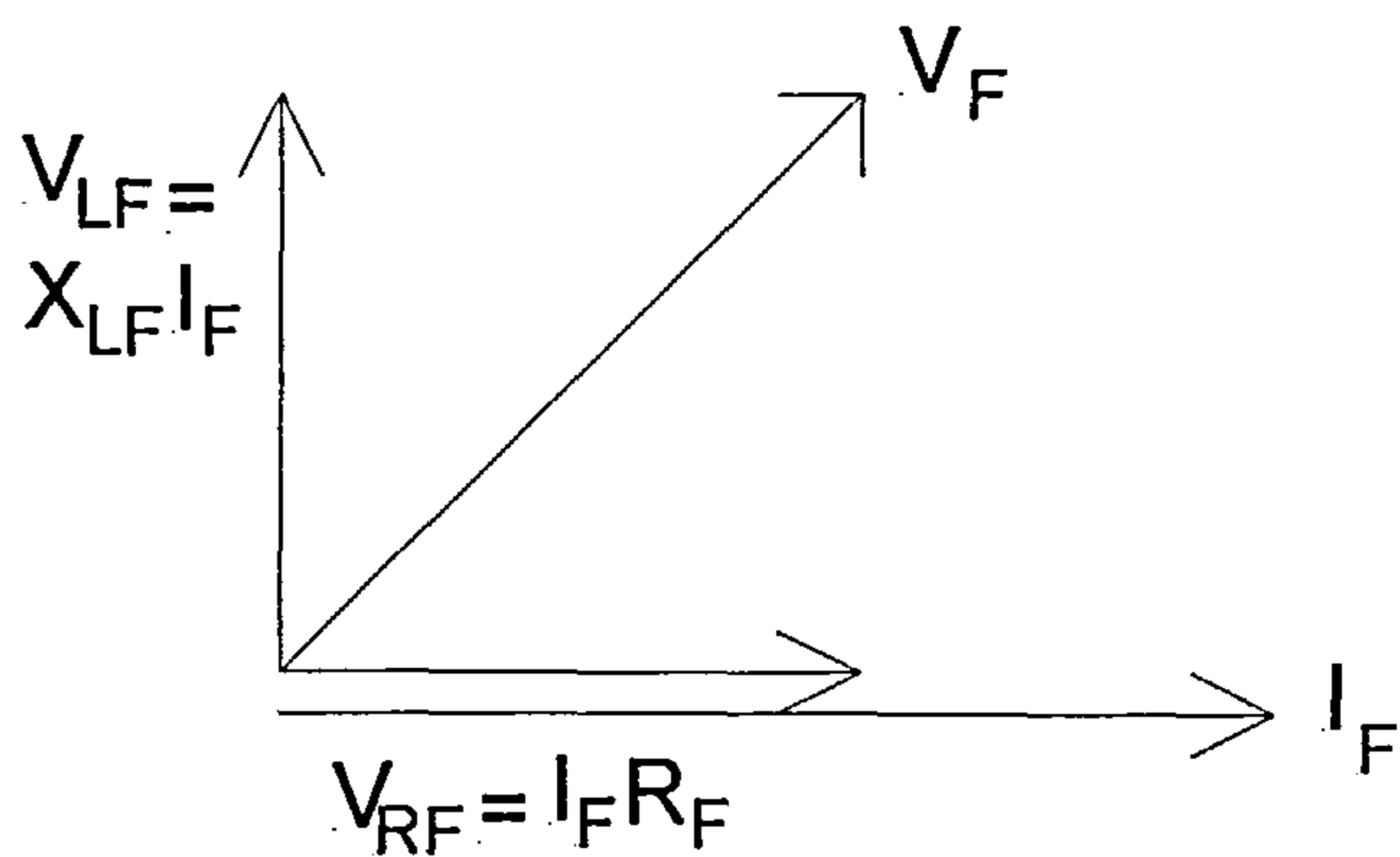


Figure 6.3 Phasor diagram of the electrical circuit given in Figure 6.2

primary will vary depending on how much of the movable iron-core is inserted through the primary and secondary coils.

The phasor diagram for the electrical circuit, given in figure 6.2, is shown in figure 6.3. To obtain a figure for coupling-coefficient k , the percentage of flux linking the two windings, the referred primary reactive-voltage needs to be calculated as follows

$$k = \frac{V_{A1}}{V_{LF}'} \quad (6.1),$$

$$V_{LF}' = V_{LF} \times \frac{N_{A1}}{N_F} \quad (6.2),$$

$$V_{LF} = \sqrt{V_F^2 - V_{RF}^2} \quad (6.3),$$

$$V_{RF} = I_F R_F \quad (6.4),$$

where N_F is the number of field-turns, with the field-winding used as the excited primary winding, and N_{A1} is the number of armature-turns on the first armature-winding, labelled 1, which was used as the secondary winding.

The motor was mounted on the static test-rig, as described earlier, and locked in the zero advance position. The zero advance position was determined as the reference position that corresponded to the zero-crossing of the back-EMF waveform. In this position the rotor was either in the fully aligned or unaligned position with respect to the stator. The field-winding (primary) was then excited with mains-alternating-current through a Variac to deliver a current such that an

MMF of approximately 1300 A t (Ampere turns) was used. The duration of the current excitation was kept to a minimum to restrict the heating of the field-winding. However, the temperature of the field-winding was measured via a thermocouple inserted in the winding to compensate the cold resistance measurement. Peak-to-peak values of field voltage, field-current and induced armature voltage were recorded. These measurements were repeated at 5° intervals over 45° (half an electrical-cycle). The measurements and calculations for coupling-coefficient k , self-inductance and mutual-inductance are given in Table 6.2. Figure 6.4 allows a comparison between the predicted values, from Finite Element Analysis, used in the modelling of the motor in Chapter 4, and the calculated values from Table 6.2. It can be seen that the correlation between the two is very good.

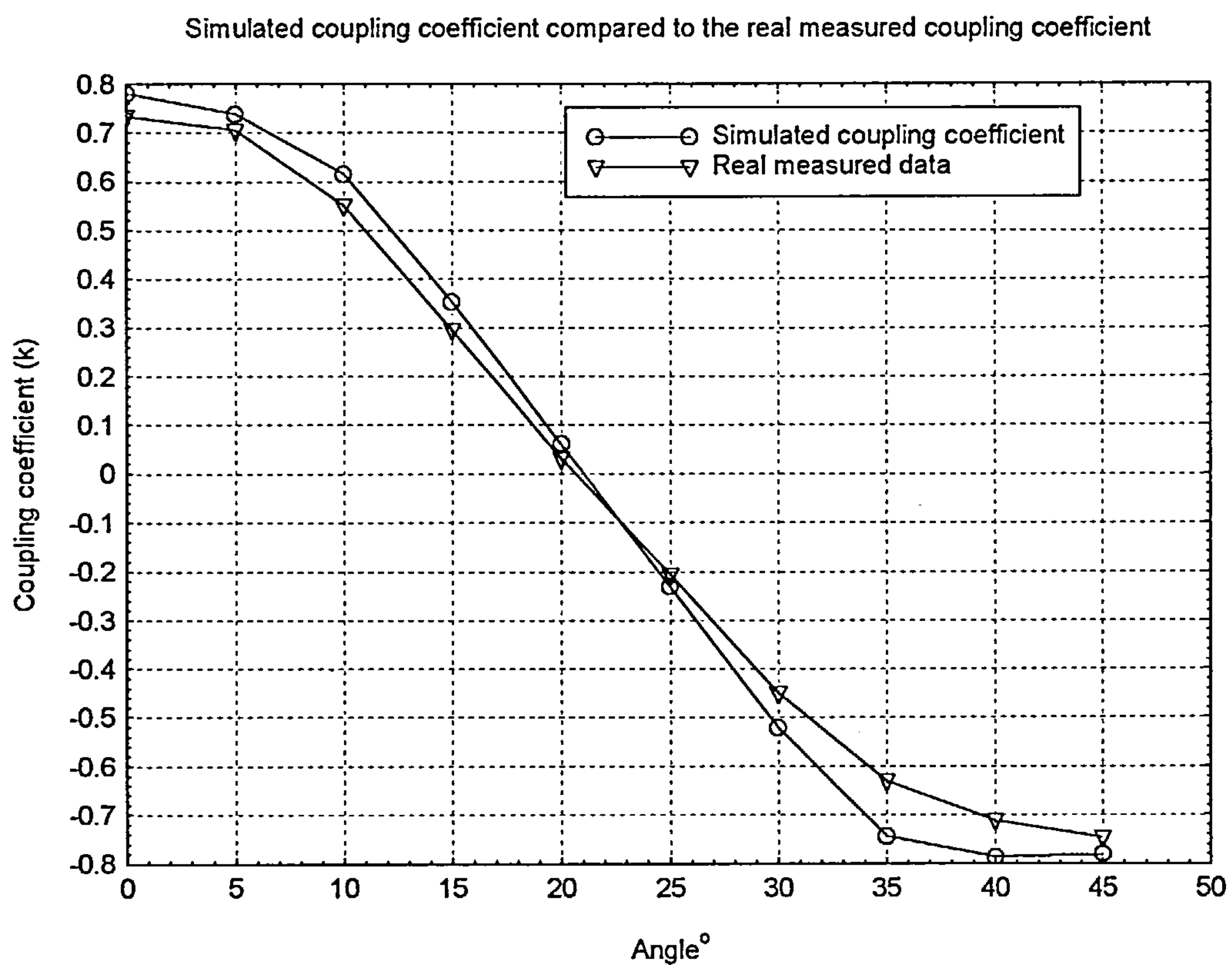


Figure 6.4 Comparison of the measured coupling-coefficient and that predicted using Finite Element Analysis

Rotor Angle	Primary Voltage V_F (p-p) V	Secondary Voltage V_{A1} (p-p) V	Primary Current I_F (p-p) mA	Field Resistance Ω	V_{RF} V	V_{LF} V	K	L_F H	M H	\mathfrak{M}_F H ⁻¹
0°	600	13.36	352	354	125	587	0.717	5.308	0.123	1196383
-5°	600	13.28	352	354	125	587	0.713	5.321	0.123	1193460
-10°	600	12.08	368	354	130	586	0.650	5.066	0.108	1253533
-15°	600	9.28	392	354	139	584	0.501	4.736	0.078	1340878
-20°	600	2.56	384	354	136	584	0.138	4.844	0.022	1310983
-25°	600	0.40	380	354	134	585	0.022	4.892	0.004	1298119
-30°	600	4.72	380	354	134	585	0.254	4.898	0.040	1296529
-35°	600	9.60	392	354	139	584	0.518	4.740	0.080	1339747
-40°	600	13.20	372	354	132	585	0.710	5.009	0.116	1267798
-45°	600	13.36	352	354	125	587	0.717	5.308	0.122	1196383

Table 6.2 Measurements and calculations for coupling-coefficient k , self-inductance and mutual-inductance. Negative angle owing to gearbox

The theory used to model this motor, given in Chapter 3, is predominantly formed around the rate-of-change of coupling-coefficient k with respect to position. According to the theory the back-EMF is constructed from a linearly scaled rate-of-change of coupling-coefficient. Differentiating the coupling-coefficient in figure 6.4 with respect to position gives the rate-of-change of coupling-coefficient as shown in figure 6.5. The differential of the real measured coupling-coefficient is different to the differential of the simulated coupling-coefficient. The reason being that both values were not exactly synchronised to achieve a commutation point corresponding exactly to the aligned/unaligned position. The amount that each was unsynchronised was also not the same. The commutation point corresponding exactly to the aligned/unaligned position is defined as the point at which the differential of the coupling-coefficient passes through zero at zero degrees.

6.4 Specification review

This section contains a review of the dynamic performance requirements of the specification, and the methods in which they were delivered in practice. The specification given in Appendix 1 was split into three main areas of requirements, namely performance, starting, and, braking which are reviewed in the following subsections.

6.4.1 Performance

The performance section of the specification stated that at the rated operating point the motor had to deliver 2.5 HP (1864 Watts) at a rotor torque of 2 Nm,

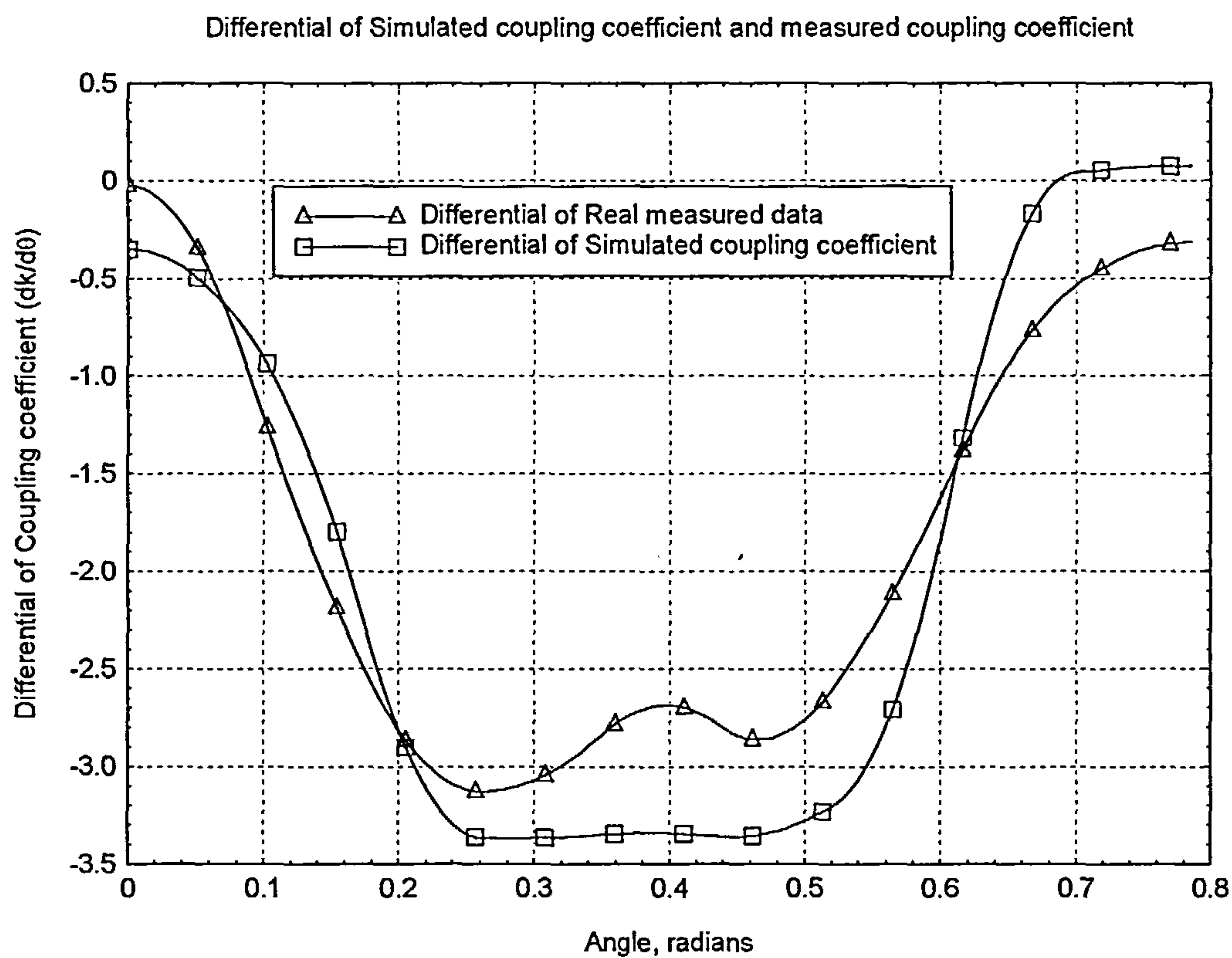


Figure 6.5 The rate-of-change of coupling-coefficient with respect to position, the differential of Figure 6.4

which corresponded to a speed of 9000 rpm. The idle rotor, or no-load, speed had to be capable of being maintained and restricted to 14000 rpm. A further maximum torque, or reserve-torque, of 3 Nm also had to be achieved for short durations of operation. Reserve-torque was necessary because of the nature of the load and the expectations of the user. The user detects decreasing availability of power as a reduction in speed, therefore speed must be reduced by a certain amount such that the user 'pulls out' before the motor stalls.

The motor also had to maintain a continuous rating of 1800 W power-input, whilst maintaining an 85 °C temperature rise on the windings. There was also a target efficiency of 75 % at the rated operating point. The motor was designed to function at the rated operating point. An understanding of how it would reach that operating point, and what the motor's natural torque-speed curve looked like was unknown, other than using the behaviour of the proof-of-principle motor for guidance. However, it was envisaged that the motor would be able to be controlled, within the torque-speed envelope, defined at the outer limits by the natural torque-speed curve, by cutting back the on-time of the IGBTs. Thus a controlled torque-speed curve could be delivered, as required, by the load and operating expectations.

6.4.2 Starting

The motor had to start from full-line voltage without drawing excessive current (maximum current = 60 A from the DC link) or having a noticeable time-delay. It also needed to accelerate smoothly to the no-load speed of 14000 rpm in

under 0.5 s. This had to be achieved with the correct inertia at the output shaft of 0.008 Kg m². The process of testing the starting of the motor was similar to that of testing the performance. A PIC micro-controller program was developed and tested with those characteristics that worked being kept and built upon to deliver in the next PIC program. This refinement continued until an optimum start-up routine was found. The only potential problem was whether, or not, the motor could be started in all rotor positions, a necessary requirement.

6.4.3 Braking

Braking was also a requirement, with a stopping time from, the no-load speed of, 1.5 s. The inductance profile of the lamination had been designed to enable a very simple braking operation of leaving a single winding permanently excited, however doing this in a series wound configuration was difficult because of the series connection.

6.4.4 Other deliverables

There were other deliverables that were not included in the specification, but they highlighted two very important points, firstly that the original objective of producing a low-cost drive had to be considered throughout, and secondly that the motor characteristics were designed for a specific-user application. The first point was discussed in detail in the previous Chapter. The second point demonstrates that the user also had qualitative expectations of the performance, such as a feeling of power, acceleration, and no unexpected feedback from the motor.

6.5 Dynamic testing of a prototype motor

The significant dynamic tests carried out with this prototype motor are presented in chronological order to demonstrate the developmental process taken. The developmental process itself was based upon designing a PIC micro-controller program (as discussed in Chapter 5) that would deliver the desired torque-speed curve from the capabilities of the motor. Each change in the PIM micro-controller program was tested and built upon until a set of optimum operating conditions had been reached. As mentioned at the start of this Chapter it was found that this first prototype motor needed to be developed, and tested further, as a result of design changes. This meant using subsequent prototypes that are described in detail in Chapter 7. This prototype motor was configured to operate with a shunt wound field-winding.

6.5.1 Initial operational tests

The initial operational testing phase was carried out to establish the operational characteristics of the motor, how it behaved, and how the PIC micro-controller program affected the motor performance. By the end of this phase of testing the method of advancing the commutation angle of the motor had been decided and the speed limitation was implemented successfully such that more detailed power tests could be performed.

i Limitation of no-load speed

Testing of the proof-of-principle motor had shown that one method of limiting speed was to cut back the on-time of the IGBTs as described in Chapter 4.

The correct amount of on-time was found by testing the motor at its no-load speed at 240 V DC and increasing or decreasing the time as necessary.

Limiting speed by removing the latter half of the current pulse also removed the relatively high turn-off currents, thus reducing the switching and snubber-circuit losses. Figures 6.6 and 6.7 show the oscilloscope waveforms recorded at a no-load speed of 11200 rpm at full volts for two separate tests. With regard to figure 6.6, speed was measured on the oscilloscope as frequency from the position-sensor signal, before being converted to rpm with a simple calculation. The DC field-current was assumed to be constant in the mathematical model. However, figure 6.6 shows that there is a degree of ripple on the field-current which, is due to the combination of self-induced and mutually-induced effects.

Figure 6.6 also shows the two unipolar currents in each of the bifilar armature-windings. The current sensor giving the bottom waveform was reversed, such that the current measured was negative. The current in one half of the bifilar-winding was measured in this way to demonstrate that the corresponding MMF opposed that in the other half of the bifilar-winding.

Figure 6.7 shows another set of no-load waveforms. The difference from figure 6.6 is that the unipolar bifilar-armature-currents are combined in one waveform. This is the same armature-current that would flow in a single armature-winding,

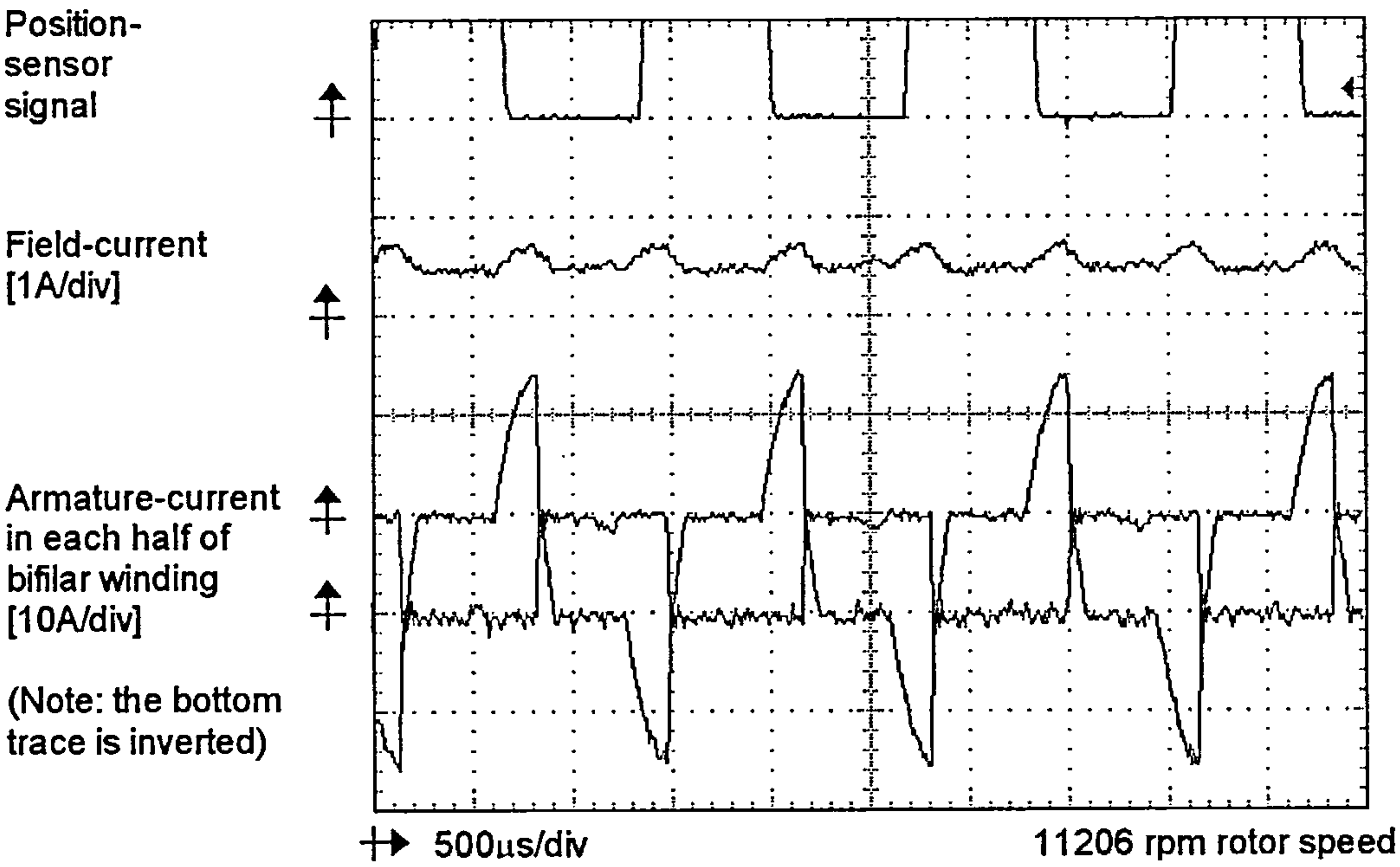


Figure 6.6 Power Test V no-load speed waveforms

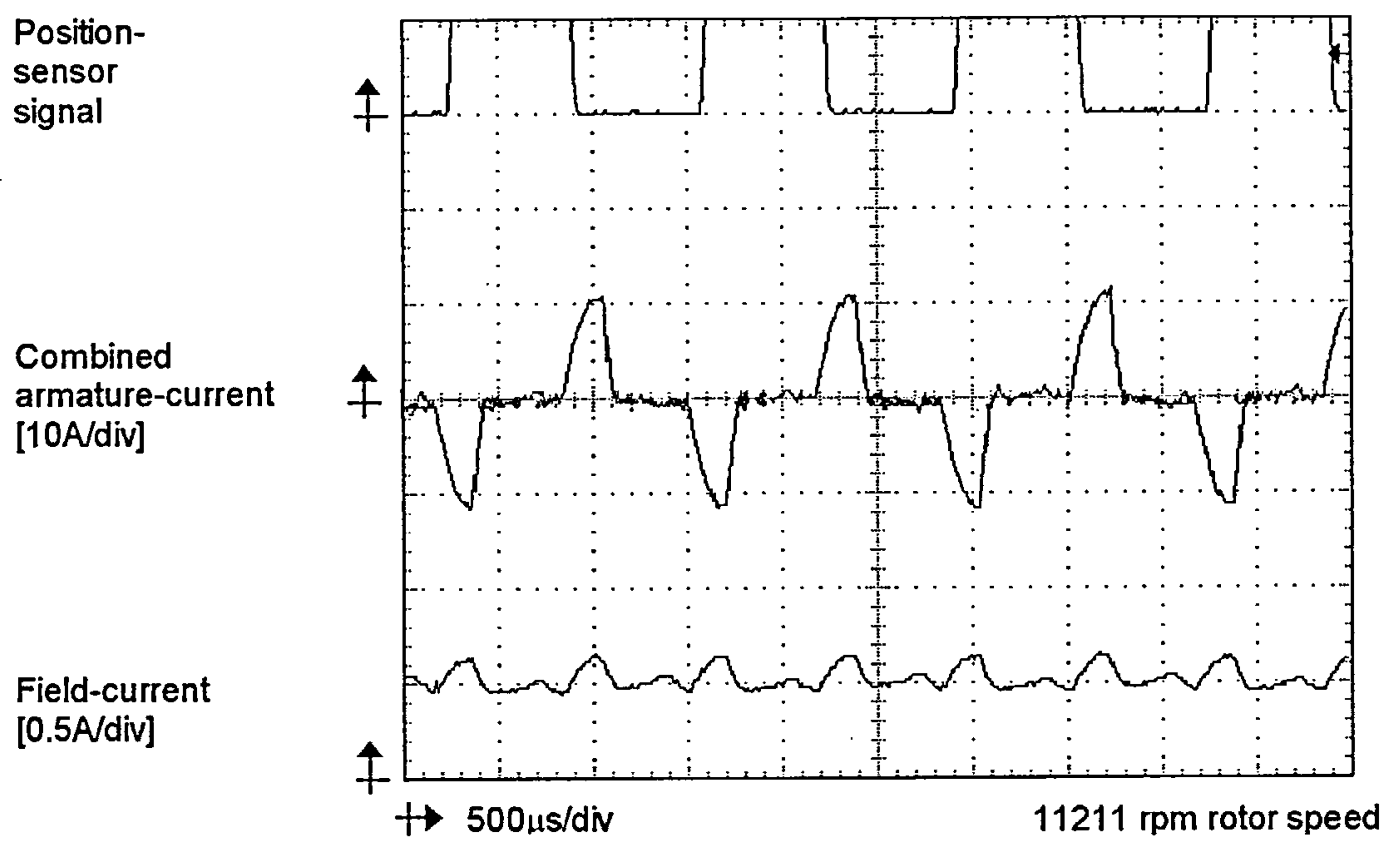


Figure 6.7 Power Test VI no-load speed waveforms

of a motor of this design, with a power converter supplying bipolar-current. Passing both bifilar armature-current-carrying conductors through the same current transducer in opposition produced this combined current. Comparing the duty-cycle of the combined armature-current to the position-sensor signal shows that to limit the speed of the motor to 11200 rpm, with this particular advance-angle, the duty-cycle of the gate-drive signals to the IGBTs needs to be approximately 30 %.

ii Choice of method of advancing the commutation angle

The change in logic state of the position-sensor caused by moving from a slot to a tooth (or vice versa) is referred to as an edge. An edge was synchronised with the zero-advance position so that the commutation of the armature-current coincided with a zero back-EMF. The slotted disk was fixed to the stator giving a position that remained constant. However the optical-sensor could be physically moved relative to stator thus changing the position of the position-sensor making advanced or retarded commutation possible. This is referred to as changing the static-advance-angle. Advanced commutation occurs prior to the zero back-EMF position and is discussed in terms of positive advance-angle. Retarded commutation occurs after the zero back-EMF position and is discussed in terms of negative advance-angle. Dynamic advance is also possible by advancing or delaying the edge electronically, calculating the speed of rotation and moving the edge by a related time is one method of doing this. Advanced commutation is required to allow the current to build-up in overcoming the winding inductance to a level in which it becomes useful.

Previously from testing the proof-of-principle motor, Chapter 4, it had been thought that a static advance of 90° (electrical) was the optimum setting for the motor at the load point. However setting this amount of static-advance, caused problems when starting the motor, in some cases causing the motor to run in reverse. Therefore it was initially decided to set the static-advance to zero to ease starting and to advance the gate-signals electronically with respect to the position-sensor signal and with increasing speed, such that the 90° (electrical) advance was reached at the load point.

This method of advancing the commutation angle of the motor was ruled out early on because it proved computationally intensive for the PIC micro-controller. The easy solution to overcome this was to increase the processing size of the micro-controller, however the original aim of producing a low-cost drive had to be adhered to so a larger, more expensive, micro-controller was not used. Maintaining the advance-angle accurately was also very difficult to achieve using this method.

iii Back-EMF waveforms

The motor was set up on the dynamic test-rig and it was back-driven in its direction of rotation at a speed of 9000 rpm, via the gearbox, using a stepper motor. The field-winding was connected to a separately-excited power supply that was steadily increased from zero to 180 V, with the armature-windings being left open-circuited. As the rotor turned, within the flux produced by the

field-windings, a back-EMF was generated across the armature-windings.

Figure 6.8 shows the back-EMF waveforms obtained. It is important to note that the supply voltage to the field-windings of the motor could not be increased above 180 V as the load torque then became too great for the stepper motor to drive so it stalled.

According to theory the back-EMF is a linearly-scaled version of the rate-of-change of coupling-coefficient, as given earlier in this Chapter. In practice however this is not true, as can be seen by comparing the back-EMF in figure 6.8 with the rate-of-change of coupling-coefficient in figure 6.5. The reasons for this are that the field-current is not constant, due to changing self-inductance effects, and that no saturation effects were taken into account in the theory. The most important aspect was demonstrated in that the motor behaves as a DC motor, by generating a bipolar back-EMF across the armature-windings.

6.5.2 Power tests

With the initial operational tests completed the motor was tested, under load, in order to observe its power producing capabilities. The aim was not only to reach the desired power-output, but also to deliver power efficiently. In practice this required the optimum combination of advance-angle and duty-cycle being identified.

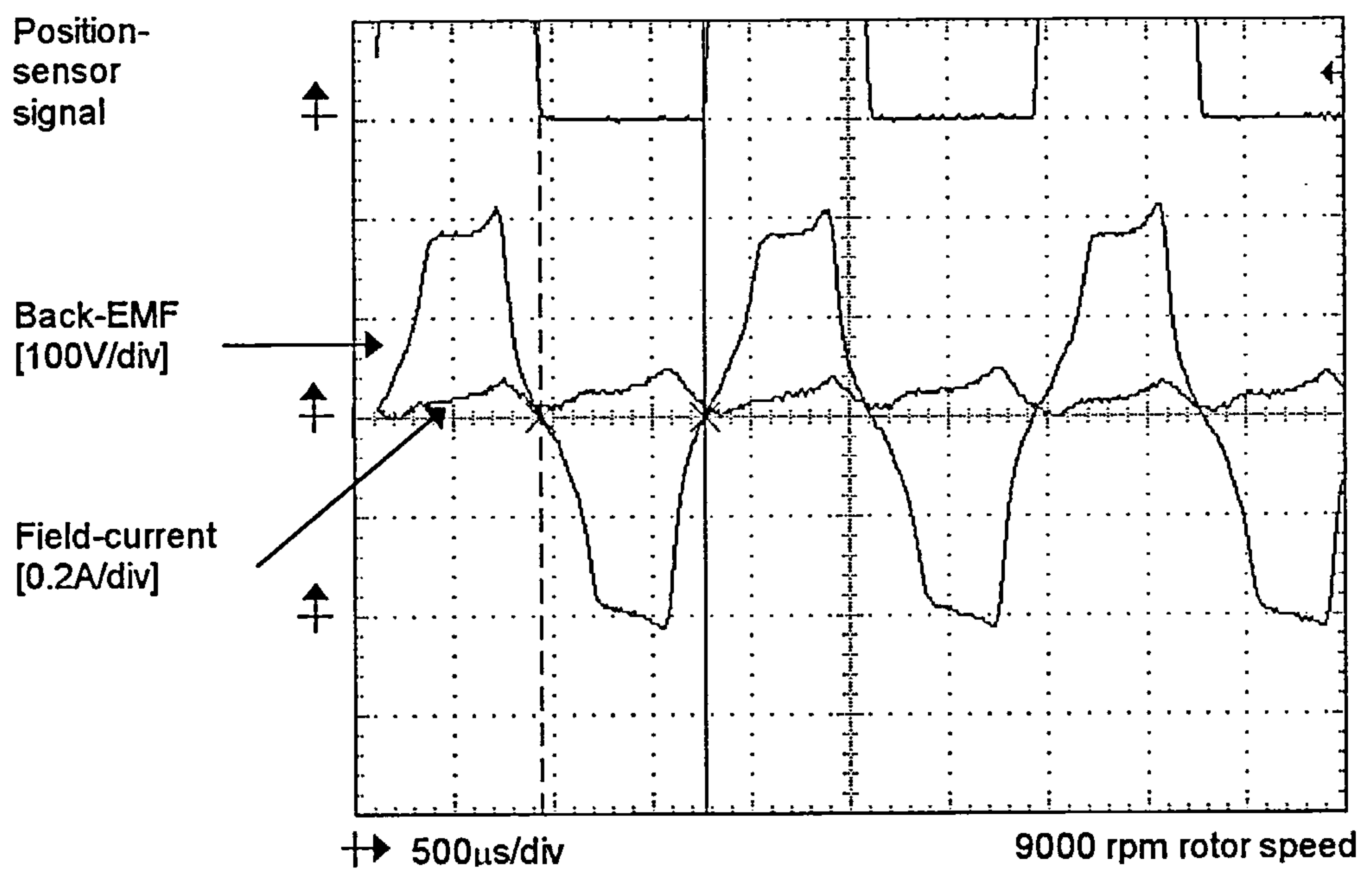


Figure 6.8 Back-EMF waveform generated across one half of the bifilar armature-winding

i Duty-cycle

The optimum duty-cycle of the IGBTs had to be set such that the current in one half of the bifilar armature-winding could rise from zero, and return to zero, before the other IGBT was excited. That is, there was a minimum dead-time between the current falling in one half of the bifilar winding before it began to rise in the other half of the bifilar winding. If current were allowed to flow in both halves of the bifilar winding simultaneously, the net effect would be regions of either zero or negative torque. The setting of the duty-cycle largely depended on the level of the current in the winding when the corresponding IGBT was switched off, which was itself dependent on the advance-angle.

The motor was tested with a static advance of 8° (mechanical) using two separate PIC micro-controller programs that were designed to deliver a duty-cycle of $3/4$ and $7/8$ at the specified load speed of 9000 rpm. Figures 6.9 and 6.10 show the respective current waveforms at an approximate rotor-speed of 9630 rpm (642 Hz). Both sets of waveforms appear to be the same. However, referring to the gate-signals applied to one of the IGBTs, it can be seen that in figure 6.10 the duty-cycle is greater. As expected, increasing the duty-cycle increases the torque due to the longer current duration, as is evident in figure 6.9 corresponding to a torque of 1.0 Nm, and in figure 6.10 corresponding to a torque of 1.2 Nm. Figure 6.11 gives a comparison between a $3/4$ and a $7/8$ duty-cycle in terms of the torque-speed curve. The $7/8$ duty-cycle gives approximately 20 % more torque than the $3/4$ duty-cycle does in the latter half of the curve. Also, if the curve is projected with the same gradient, it can be

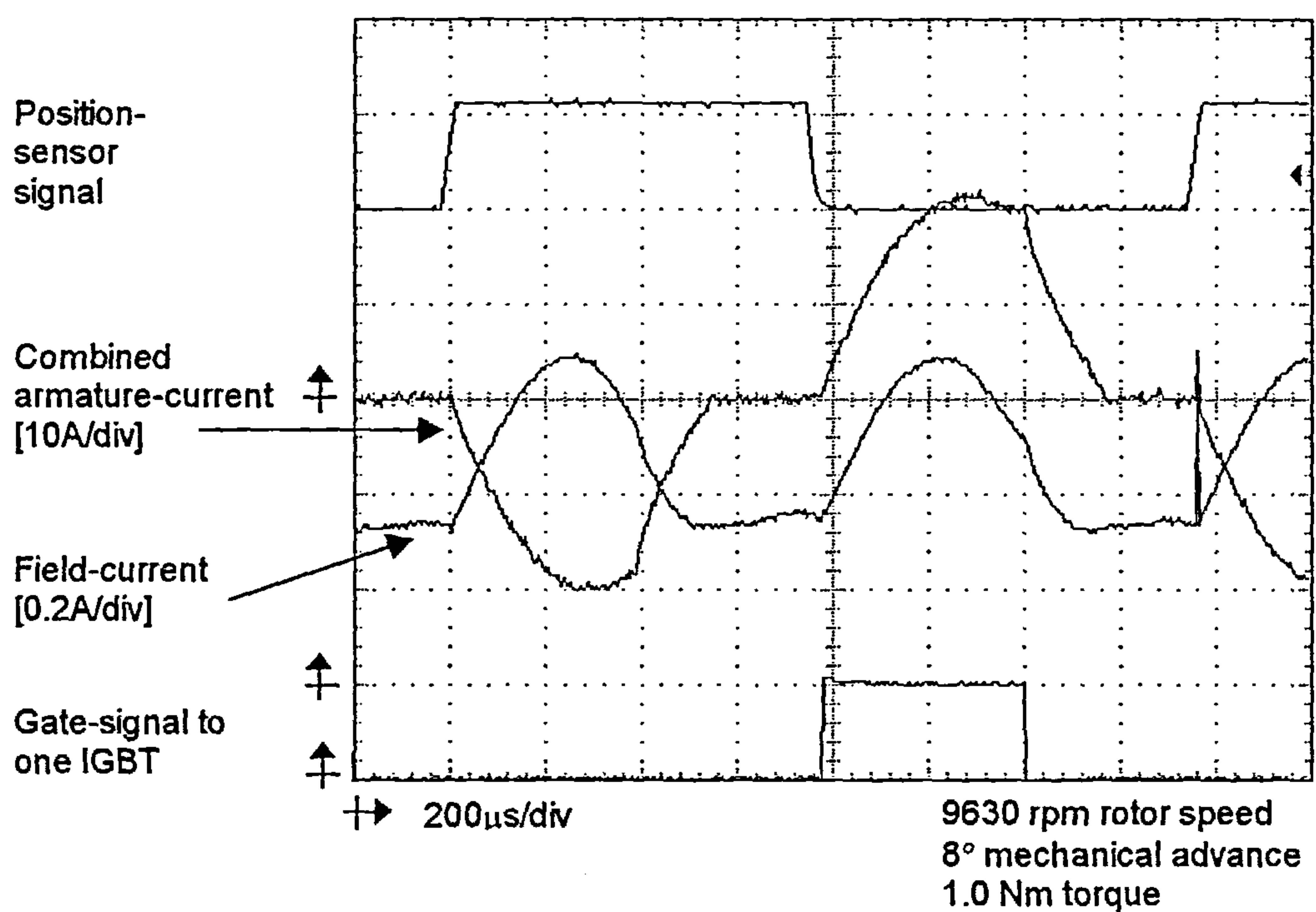


Figure 6.9 Power Test XIII, 3/4 duty-cycle current-waveforms

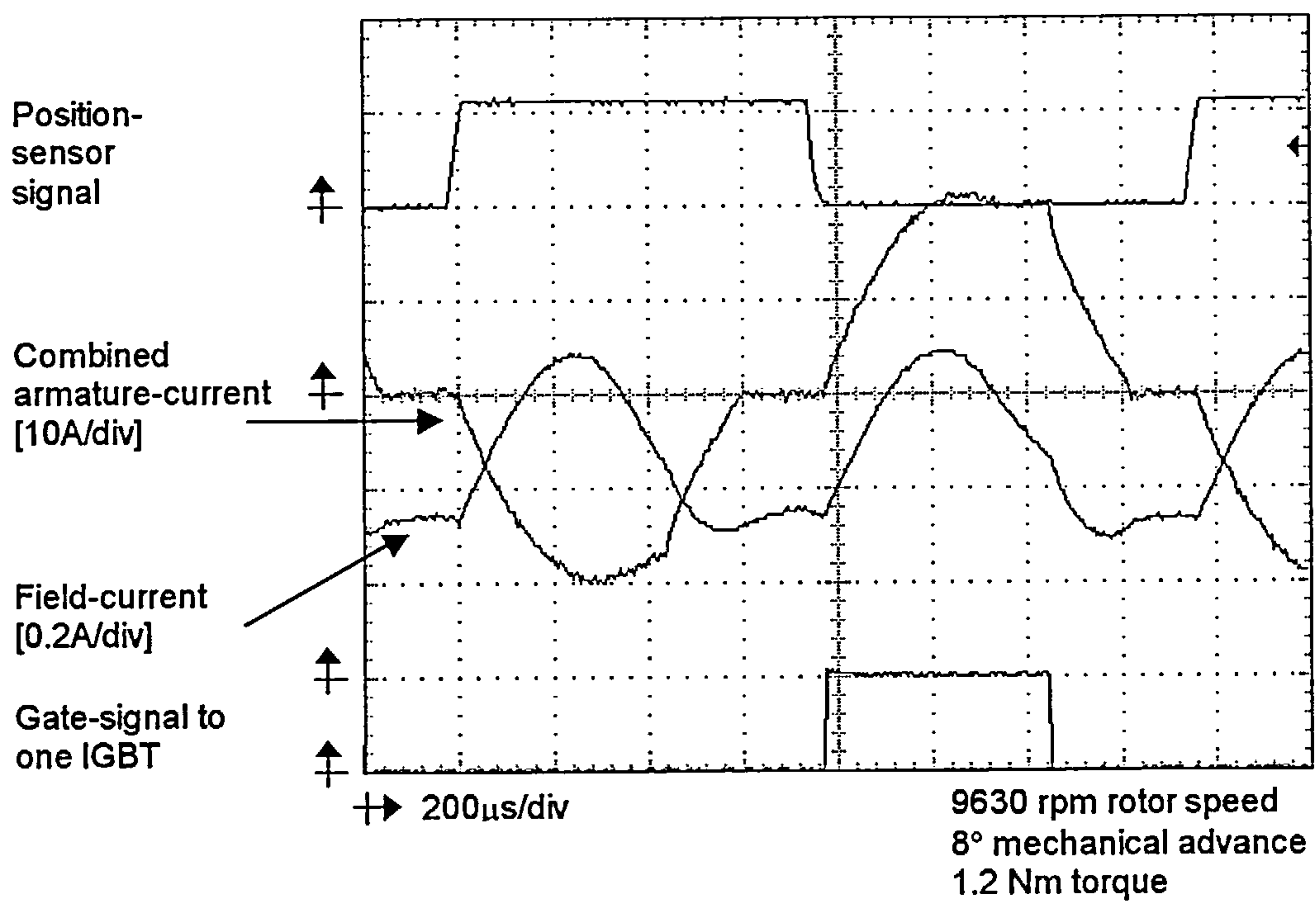


Figure 6.10 Power Test 14, 7/8 duty-cycle current waveforms

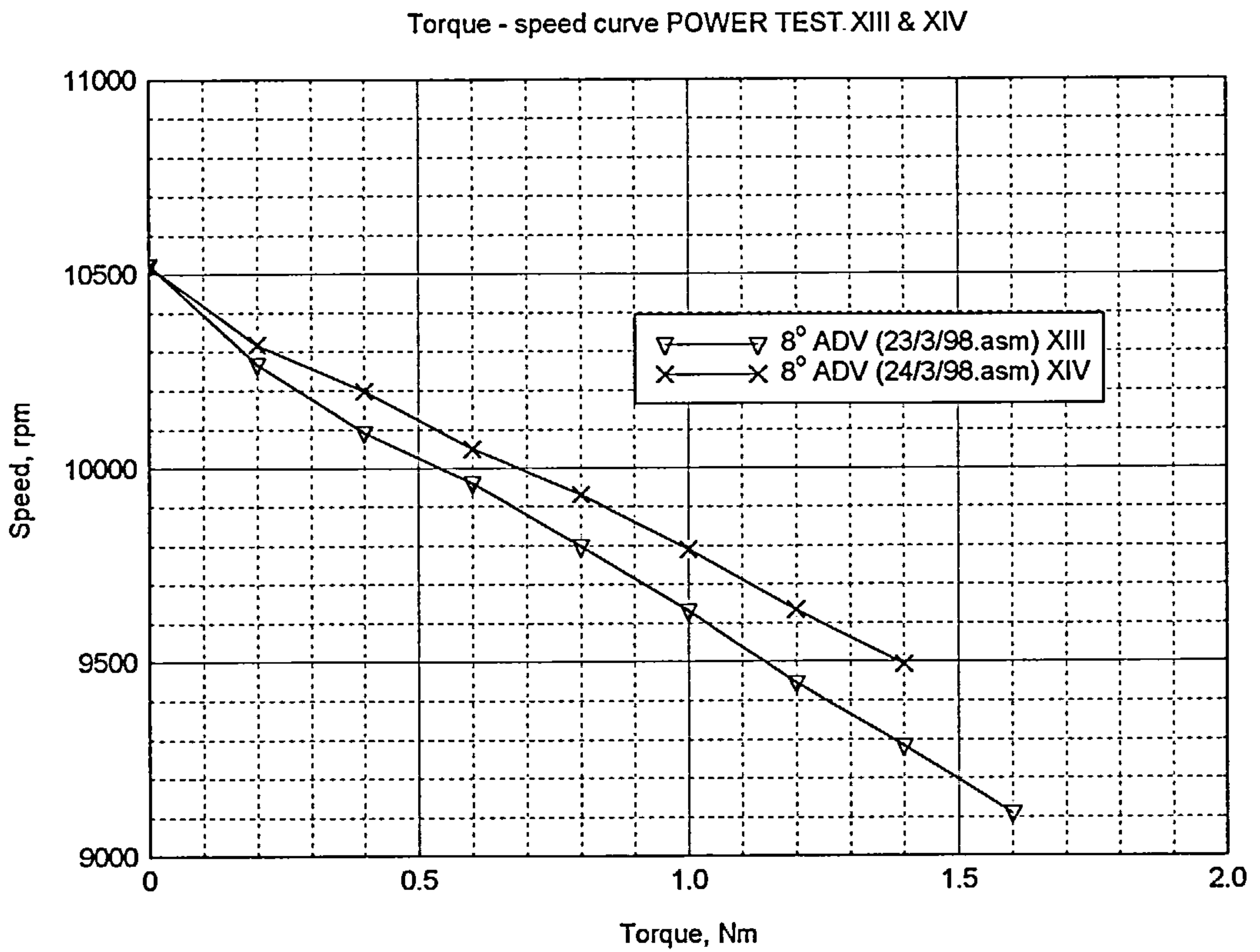


Figure 6.11 Power Tests XIII and XIV, Torque – speed curves comparing 3/4 duty-cycle with 7/8 duty-cycle using an advance-angle of 8° (mechanical)

seen that the target load point would have been hit assuming that the operating characteristics remained the same.

ii Advance-angle

In conjunction with the tests to find the best duty-cycle, the optimum static advance setting needed to be identified. Previously, from testing the proof-of-principle motor it was found that the optimum setting of the advance-angle was 90° (electrical) for delivering the highest torques. Testing began, with this first prototype, with the same advance-angle reached electronically as described earlier. An electronic advance method had to be used as starting proved very difficult using a static advance of 90° (electrical), or 22.5° (mechanical). The results showed that torque could be delivered at this advance-angle but, that the armature-current was high and efficiency did not reach above 60%. Theory contradicted the testing of the proof-of-principle motor as it suggests that to obtain the optimum torque the back-EMF and armature-current waveforms need to be synchronised. Therefore lower advance-angles were tested once again to see if they were more suitable.

Figure 6.12 shows the torque-speed curves for the four power tests X, XI, XII & XIII carried out at 5° , 6° , 7° and 8° mechanical advance-angles respectively. Each extra degree of advance corresponds to an approximate 100 rpm rise in speed for the same torque. Figure 6.13 gives the associated torque-efficiency curves for these power tests, they show that there is less than a 2 % difference in efficiency over this range of advance-angles. In conclusion it can be seen

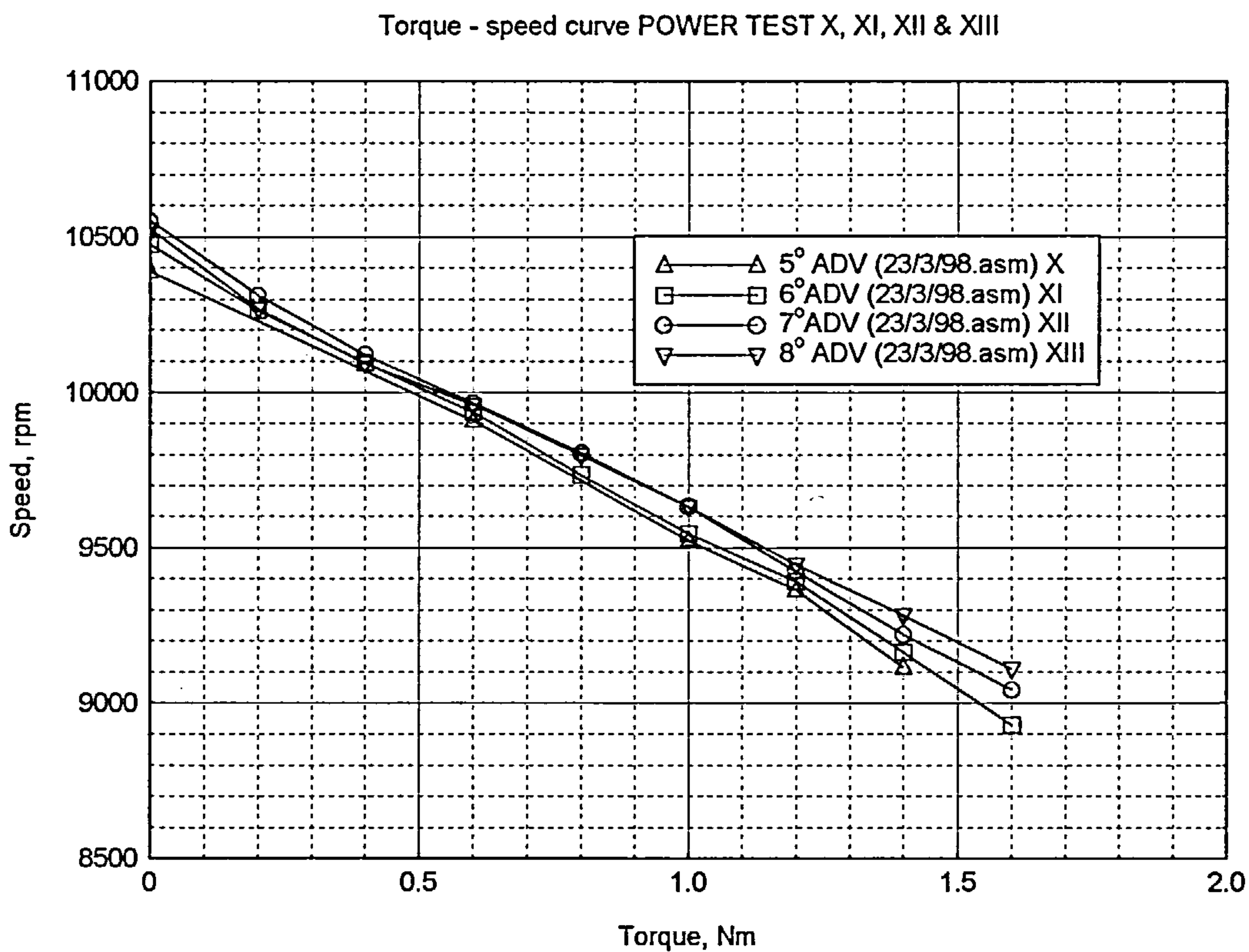


Figure 6.12 Power Tests X, XI, XII and XIII, Torque – speed curves comparing advance-angles of 5°, 6°, 7° and 8° respectively using the same PIC micro-controller program

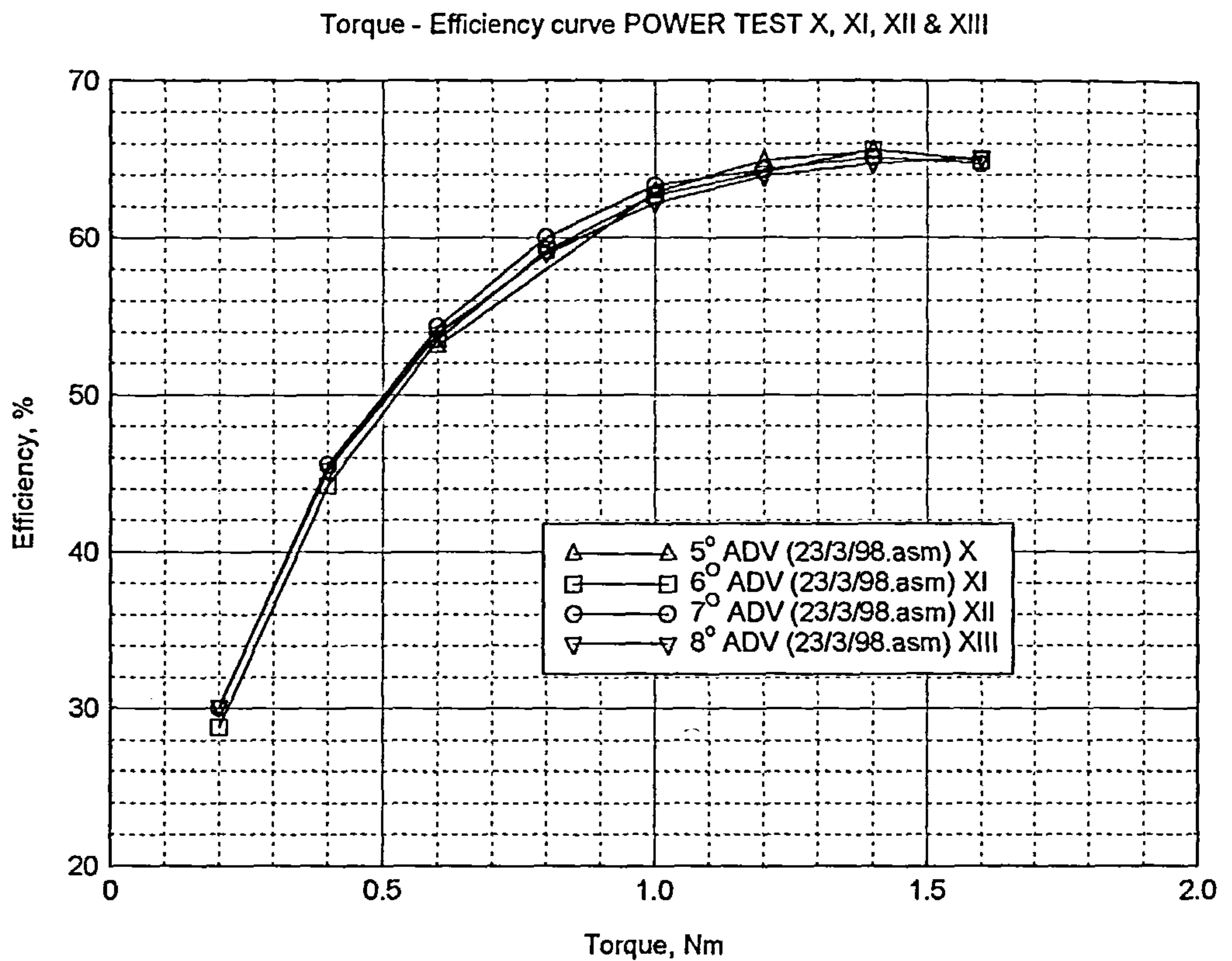


Figure 6.13 Power Tests X, XI, XII and XIII, Torque – efficiency curves comparing advance-angles of 5°, 6°, 7° and 8° respectively using the same PIC micro-controller program

that for the same speed, torque increases when advance-angle is increased. It was decided that, as there was no real improvement in advancing the commutation angle further, testing was to continue with these lower settings.

iii The natural torque-speed curve

The projected torque-speed curve of power test XIV would have hit the desired operating point assuming that the motor would have followed the same linear torque-speed characteristic. However, this was not to be. Having also achieved a torque of 1.6 Nm on the same linear function, the next value of torque aimed for was 1.8 Nm. Before this load could be fully applied the motor stalled unexpectedly. To understand why this stall had occurred the motor was tested with a greater torque resolution between 1.6 Nm and 1.8 Nm, as shown in the torque-speed curve from power test XX in figure 6.14. The torque-speed curve followed a linear characteristic up to a torque of 1.7 Nm, and then at 1.74 Nm another measurement was taken and plotted. As can be seen there is a significant drop of at least 200 rpm from where the torque-speed curve was expected to be.

The corresponding current waveforms for the last four torque measurements of power test XX are given in figure 6.15. Referring to the current waveforms at the torque of 1.4 Nm, both the positive and negative halves of the combined armature-current waveform are balanced with a significant period of on-time remaining. As with all the previous tests the ripple on the field-current waveform, which is caused by the mutually induced effects from the changing

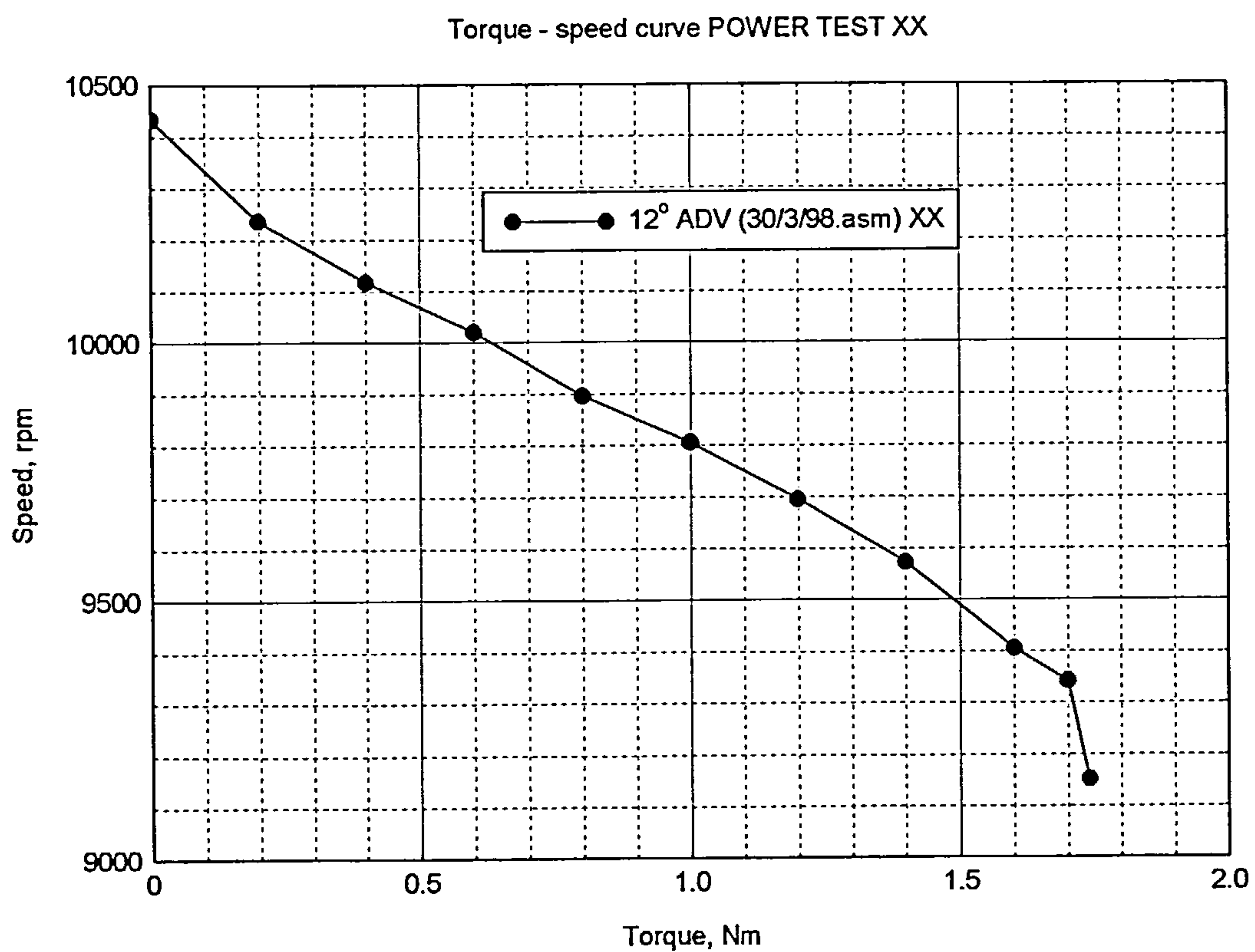


Figure 6.14 Power Test XX, Torque – speed curve using an advance-angle of 12° (demonstrates the sudden drop in torque-output)

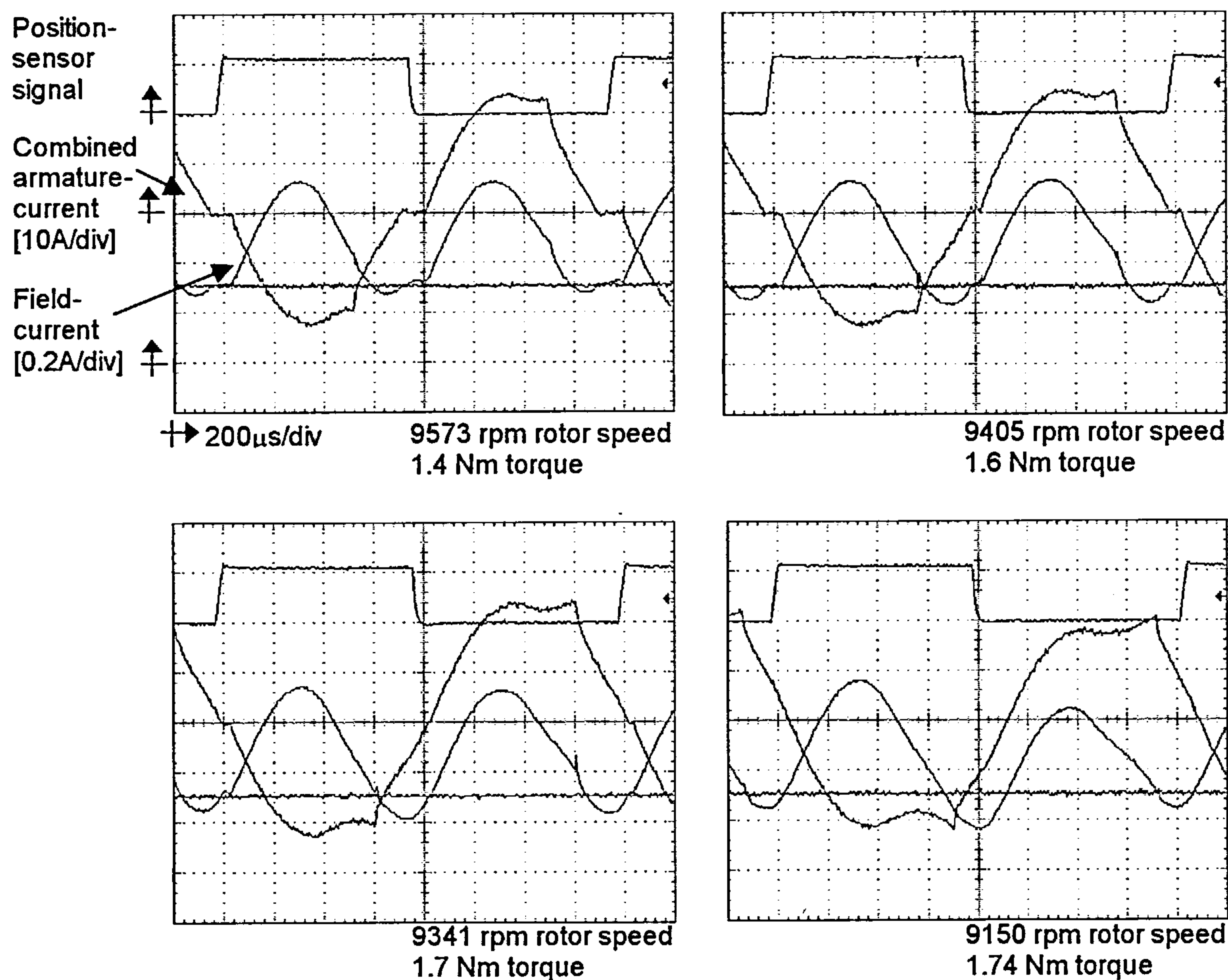


Figure 6.15 Power Test XX, current waveforms for the final four measurements of this test

armature-current, is very significant. By the torque of 1.7 Nm in figure 6.15 the combined armature-current is almost continuous and the dips in the field-current are even lower than before. Figure 6.15 at the torque of 1.74 Nm reveals what was starting to happen; the combined armature-current is now continuous and the commutation point to the positive half-cycle is lagging and is not synchronised to the position-sensor signal as before. This has a direct effect on the field-current waveform and it can be seen to be unbalanced also. This operating point at the torque of 1.74 Nm gave the maximum power-out recorded from the motor with a value of 1668 W.

In addition to the temporary drive-protection circuit, the drive and the IGBTs were protected from being destroyed by an over-current due to a stall condition by interpreting a low speed as the motor beginning to stall. The PIC micro-controller was programmed to shutdown and switch-off all of the power-devices at approximately 585 Hz, which corresponded to a speed of 8775 rpm. A motor stall was captured in figure 6.16 by triggering the oscilloscope on the falling edge of the field gate-signal to the MOSFET. Both the combined armature-current and the field-current were unbalanced such that, the negative half of the combined armature-current was clearly dominating, and to the degree that the field flux had collapsed in places. This imbalance became so severe that one half of the armature overpowers the other, and the rotor locks in alignment with this phase stalling the motor.

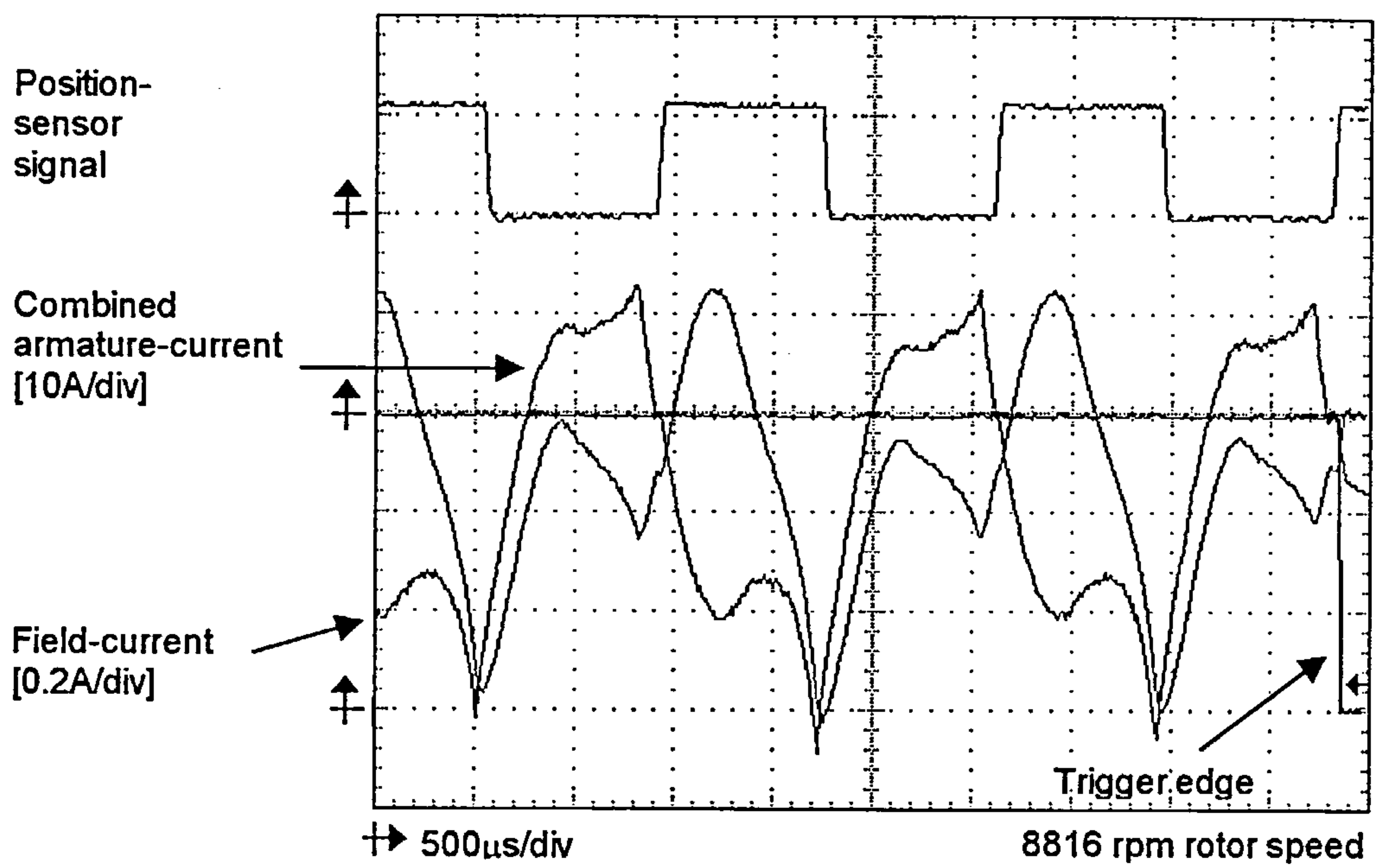


Figure 6.16 Current waveforms just prior to a stall

The explanation for this occurrence is that under these particular operating conditions the motor had reached the limits of its operation, as defined by the natural torque-speed curve of the motor that would be described if the duty-cycle of the IGBTs on-time was 100 %. As the motor had reached the limit no further testing could be carried out apart from changing the advance-angle. The motor was tested again with an advance of 14° , which had no real effect on performance, and still resulted in a stall occurring. The only other options to try were to change one of the fixed values or rewind the motor.

6.5.3 High-speed power tests

The new prototype motor had been designed to be a drop-in replacement for the previous series universal-motor, which drove the load through a gearbox. For this reason the performance figures quoted, in terms of torque and speed, were specified according to the gearbox ratios of this design. The gearbox ratios could be easily changed, thus implying that the power-out could be developed at any practical motor speed.

i New PIC micro-controller programs

Four further PIC micro-controller programs were developed, each with different target operational speeds that would help find the natural torque-speed curve of the motor, with the aim of delivering the target power-out of 1864 W. In the PIC micro-controller programs a higher operational speed was achieved by increasing the duty-cycle such that a larger pulse-width was applied to the

IGBTs at a higher speed. Conversely a lower speed was achieved by decreasing the duty-cycle.

The effect of this simple change is illustrated in figure 6.17, which shows the four torque-speed curves developed by the motor. It can be seen that the motor is capable of operating over a wide-speed range. Figure 6.18 gives the end-point current waveforms for each torque-speed curve, which are very similar in that the applied pulse-length in terms of duty-cycle is almost identical. This shows that the motor is approaching its limit again in each case, and that these end-points could be considered to be near to the natural torque-speed curve of the motor. Figure 6.17 has a constant power-out curve of 1600 W shown upon it for reference, this suggests that the motor's natural power-out curve is constant. Therefore changing the speed of the motor would neither increase nor decrease the power delivered. The only remaining solution to increase the power-out, with the specified inputs, was to change the winding design. A new design could have been achieved by returning to the mathematical model but it was decided that the motor would be tested further to give some experimental evidence that might be useful in producing a winding design change.

ii Raising the input-power

To increase the torque of a DC motor the armature-current has to be increased. This implies that, either the resistance of the armature-winding has to decrease, or, the applied armature voltage has to increase. This theory was

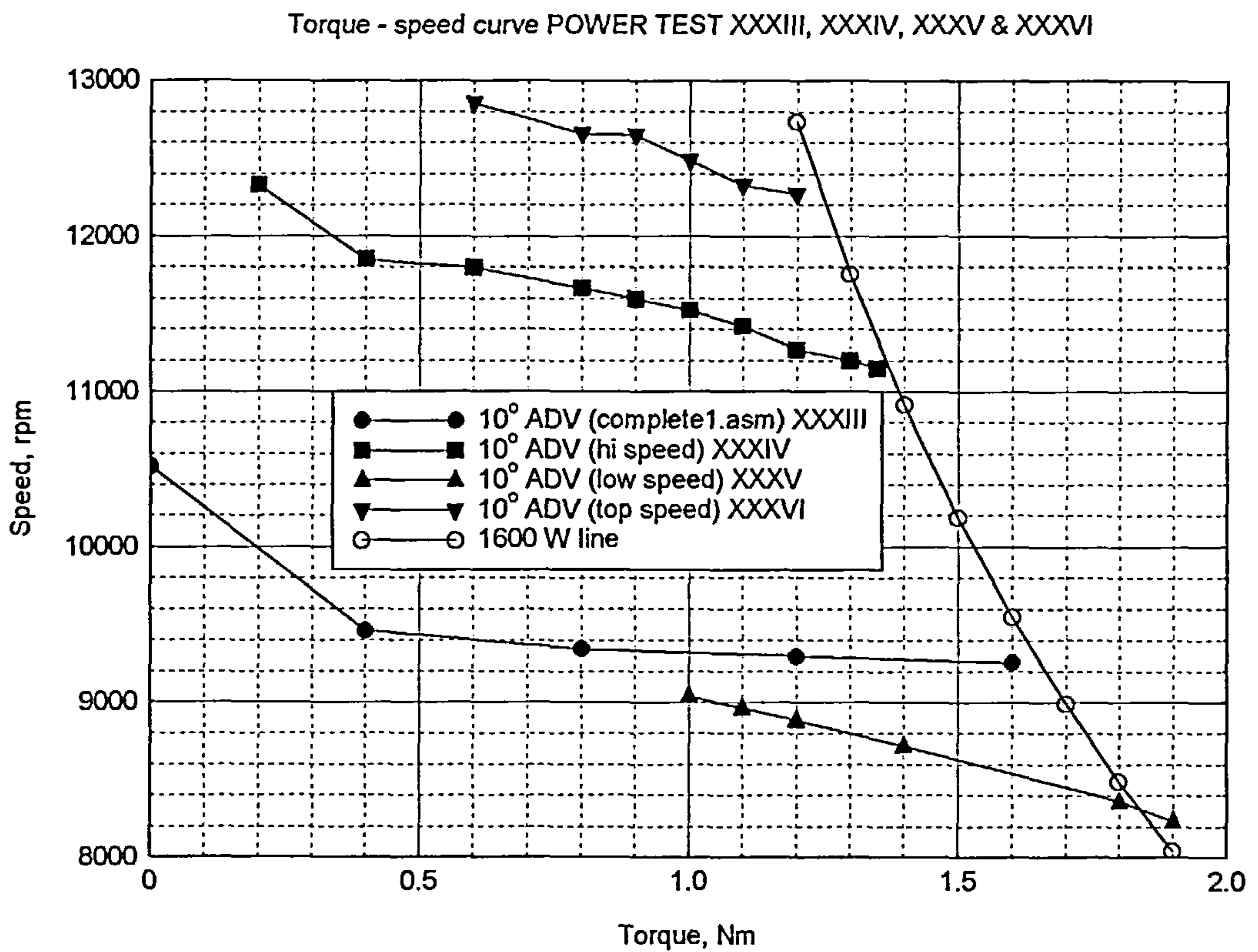


Figure 6.17 Power Tests XXXIII, XXXIV, XXXV and XXXVI, Torque – speed curves at an advance-angle of 10° (mechanical)

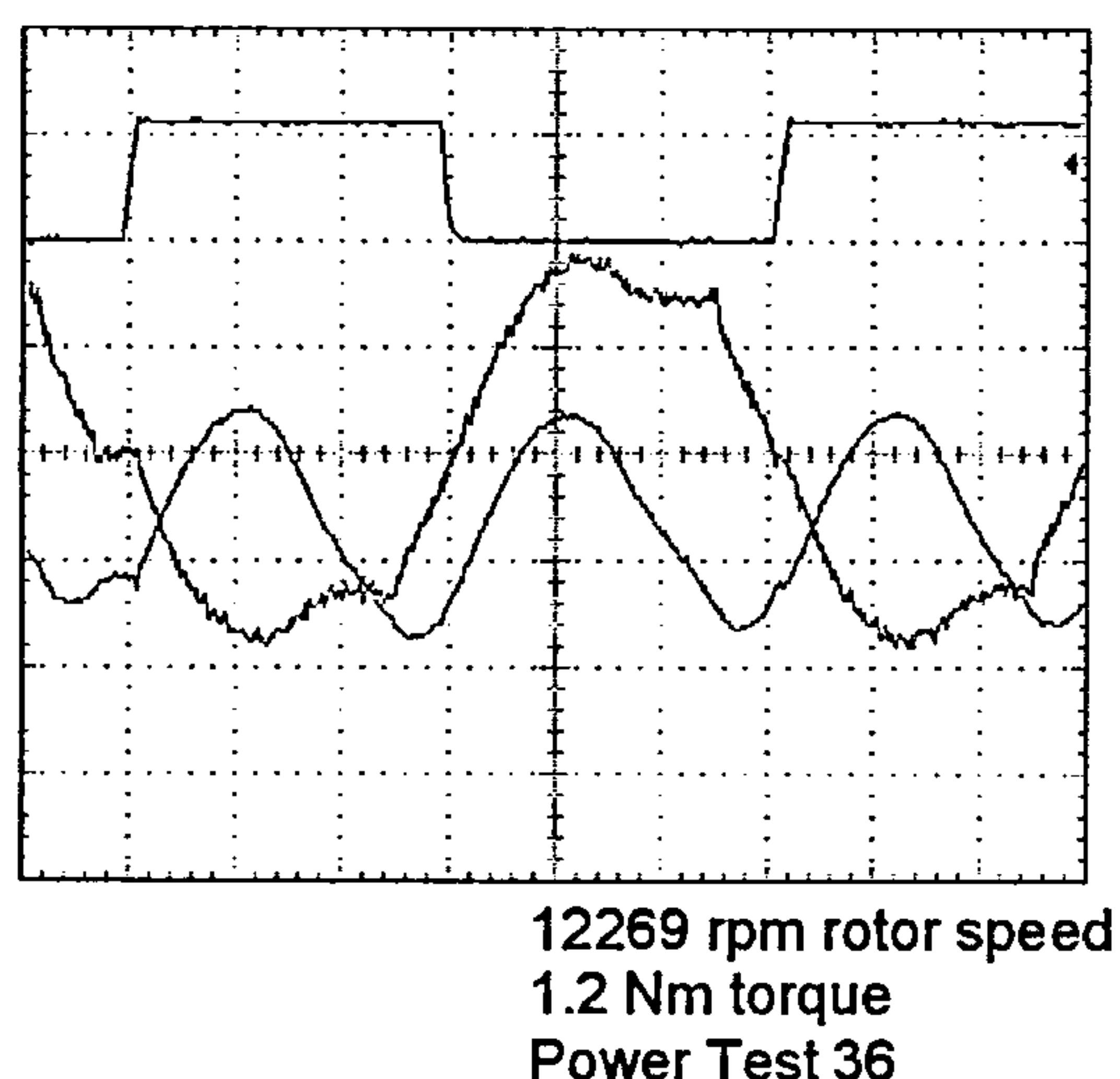
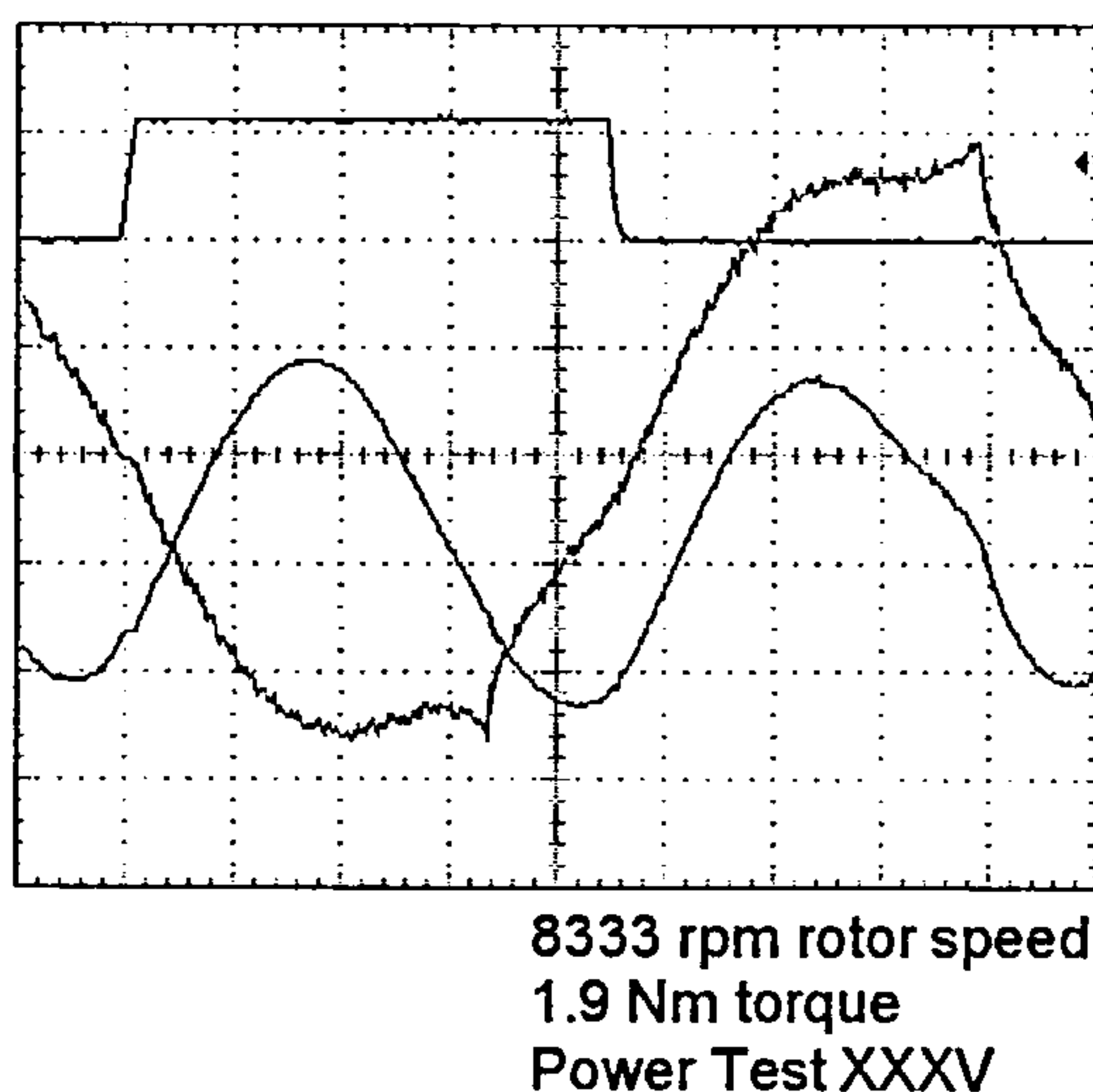
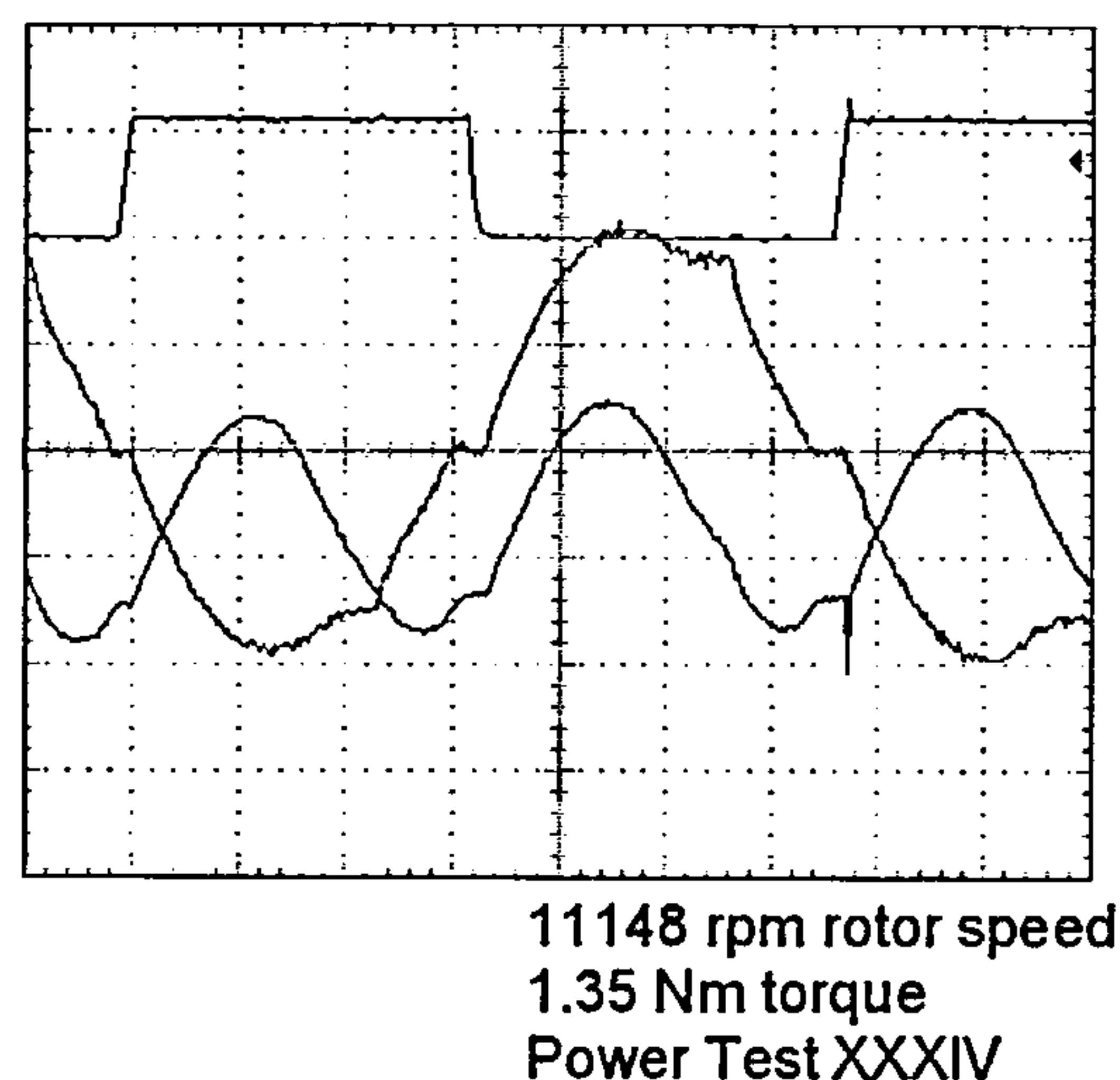
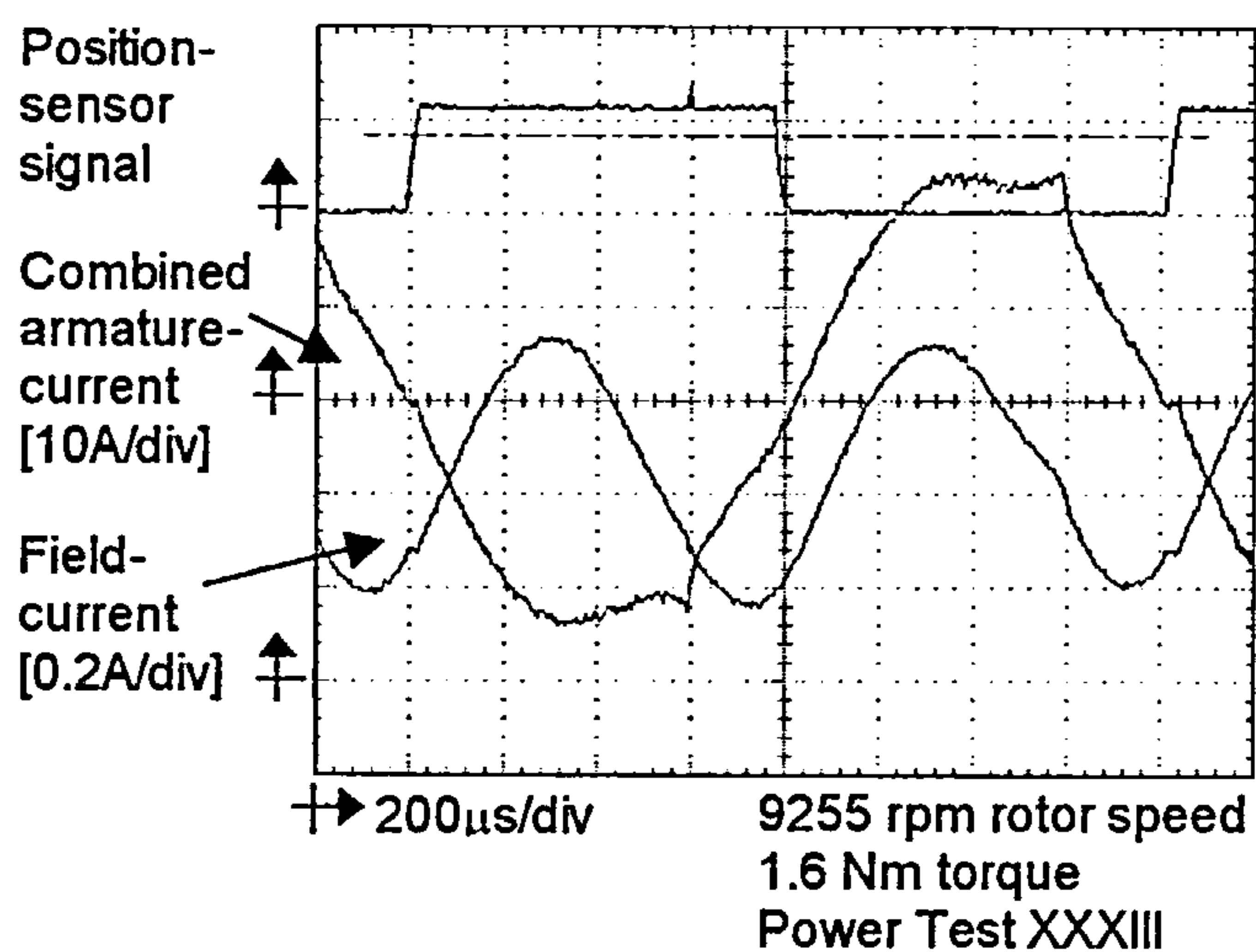


Figure 6.18 Current waveforms for the end test points shown

applied to this motor very simply. The output power had to rise by approximately 16.5% from 1600 W to 1864 W. Therefore the input voltage across the armature was raised by a similar percentage from 240 V to 280 V. The voltage across the field-winding was kept to 240 V when the armature had 280 V applied by the use of an external dropping resistor. The motor was tested again with the “Hi speed” and “Top speed” PIC micro-controller programs at 280 V supply voltage. These two programs were chosen because at the load point, as tested at 240 V, there was still scope for the armature-current to be increased. This was important because testing had demonstrated that the temperature rise on the armature-windings was restricting the motor being tested at the lower speeds. Figure 6.19 shows that the increase in input-power to the armature-winding enabled the desired power-out to be reached. The implication of this was that the motor needed a rewind to achieve the same results but at the correct supply voltage of 240 V.

6.5.4 Reserve torque tests

Referring to the performance section of the review of the specification it states that, “A further maximum torque, or reserve torque, of 3 Nm also had to be achieved for short durations of operation”. As the load torque had changed to achieve the desired power-out by increasing the speed, the reserve torque was defined as being one and a half times the load torque. The motor was capable of delivering a torque of 1.8 Nm, at a reduced power-out, without any problems. Therefore this value was set as the reserve torque, which meant that a load torque of 1.2 Nm had to be developed. With a target power-out of 1864 W this

Torque - speed curve POWER TEST XXXIV, XXXVI, XXXVII, XXXVIII & XLI

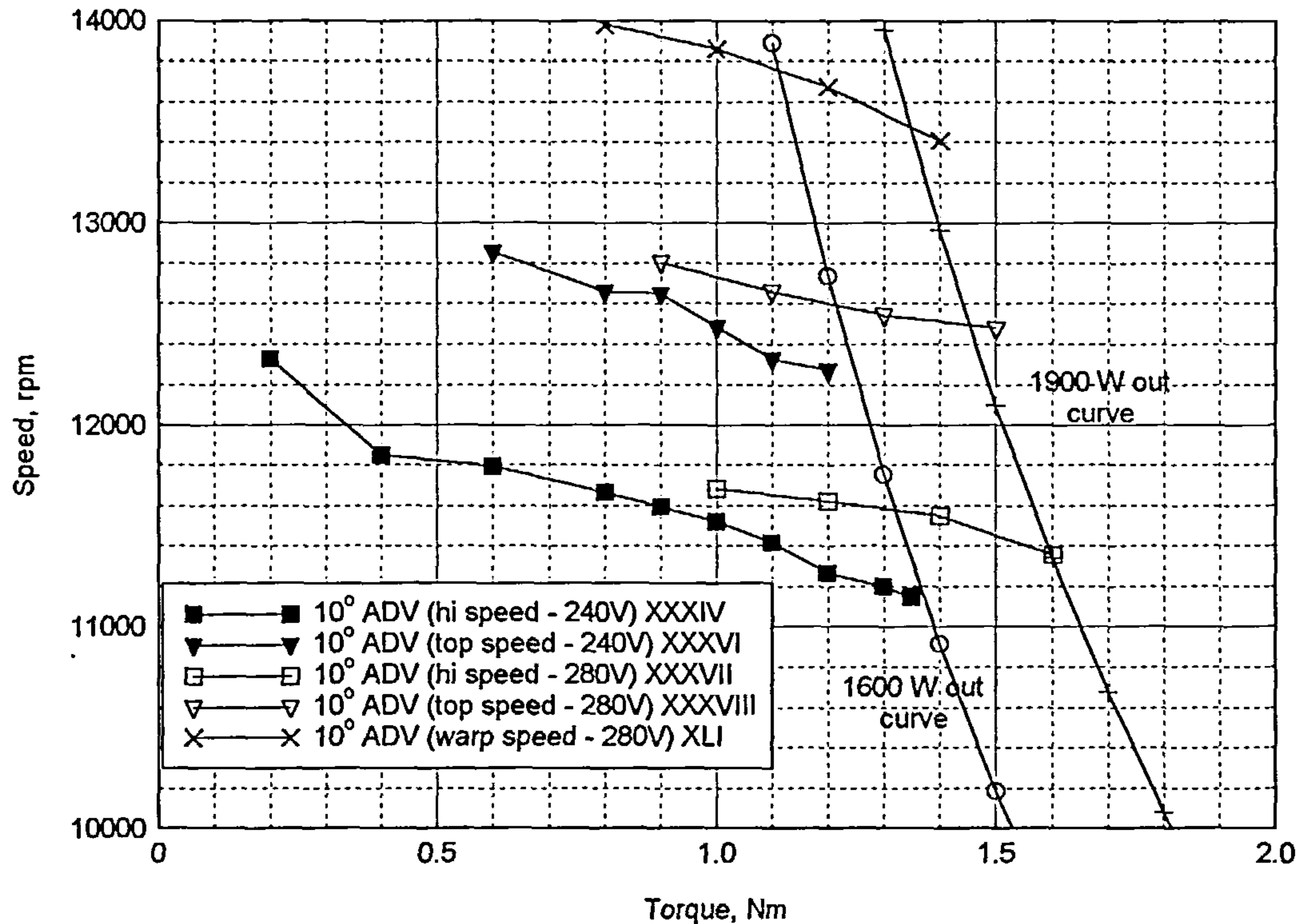


Figure 6.19 Power Tests XXXIV, XXXVI, XXXVII, XXXVIII and XLI, Torque – speed curves at an advance-angle of 10° (mechanical) at armature-voltages of 240 V and 280 V

torque had to be produced at a speed of 14833 rpm. Figure 6.19 also shows the first attempt at operating, at an even higher speed, using a new PIC micro-controller program called "Warp speed", which gave a speed of 13700 rpm at 1.2 Nm.

The reserve torque did not have to be delivered at a higher power than that specified for the load torque. Therefore in terms of the load routine within the PIC micro-controller program it was envisaged that the torque-speed curve would be shaped such that the initial slope was as flat as possible up to a knee-point at 1.2 Nm. Then the power-out would stop increasing, and the curve would follow a constant power-out curve to the reserve torque of 1.2 Nm. A new PIC micro-controller program "Warp II speed" was developed to implement this load routine. The resulting torque-speed curve is shown in figure 6.20 together with the previous 280 V curves already found. Firstly this torque-speed curve demonstrates the desired characteristics, the flat initial slope, the knee point at 1.2 Nm, and the steeper section that attempts to follow constant power. However, the speed still needed to be increased by a further 600 rpm, at the desired load point, and the reserve torque had to be cut-back in terms of power-output.

The corresponding curve for power-out against torque is given in figure 6.21. This clearly illustrates that the method of cutting-back the power-output is working as the curve is deviating from the previous power-out curves. Also it is important to note that the motor has delivered 2.1 kW of power. Figure 6.22

Torque - speed curve POWER TEST XXXVII, XXXVIII, XLI & XLII

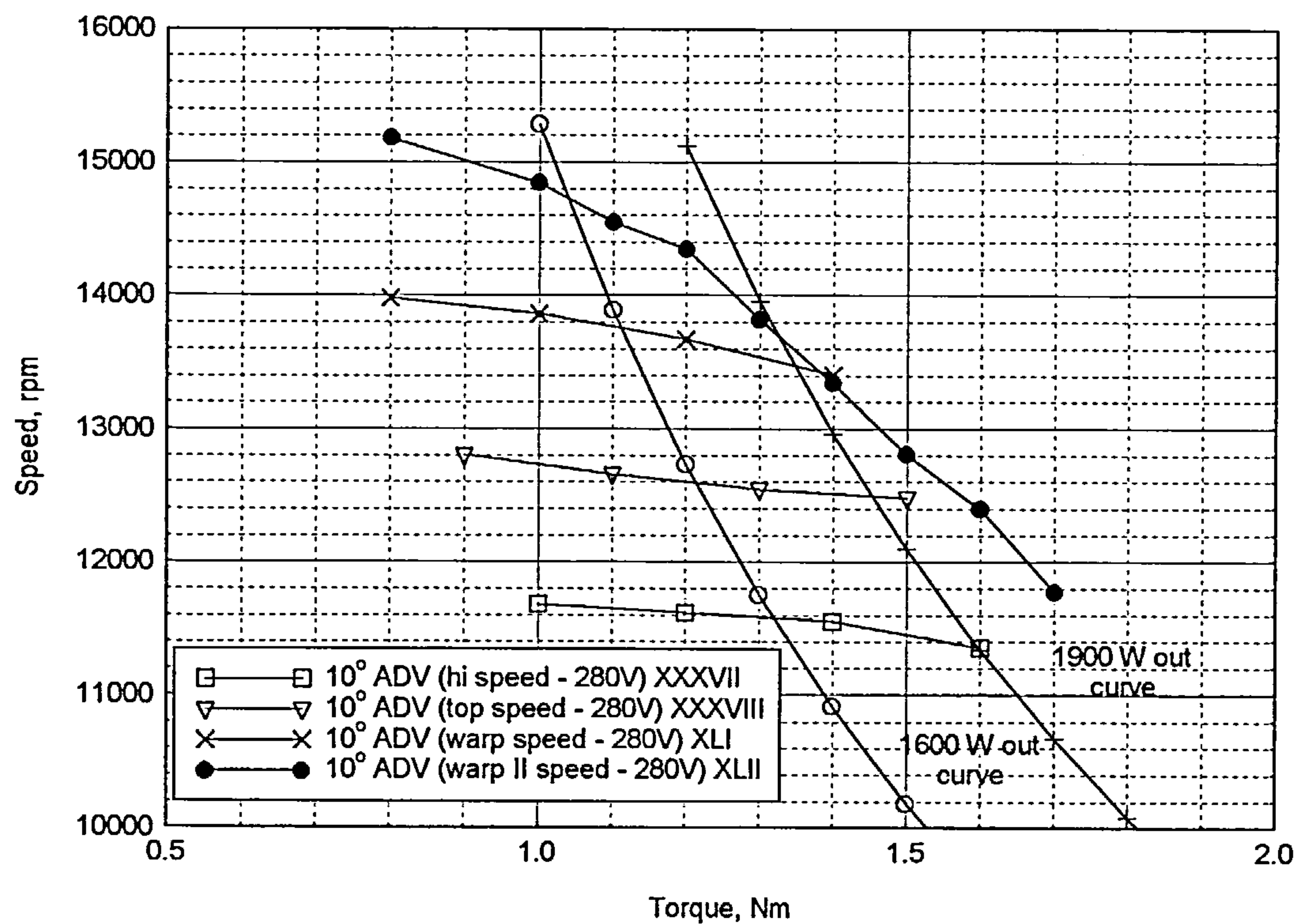


Figure 6.20 Power Tests XXXVII, XXXVIII, XLI and XLII, Torque – speed curves at an advance-angle of 10° (mechanical)

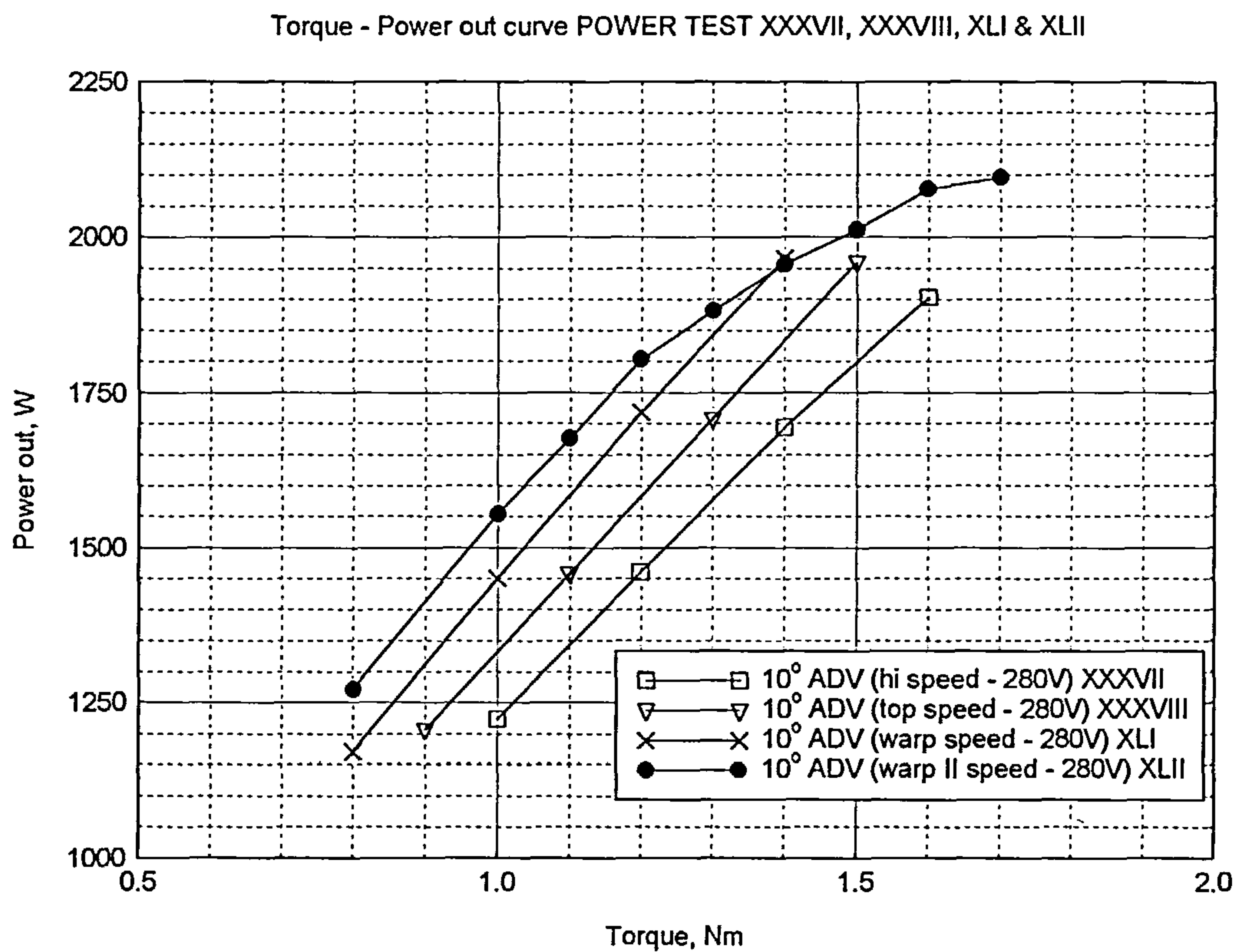


Figure 6.21 Power Tests XXXVII, XXXVIII, XLI and XLII, Torque – power out curves at an advance-angle of 10° (mechanical)

shows the power-in curve, and figure 6.23 gives the efficiency of the motor against torque. The latest PIC micro-controller program “Warp II Speed” gave the highest recorded efficiency of 67 %.

Further testing with different programs, using this motor, showed no significant improvement in obtaining the desired torque-speed curve.

6.5.5 Start-up tests

The starting requirements of this type of motor were examined in detail in Chapter 2, and Chapter 5 presented the lamination design characteristics chosen to enable self-starting. Basically the motor had to be started without exceeding the limits specified or the drive being damaged.

To start the motor the correct combination of chopping frequency and duty-cycle of the PWM scheme were needed. Through a set of extensive tests using a signal generator to drive the IGBTs and field MOSFET it was found that the best PWM scheme had a chopping frequency of 10 kHz and an initial duty-cycle of 52.5 %. Once this initial combination of values had been found they were incorporated into a complete starting routine contained in a PIC micro-controller program, which was designed to start the motor and then accelerate it up to no-load speed. This was achieved by increasing the duty-cycle of the PWM in steps with increasing rotor speed, until the full duty-cycle was applied, then, as the no-load speed was approached, the pulse-length was reduced as before.

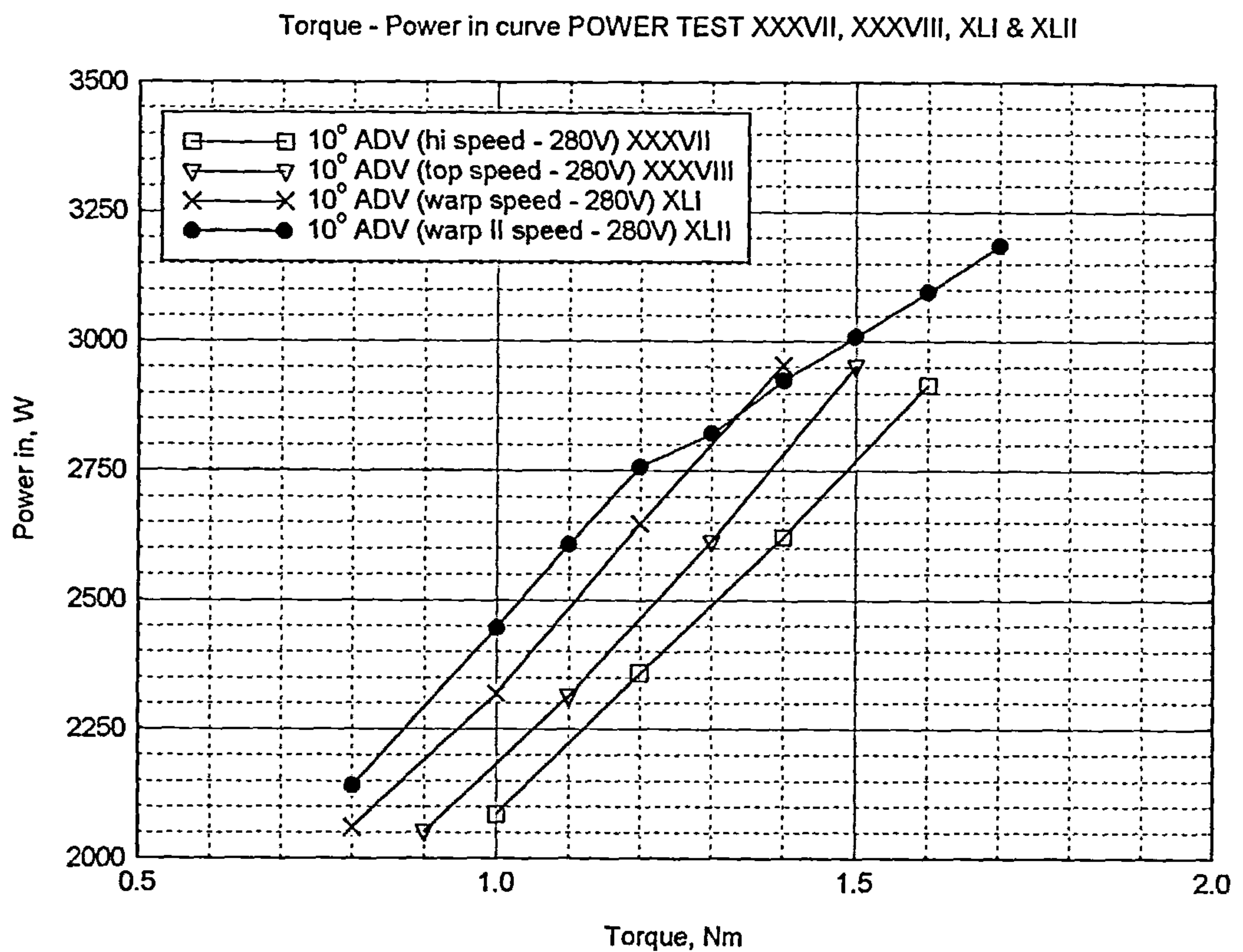


Figure 6.22 Power Tests XXXVII, XXXVIII, XLI and XLII, Torque – power in curves at an advance-angle of 10° (mechanical)

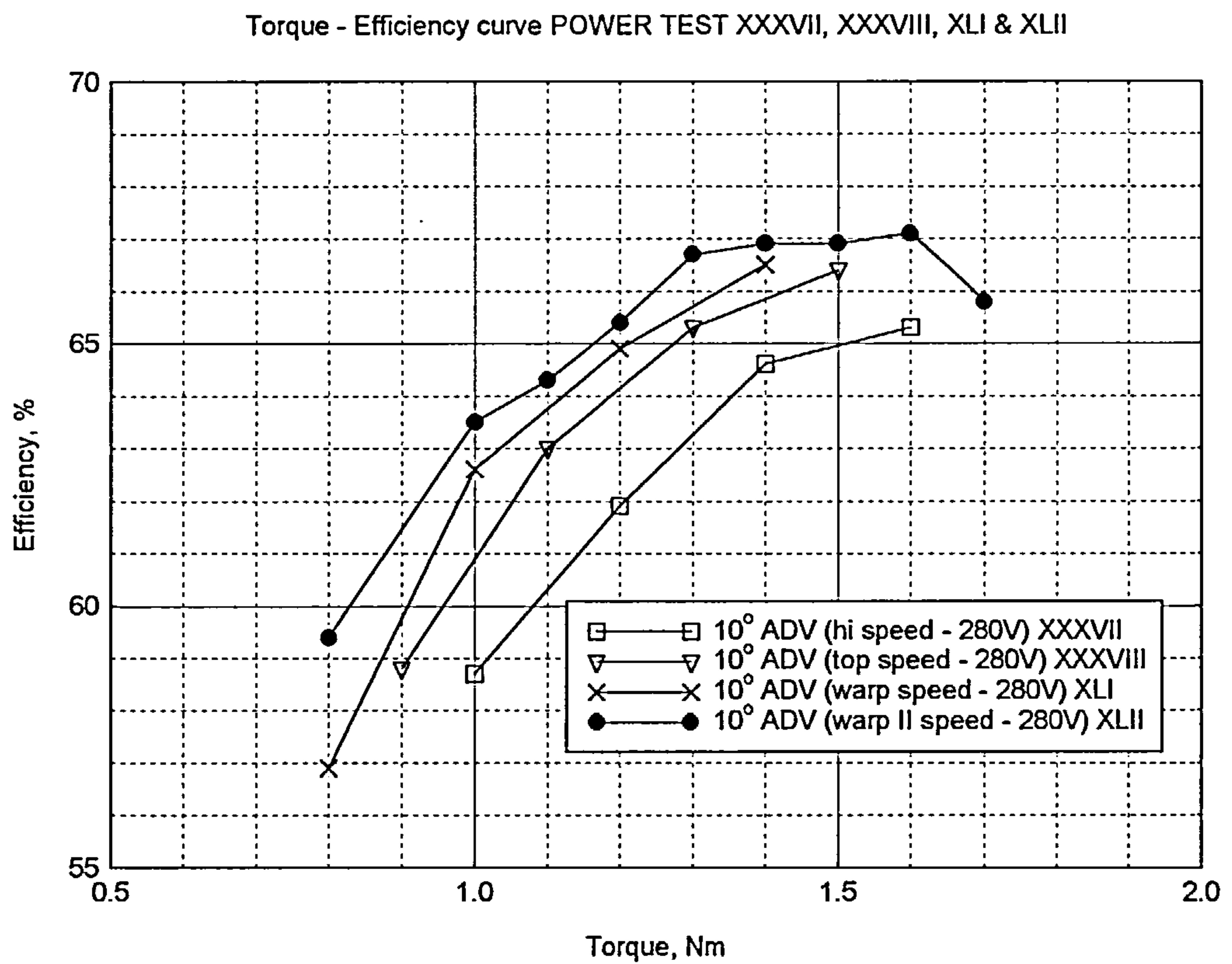


Figure 6.23 Power Tests XXXVII, XXXVIII, XLI and XLII, Torque – efficiency curves at an advance-angle of 10° (mechanical)

Figure 6.24 shows a complete start-up sequence of the motor in ten oscilloscope frames. From the early section of this sequence the duty-cycle step increases can be clearly seen. The time taken to accelerate the motor to no-load speed was approximately 1.46 s, which is evident by the consistency of the aliasing of the position-sensor signal and the rotor speed signal reaching its peak value within the 8th oscilloscope frame. The desired acceleration time as given in the specification was 0.5 s meaning that the routine still had to be optimised to achieve this value. The combined current waveform never went above 20 A, so there was plenty of scope for the duty-cycle to be stepped-up earlier with a higher percentage.

One other important detail to note was that this series of start-up tests was carried out with only the inertia of the dynamometer ($1.55 \times 10^{-3} \text{ kgm}^2$) and the flexible coupling ($0.0887 \times 10^{-3} \text{ kgm}^2$), linking the motor to the dynamometer, resisting the acceleration, that totalled $1.6387 \times 10^{-3} \text{ kgm}^2$. The specified inertia was almost five times greater at $8 \times 10^{-3} \text{ kgm}^2$. With the correct inertia in place the requirements of the drive were even greater.

The average-torque exerted during start-up to accelerate the motor from standstill to 11100 rpm in 1.46 s was calculated as,

$$T = I_o \alpha \quad (6.5),$$

$$\text{where } \alpha = \frac{d\omega}{dt} \quad (6.6),$$

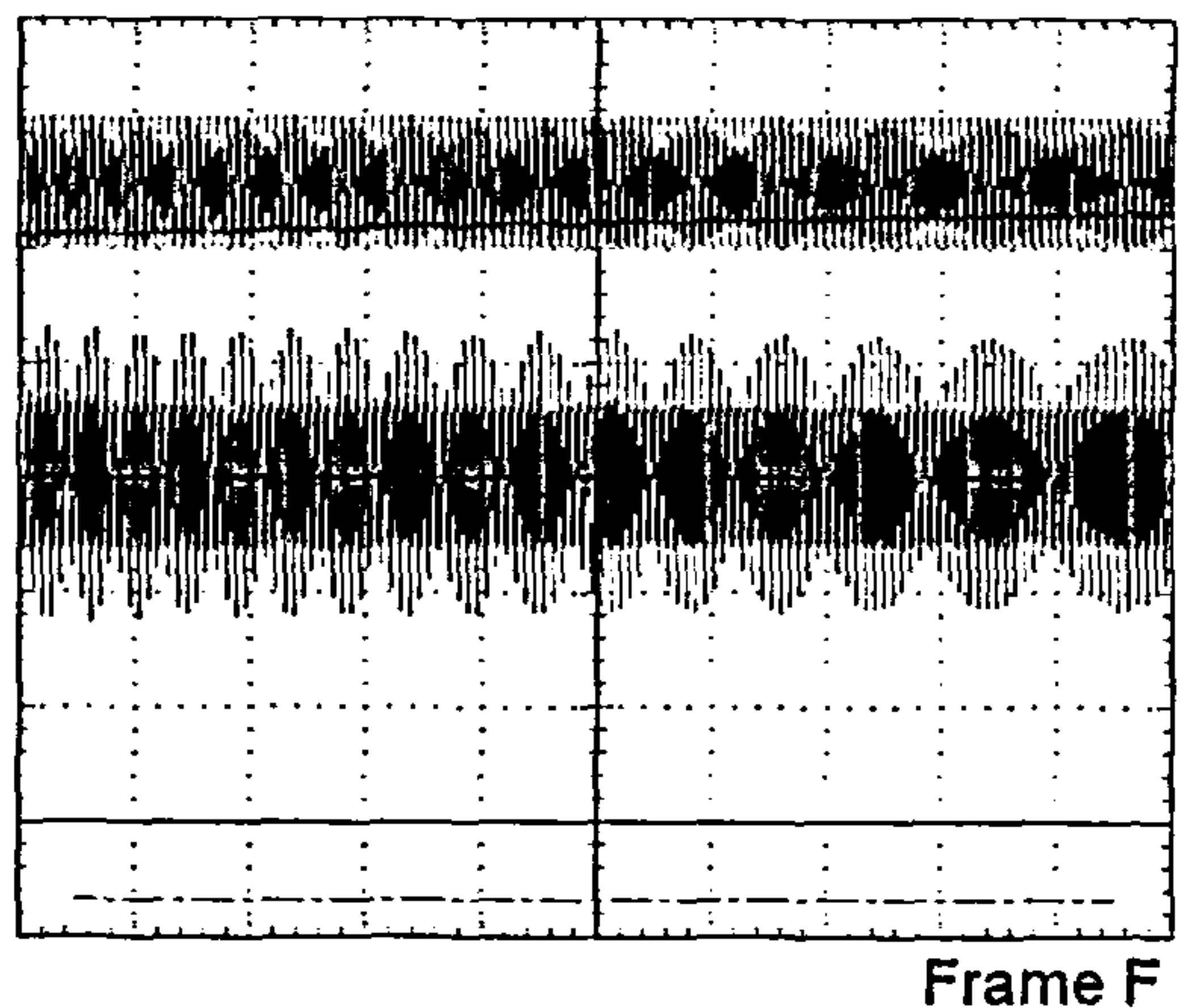
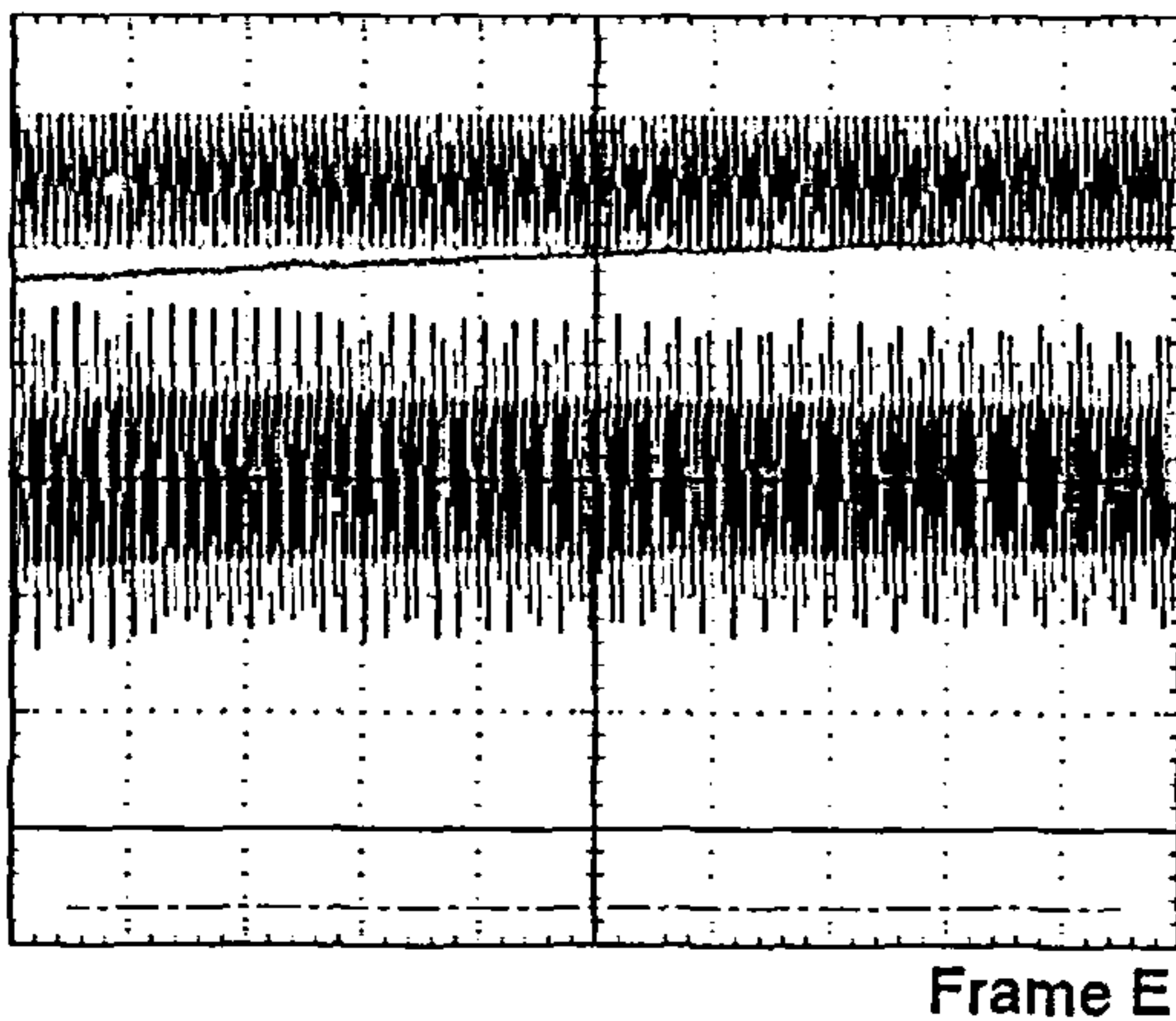
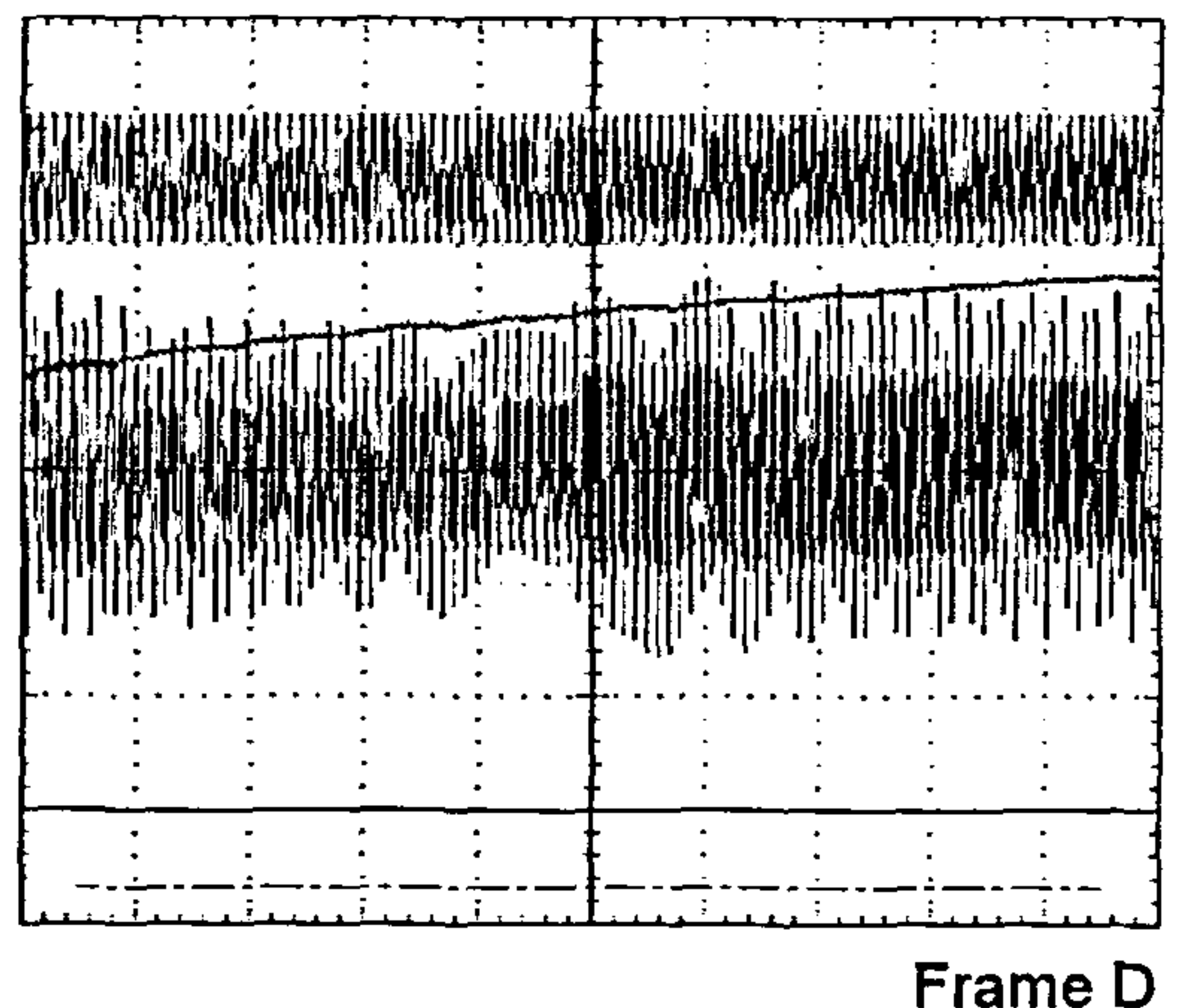
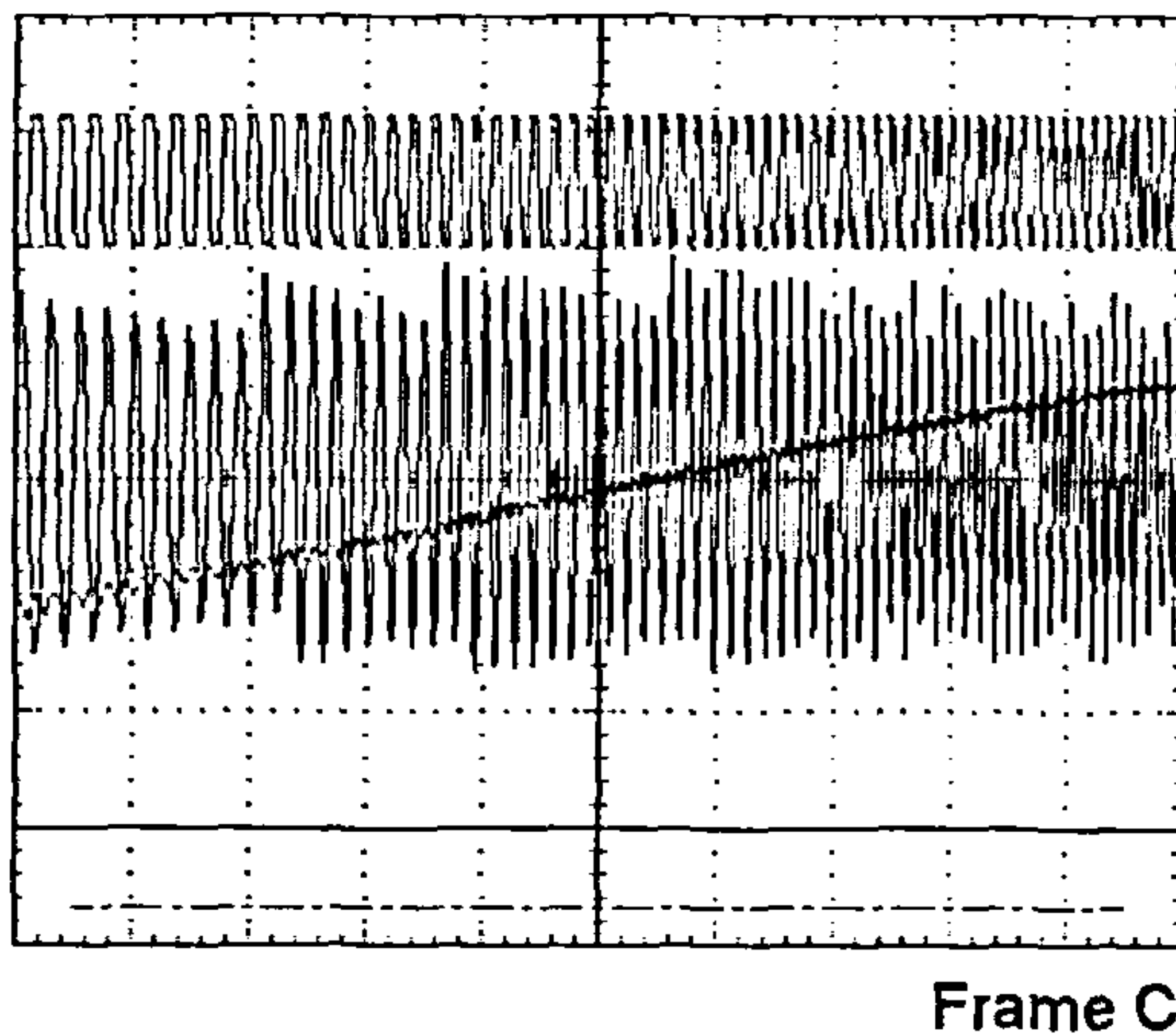
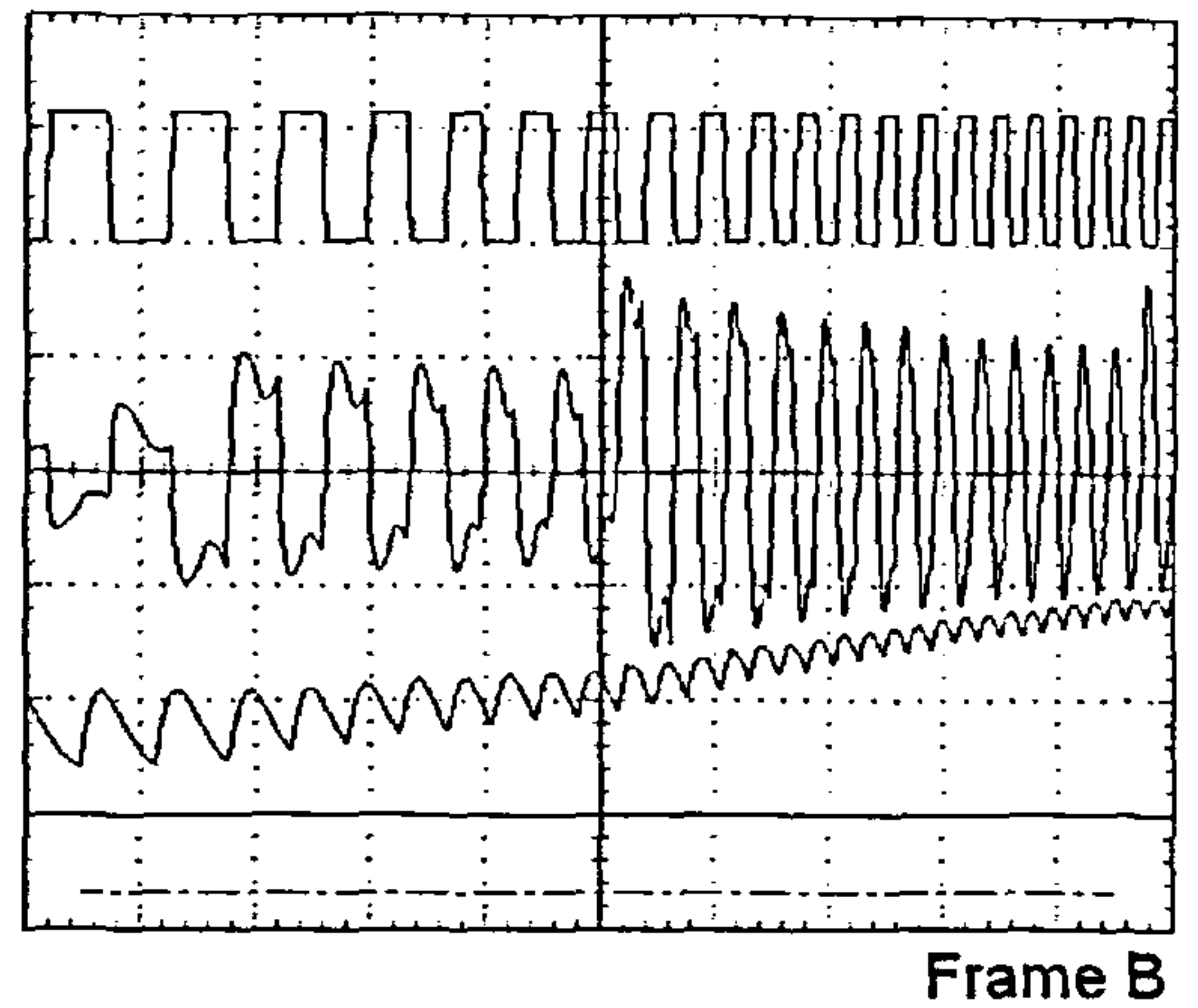
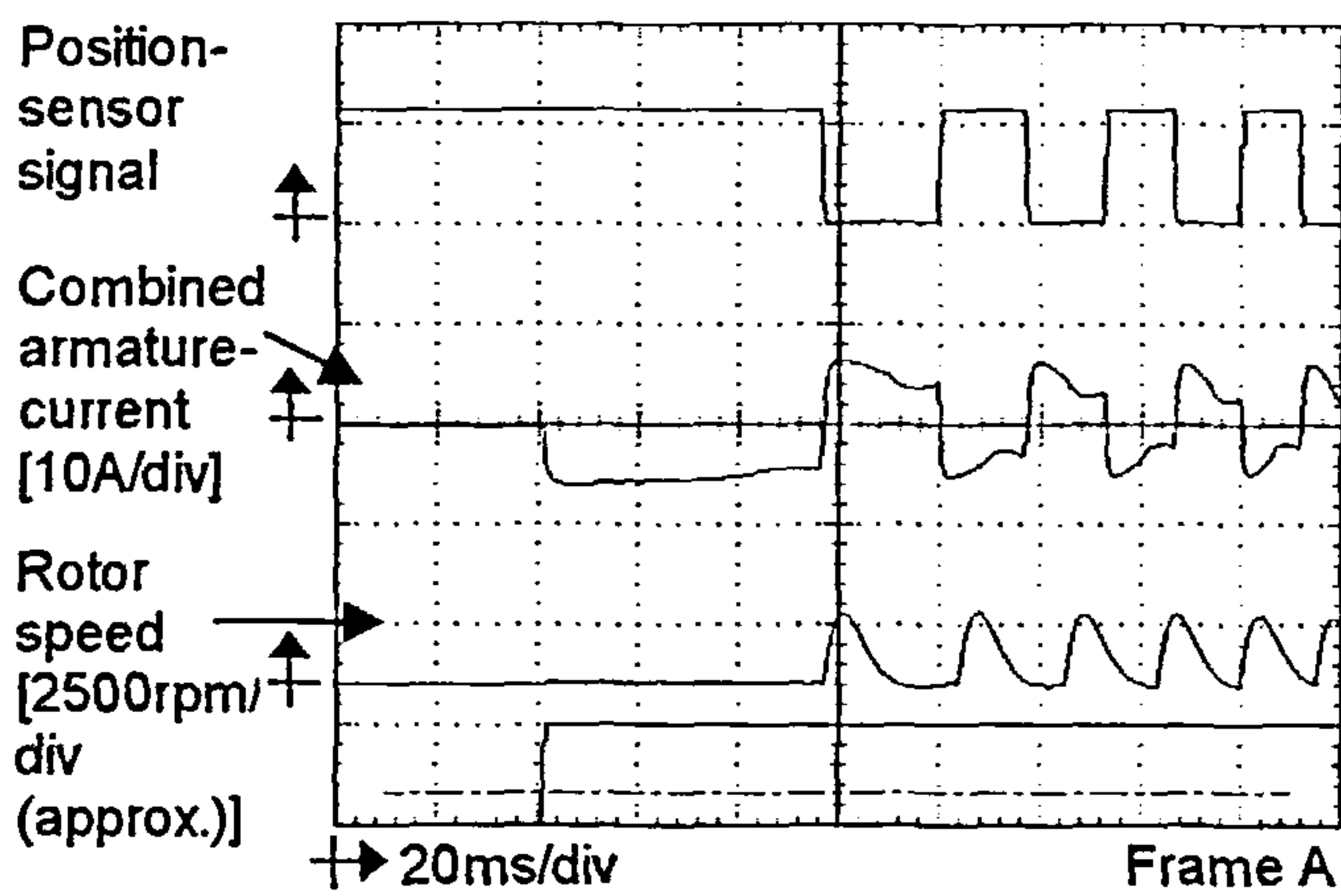


Figure 6.24 A complete start-up sequence using the first prototype motor – continued on next page

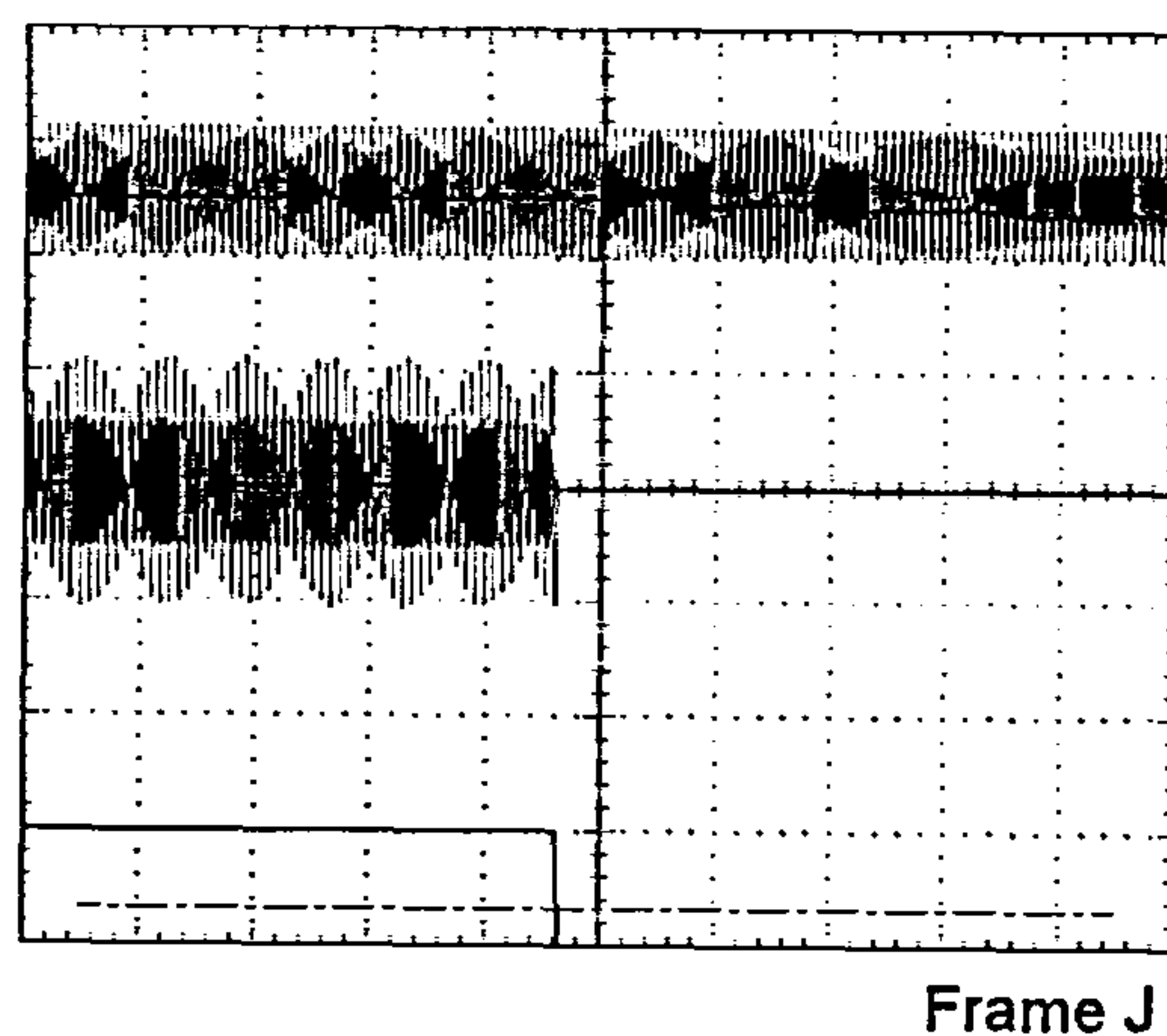
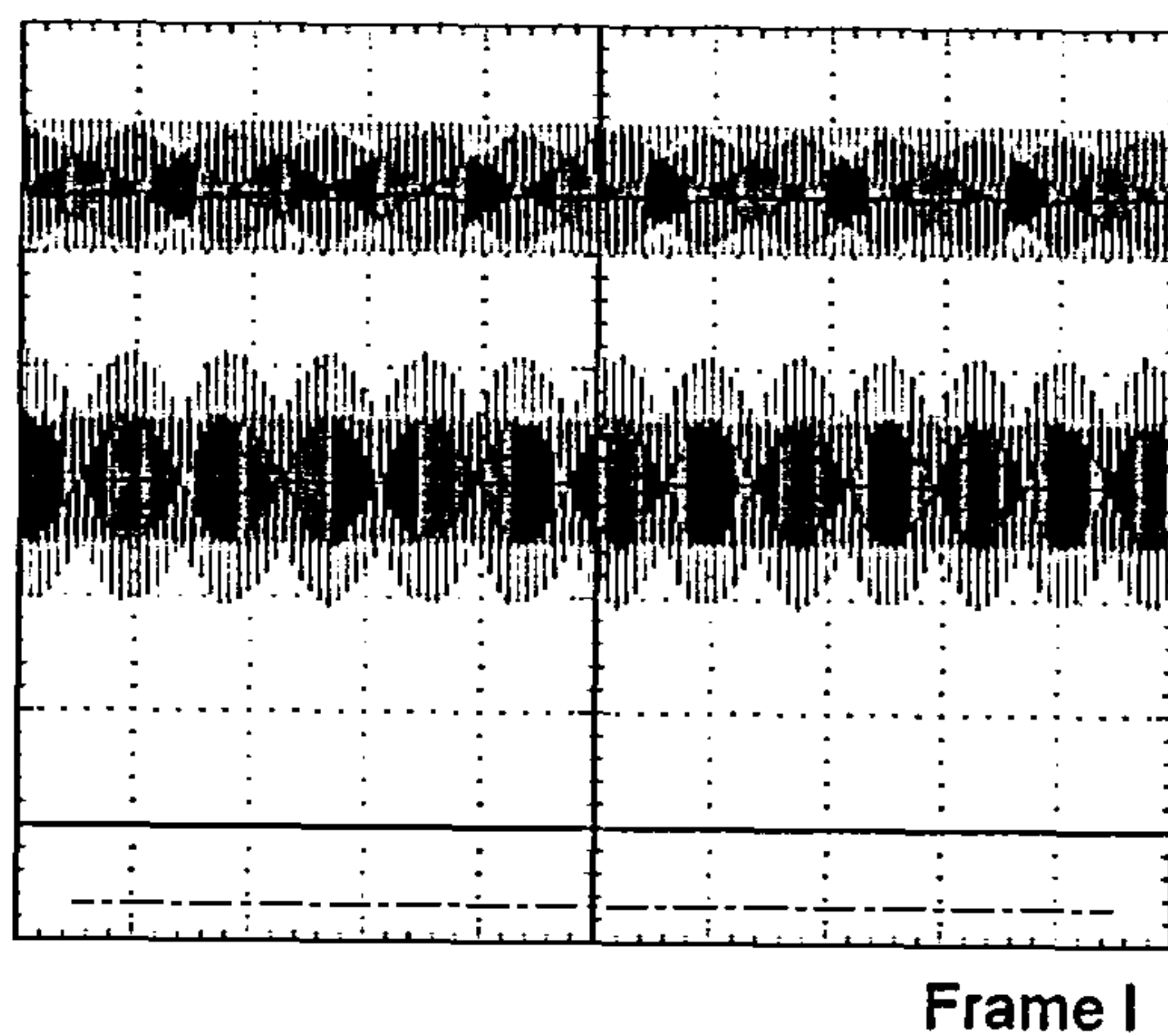
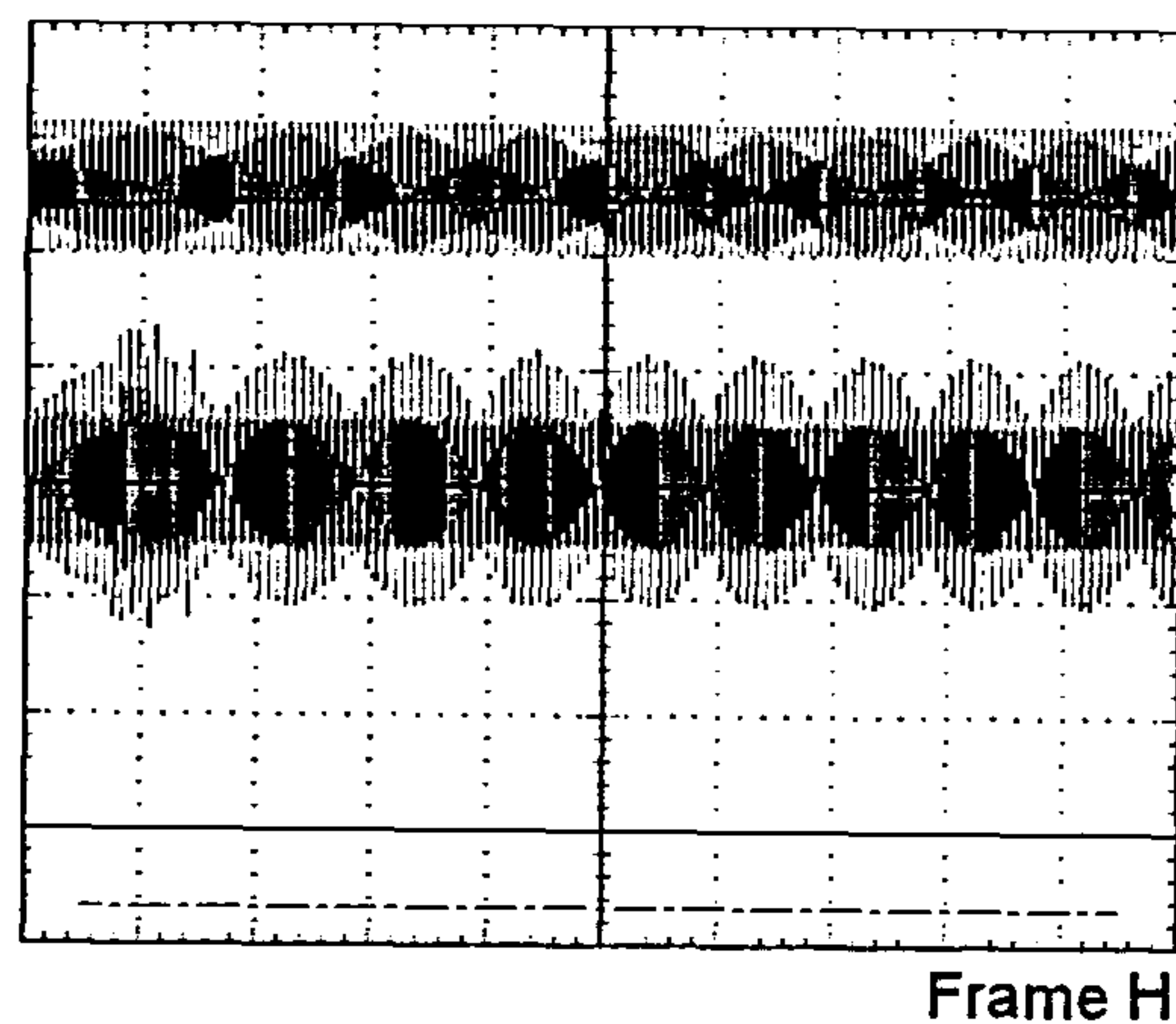
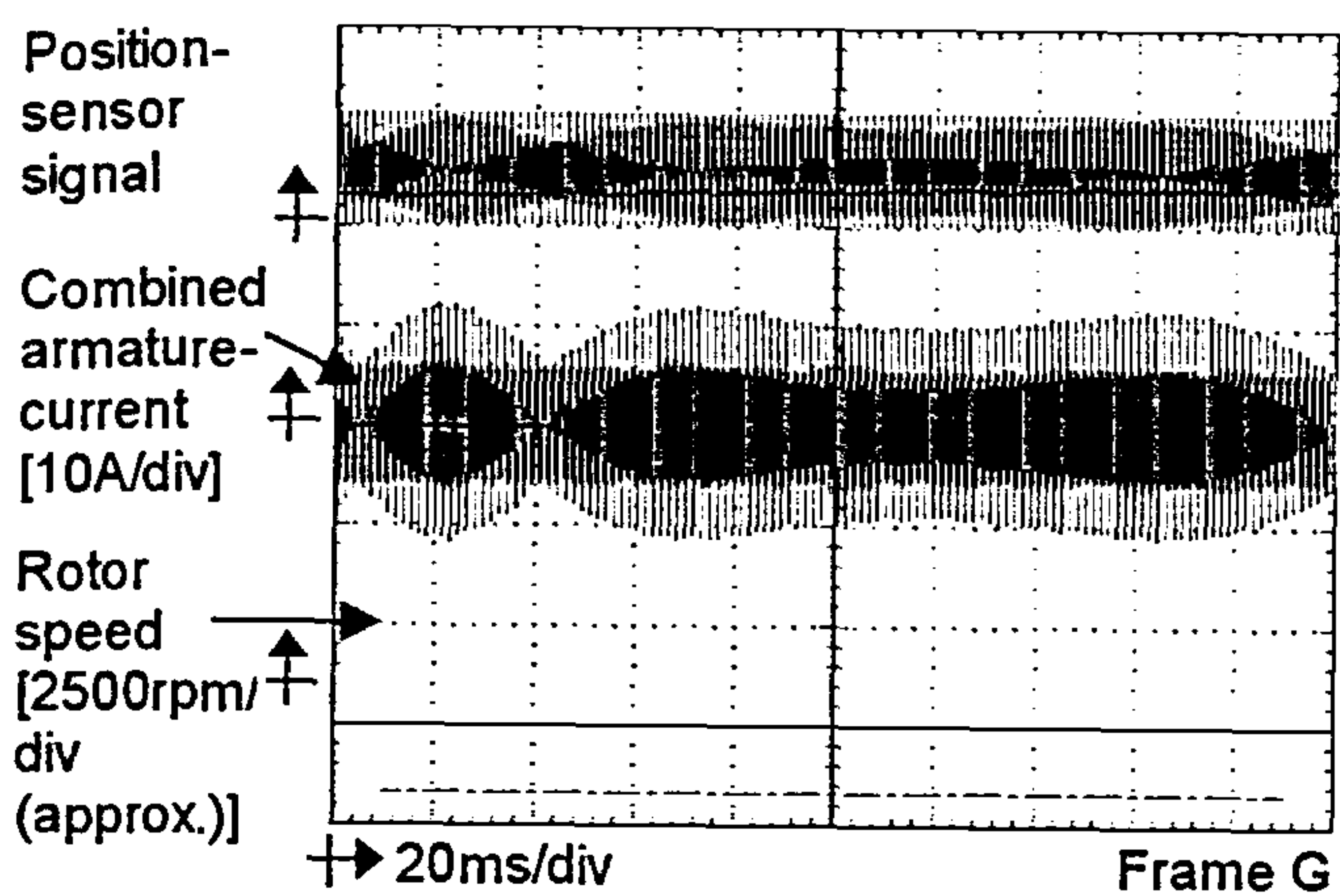


Figure 6.24 A complete start-up sequence using the first prototype motor – continued from previous page

$$\omega = 11100 \text{ rpm} = 1162 \text{ rads}^{-1} \quad (6.7),$$

$$t = 1.46 \text{ s} \quad I_o = 1.6387 \times 10^{-3} \text{ kgm}^2 \quad (6.8),$$

$$\text{hence } T = 1.30 \text{ Nm} \quad (6.9).$$

With a start-up routine found that worked successfully, it was necessary to test the starting more rigorously at every possible starting position of the rotor. In certain positions, particularly in the regions around a position-sensor edge, starting was unsuccessful. The motor oscillated around the edge as it tried to find the correct direction to rotate in. As these oscillations increased in frequency this was interpreted as an increase in speed and the duty-cycle of the applied current pulses was increased. This resulted in the drive failing as too much current was allowed to flow through the power devices. This problem was caused by the limited positional information available. No further testing was carried out on this prototype at this stage to remedy this problem.

6.5.6 Braking tests

In addition to starting the motor it also had to be stopped from no-load speed in a time of 1.5 s. The lamination had been designed to retain a small change in field-winding self-inductance so that when the field was excited on its own a torque was generated, which was used to brake the motor. The motor was allowed to run at no-load speed with the full supply voltage applied, both of the IGBTs were then switched-off leaving the field excited. Figure 6.25 shows the

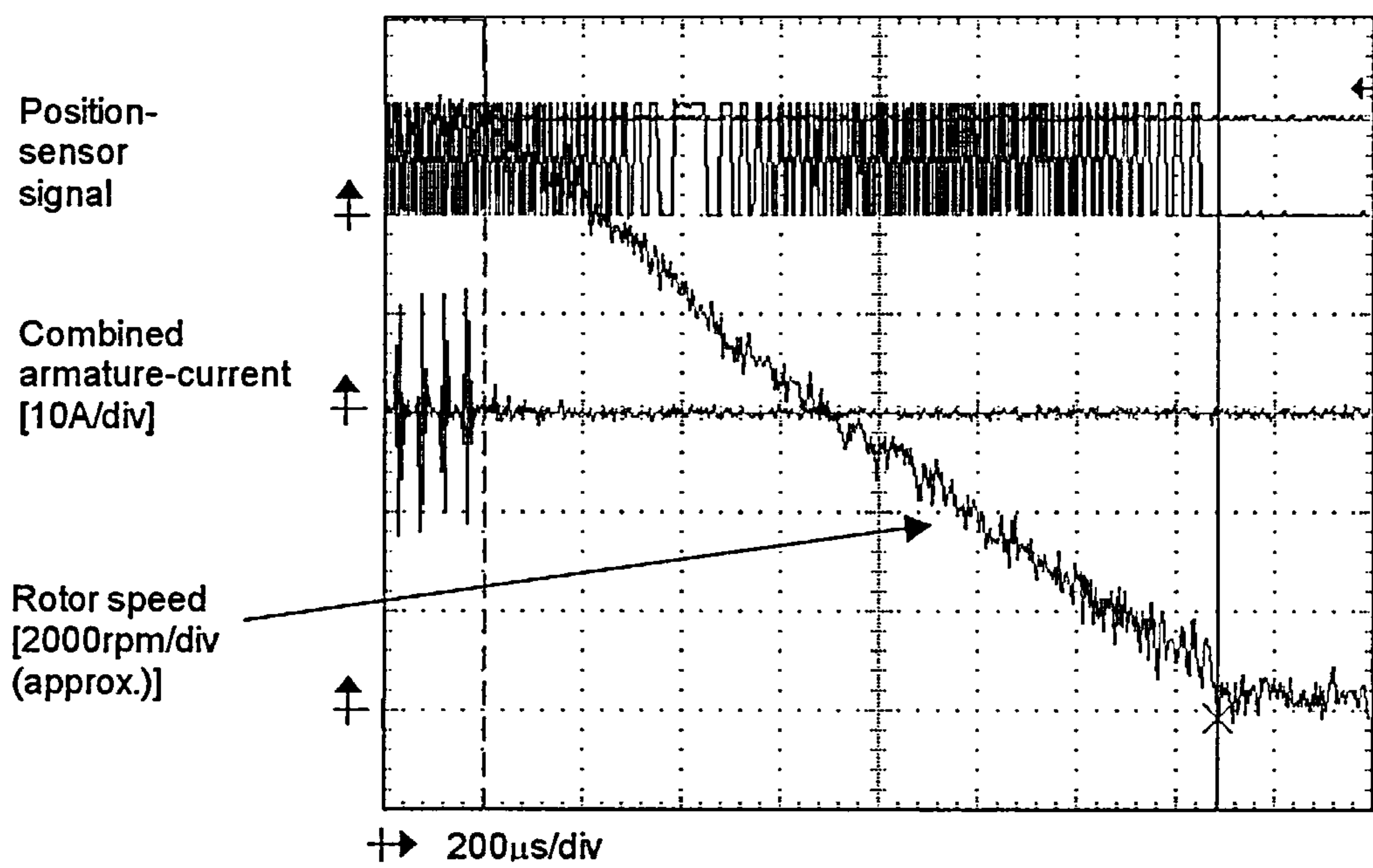


Figure 6.25 Braking performance waveforms

braking performance waveforms recorded on the oscilloscope. The time taken to stop was measured as 740 ms.

Assuming that the deceleration was linear the torque exerted during braking was calculated as,

$$T = I_o \alpha \quad (6.10),$$

$$\text{where } \alpha = \frac{d\omega}{dt} \quad (6.11),$$

$$\omega = 11100 \text{ rpm} = 1162 \text{ rads}^{-1} \quad (6.12),$$

$$t = 740 \text{ ms} \quad I_o = 1.6387 \times 10^{-3} \text{ kgm}^2 \quad (6.13),$$

$$\text{hence } T = 2.57 \text{ Nm} \quad (6.14).$$

With the same braking torque and no-load speed, and the correct inertia of $8 \times 10^{-3} \text{ kgm}^2$ in place, the braking time can be recalculated as taking 3.62 s, which is over twice that required.

6.6 Conclusions

Testing of the first prototype motor gave an insight into the operational characteristics of the motor and demonstrated its performance capabilities. The initial operational tests gave two very important results that formed the basis of the remaining tests. They showed that the speed of the motor could be controlled very easily, and that the best method of advancing the commutation point of the motor was statically. They also showed how the motor behaved as

a DC motor by generating a back-EMF across the armature-windings by rotating the rotor with the field-winding excited.

The power tests would have hit the desired operating point of a power-out of 1864 W at a speed of 9000 rpm, assuming that the motor would have followed the same linear torque-speed characteristic. However, the motor stalled after having reached a maximum torque of 1.74 Nm. The explanation for this was that the motor had reached the limits of its operation, as defined by its natural torque-speed curve and that no further testing could be carried out.

Furthermore, the torque-speed curve, described, gave constant power-out, so that changing the speed had no effect on output-power. The only other option to try with this motor was to increase the power-input. Based on a simple calculation the supply voltage to the armature-winding was raised to 280 V, and the motor was tested again at a higher speed to restrict the temperature rise of the armature-windings. The desired power-out was reached.

The reserve torque tests were not able to deliver the one and a half times load torque required, but they demonstrated the principle in which this torque could be achieved in future tests. Problems were encountered in the start-up tests as there were certain positions around a position-sensor edge that the motor was unable to start from. These problems remained unsolved at this stage. The procedure for braking was also demonstrated effectively.

In conclusion testing of the first prototype motor showed that it was capable of starting, delivering the power-out, and braking as required, thereby providing a convincing demonstration of the performance of the motor. However, there was still need for further improvement, and, in particular a need to operate within specification at the correct supply voltage. Therefore it was necessary to produce a further prototype with a rewound armature-winding, but keeping the same shunt field-winding. Also, having seen that the operation of the motor was so successful, and that it needed no major design changes, another prototype motor with a series field-winding was manufactured. The following Chapter discusses the further testing carried out using these additional prototype motors.

CHAPTER 7 FURTHER TESTING AND DEVELOPMENT OF FLUX-SWITCHING MOTORS

7.1 Introduction

The conclusions drawn from testing the first prototype motor, described in Chapter 6, were that although the motor was capable of starting, delivering the power-out, and braking as required there was still scope for improvement. Furthermore, the need to deliver the desired performance against the specification had yet to be met. The performance capabilities of a series-wound field motor also had to be investigated, and the results compared with that of the shunt-wound field motor.

This Chapter describes and discusses the further development and testing of the flux-switching motor carried out using three additional prototype motors. The second and third prototypes both had the same new rewind armature-winding, and the same shunt-field-winding used, in the first prototype. The only difference between the two prototypes was that the third was manufactured with a more robust casing design and the gearbox was omitted from the design. The fourth prototype motor used the new casing design, without the gearbox, and a motor with a series-field-winding.

7.2 Dynamic testing of the second prototype motor

7.2.1 Power tests

The armature-winding of the first prototype motor was rewound with twelve less turns, and an increased wire diameter of 1 mm, according to the very simple design calculations given in Chapter 5. The intention of this second prototype motor was basically to deliver the desired power-out, with the correct supply voltage of 240 V across both windings. The first power test that was carried out used the same PIC micro-controller program “Warp II Speed” and, the same static advance-angle of 10° (mechanical) that were last used with the first prototype. The objective was that this repeat test would enable a direct comparison to be made as to the performance of the motor with a rewound armature. Figure 7.1 shows the torque-speed curve obtained, and, as expected, the shape of the curve is much the same as before, the only difference is a 200-300 rpm speed offset. The conclusion from this test was that the rewind of the armature-winding was successful, allowing the motor to deliver the desired power-out.

7.2.2 Reserve-torque tests

In order to deliver the correct reserve-torque, the torque-speed curve had to be shaped. As discussed previously, the aim was to design an ideal curve that would peak at the operating point with the required power-out, at a speed of 15000 rpm, and a torque of 1.2 Nm, and then follow a constant power-out curve that would end at the reserve-torque of 1.8 Nm. To achieve this aim the duty-cycle of the gate-drive signal, applied to the armature IGBTs, had to change

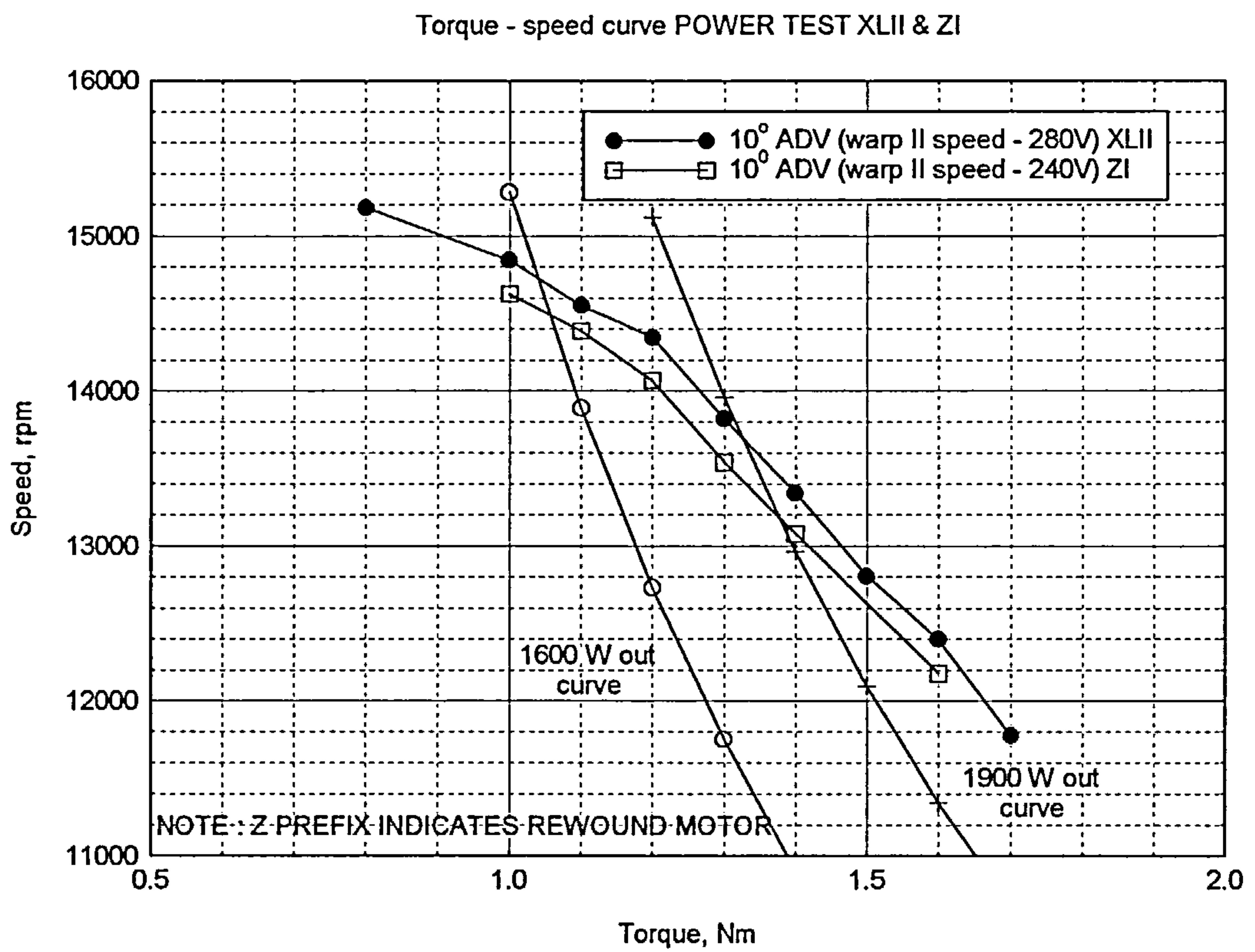


Figure 7.1 Power Tests XLII (First Prototype) and ZI (Second Prototype)
Torque – speed curves

with speed as the torque was applied. A number of different methods and calculations were used within the PIC micro-controller programs to do this.

In figure 7.2 two characteristics obtained from employing the PIC micro-controller program, "Warp II Speed", are shown with the changing applied duty-cycle. As the motor accelerates from rest the motor follows the "Increasing Speed Routine" before reaching the no-load speed. Then, as torque is applied, the motor switches to the "Load Routine". Initially the "Load Routine" changes very rapidly with motor speed (position-sensor frequency) until approximately 14800 rpm when the duty-cycle is fixed at around 75 %. This load routine produced the torque-speed curve shown in figure 7.1. From this torque-speed curve a number of conclusions can be drawn with regard to the 75 % applied duty-cycle, firstly it was instigated at too low a speed resulting in the load-power not being delivered at the torque of 1.2 Nm, and secondly it is too high at the higher torques causing the motor to exceed the constant power-output down to the torque of 1.8 Nm. Figure 7.3 shows the same characteristics in terms of the pulse-width of the signal applied to the IGBTs.

Instead of fixing the duty-cycle, of the applied signal to the IGBTs, in terms of percentage, it was fixed in terms of time with the pulse-width being kept constant. Figure 7.4 shows three torque-speed curves with different pulse-widths and the 75 % fixed duty-cycle curve for comparison. Clearly neither of these programs delivered the desired torque-speed curve, although it is important to note that some of the points recorded are actually on it. These

PIC Program "Warp II Speed" Characteristics

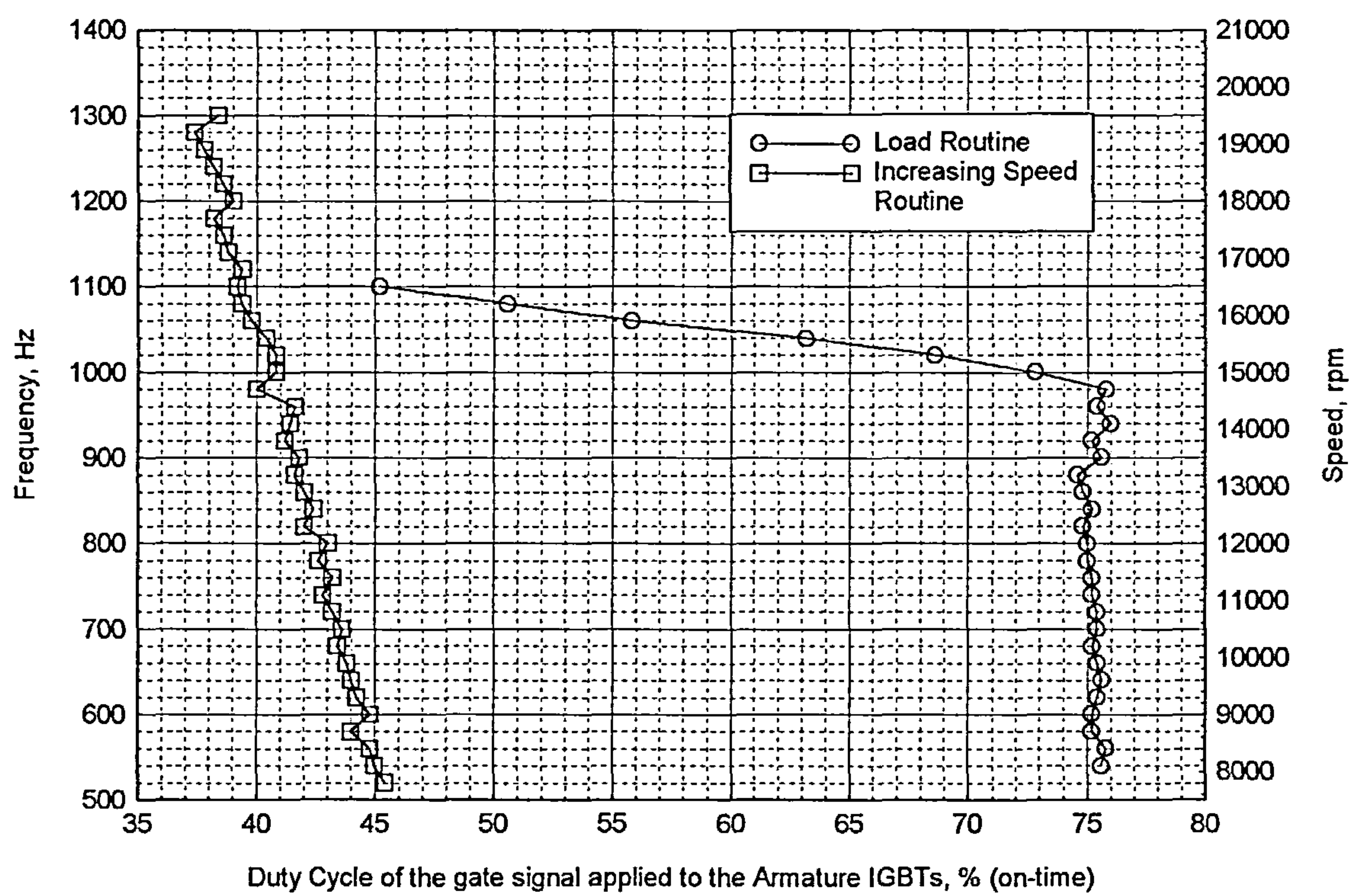


Figure 7.2 Characteristics of PIC micro-controller program "Warp II Speed"

PIC Program "Warp II Speed" Characteristics

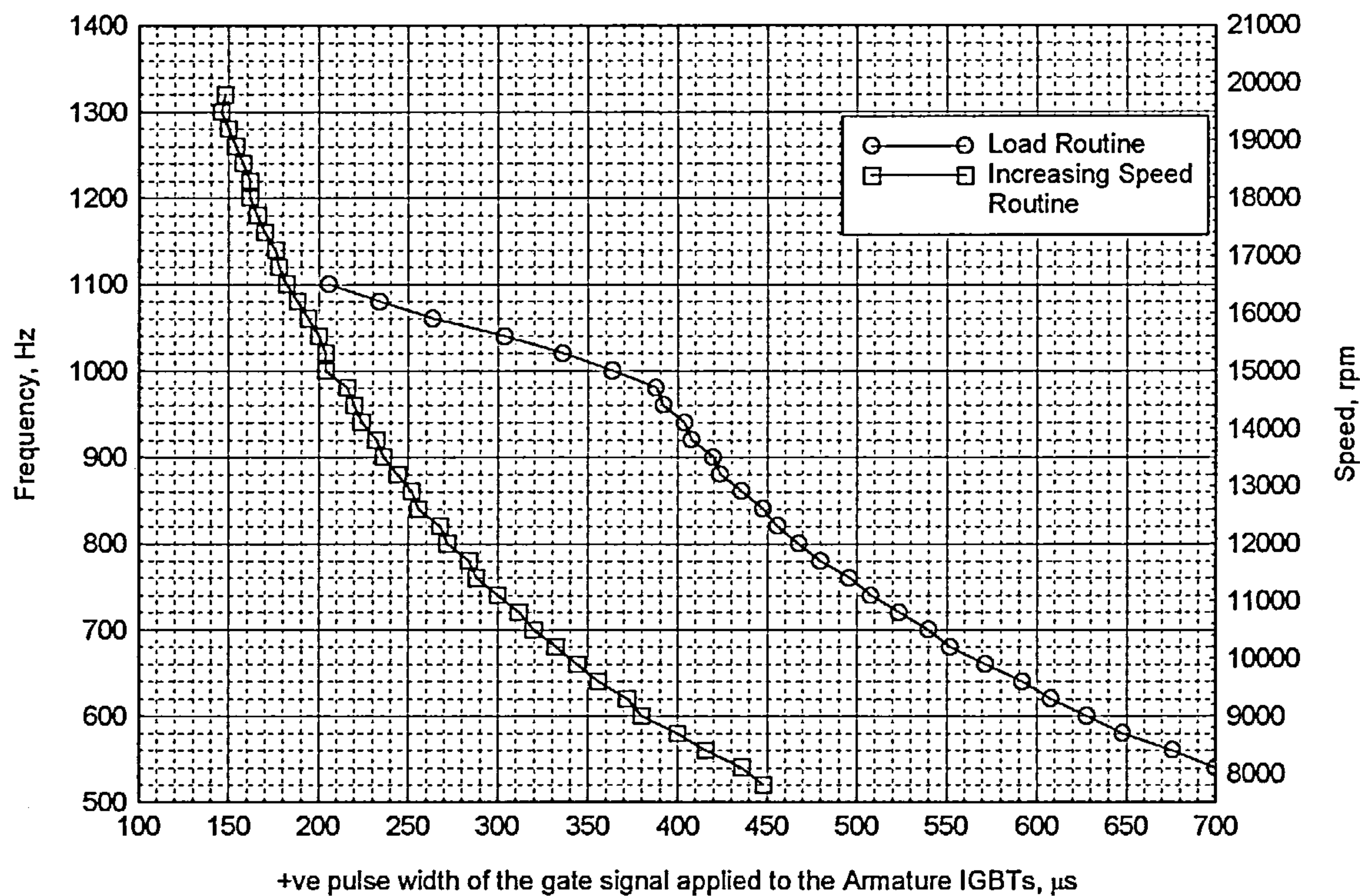


Figure 7.3 Further characteristics of PIC micro-controller program "Warp II Speed"

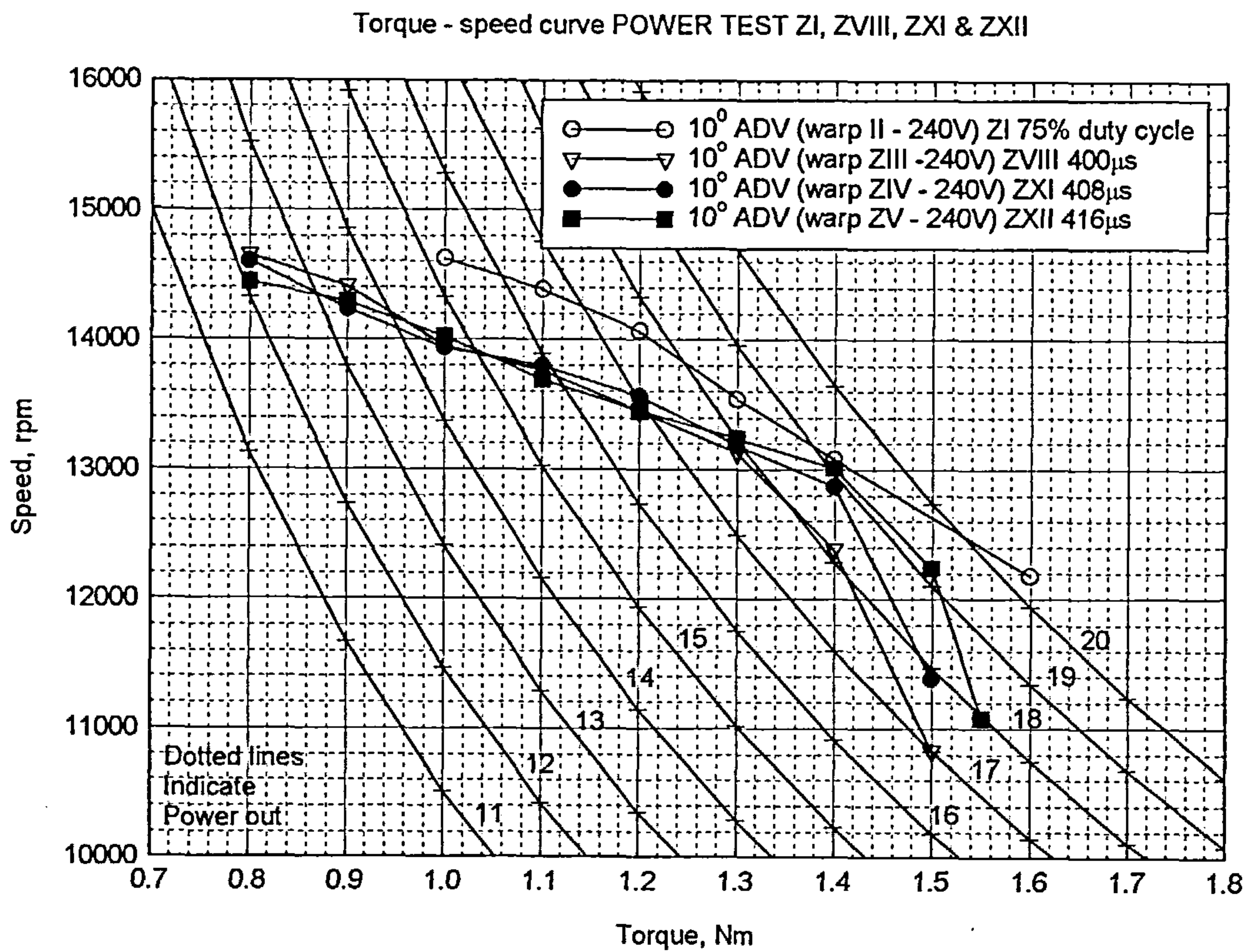


Figure 7.4 Power Tests ZI, ZVIII, ZXI, and ZXII, Torque – speed curves

tests also demonstrated that changing the applied pulse-width by only 2 % and 4 %, respectively, gave very different torque-speed curves. Figure 7.5 shows the duty-cycle of the signal applied to the IGBTs in terms of percentage in each case corresponding to the four torque-speed curves in figure 7.4. Referring to the triangular area formed by the fixed duty-cycle and fixed pulse-width curves, the desired curve had to fall within this area, which was a combination of fixed duty-cycle and time. It was also evident that the speed had to be raised to achieve the required load demand requirement.

A number of further tests were performed until the desired operating torque-speed curve was finalised, figure 7.6 shows this curve in power test ZXXXI. The speed was a lot higher than in previous tests, thus ensuring that the operating point was reached at a torque of 1.2 Nm and a speed of 15000 rpm. As the load was then increased the constant power-out curve was approximately followed.

Up until now, all of the prototype motors had previously been tested at a constant supply voltage of 240 V DC. However, the motor was supposed to operate from a single-phase line voltage of 240 V AC. Power test ZXXXII indicates the effect of maintaining a fixed voltage of 240 V AC prior to rectification rather than 240 V DC. With a few minor changes to the program the desired curve was obtained once again. Figures 7.7, 7.8 and 7.9 show the corresponding power curves for power-out, power-in and efficiency. From these it can be seen that efficiency peaks, at the operating point, with a value

PIC Program Characteristics Warp II, Warp ZIII, Warp ZIV & Warp ZV

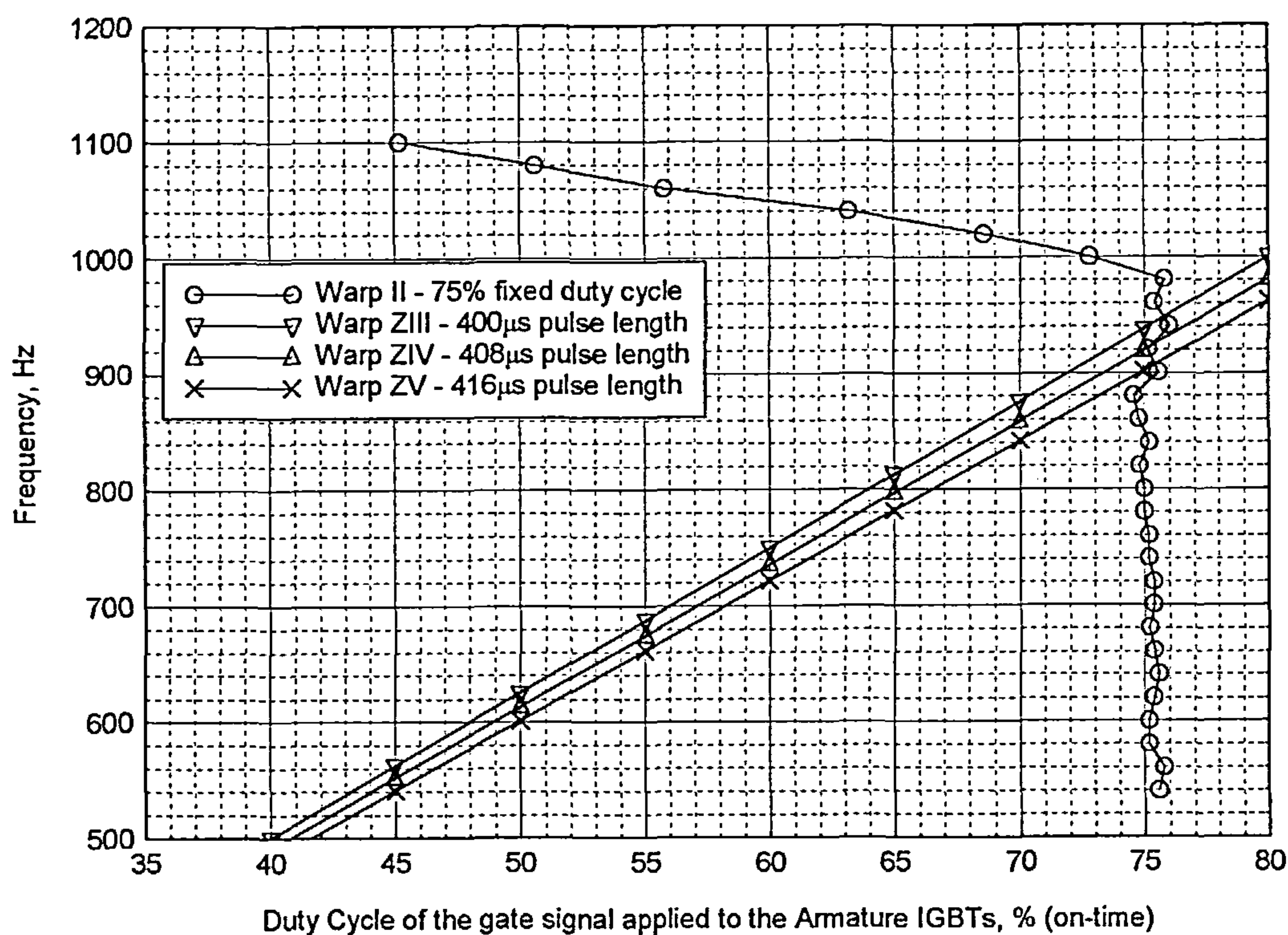


Figure 7.5 Characteristics of PIC micro-controller programs “Warp II (Speed)”, “Warp ZIII”, “Warp ZIV”, and “Warp ZV”

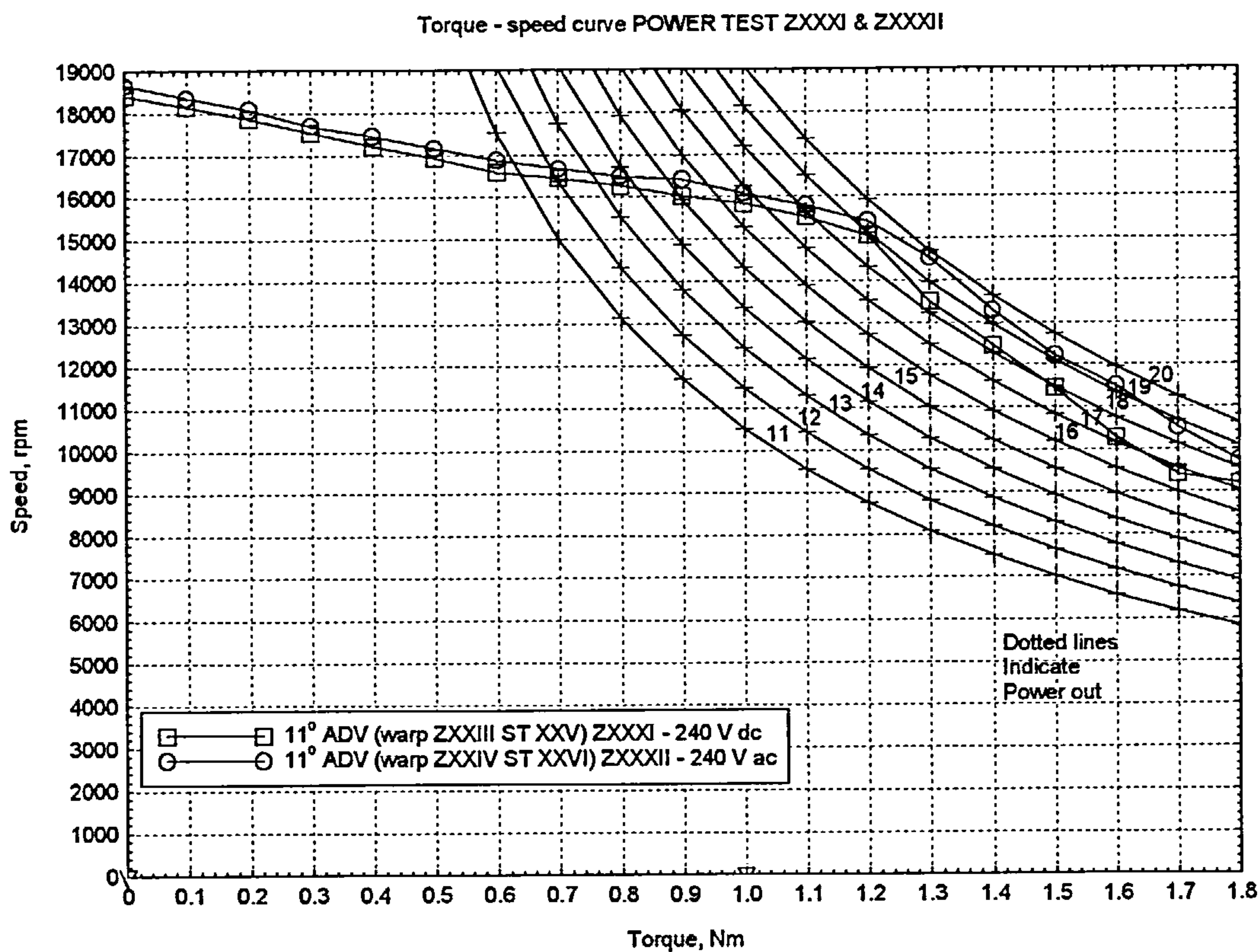


Figure 7.6 Power Tests ZXXXI and ZXXXII, Torque – speed curves

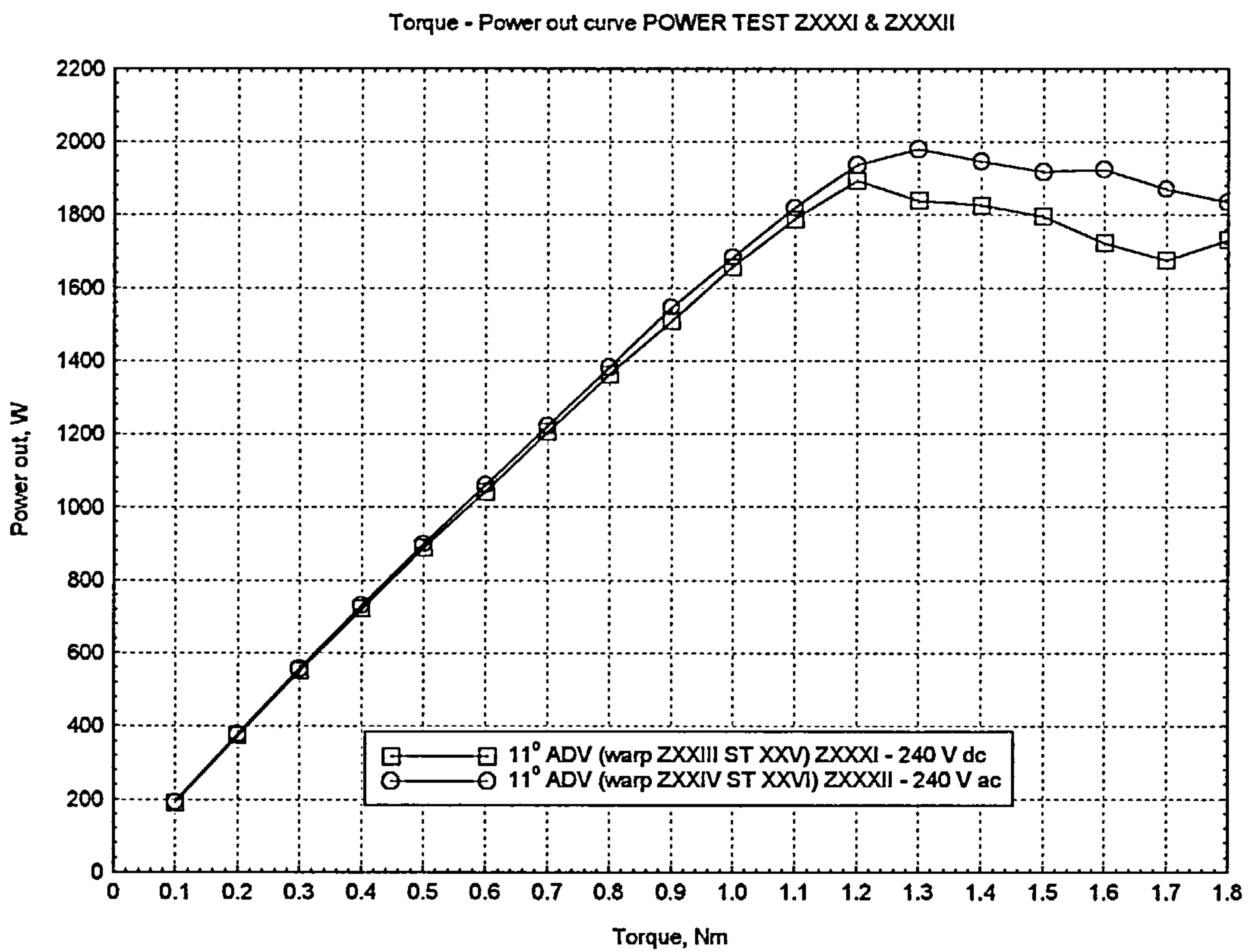


Figure 7.7 Power Tests ZXXXI and ZXXXII, Torque – power-out curves

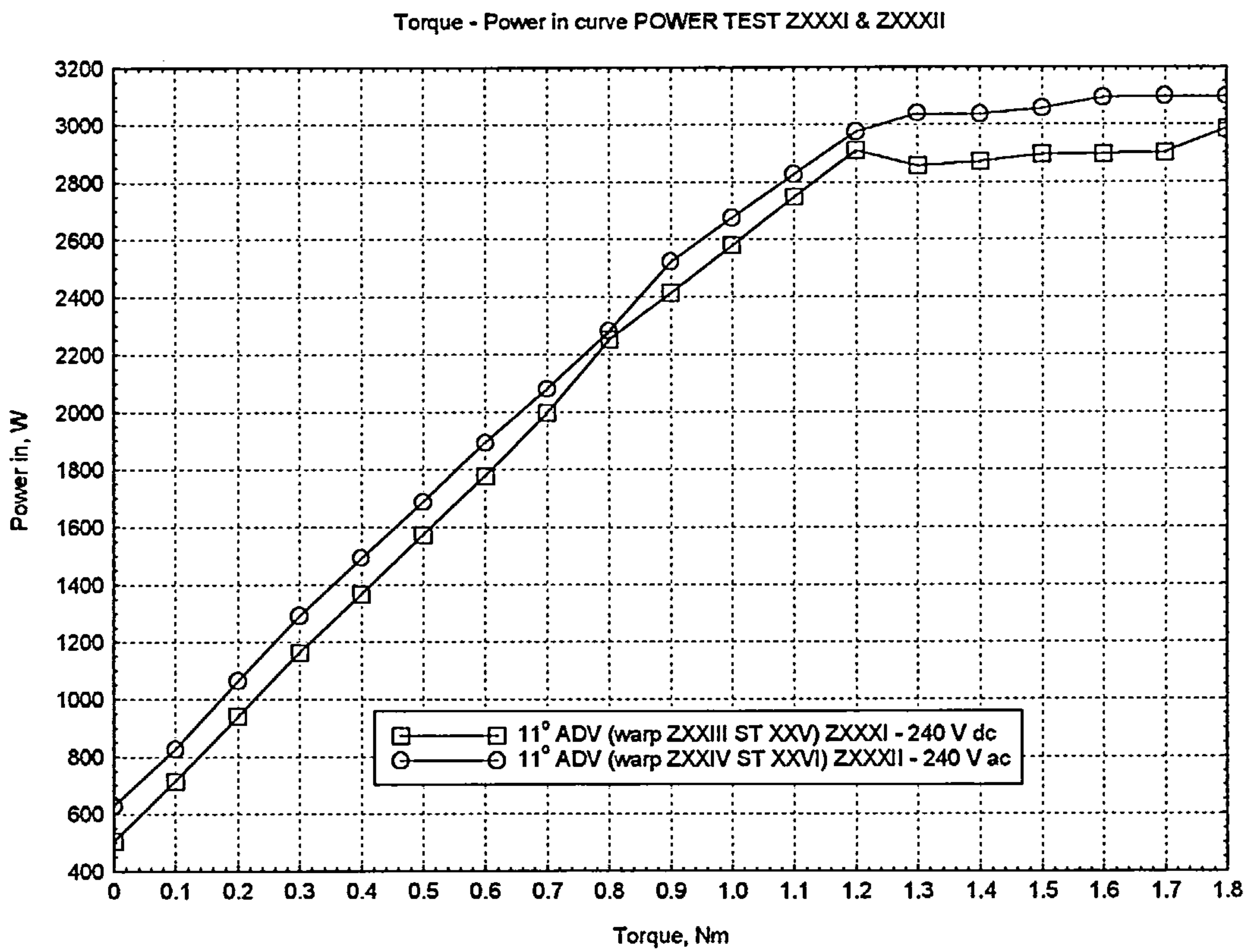


Figure 7.8 Power Tests ZXXXI and ZXXXII, Torque – power-in curves

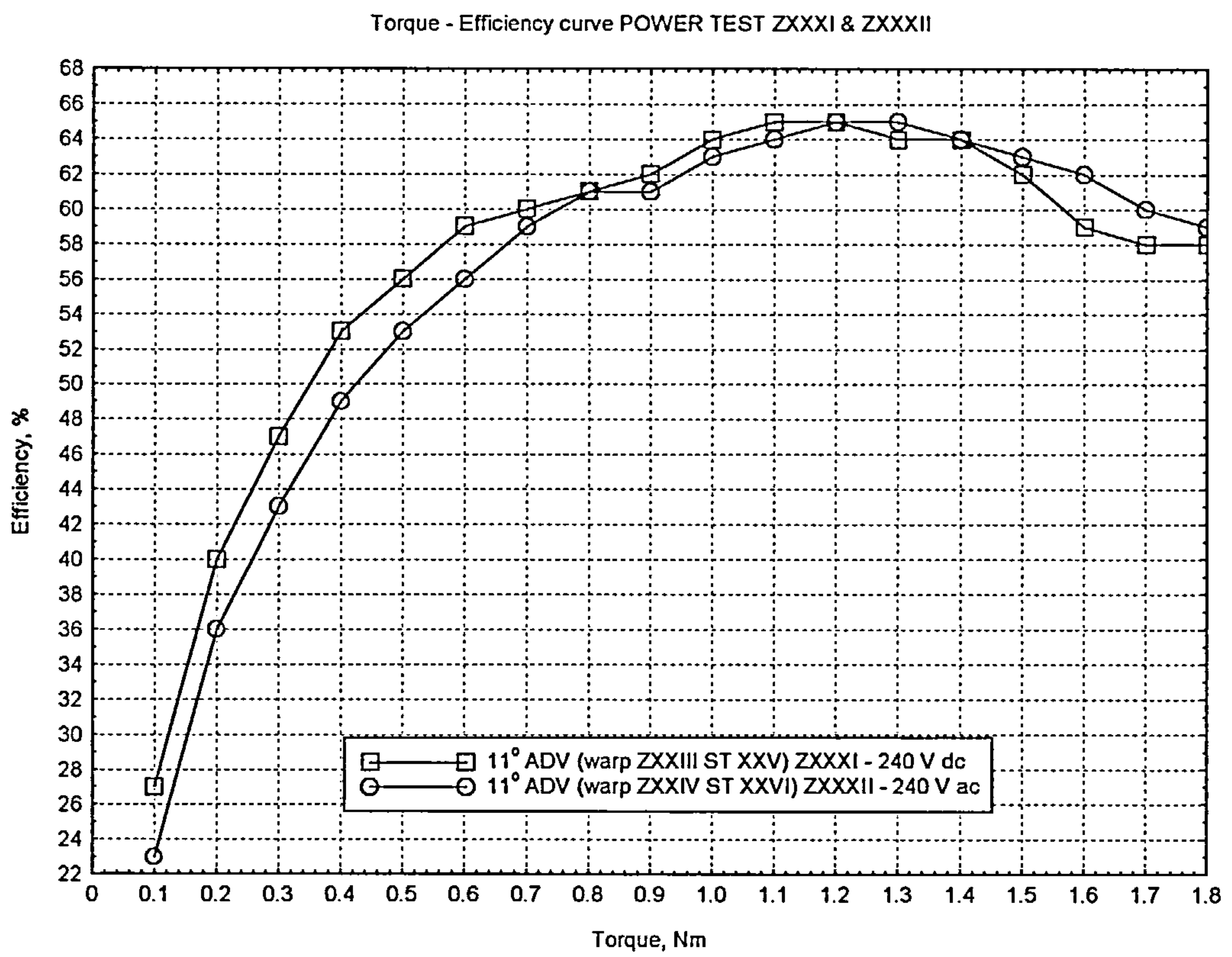


Figure 7.9 Power Tests ZXXXI and ZXXXII, Torque – efficiency curves

of 65 %, and that maintaining a comparatively constant power-in has the effect of letting the power-out decline slightly with increasing power-in.

7.2.3 Continuous power rating tests

Having achieved the desired torque-speed curve the focus shifted to the other requirements of the specification, one of which was a continuous power rating test. The motor had to be capable of maintaining a power-input of 1800 W whilst operating with a maximum 85 °C temperature rise on the windings. A test was set up whereby the power-in was kept at 1800 W by modifying the load torque in accordance with the temperature rise on the windings.

Figure 7.10 shows the results from the tests carried out with the first and second prototype motors. Immediately it can be observed that the field-winding of the first prototype is pushing the limit of the 85 °C temperature rise barrier whilst the other windings are not experiencing this. In fact, the temperature rises on both windings, of the second prototype, are considerably lower than those of the first prototype. One reason for this was that, when the motor was being rewound, the nylon outer casing was modified with air channels milled-out, to allow the circulation of the air around the outside of the stator as well as the inside. Another reason was that at the time of the two tests the second prototype was running approximately 1700 rpm faster, thus increasing the flow of air across the windings, and hence improved the cooling of them. The flow constant characteristic of the fan was 9.96×10^{-4} litres $\text{s}^{-1}\text{rpm}^{-1}$, so at 15500 rpm, with the first prototype, the fan was able to move 15.44 litres of air per

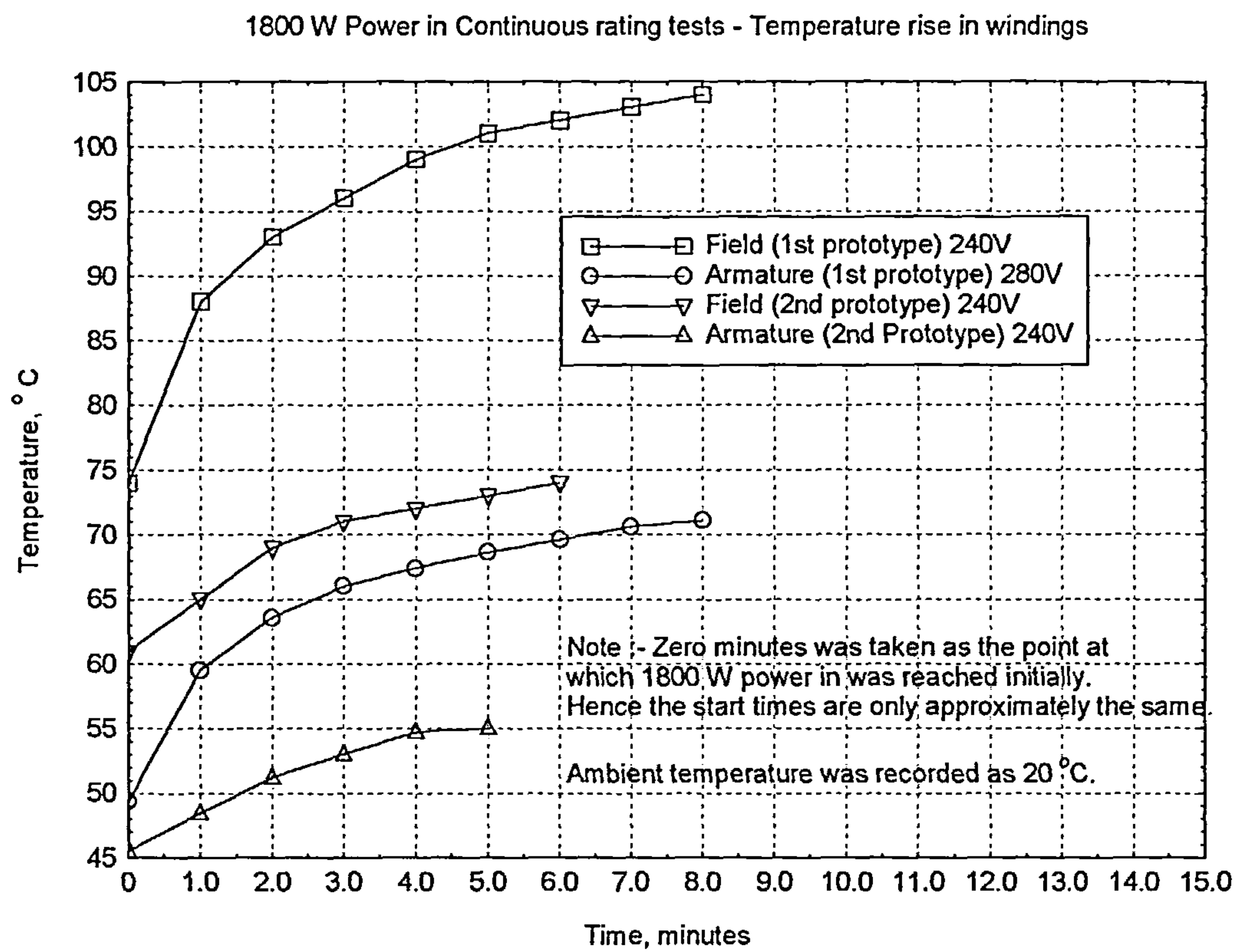


Figure 7.10 Comparison of temperature-rise in the windings of the first and second prototypes

second, and at 17000 rpm, with the second prototype, the fan was able to move 16.93 litres of air per second.

The continuous power rating test with the second prototype motor shows that the motor was easily capable of maintaining this level of power-input, and, on this basis, the motor power could be rated much higher than the present 1800 W.

7.2.4 Start-up tests

A set of start-up tests were performed with the objective of ensuring that the motor could reliably start from any rotor position using the correct inertia of $8.00 \times 10^{-3} \text{ kgm}^2$. The inertia that was already present in the system, $1.64 \times 10^{-3} \text{ kgm}^2$, included that of the dynamometer ($1.55 \times 10^{-3} \text{ kgm}^2$) and the flexible coupling ($0.09 \times 10^{-3} \text{ kgm}^2$) linking the motor to the dynamometer, subtracting these left a shortfall of $6.36 \times 10^{-3} \text{ kgm}^2$. A flywheel was manufactured to add the correct inertia to the mechanical system. As the flywheel had to rotate at speeds in excess of 19000 rpm, it was dynamically balanced to avoid potential damage, to the mechanical system, by vibration. For the purpose of the start-up tests the flywheel was mounted on the non-drive end of the dynamometer.

Unfortunately, when the calculations for the flywheel were performed they were a factor of π out due to an error. The flywheel's inertia was $19.98 \times 10^{-3} \text{ kgm}^2$ that led to a total inertia of $21.62 \times 10^{-3} \text{ kgm}^2$, which was 2.7 times larger than specified. This error was only realised after the testing had been completed.

With the “correct” inertia (as designed) in place testing resumed. As before it was found that the motor had particular difficulty starting around the position-sensor edges. The motor had been designed such that a starting-torque could be developed in any position, assuming that the commutation axis of the IGBTs was synchronised with the motor’s neutral axis, as defined by the zero-crossing of the back-EMF. However, because the commutation-axis was statically in advance of the neutral-axis, as shown in figure 7.11, there was a period in which negative torque was developed before the neutral-axis as the armature-current was reversed. If the motor had not accumulated enough momentum to carry it through the small negative torque region, it would have decelerated and stopped before rotating in reverse. Thus, initiating the same sequence of events to occur in reverse so producing an oscillation. As the oscillation increased in frequency, it was interpreted by the PIC micro-controller as an increase in speed, as there was no discernable difference from normal motoring acceleration in one direction. This caused the PWM duty-cycle applied to the IGBTs to increase and, because a negligible back-EMF was generated, the full supply voltage was still available. A large current, therefore, was passed through the IGBTs and the windings. The drive-protection circuit prevented the drive from being damaged, by shutting down the power devices, before the current got too high. This problem had to be overcome, as the drive-protection circuit was only being used as a temporary development tool.

Figure 7.12 shows the motor experiencing normal starting operation with the rotor positioned three degrees prior to commutation, sufficient momentum was

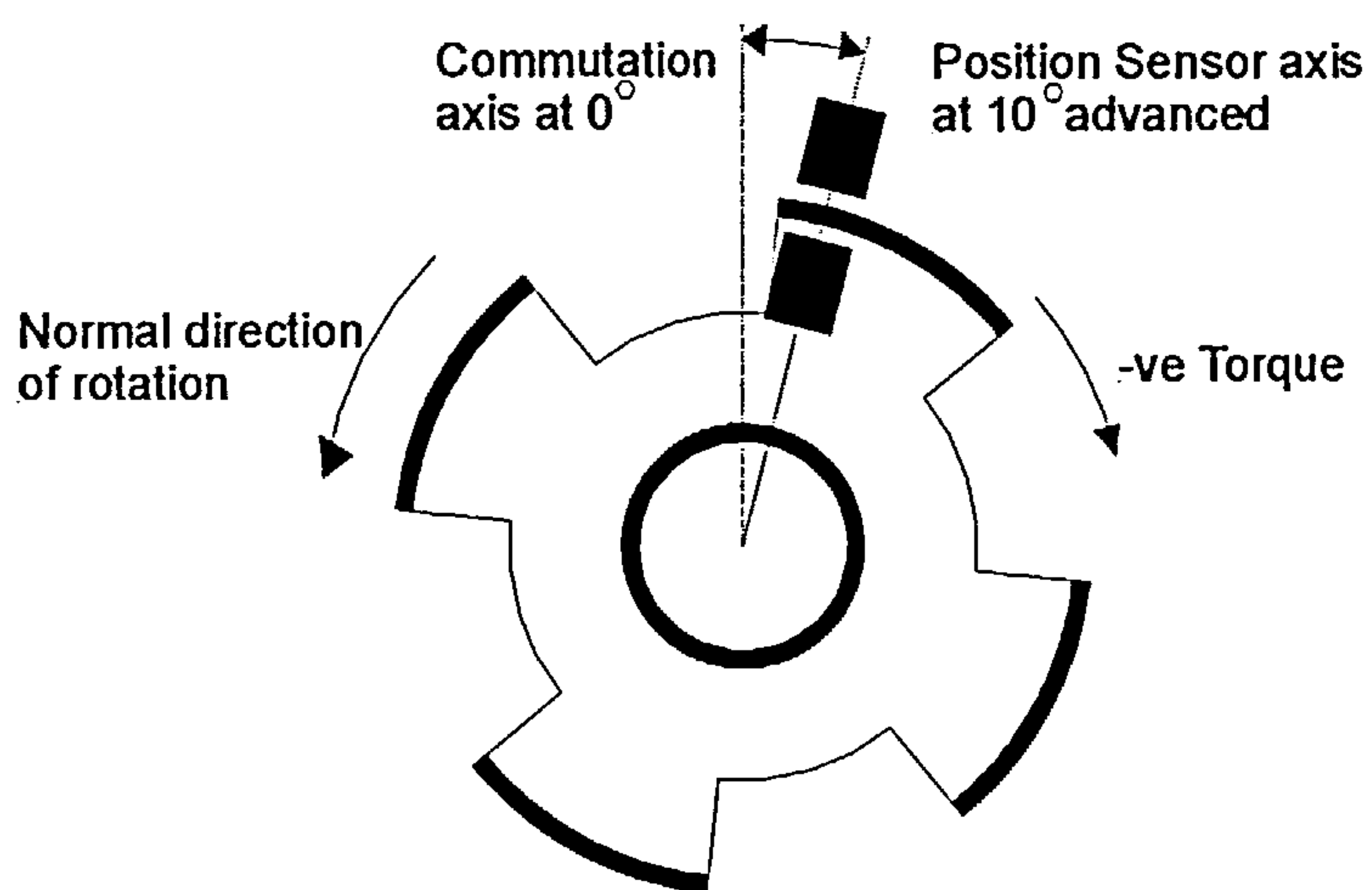
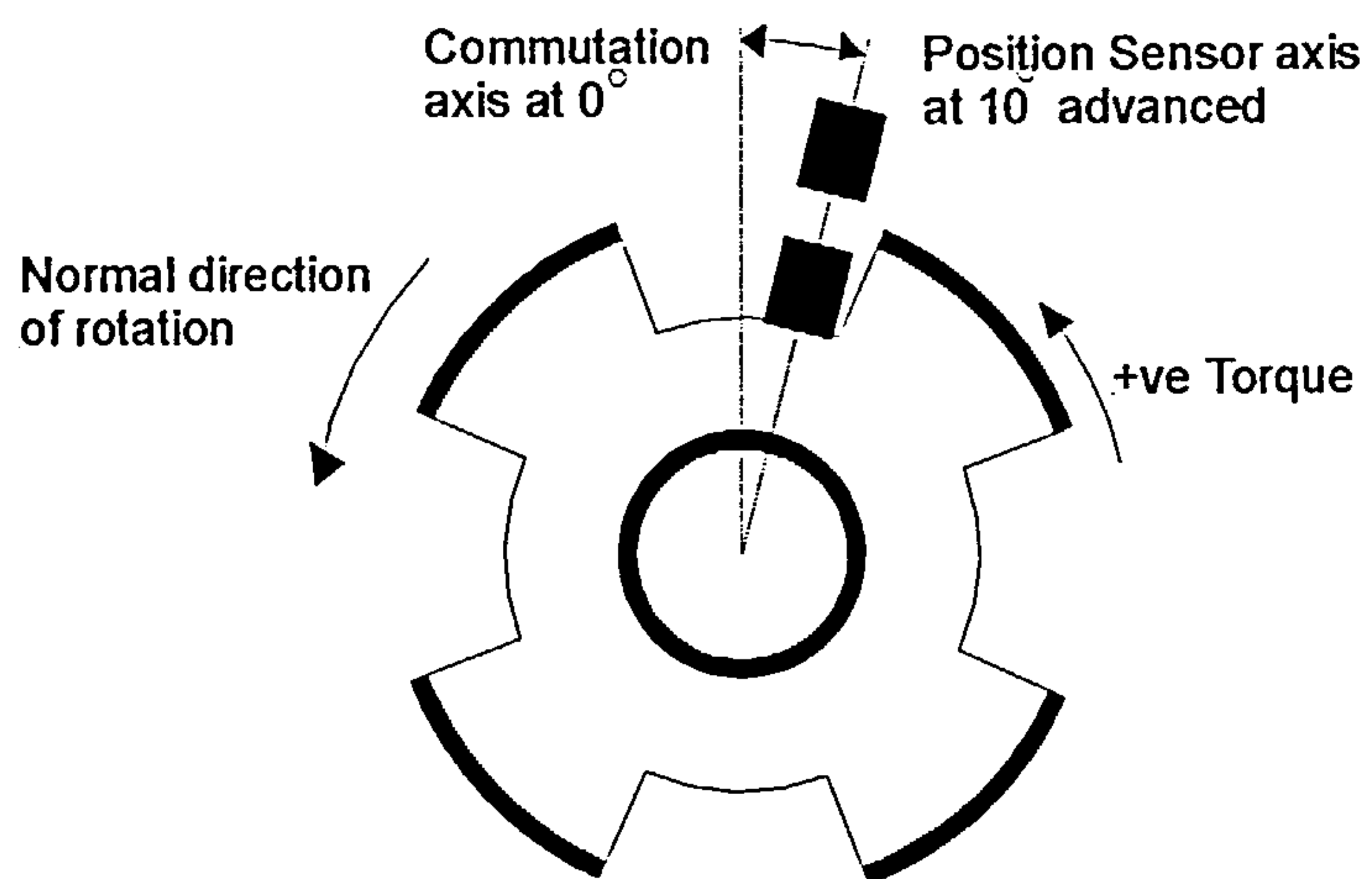


Figure 7.11 Position sensor showing the effects of the advance-angle

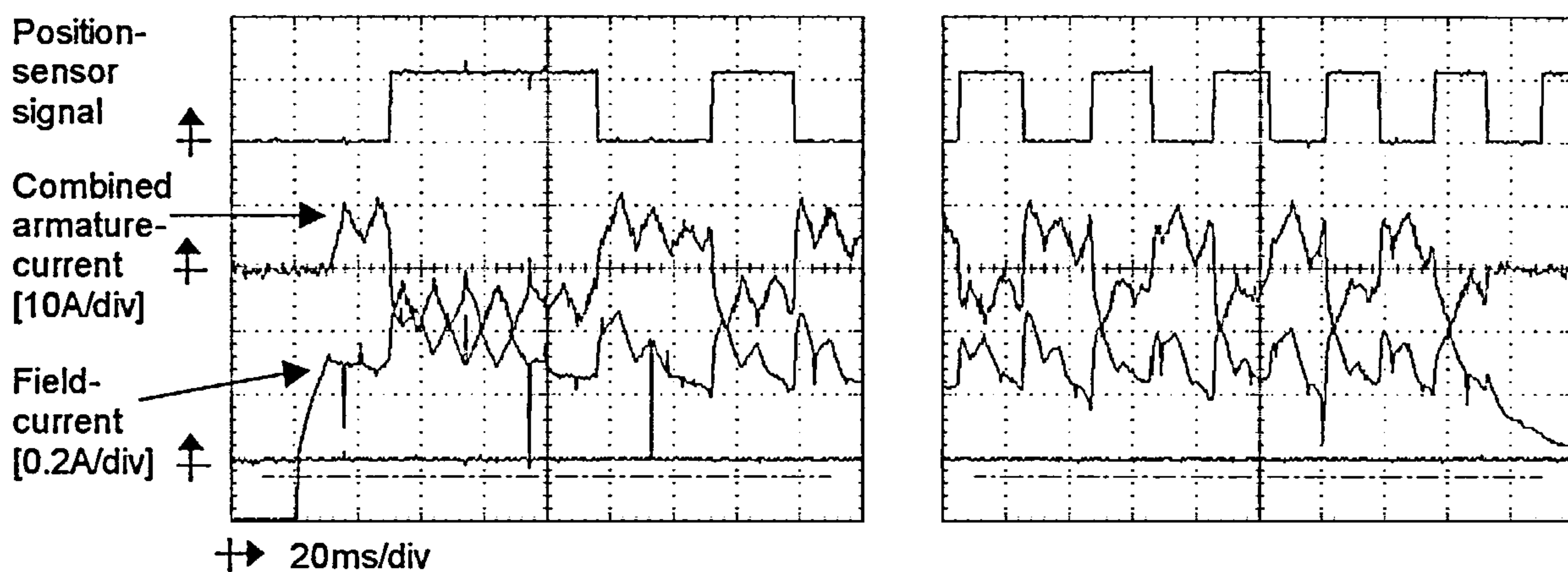


Figure 7.12 Normal starting operation with rotor positioned three degrees prior to commutation, sufficient momentum is accumulated to overcome the negative torque region

accumulated to overcome the negative torque region. Figure 7.13 shows the motor starting and oscillating around a position-sensor edge with the rotor initially positioned one degree prior to commutation. Insufficient momentum was accumulated to overcome the negative torque region in this case.

A solution to this problem was to delay and realign the advanced commutation axis with the neutral axis. As the motor needed a static advance to operate, as previously described, the best option was to perform this realignment electronically. With the stated inertia present it was found, via a series of tests, that a 15 ms delay to commutation, after a position-sensor edge, was enough to ensure starting without oscillation. The 15 ms delay was removed after four commutations had occurred, reverting back to the normal advanced mode of operation. Figures 7.14 and 7.15 show the effect of the time-delay when the rotor was positioned just before and just after a position-sensor edge respectively.

The task remaining was to push the IGBTs nearer to their limit in order to achieve the desired acceleration-time. The finalised starting routine is shown in Figure 7.16 with a selection of 20 ms oscilloscope frames taken from the complete starting routine. Figure 7.17 shows the acceleration ramp of the motor from this test, and it can be observed that the no-load speed of 18000 rpm was reached in just over 2.2 s. The average-torque exerted during start-up to accelerate the motor from standstill to 18000 rpm in 1.2 s was calculated as,

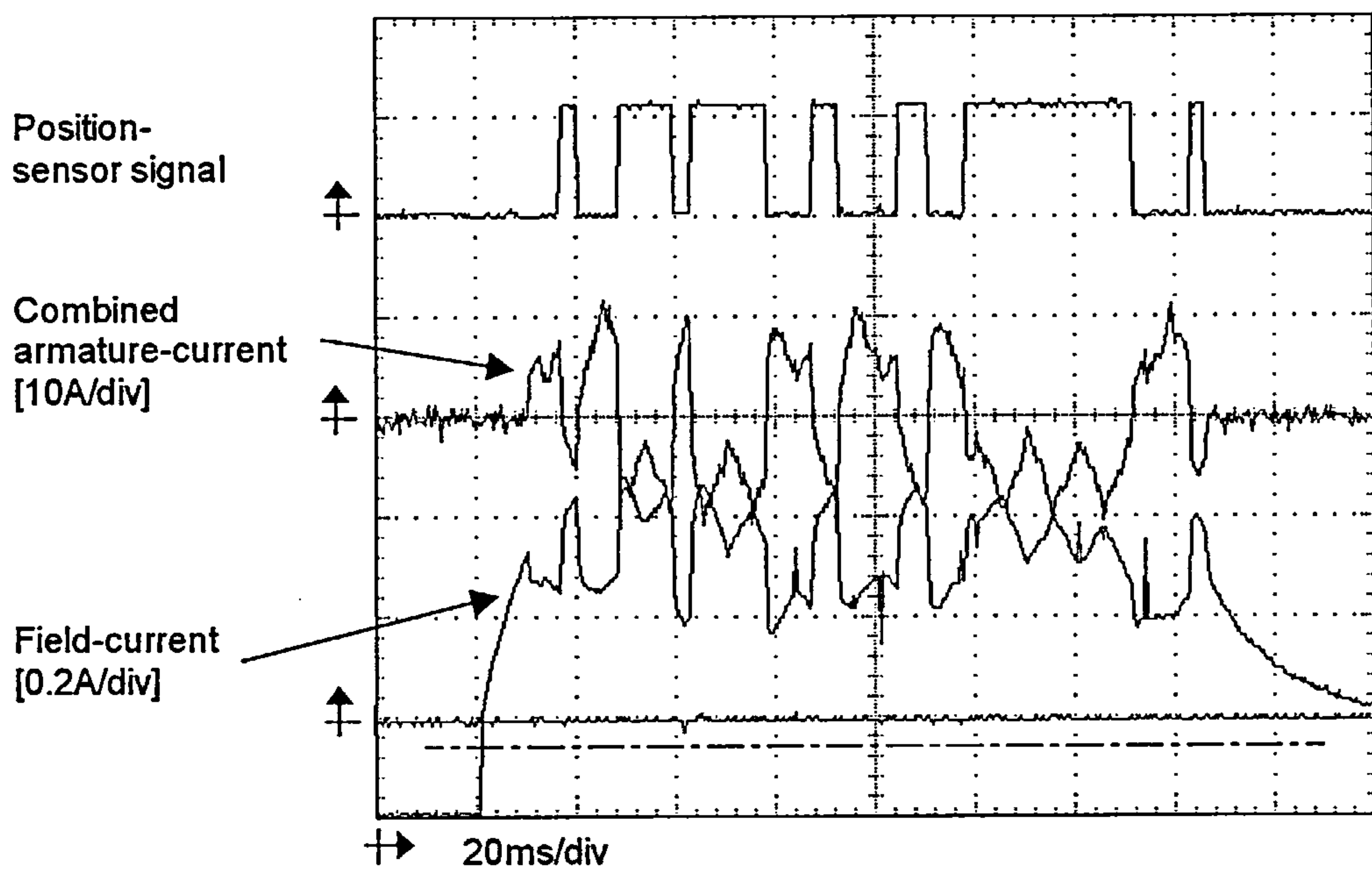


Figure 7.13 Oscillation of motor at starting around a position-sensor edge with rotor positioned one degree prior to commutation; insufficient momentum is accumulated to overcome the negative torque region, (Each high and low position-sensor edge consists of forward and backward motion, which shouldn't be confused with rotation)

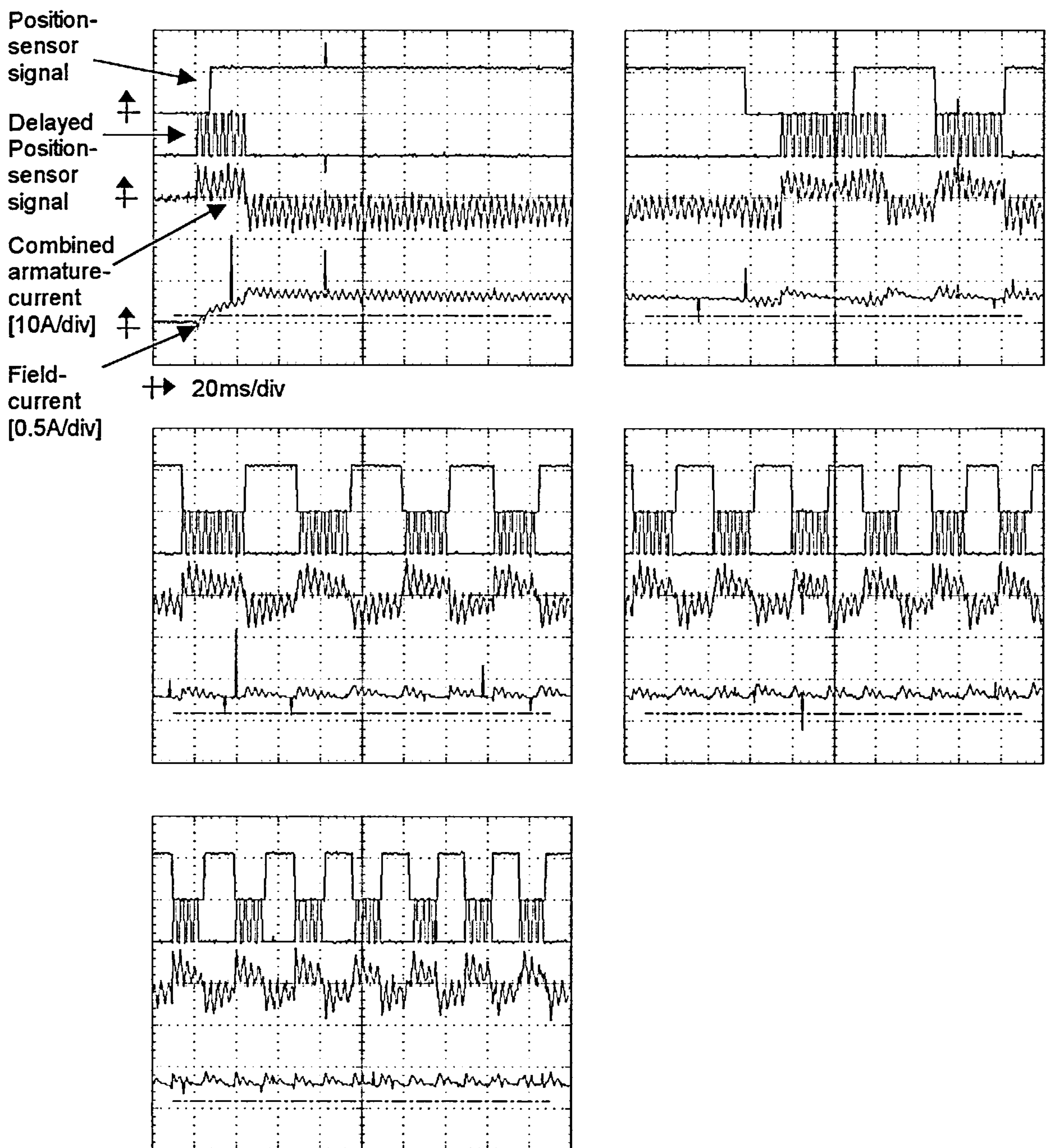


Figure 7.14 Starting operation with 15ms delay with rotor positioned in low state just prior to commutation. In the low state the motor starts in the correct direction of rotation with no negative torque, on the 4th edge normal operation resumes and the motor continues to rotate

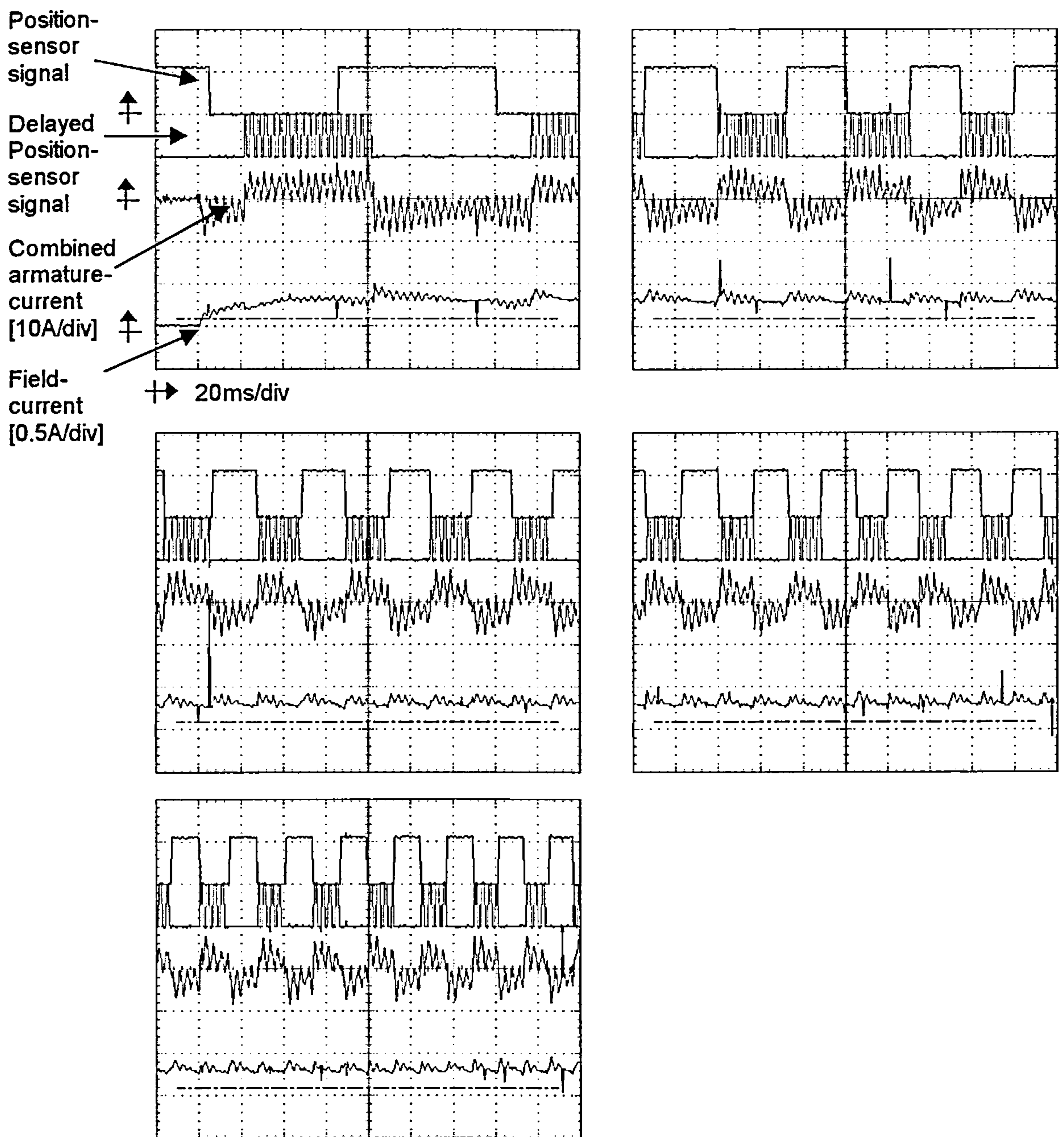


Figure 7.15 Starting operation with 15ms delay with rotor positioned in high state just prior to commutation. In the high state the motor starts in the reverse direction of rotation due to negative torque. Rotation continues in reverse passing a position sensor and so initialising the delay. Commutation occurs after the duration of the delay allowing the rotor to turn back in the correct direction and continue to rotate. On the 4th edge normal operation resumes

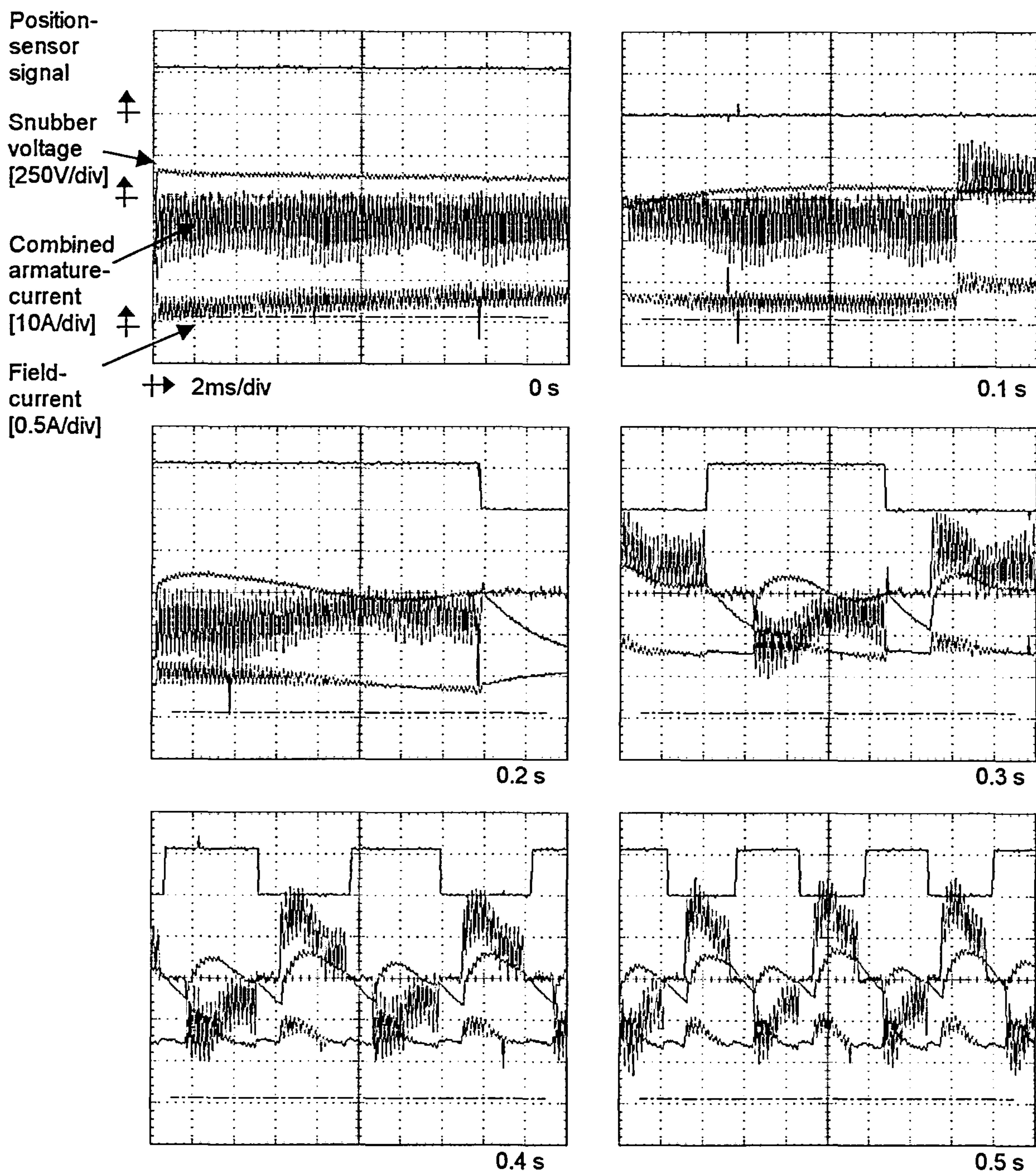


Figure 7.16 Final starting routine shown with selected waveforms with time from start indicated (continued on next page)

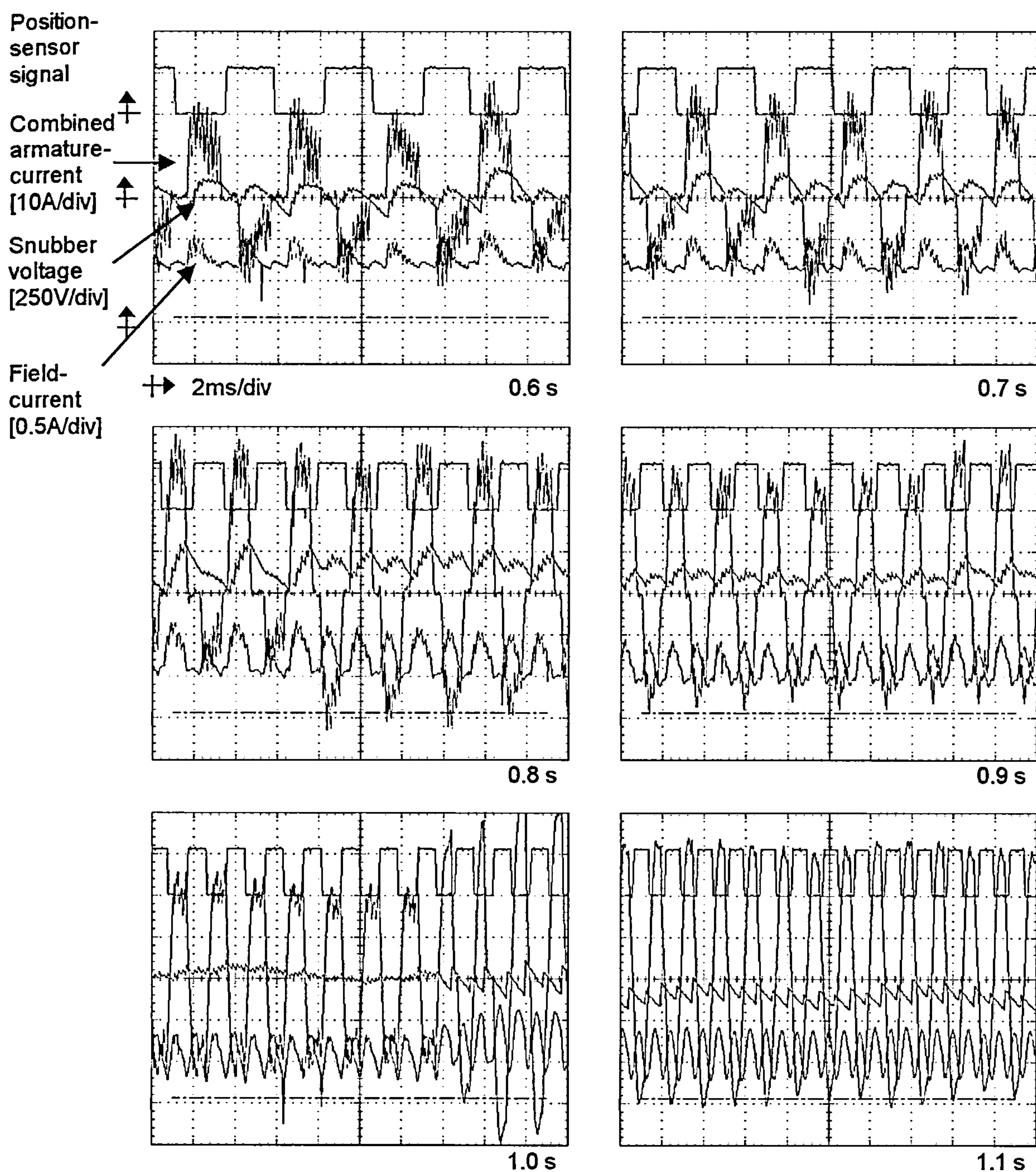


Figure 7.16 Final starting routine shown with selected waveforms with time from start indicated (continued from previous page and on next page)

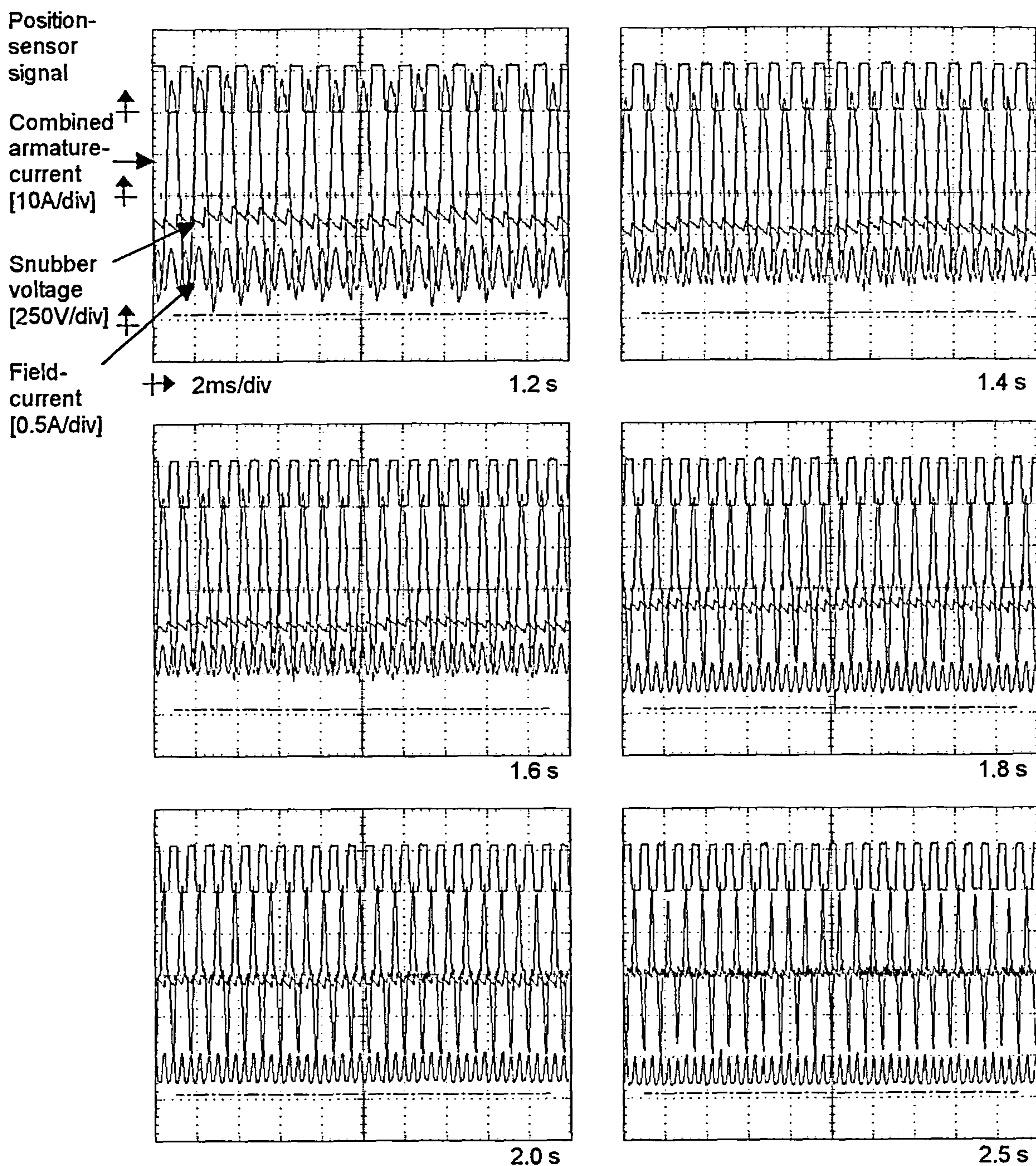


Figure 7.16 Final starting routine shown with selected waveforms with time from start indicated (continued from previous page)

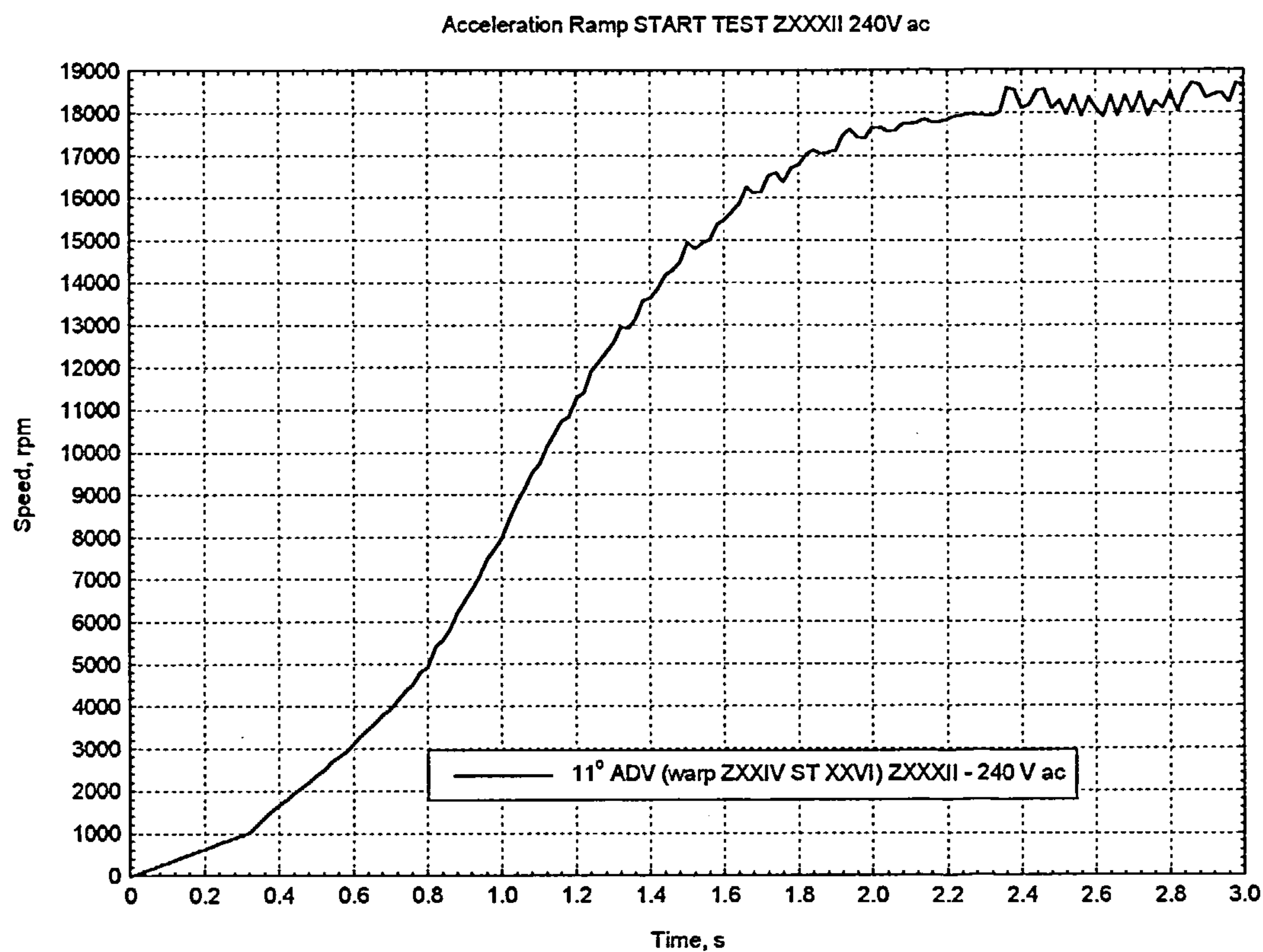


Figure 7.17 Acceleration ramp of second prototype motor

$$T = I_o \alpha \quad (7.1),$$

$$\text{where } \alpha = \frac{d\omega}{dt} \quad (7.2),$$

$$\omega = 18000 \text{ rpm} = 1885 \text{ rads}^{-1} \quad (7.3),$$

$$t = 2.2 \text{ s} \quad I_o = 21.6 \times 10^{-3} \text{ kgm}^2 \quad (7.4),$$

$$\text{hence } T = 18.5 \text{ Nm} \quad (7.5).$$

If the same starting torque had been applied to the correct inertia the acceleration time would have been reduced by a factor of 2.7 to 0.82 s. The specification had originally called for an acceleration time of 0.5 s for a no-load speed of 14000 rpm, assuming a linear acceleration profile the time taken to reach 18000 rpm would have been 0.64 s. Therefore the tested time taken was still 28 % greater than that desired.

7.2.5 Test conclusions

Testing of the second prototype motor developed from the experience gained from testing the first prototype. First of all, it was demonstrated that the armature rewind was successful. The motor performed as expected, and delivered the desired power-output. Then, through a series of tests the required reserve-torque of one-and-a-half times load-torque was achieved, and this was produced with a constant power-output. The start-up tests were completed successfully in that the motor was able to start from any rotor position. The problems with starting at positions around a position-sensor edge were resolved with a simple change to the starting routine. A continuous

power rating test was carried out and the results from this showed that the motor was easily capable of maintaining the 1800 W level of power-input required with a moderate temperature rise of the windings. In fact, on this basis the motor could be rated much higher.

In conclusion, testing of the second prototype motor showed that it was able to start efficiently from any position, deliver the power-out required at rated torque, deliver the reserve-torque required, and perform within the desired continuous power rating. The only remaining questions were concerned with the efficiency of the gearbox, and whether a series-wound motor would produce better results. To address these questions testing was continued with two further prototypes.

7.3 Dynamic testing of the third prototype motor

7.3.1 Power tests

A motor-failure problem that had occurred with both previous prototypes was investigated. This revealed that the rotor did not remain concentric with the stator. During tests at the higher torques, the imbalance of forces caused the airgap to close completely at the narrowest point, thus stalling the motor. The reason for the loss of concentricity was that the surrounding glass-reinforced-nylon casing construction was not sufficient to withstand the large radial forces produced [61]. To overcome this problem a new aluminium casing was designed. As it would no longer drop in to the application as a replacement, it

was decided that the gearbox did not have to be incorporated for present purposes.

Testing of the shunt-motor, without a gearbox, was achieved with this third prototype via a single power test that was carried out as a comparison with the last test performed on the second prototype. The results are shown in figures 7.18, 7.19, 7.20 & 7.21. Referring to the efficiency of the two motors, in figure 7.21 it can be seen that the largest difference between the two was 5 % at a torque of 1.7 Nm. At this point both power-inputs were the same at 3.1 kW. However, the third prototype without a gearbox was able to deliver an additional 135 W, and this accounted for the rise in efficiency to 65 %. It was predicted that, at worst case, the efficiency of the gearbox would be 92 %. However owing to the difficulties referred to above this figure could not be verified.

7.3.2 Test conclusions

In conclusion, the results of the test showed that despite modifications that improved the performance, the target efficiency, given in the specification, of the motor (75 %), was not reached.

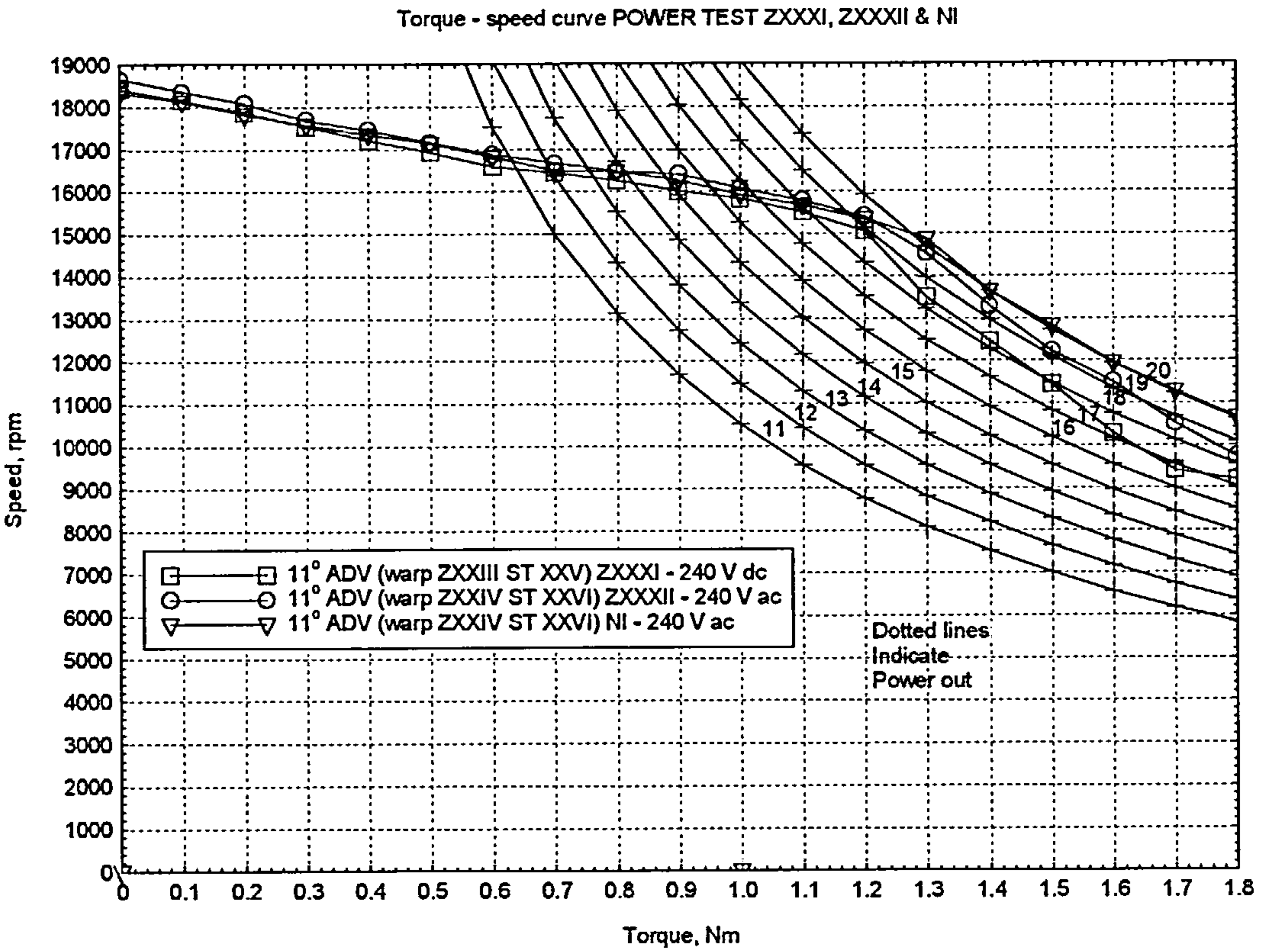


Figure 7.18 Power Test NI, Torque – speed curve of third prototype motor (without gearbox)

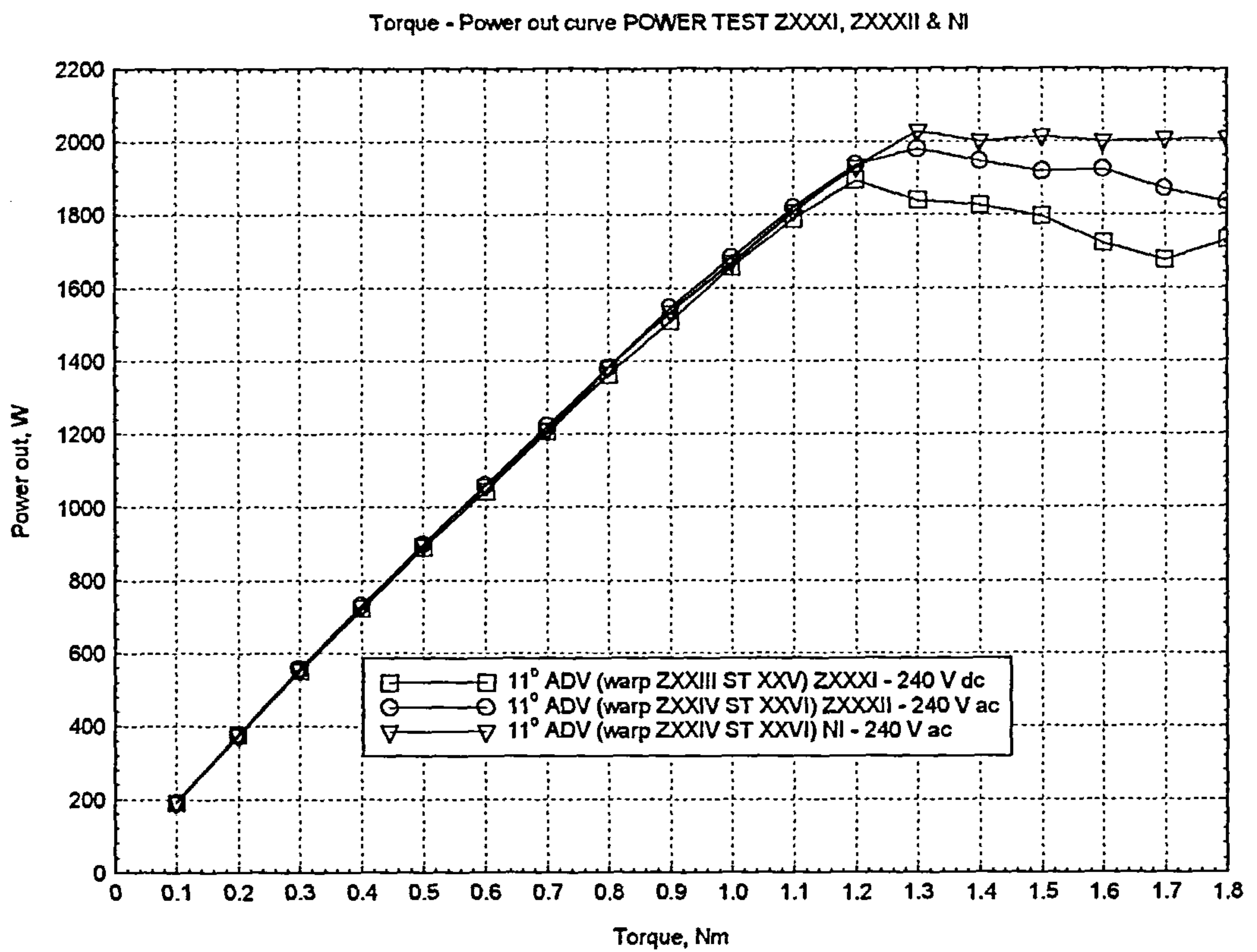


Figure 7.19 Power Test NI, Torque – power out curve of third prototype motor (without gearbox)

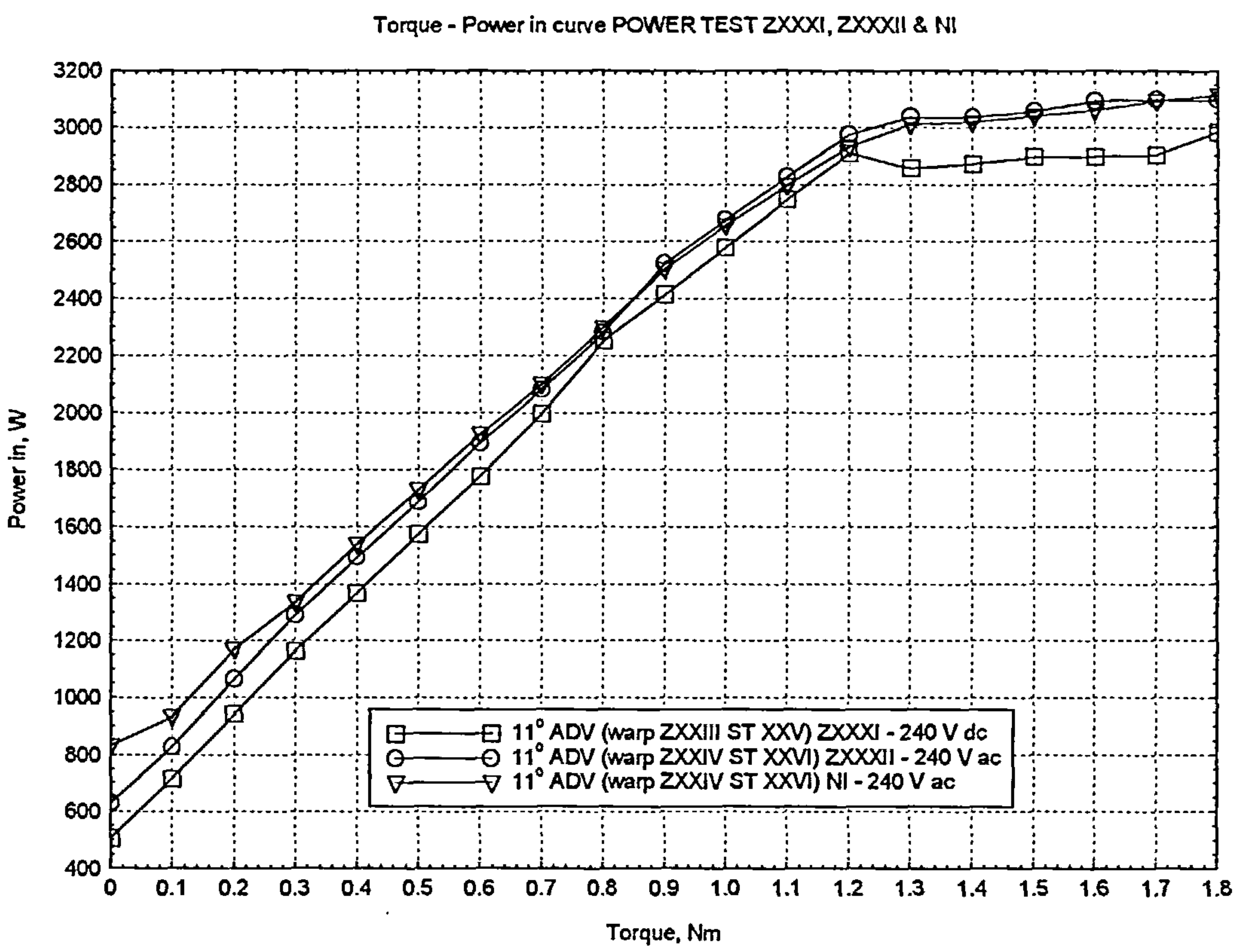


Figure 7.20 Power Test NI, Torque – power in curve of third prototype motor (without gearbox)

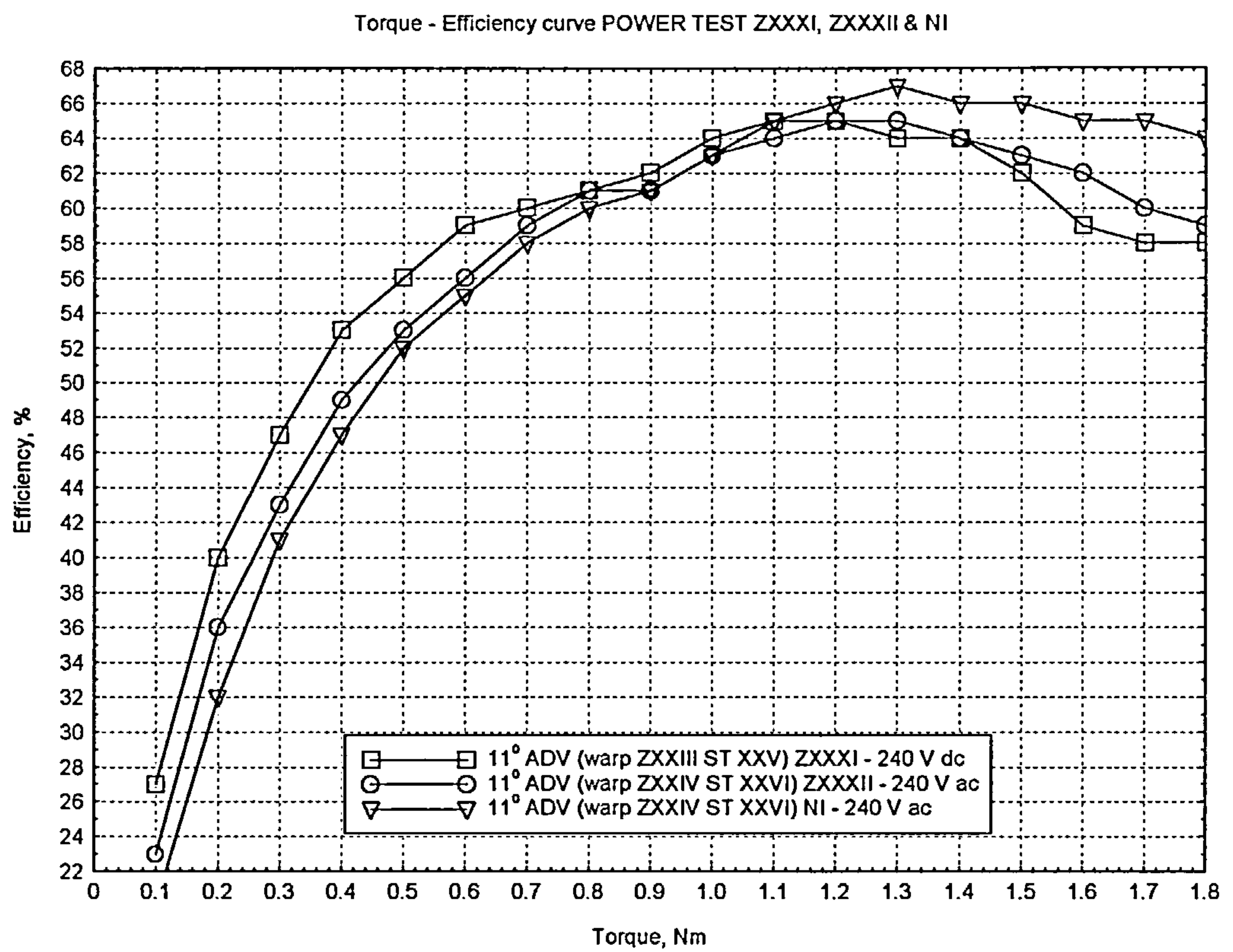


Figure 7.21 Power Test NI, Torque – efficiency curve of third prototype motor (without gearbox)

7.4 Dynamic testing of the fourth prototype motor

7.4.1 Power tests

The armature-winding of this fourth prototype motor remained unchanged from that of the second prototype (that is 68 turns and a wire diameter of 1 mm).

The field-winding was rewound, according to the calculations given in Chapter 5, with a base number of 112 turns, and, in addition, two further windings of 8 turns each. All of the field-windings used a wire diameter of 0.85 mm. These additional windings were able to give flexibility to the testing, that is, it gave a choice of 112, 120 or 128 turns, without the need for a further rewind. The intention of this fourth prototype motor was simply to deliver the desired power-out, with the correct supply-voltage of 240 V, and to demonstrate whether, or not, the series-motor, would be a better option than the shunt-motor for the application in question.

The power-converter of the series-motor prototype could be connected in a number of different configurations, as described in Chapter 5, which gave scope for a range of tests using these configurations. Initially, as shown in figure 5.6, capacitor values of 3300 μF and 3470 μF were used for capacitors C1 and C2 respectively. Capacitor C1 was the DC-link capacitor, used to smooth the rectified DC-output, and capacitor C2 was the capacitance across the armature circuit that was needed to contain the returned energy from the armature circuit. Both capacitors were of electrolytic type.

The three field-windings of the motor were connected in series (total number of turns 128), and the motor was tested using the same PIC micro-controller program (Warp ZXXIV STXXVI) and test conditions (11° mechanical advance and 240 V AC) that were last used with the third prototype. The resulting torque-speed curve is shown in figure 7.22, with power-out, power-in and efficiency shown in figures 7.23, 7.24 and 7.25 respectively. It can be seen that the motor delivers the desired torque-speed curve, and is very similar in performance to the third prototype shunt-motor. Figure 7.26 shows the current-waveforms recorded for the third prototype shunt-motor and the series-motor for comparative purposes. The combined armature-currents, in both waveforms, are almost identical in magnitude and shape. The field-current waveform for the shunt-motor is on a scale of 200 mA per division, whereas the scale for the series-motor is 10 A per division. Taking these scales into account the ripple on both waveforms is in the order of 40 %, and, again, the shape of the waveforms is very similar. In conclusion, the behaviour of the two motors was comparable in terms of the outputs obtained.

Bearing in mind that the overall objective is to produce a low-cost implementation, the use of these electrolytic capacitors is not realistic because they are too expensive, owing to their large value of capacitance required. The physical size of the capacitors also made them impractical for a real product implementation. Although it had been decided that the refinement of the component sizes would occur at a later date, these capacitors were integral to the operation of the power-converter circuit. Therefore this needed to be

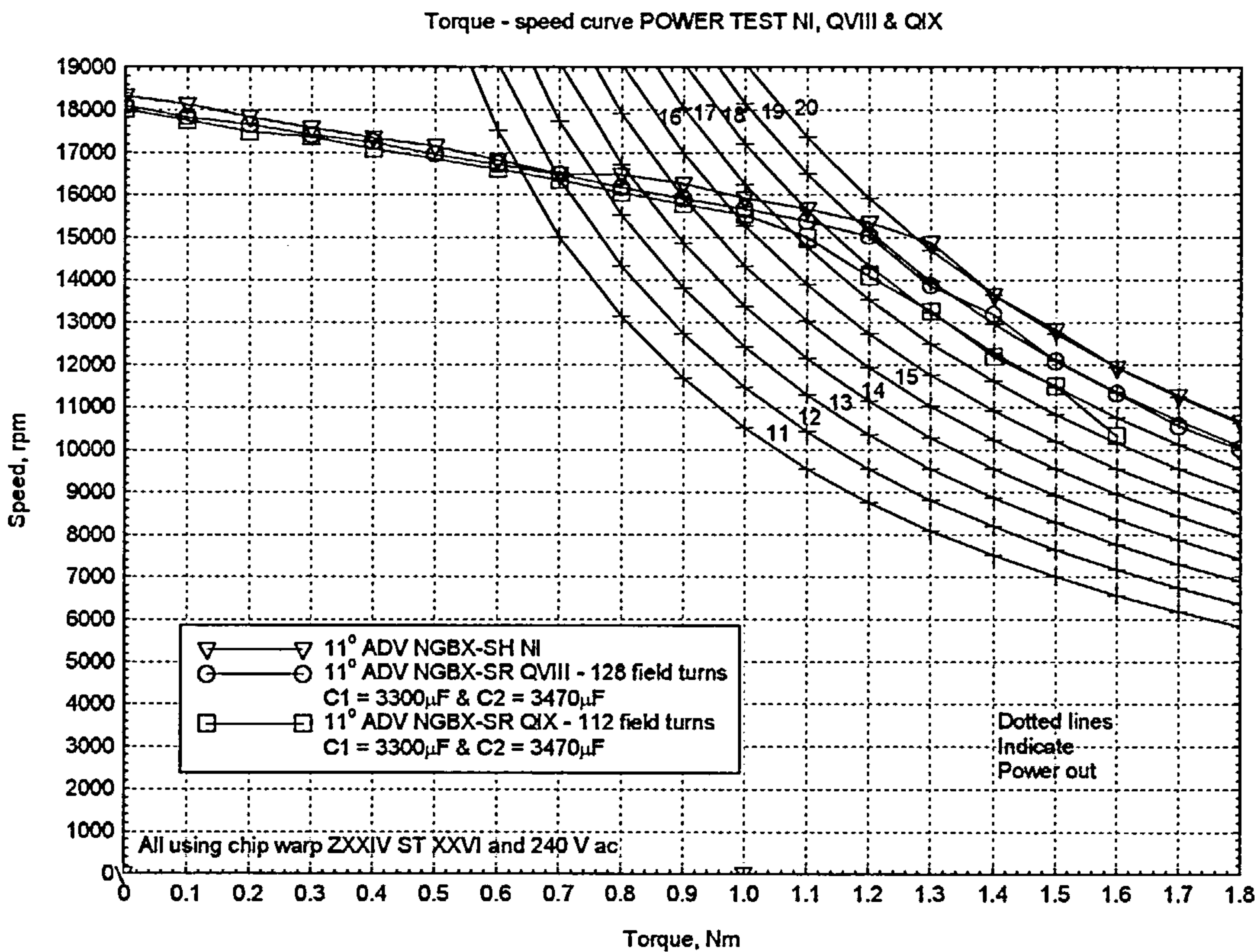


Figure 7.22 Power Test QVIII and QIX, Torque – speed curves of fourth prototype series-motor

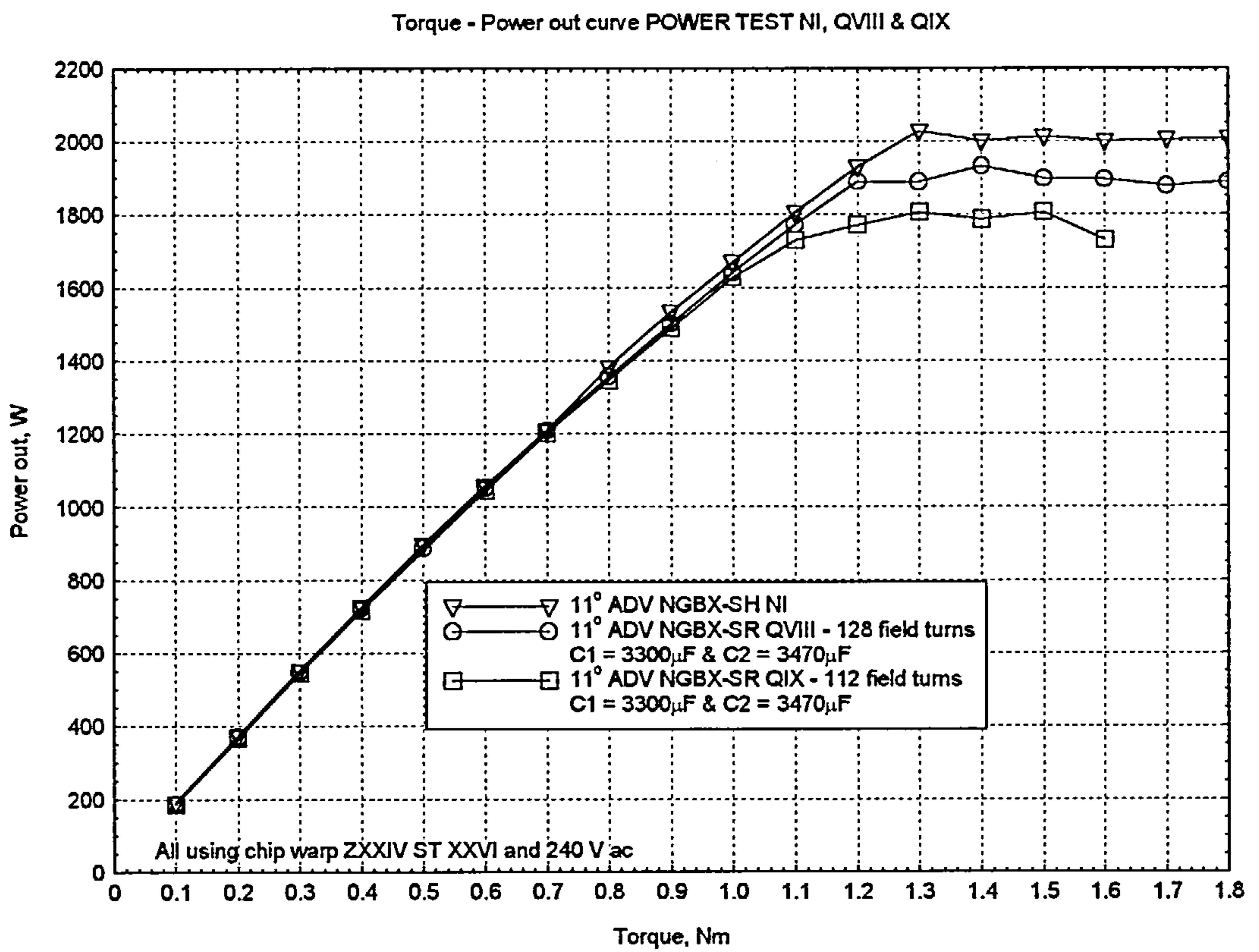


Figure 7.23 Power Test QVIII and QIX, Torque – power out curves of fourth prototype series-motor

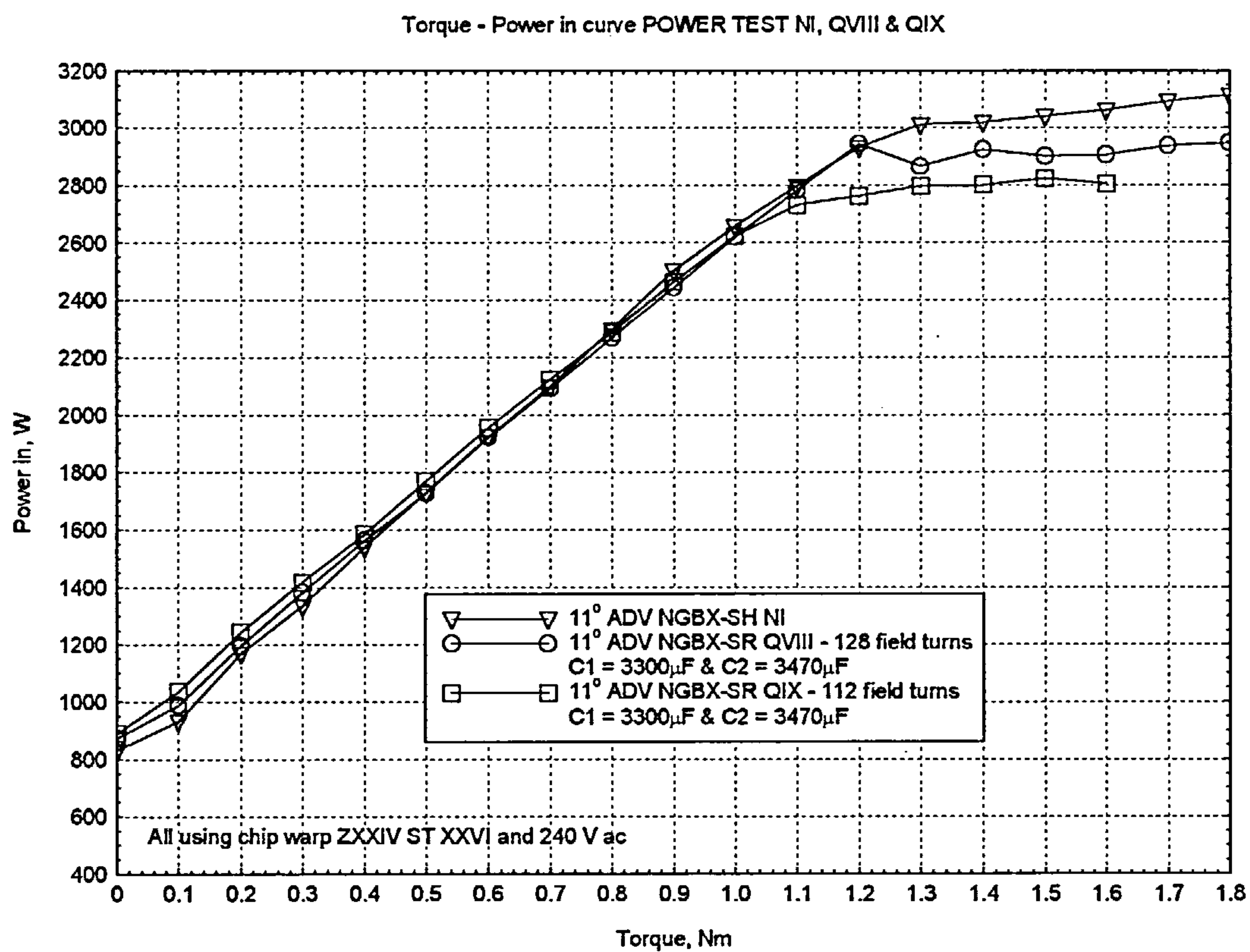


Figure 7.24 Power Test QVIII and QIX, Torque – power in curves of fourth prototype series-motor

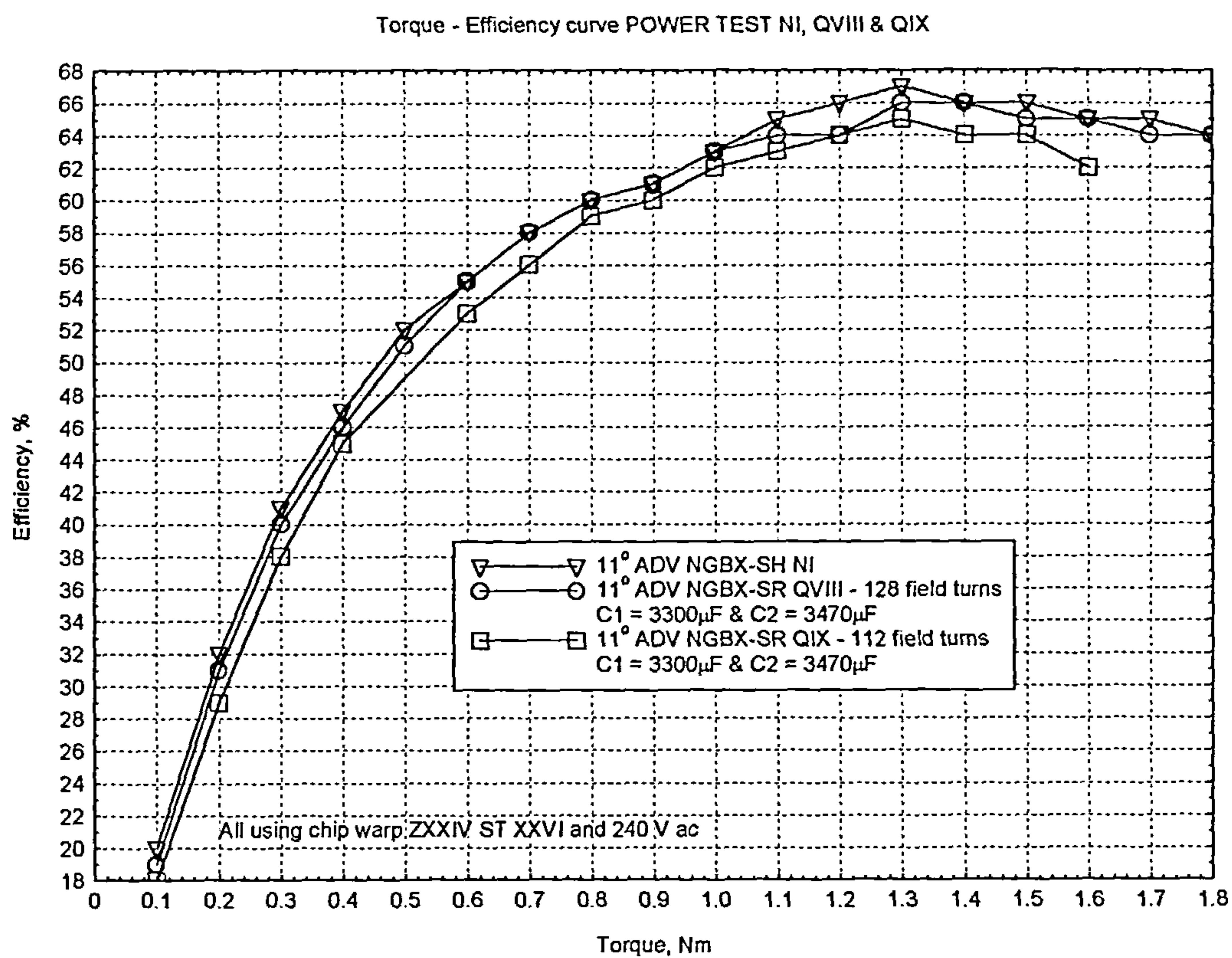
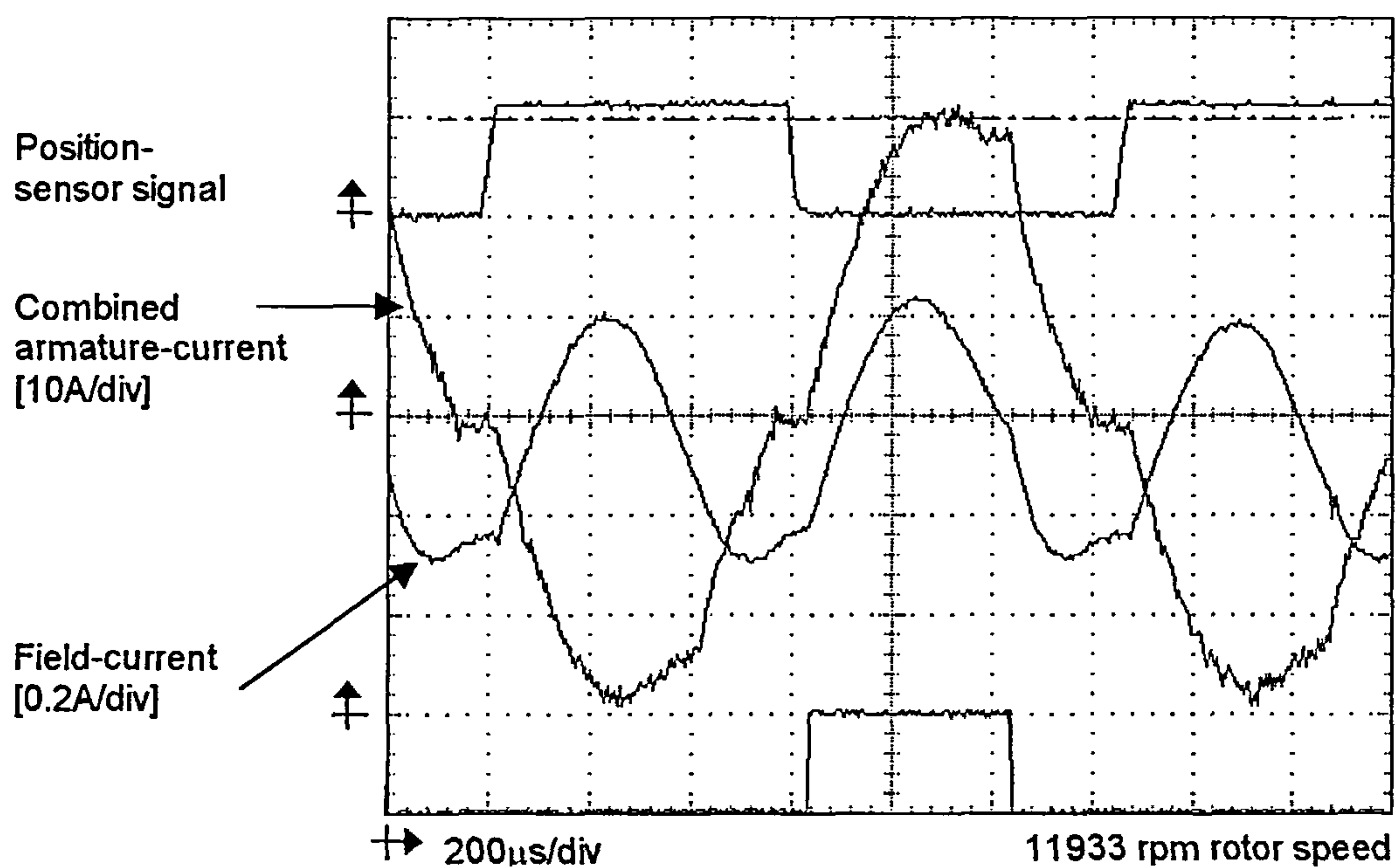
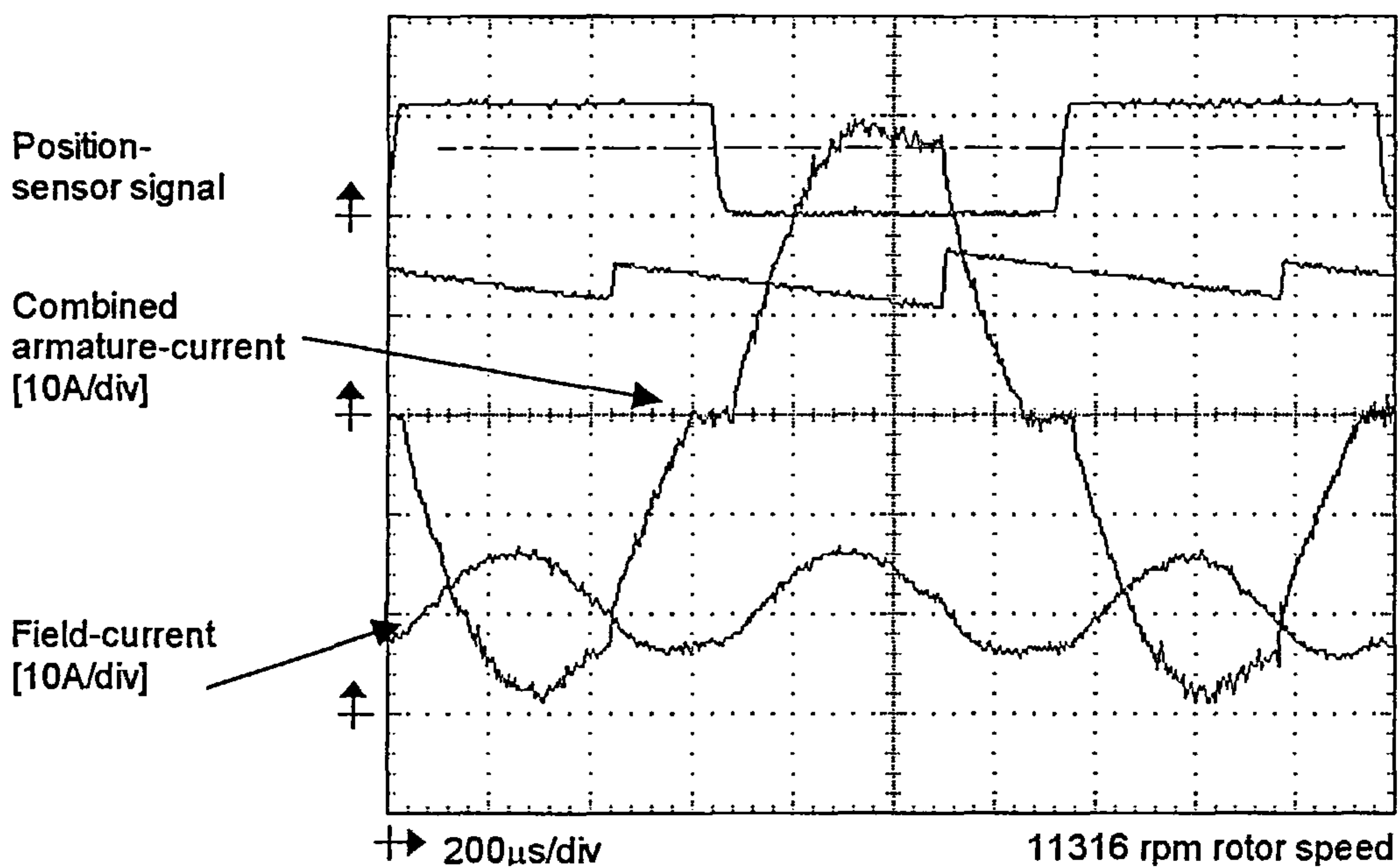


Figure 7.25 Power Test QVIII and QIX, Torque – efficiency curves of fourth prototype series-motor



(a) Power Test NI, third prototype shunt-motor



(b) Power Test QVIII, fourth prototype series-motor

Figure 7.26 Comparison of current waveforms recorded at 1.6 Nm

optimised to some extent at this stage. The capacitance of both capacitors was reduced to 470 μF and the motor was retested. The resulting torque-speed curve is given in figure 7.27. It shows that there was a significant drop in torque production and, hence, power-output. This can be explained with reference to the current waveforms in figure 7.28, which show that there is a significant proportion of regenerative armature-current, that created an opposing negative torque. However, figure 7.29 shows that the reduction in the size of the two capacitors had the unexpected effect of increasing the available DC supply-voltage quite considerably, approximately 11 % at 1.2 Nm. The reason for this was that the larger capacitors could not follow the peaks of the AC supply voltage too closely, whereas the smaller capacitors could, thus allowing a higher-mean DC supply-voltage.

To prevent the effects of regeneration a diode was included in the power circuit after the series armature-winding, see figure 5.7. This stopped the flow of negative armature-current back into the supply, and also allowed the full armature voltage to be placed across the armature-capacitor C2. Lowering the capacitance of capacitor C2 allowed it to be charged to a higher voltage, when the armature was switched-off, because of the reduced time-constant. Then, at the start of the next armature-pulse the energy stored in the capacitor, as a result of the boosted voltage across it, was available to give a shorter rise-time of the armature-current, which, in turn, increased the torque output. Figure 7.30 shows the effect of reducing the capacitance of the armature-capacitor C2 to 30 μF , on the torque and power-output of the motor. Figure 7.31 gives the

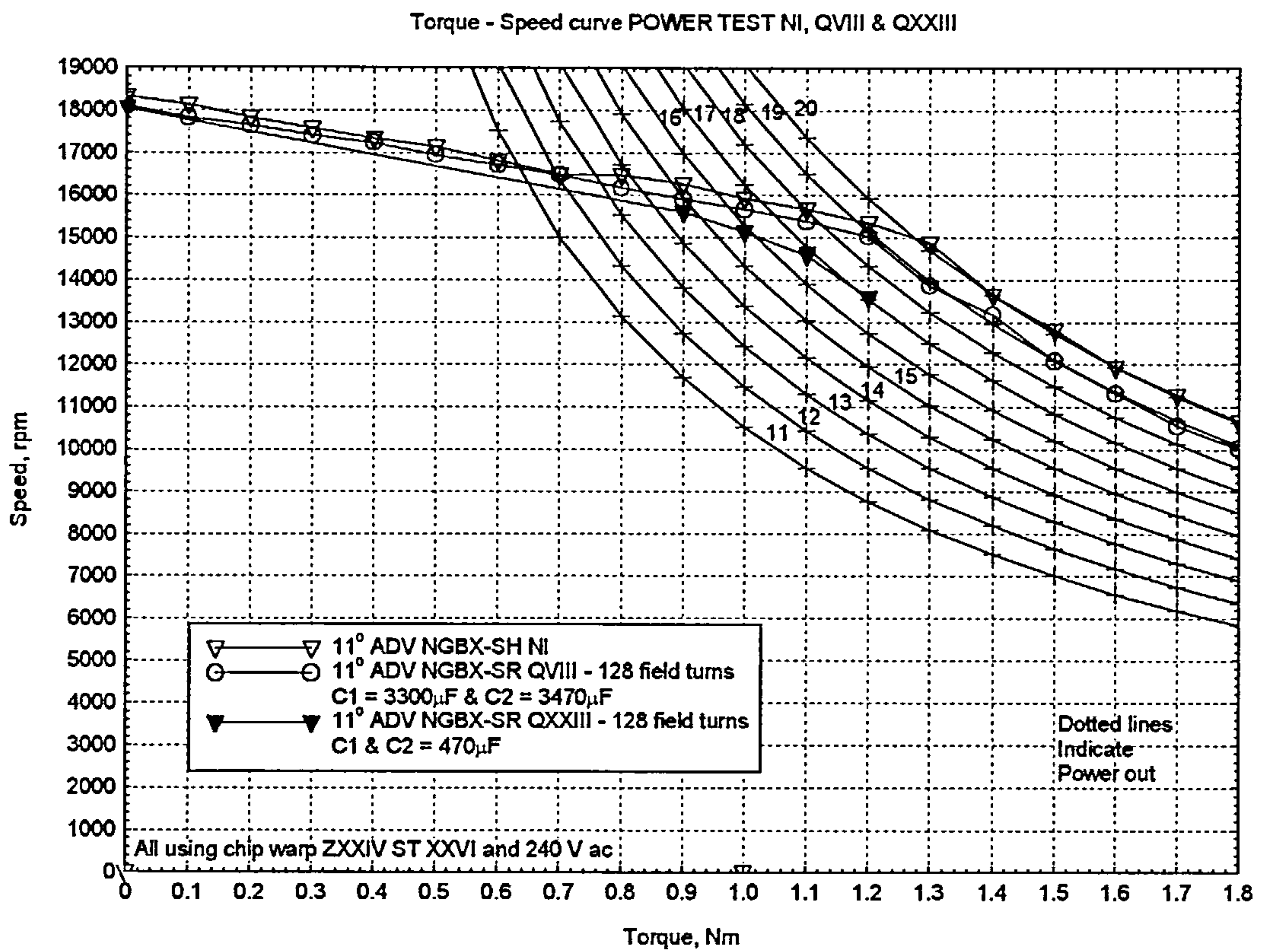


Figure 7.27 Power Test NI, QVIII and QXXIII, Torque - speed curves

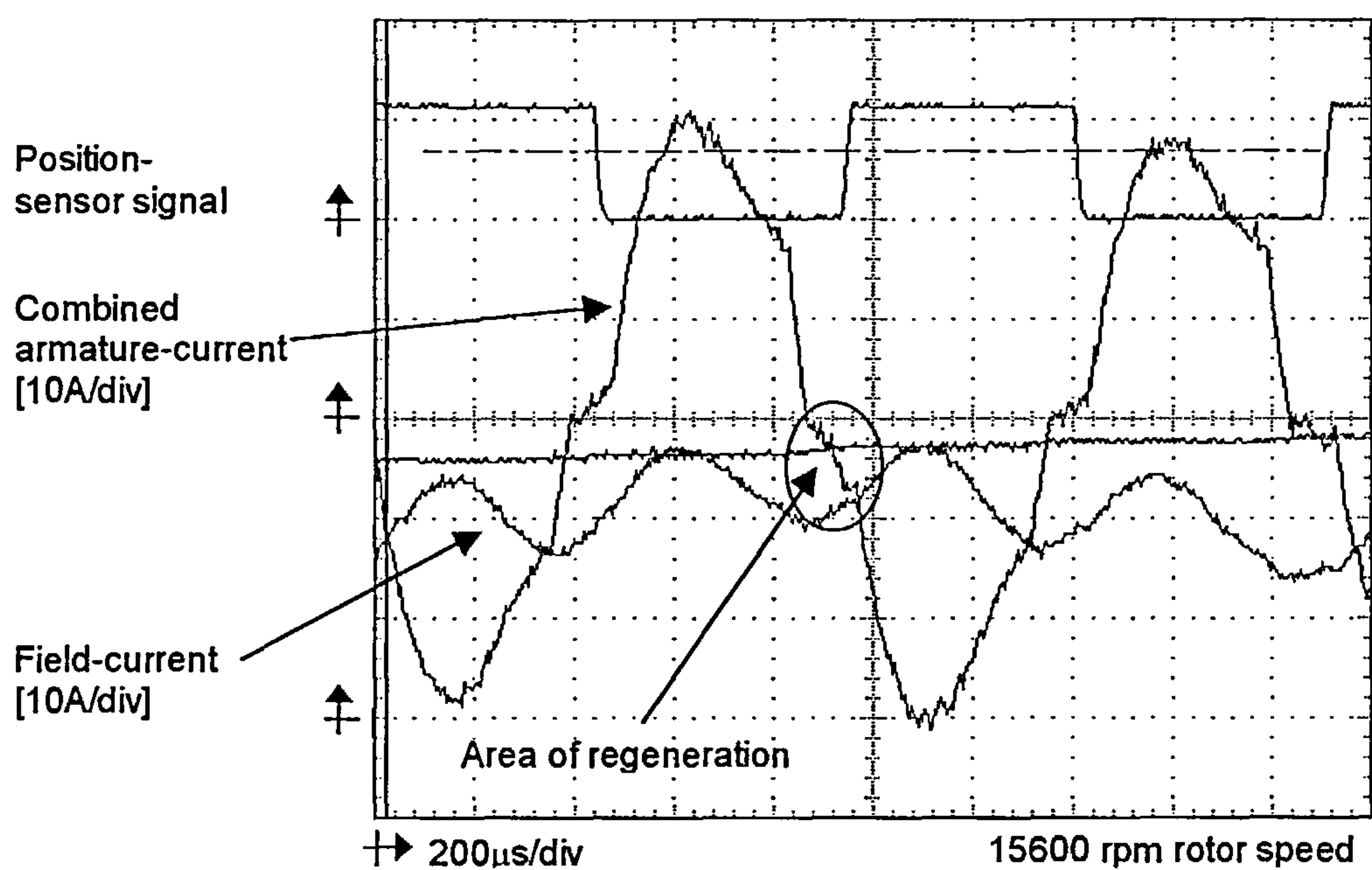


Figure 7.28 Armature-current regeneration recorded at 0.9 Nm

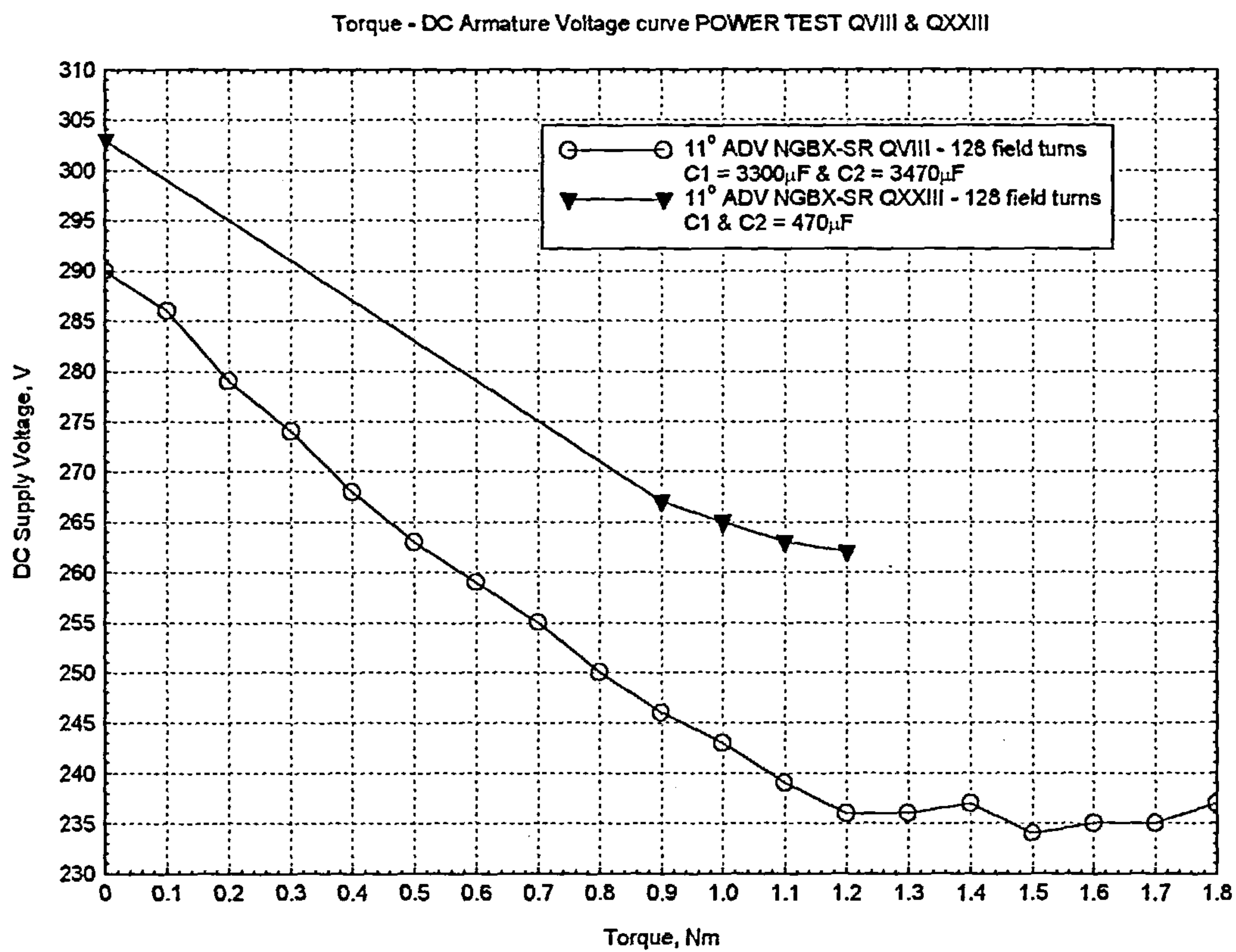


Figure 7.29 Power Test QVIII and QXXIII, Torque - DC Armature Voltage curves

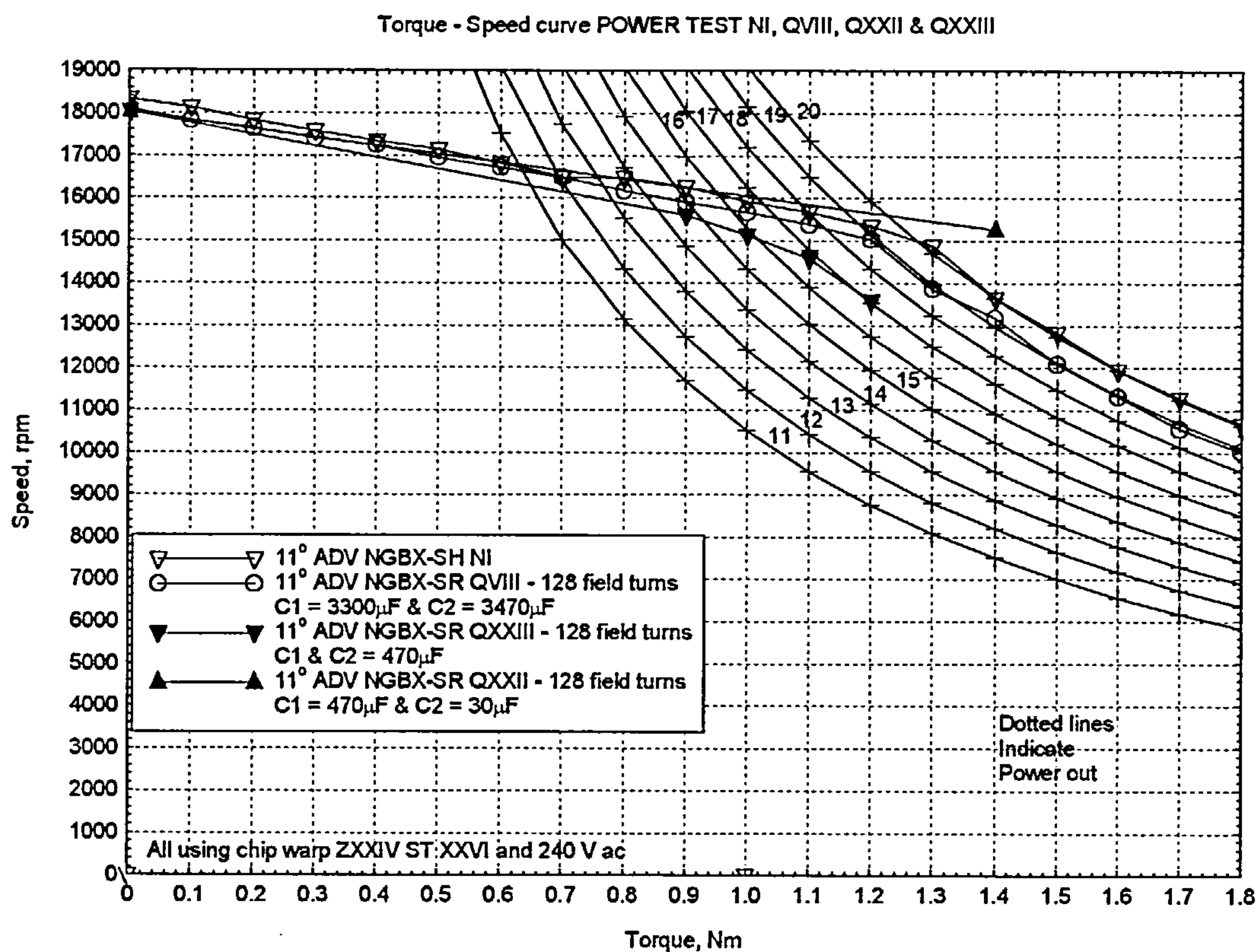


Figure 7.30 Power Test QVIII, QXII and QXXIII, Torque - speed curves comparing capacitor sizes

resulting current-waveforms, and also the armature voltage-waveform across the capacitor at a torque of 1.4Nm. Comparing the armature voltage-waveform, to that in figure 7.28, demonstrates the boosting effect of the armature-voltage, the shortened rise-time of the armature-current, and the removal of the regenerative effects.

Further tests were performed to identify the optimum value of capacitance of armature capacitor C2, and the corresponding advance-angle, that was most suitable to the operation of the motor, under these conditions. Figure 7.32 shows the torque-speed curves from these tests, and figure 7.33 gives a collection of the corresponding current and voltage-waveforms all recorded at a torque of 1.4 Nm. From these figures it was decided that the best combination of capacitance of armature-capacitor C2 and advance-angle was 15 μ F and 8°, respectively. More specifically, a capacitance of 7.5 μ F was too low because the armature voltage-ripple was excessive, peaking at 450V just before the armature was turned on. With this value of capacitance the problem was exacerbated at lower speeds giving poor performance, whereas the 15 μ F capacitor had a high-enough value to keep the voltage ripple within sensible limits (200V). With an increased supply-voltage available, owing to the boosting effect caused by lowering the value of the capacitance of armature-capacitor C2, the armature-current was able to rise quicker, thus enabling the advance-angle to be reduced to deliver the same power-output. An advance-angle of 7°, and below, gave too little power-out at the desired operating-point at a torque of 1.2 Nm, and an advance-angle equal to 9°, and above, gave too

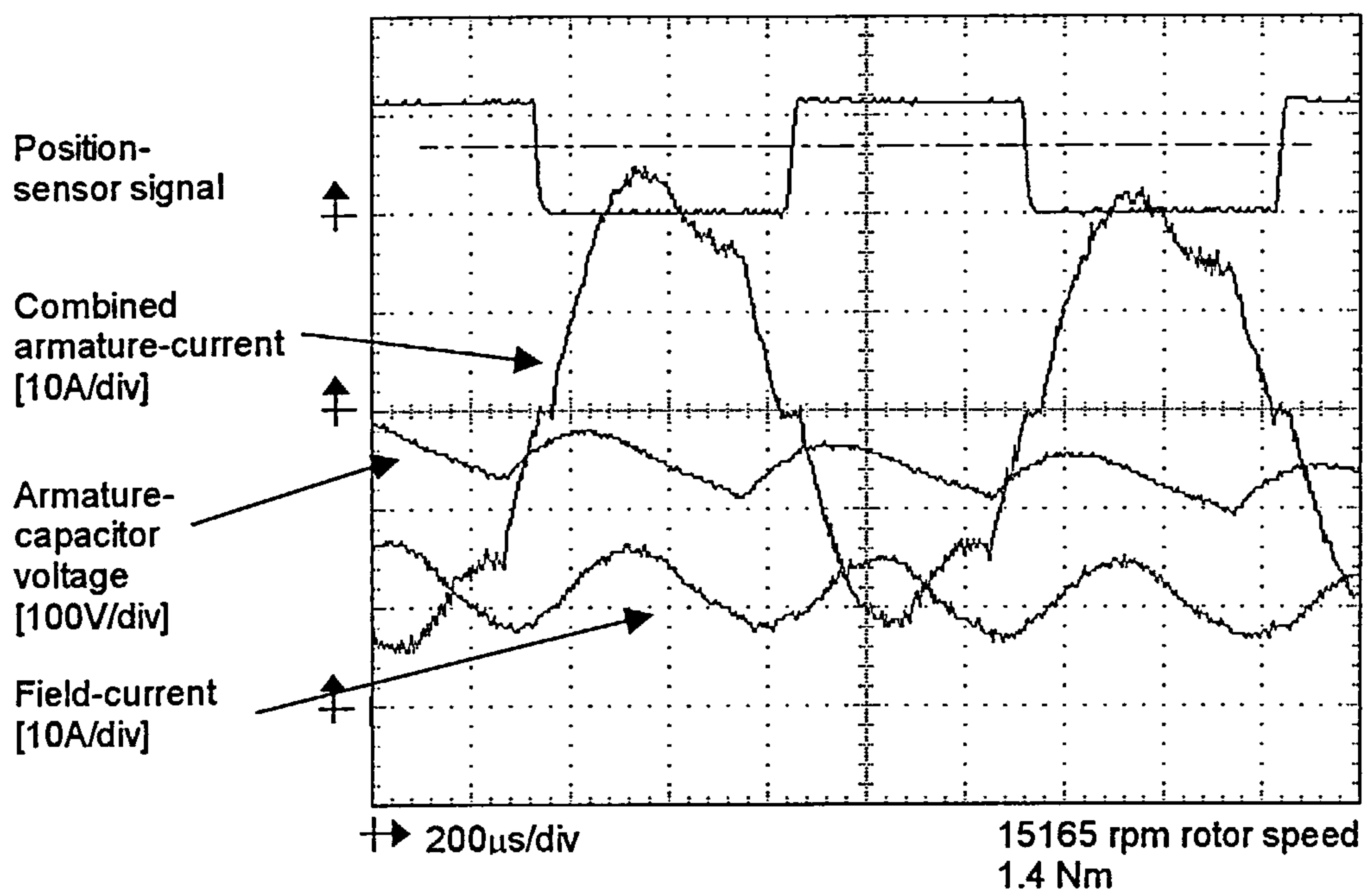


Figure 7.31 Current waveforms and armature-capacitor voltage with a capacitance C_2 of $30\mu\text{F}$

Torque - Speed curve POWER TEST NI, QVIII, QXVIII, QXIX, QXX, QXXI, QXXII, QXXIII, QXXIV & QXXV

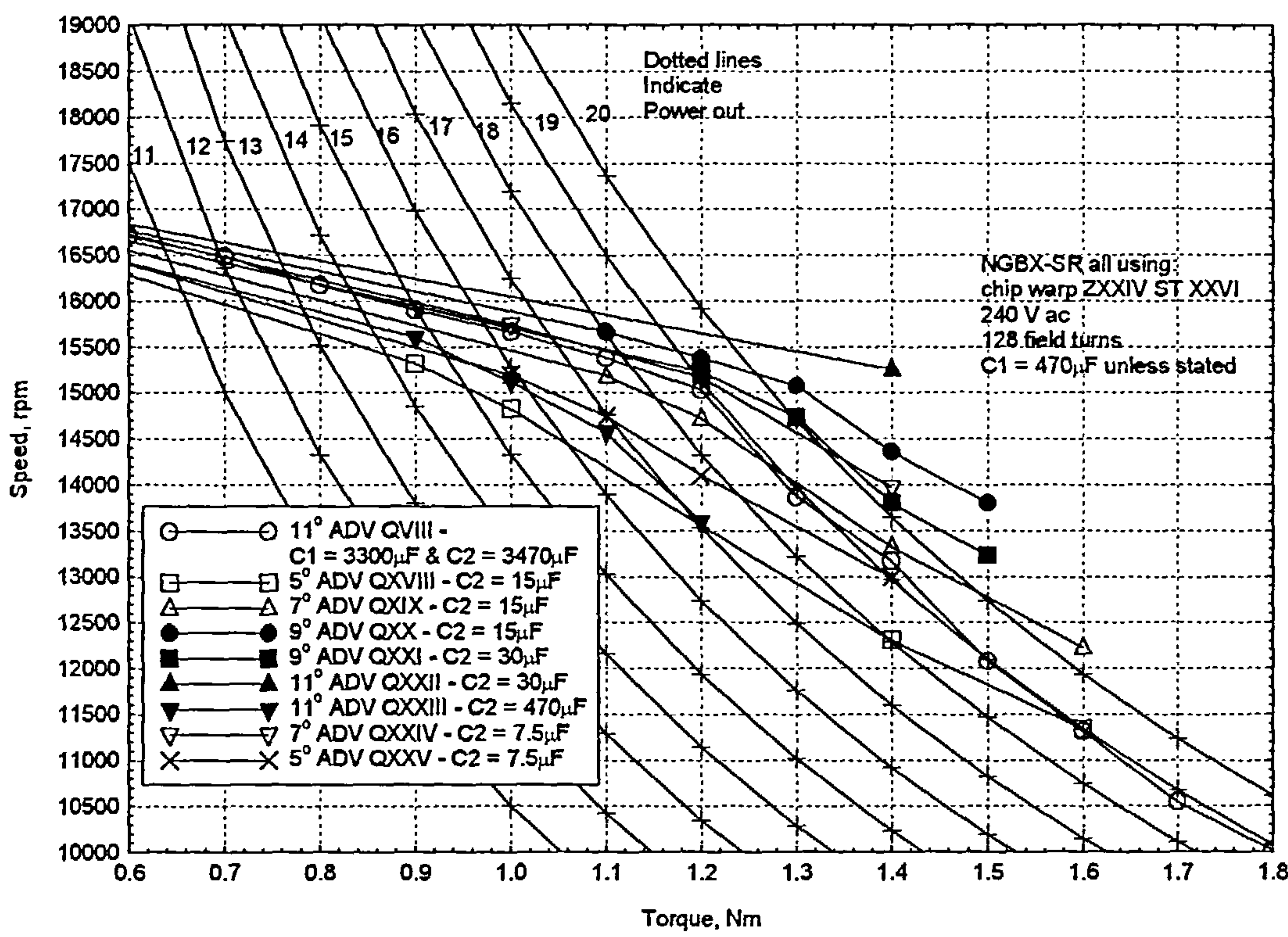


Figure 7.32 Torque – speed curve comparison

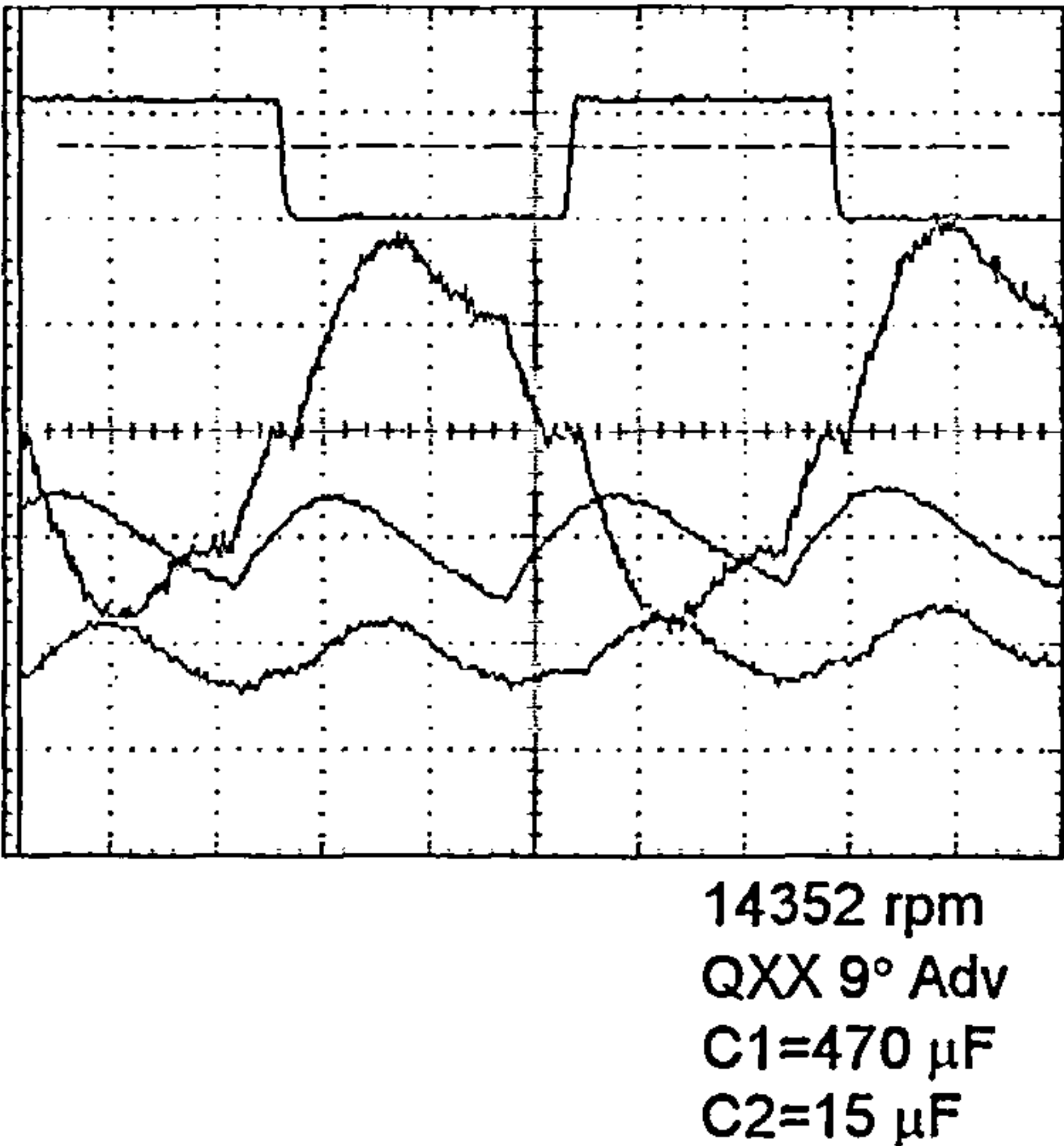
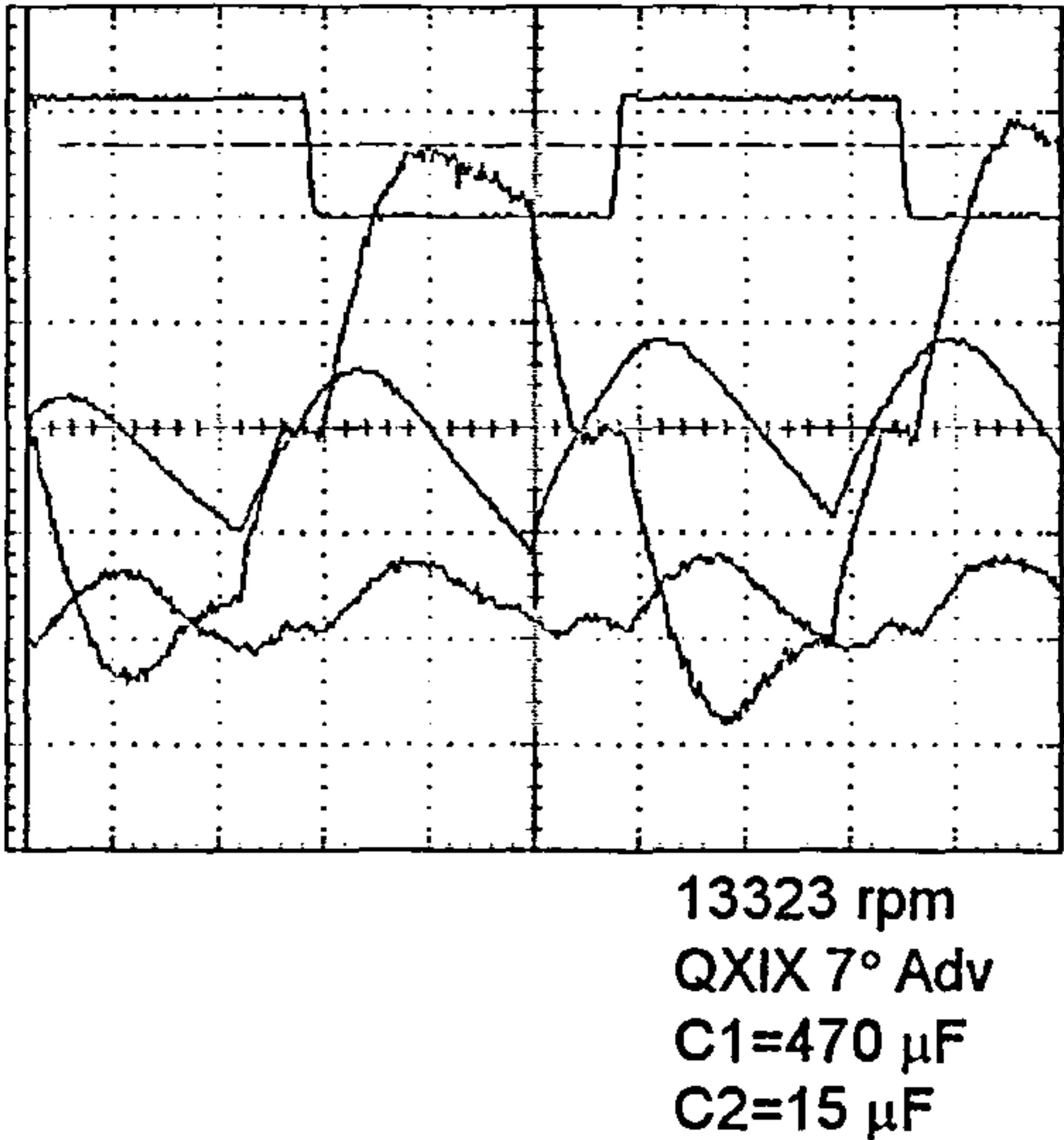
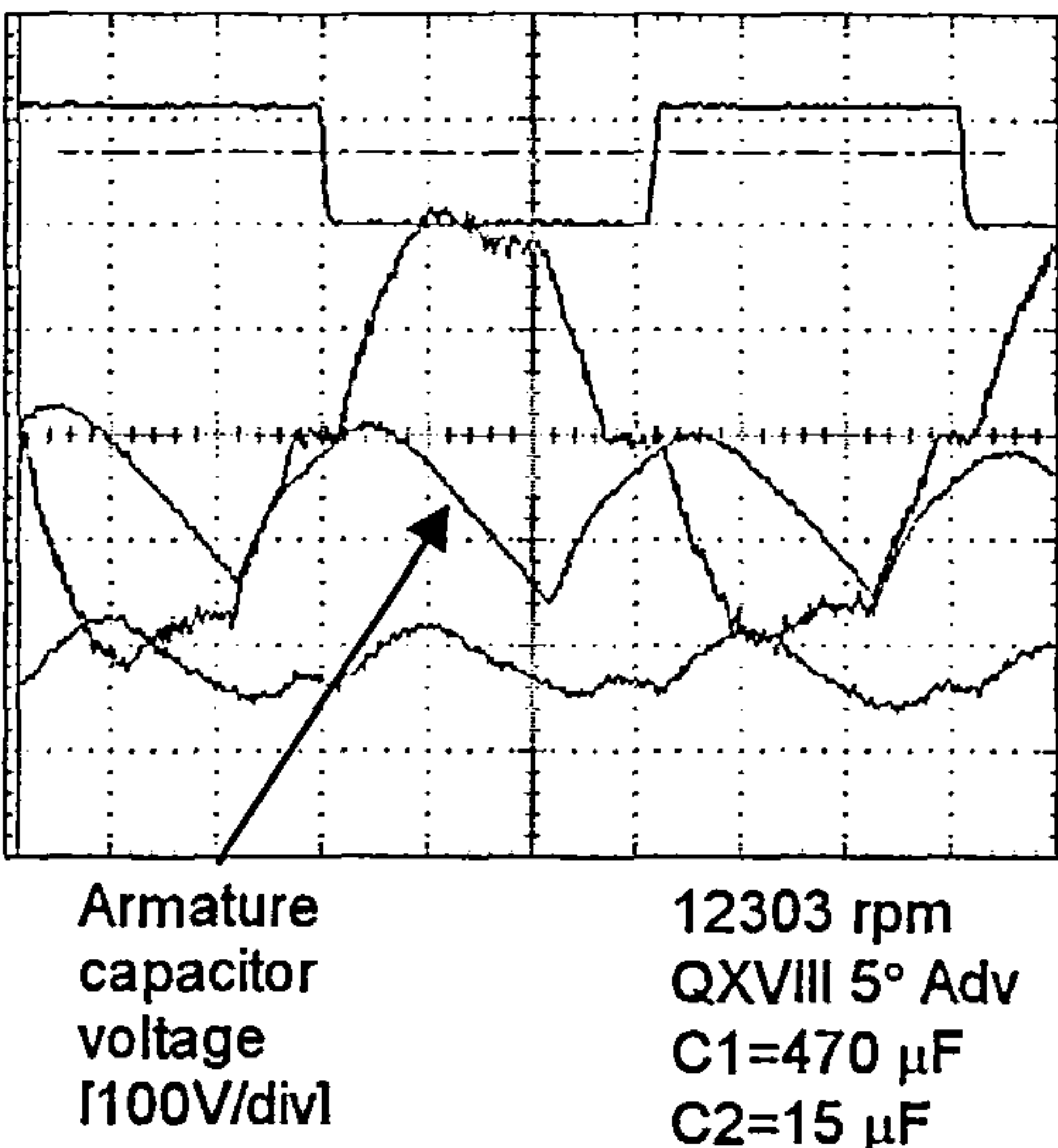
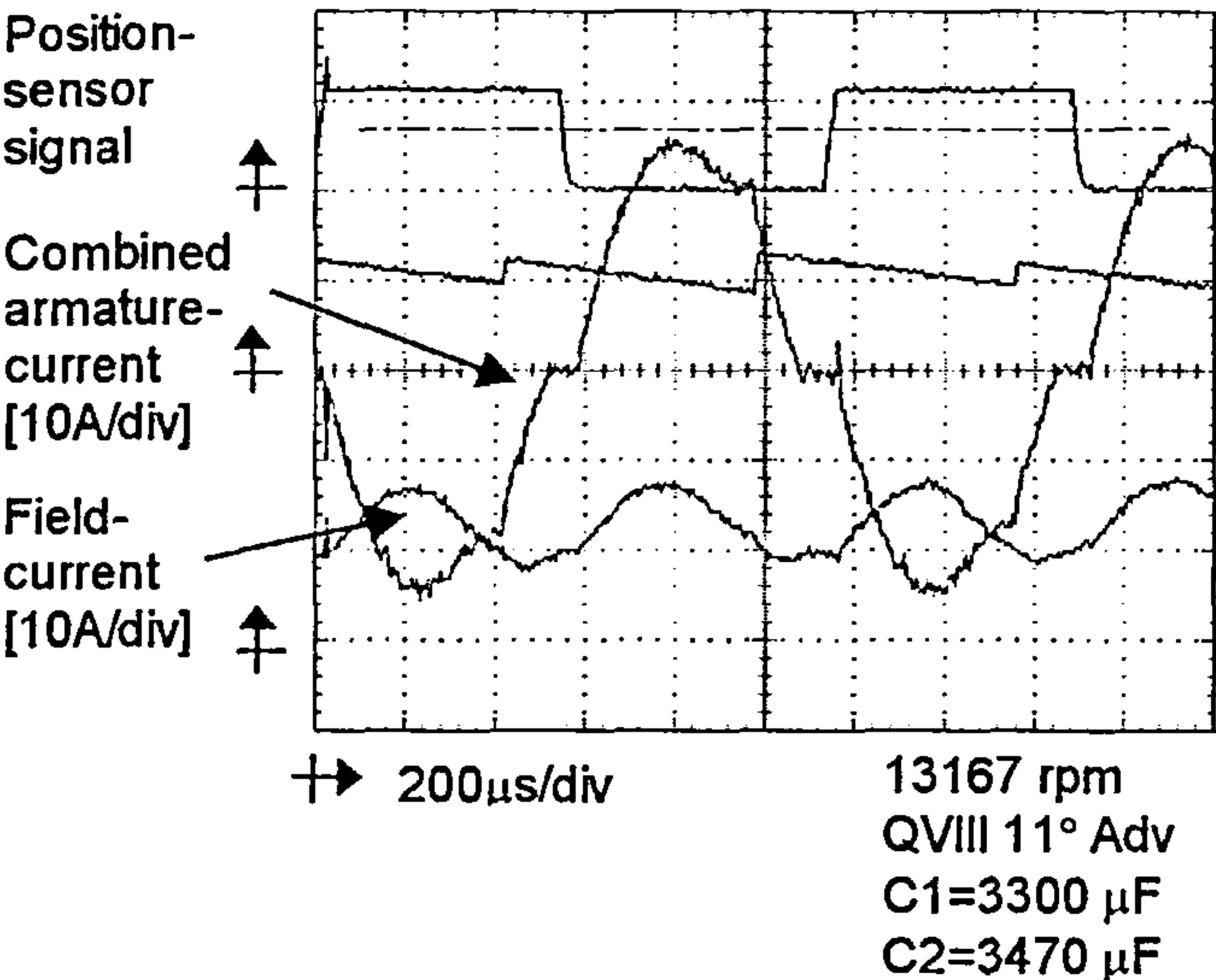


Figure 7.33 Comparison of current and voltage waveforms at a torque of 1.4 Nm (continued on next page)

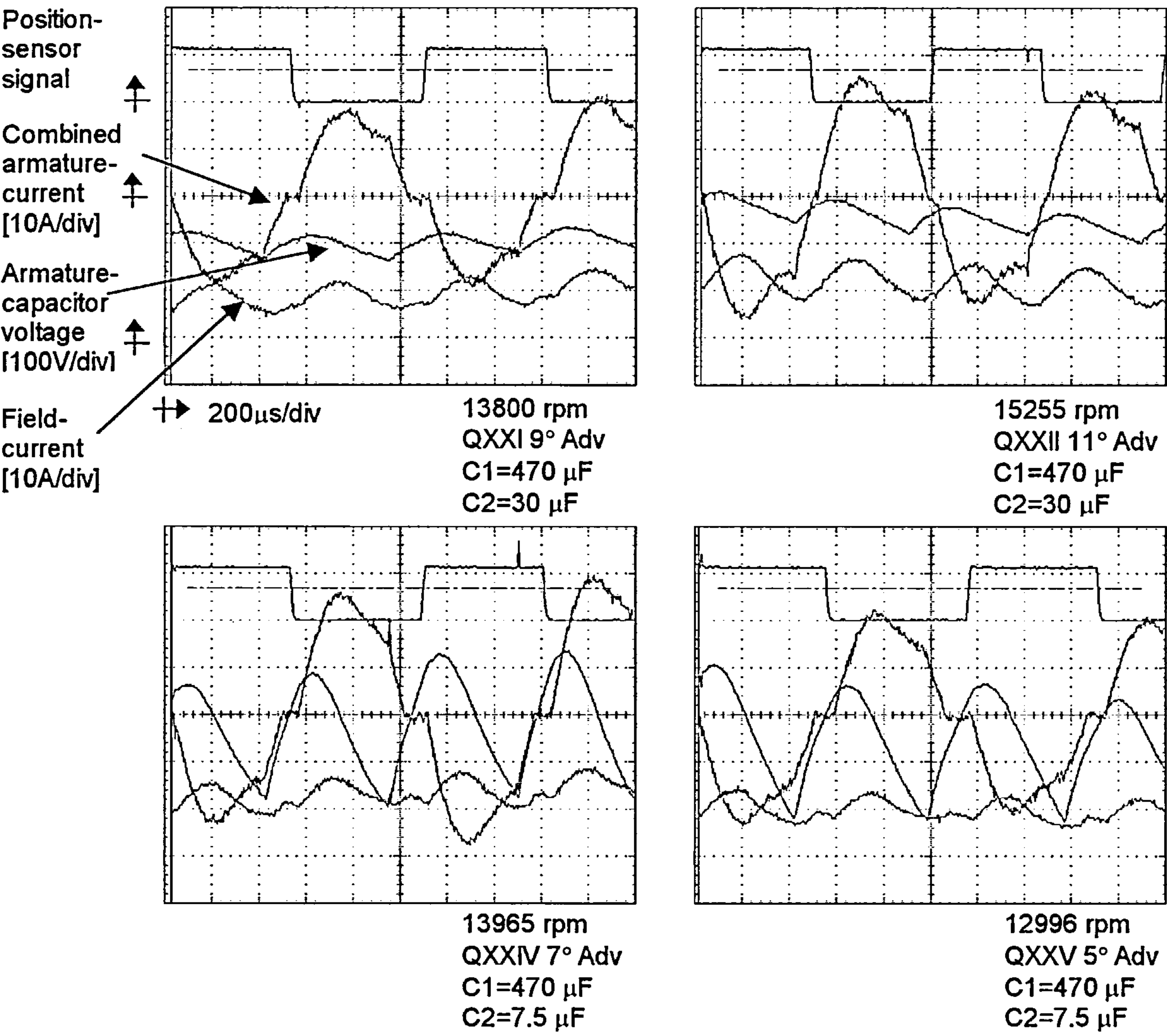


Figure 7.33 Comparison of current and voltage waveforms at a torque of 1.4 Nm (continued from previous page)

much power-out at this point. Ideally an advance of 8° would have delivered the desired power-out. With all of the combinations of advance angle and the lower values of capacitance the reserve-torque was exceeded in each case, resulting in the use of a lower duty-cycle.

7.4.2 Additional-power delivery

The prototype shunt-motors demonstrated that, as the higher torques were reached it, a stall was likely to occur owing to the collapse of the field-flux. This was owing to the suppression of the field-current by the induced effects from the armature. When a stall did occur it was usually very rapid, and without warning, and was accompanied by high armature-currents (in excess of 30 A). With the fourth prototype series-motor it was thought that this would be less of a problem because the armature-current was derived directly through the series field-winding, thus providing a self-regulatory system.

It was decided to discover what maximum power-out could be obtained when the windings were at their maximum allowable rise in temperature. In order to deliver maximum power-out the duty-cycle of the IGBTs had to be maximised also, which was achieved by maintaining the speed of the motor at 15000 rpm whilst increasing the supply-voltage and the load-torque. To deliver more power-out required a corresponding rise in power-input. This meant a change in the input-supply from single-phase to three-phase, as the power-limit of the single-phase supply would have been exceeded otherwise. The results from the tests are shown in figures 7.34 to 7.38. Table 7.1 gives the corresponding

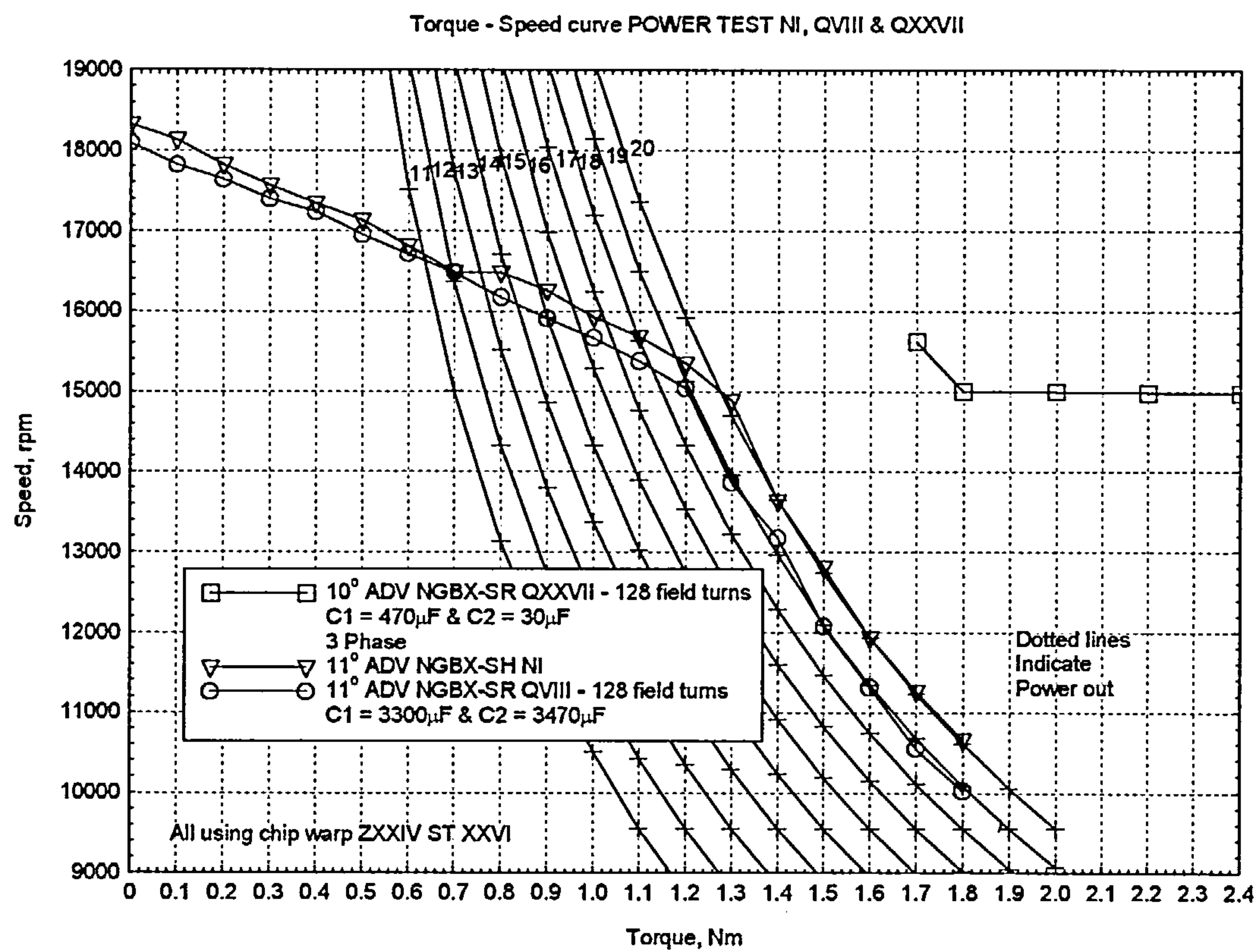


Figure 7.34 Power Test QXXVII, Torque - speed curve

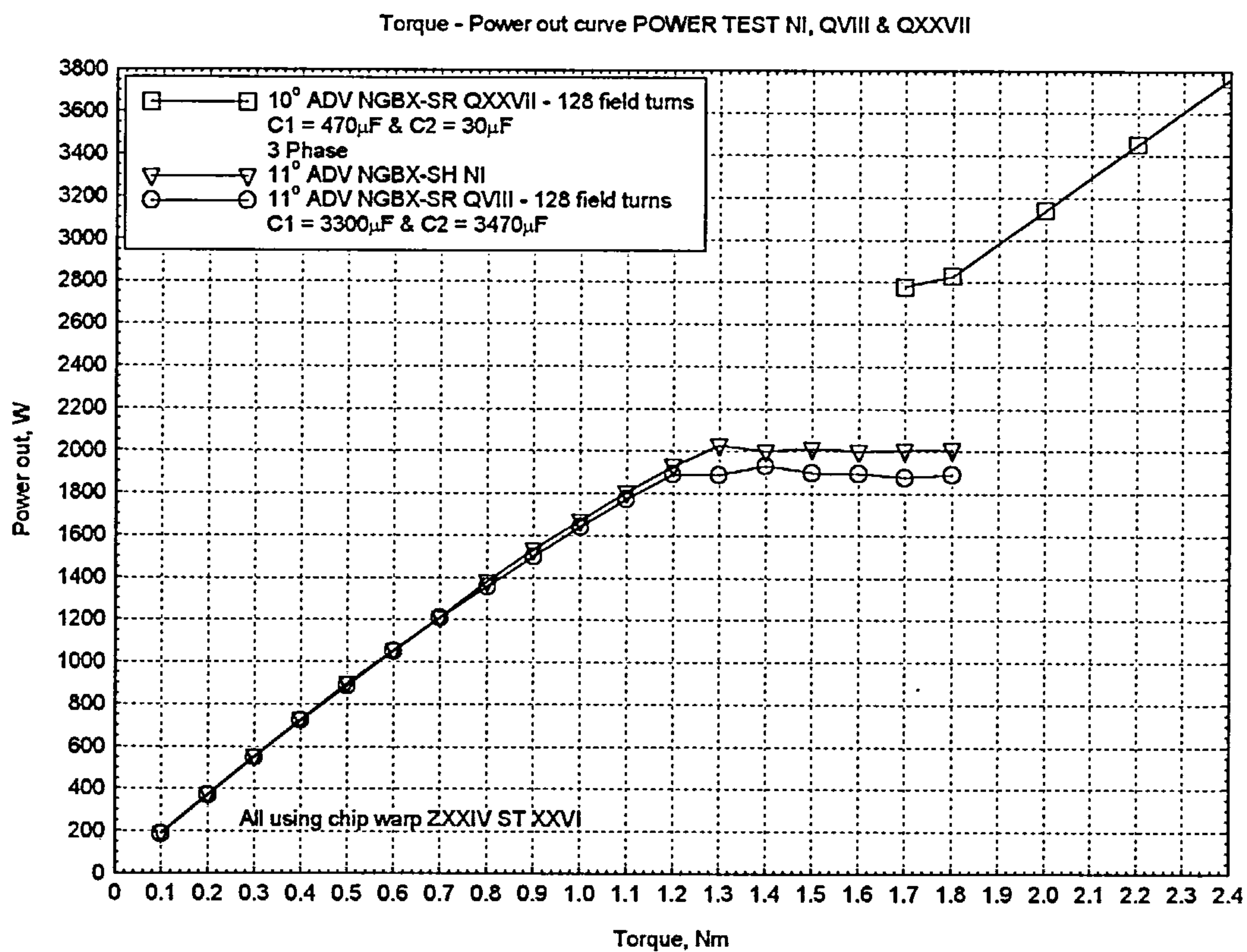


Figure 7.35 Power Test Q27, Torque – power out curve, over twice rated power-out

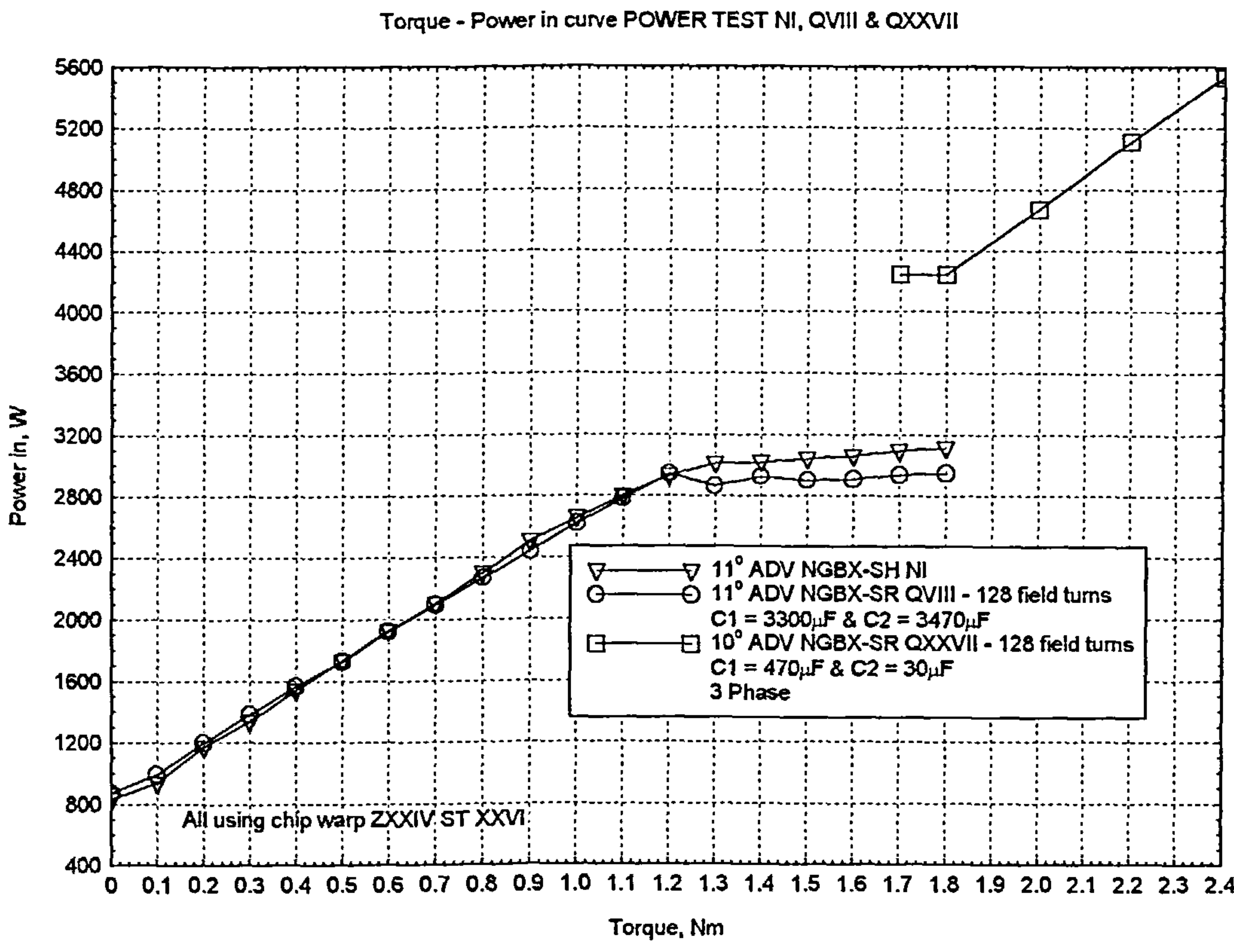


Figure 7.36 Power Test QXXVII, Torque – power in curve

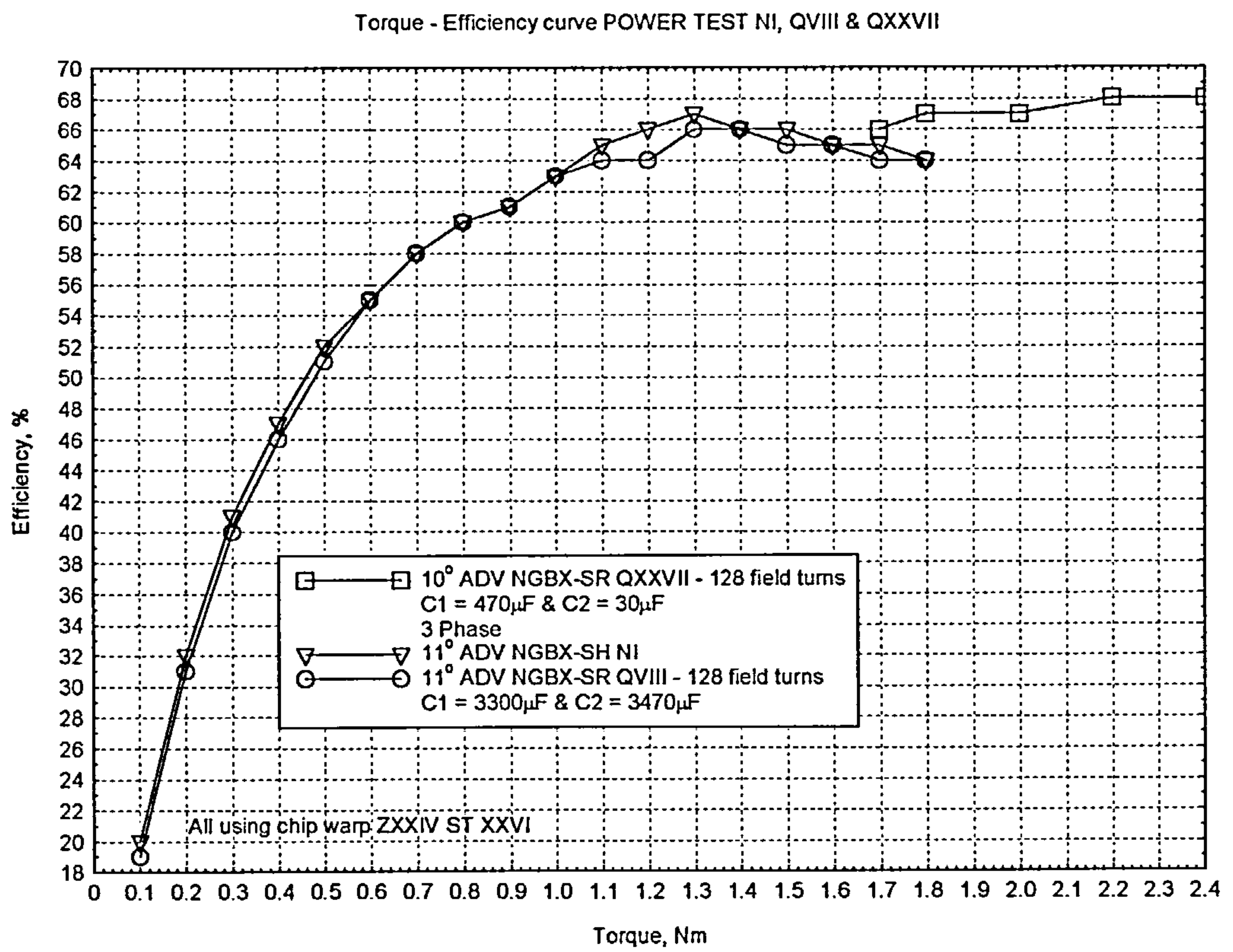


Figure 7.37 Power Test QXXVII, Torque - efficiency curve

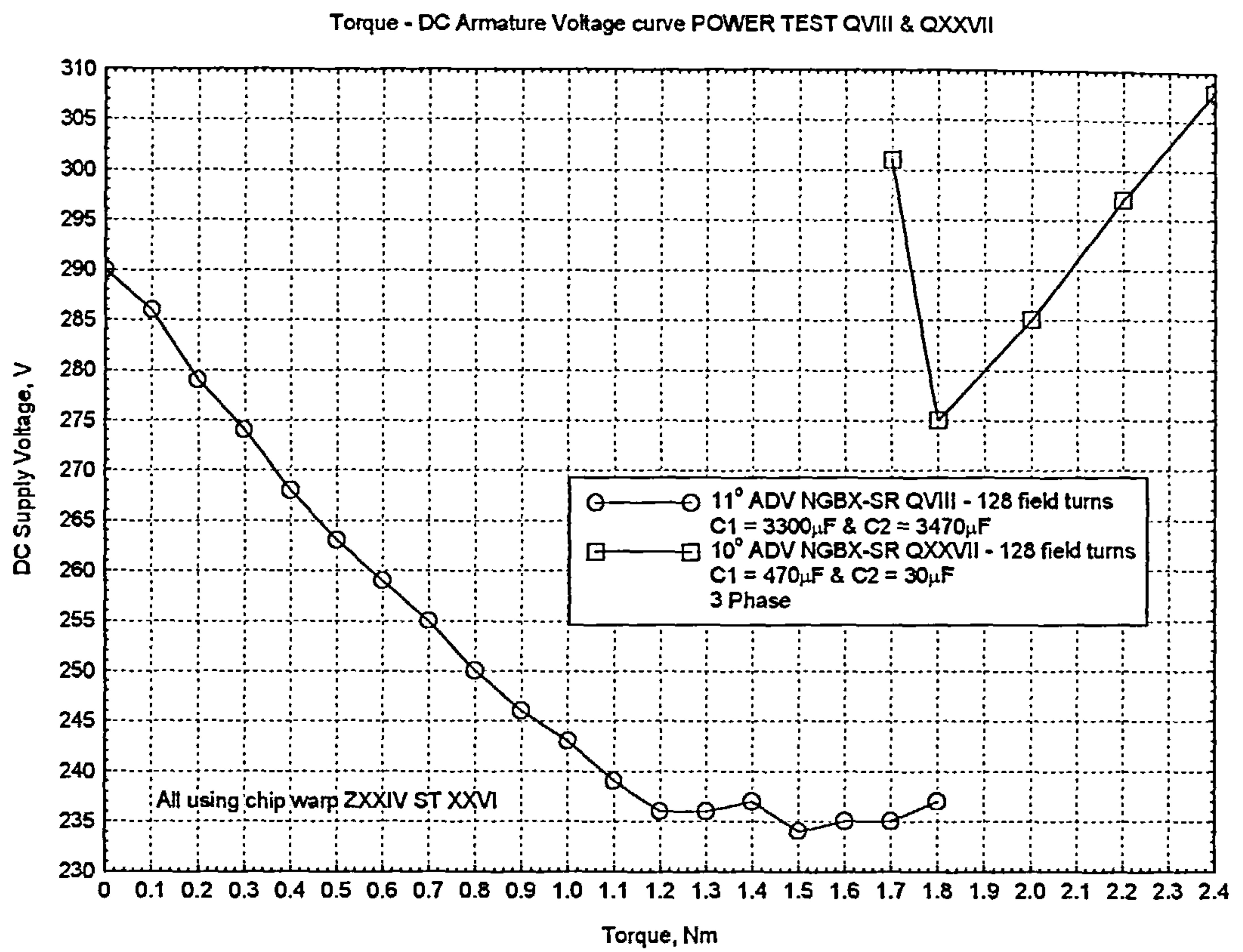


Figure 7.38 Power Test QXXVII, Torque – DC supply voltage curve

numerical data. The most impressive result shows that the series-motor was capable of developing 3763 W of power-output with an input power of 5534 W at 15000 rpm. This implies an efficiency of 68 %. This power-out was more than twice that originally specified; it was also delivered for a period of time greater than a minute before the temperature on the windings reached 100 °C. Figure 7.39 gives the current and voltage-waveforms recorded at three load-points. It can be observed that unlike the shunt-motors there is no significant suppression of the field-current, and also the armature-current does not peak above 30 A at any point.

The implications of this test are very important in that, if a motor of this size can produce twice the specified output-power, then scaling the power density, a motor of half the size should be able to deliver the specified power-out. A power density of 8641 kWm^{-3} was recorded from a motor frame size of 89 mm outside diameter and a stack length of 70 mm. Thus, a motor with the same diameter and half the stack length should, in theory, be able to deliver the desired power.

7.4.3 Testing conclusions

Testing of the fourth prototype series-wound-field motor has demonstrated its performance against that of the three previous shunt-wound-field motors. With the correct combination of advance angle, DC-link capacitor and armature capacitor the specified power-out was produced. In conclusion the operation of the motor was more robust and the series-field-winding was less prone to

Torque (Nm)	Speed (rpm)	Power out (W)	Power in (W)	Efficiency (%)	Ac phase volts (V)	Dc link volts (V)	Mean Armature volts (V)
1.7	15615	2780	4244	66	240	319	301
1.8	15000	2827	4246	67	222	297	275
2.0	14994	3140	4670	67	231	307	285
2.2	14985	3452	5110	68	240	320	297
2.4	14973	3763	5534	68	250	335	308

Table 7.1 Performance figures for Power Test QXXVII

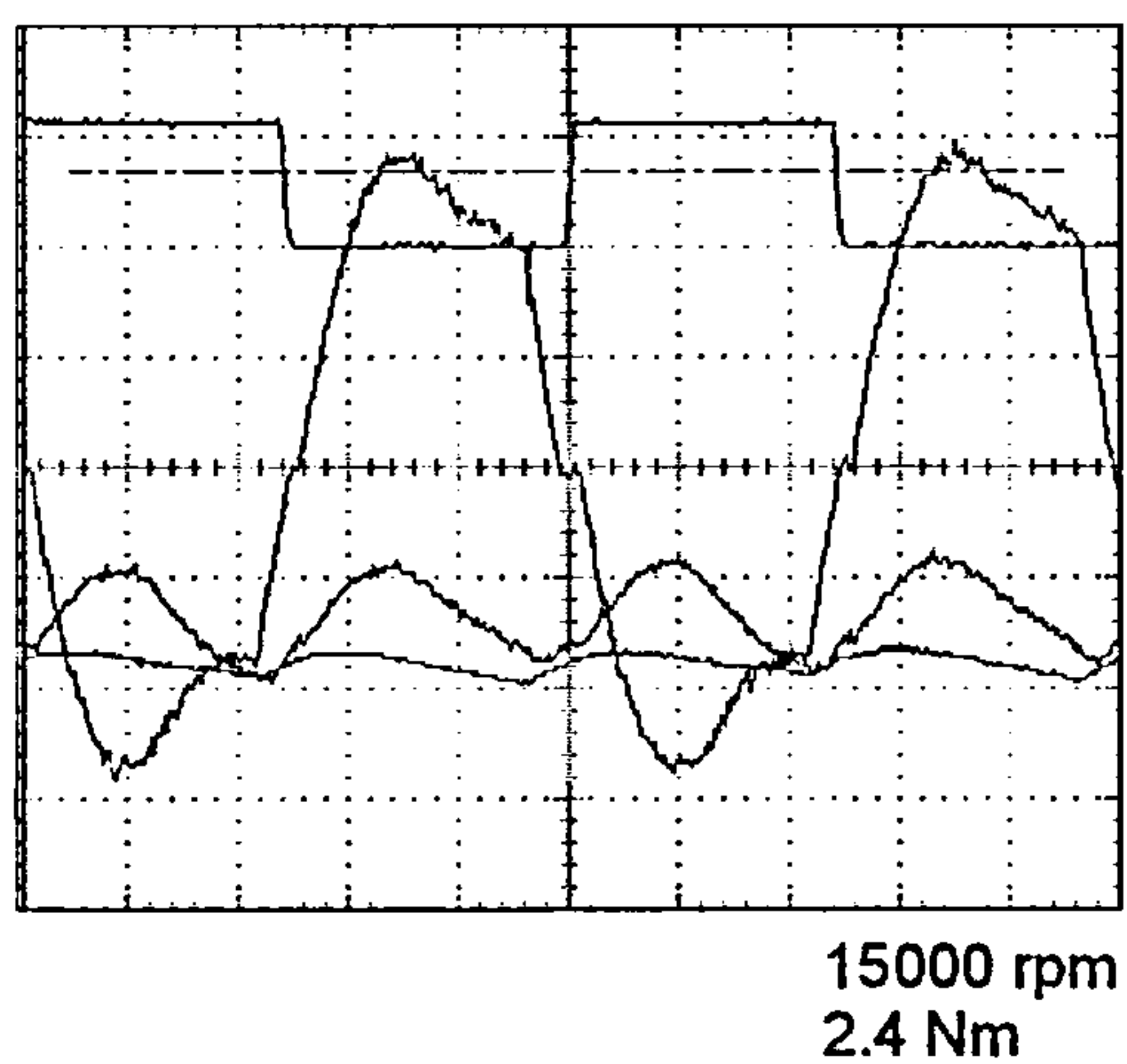
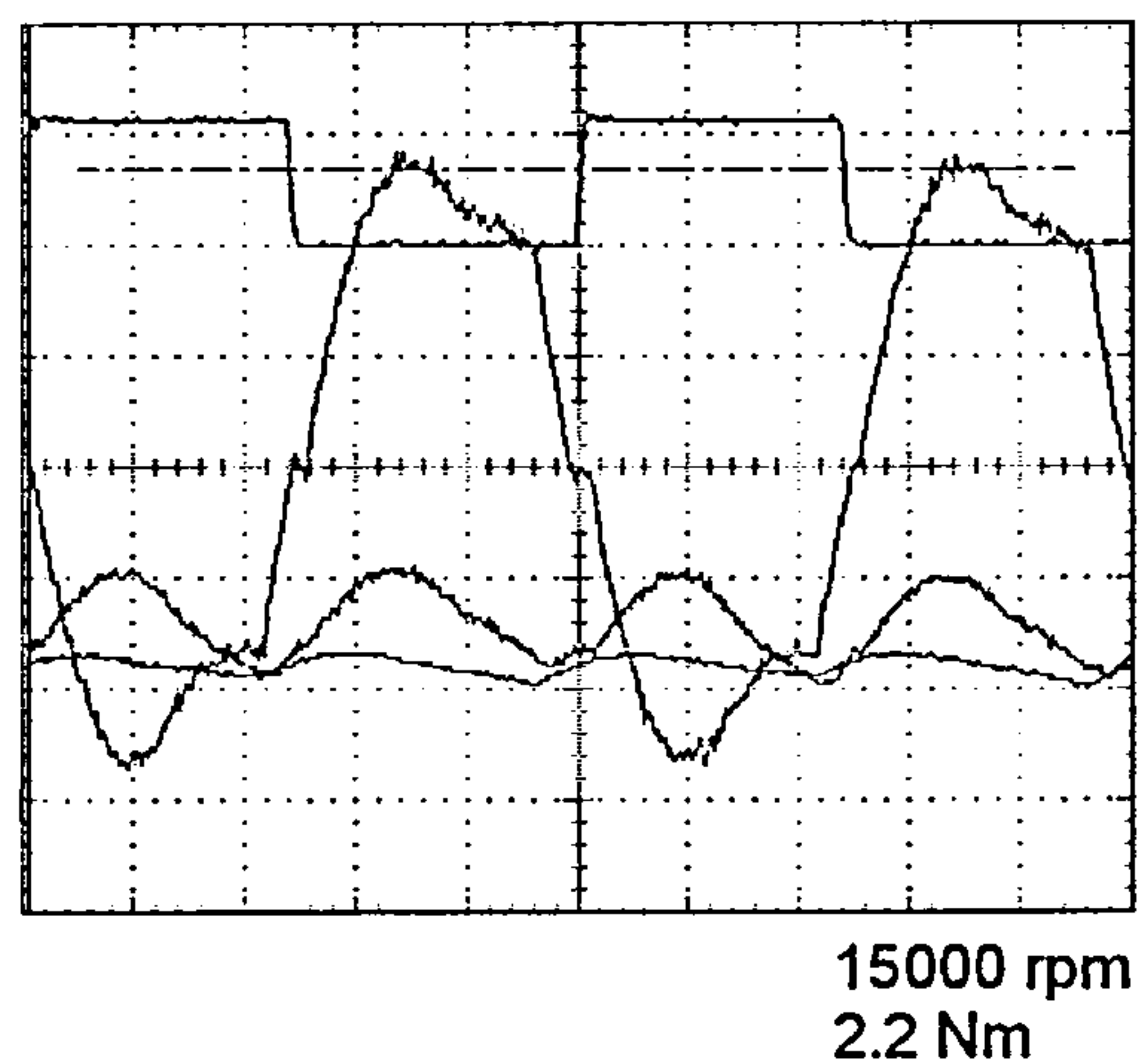
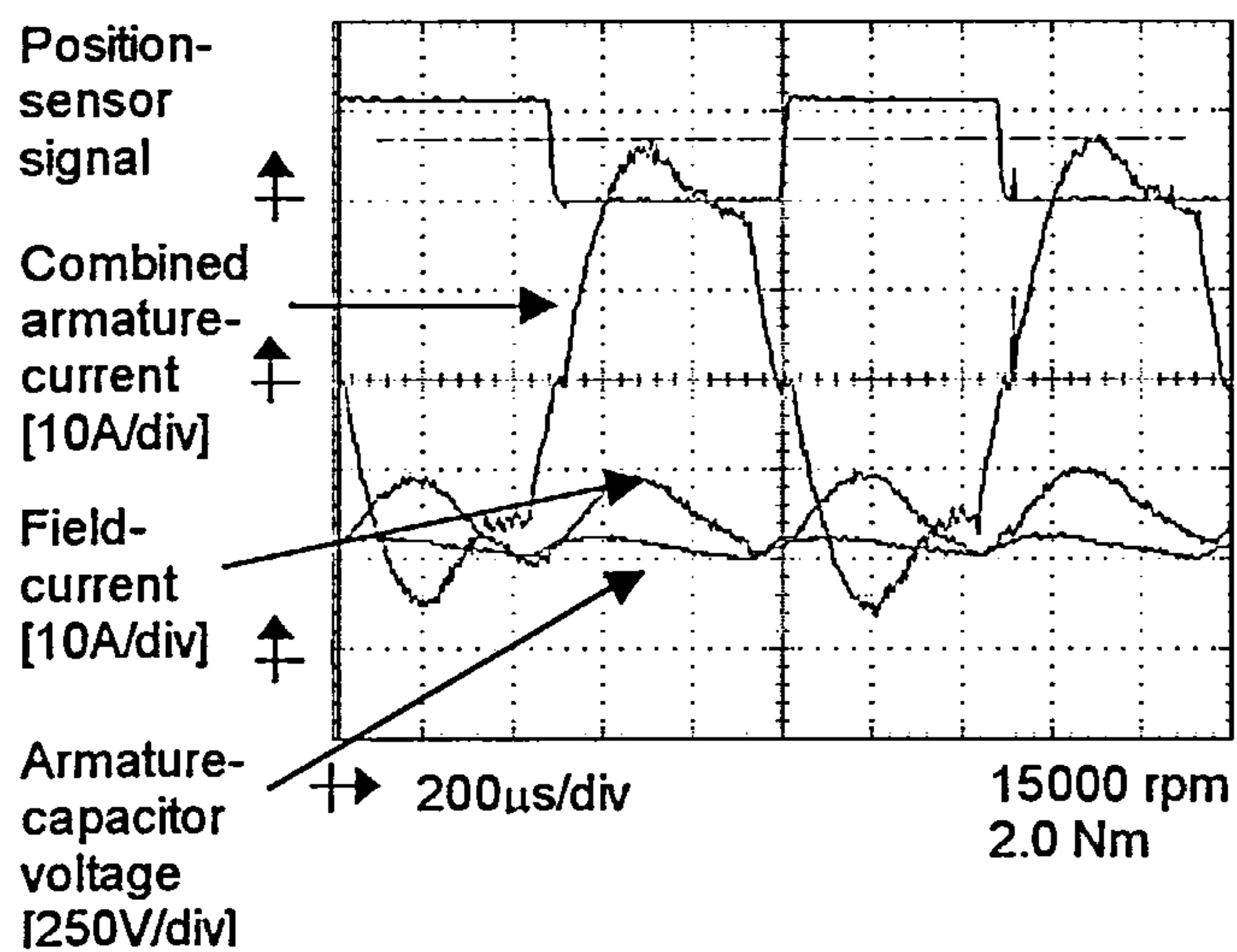


Figure 7.39 Current waveforms for Power Test QXXVII

induced effects from the armature-windings. When operated near its design limits the motor developed twice the previous output power. This level of performance was exciting because it implied that a motor of half the physical volume might be capable of delivering the required output power.

Starting and braking the motor was not tested, and further work has to be carried out to optimise these parts of the motor performance.

7.5 Conclusions

Through the testing and development of the first prototype motor and three further prototypes the majority of the specification has been achieved. It can be confidently stated that, with refinement in some areas, the specification can be exceeded. Presently the starting and braking times are slower than required, and the efficiency is 5 % down. However, apart from these, the power delivery requirement has been met in every aspect. The motor has also exhibited superb and safe control with very limited feedback.

A remaining question is which configuration of field-winding shows the most promise, series or shunt? Without completely testing the series-wound-field motor this question cannot be answered authoritatively. However, based purely upon the evidence of the delivery of power the series-motor has the most potential. In producing a low-cost solution the number of components in the circuit design is another factor to consider. The shunt-wound-field motor needs a low-powered MOSFET, a relatively-small power-diode and the

corresponding gate-drive circuitry to operate the field-winding, whereas the series-wound-field motor uses a 15 μF polypropylene capacitor and a power-diode.

In conclusion the series-motor appears to be the best choice. Not only can it deliver the power with an economic power-converter, it delivers the power-in a more controlled manner, and is altogether a more robust solution.

Chapters 6 and 7 have described the development of the motor to achieve performance measured against the specification. Chapter 8 describes the analysis of the results obtained from a further set of tests performed to validate the theory discussed in Chapter 4.

CHAPTER 8 ANALYSIS OF THE NEW FLUX-SWITCHING MOTOR

8.1 Introduction

Testing of the motor, described in Chapters 6 and 7, showed the development of the motor aimed at achieving performances to be measured against the specification. This Chapter concentrates on the analysis of the results obtained from a further set of tests carried out solely as an attempt to validate the theory derived in Chapter 3.

8.2 Validating the torque equation

8.2.1 Further tests

The evolution of the flux-switching motor from a two-phase fully-pitched wound switched-reluctance motor to a motor that exhibited similar operating characteristics as a DC-motor was presented in Chapter 2. Chapter 3 then went into more detail in describing the behaviour of the motor using DC-motor equations, with the torque equation for the motor given as,

$$T = \frac{N_a i_a N_f i_f}{\Re} \frac{dk}{d\theta} \quad (3.33).$$

Essentially this was the equation that was validated from the further set of tests carried out, as described in this Chapter.

It was necessary to carry out further tests because the data recorded from the performance tests was not in a format that could be readily processed and

hence analysed. To validate the torque equation (3.33) there were two options, either the average or instantaneous data values, could have been analysed. It was decided that analysing the instantaneous data values was a more rigorous way of processing the data. Therefore each variable within the torque equation (3.33) had to be recorded instantaneously during a test to perform the analysis.

Referring to the torque equation (3.33) it can be broken down into two parts, the product of the field and armature MMF's, and the coupling-coefficient and the reluctance. The instantaneous-current data was recorded during a power test directly into the digital storage oscilloscope. The coupling-coefficient and reluctance data was derived from a series of separate back-EMF tests.

8.2.2 Back-EMF tests

The series-motor was mounted on the dynamic test-rig, and was back-driven, using a stepper-motor (as described in Chapter 6), in its direction of rotation at three different speeds (500, 1000 and 1500 rpm). These speeds were much lower than those recorded during previous back-EMF tests using the first prototype shunt-motor, because of the lack of a gearbox to increase the speed. The stepper-motor reached the limit of its speed capability at 1500 rpm, whereas the flux-switching motor operates in the region of ten times this value. Ideally it would have been useful to observe a characteristic nearer to this speed. However, the results show that this difference was not crucial in producing meaningful characteristics.

The equation for the back-EMF induced in the armature-winding of the motor was given by,

$$e_a = \frac{N_a N_f i_f}{\Re} \frac{dk}{d\theta} \omega \quad (3.34).$$

To derive the array of values needed for the rate of change of coupling coefficient divided by the reluctance, the back-EMF was divided by, the field-current, the number of field-turns, the number of armature-turns, and the speed of the motor. To simplify this calculation the field-current was kept constant by connecting a large 500 mH inductor in series with the field-winding. This value of inductance was over one-hundred times larger than that of the field-winding, thus preventing the current from being modulated as a result of the changing self-inductance, with rotor position, of the field-winding. The field-winding was connected to a separately-excited power supply with the armature-windings left open-circuited. As the motor rotated a back-EMF was generated across the armature-windings. The motor was configured to run with an advance-angle of 11°, the reason for this was that as the power tests were also performed at 11° there was no further need to advance either of the two sets of data, mathematically, as it was already synchronised.

Instantaneous values of back-EMF were recorded at different field MMFs and speeds for use with the instantaneous analysis described later. Corresponding RMS values of back-EMF were also recorded and the results were plotted as shown in figures 8.1 and 8.2. Figure 8.1 shows that there is a linear

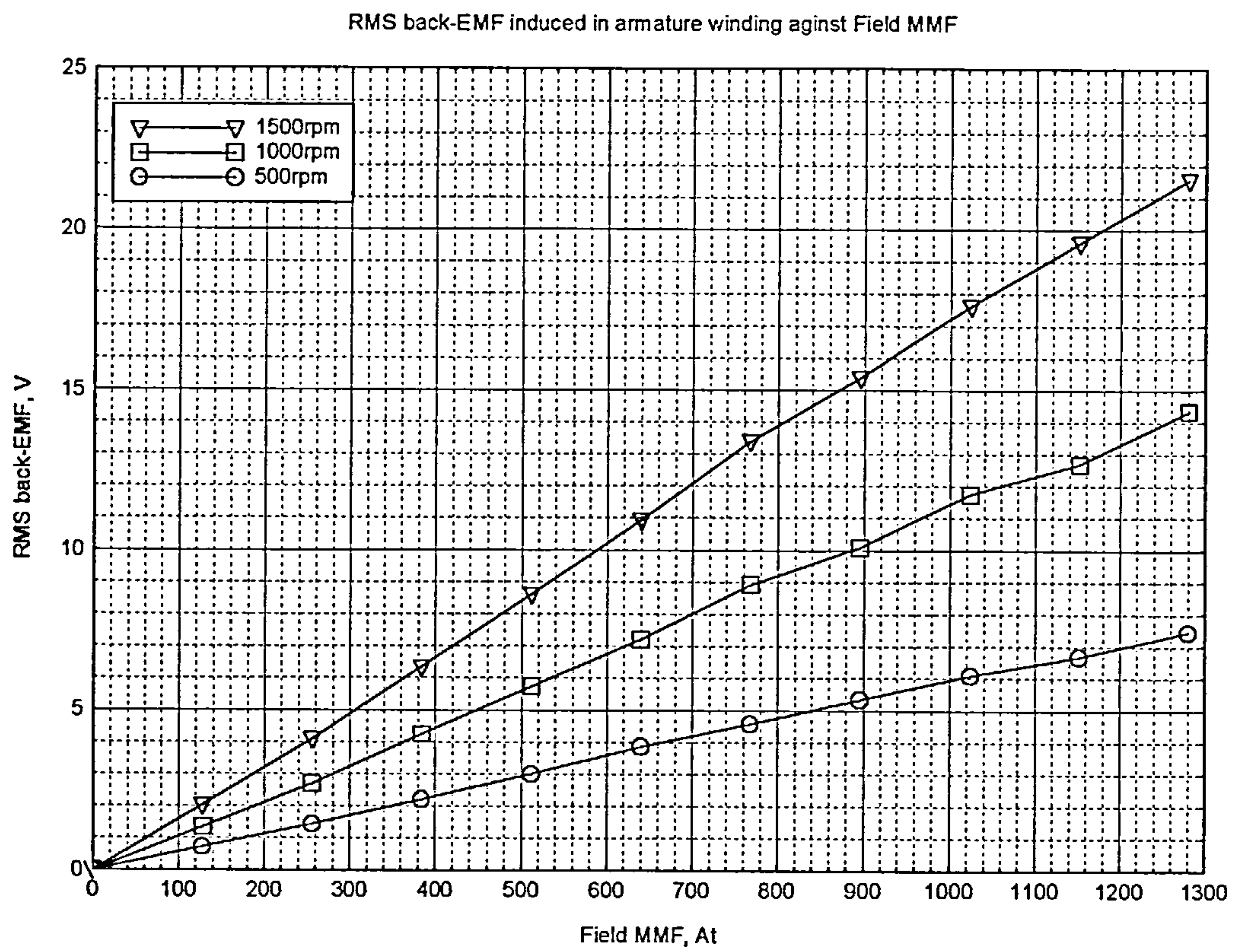


Figure 8.1 RMS back-EMF induced in armature winding against Field-MMF

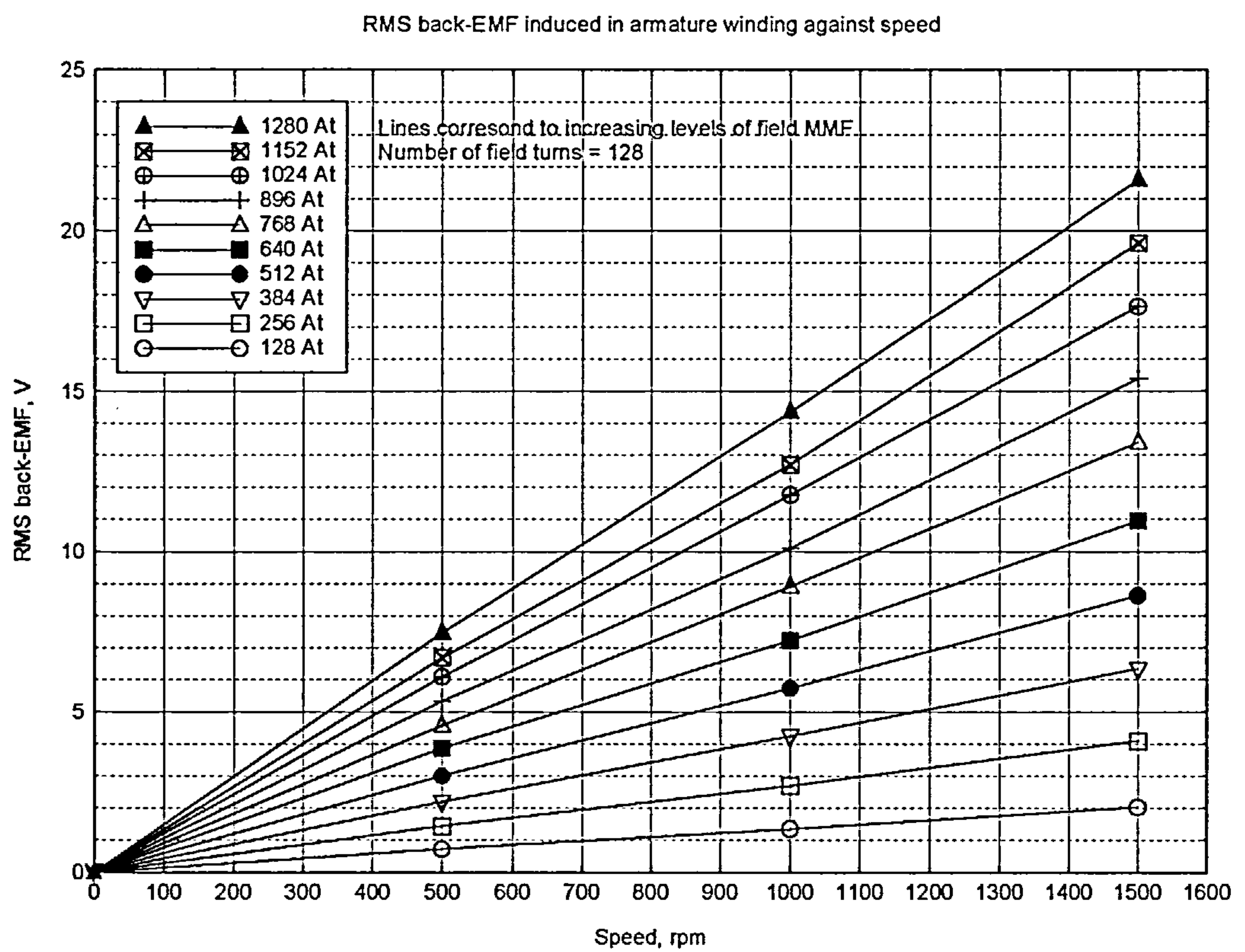


Figure 8.2 RMS back-EMF induced in armature-winding against speed

relationship between back-EMF and field-MMF, and hence field-current. Figure 8.2 shows that there is a linear relationship between back-EMF and speed for the data given. This is consistent with the characteristics exhibited by a DC-motor. The three characteristics in Figure 8.1 were each curve fitted using a straight-line and a second-order polynomial as shown in figure 8.3. The second-order polynomial curve fits, see figure 8.3, all fall below their corresponding straight-line fits, which indicates that the effects of saturation are present due to this slight downward deviation. If the second-order curve fits had appeared above the straight-line fits then possible saturation effects would not be present.

The 1500 rpm second-order polynomial curve-fit was scaled with respect to speed, and plotted against the two other second-order polynomial curve-fits for the 500 rpm and the 1000 rpm data as shown in figure 8.4. As can be seen there is only a small difference between the fitted and scaled curves in both cases, which shows that it is valid to scale the curves in order to take into account the effects of saturation.

The difference between the straight-line fit and the second-order polynomial curve-fit at any point was used to determine a saturation factor that was incorporated into the instantaneous analysis that follows.

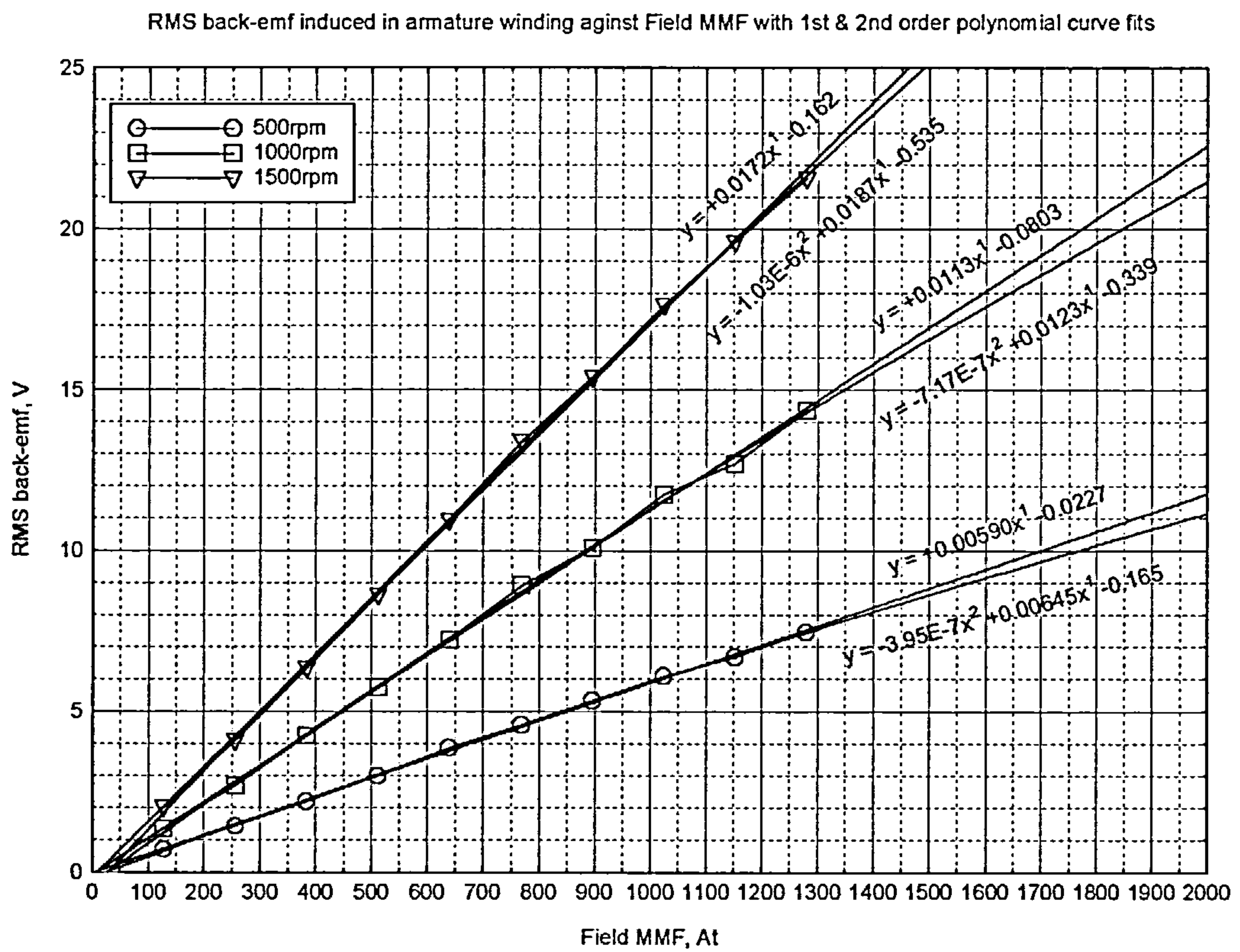


Figure 8.3 RMS back-EMF induced in armature-winding against field-MMF with 1st and 2nd order polynomial curve fits

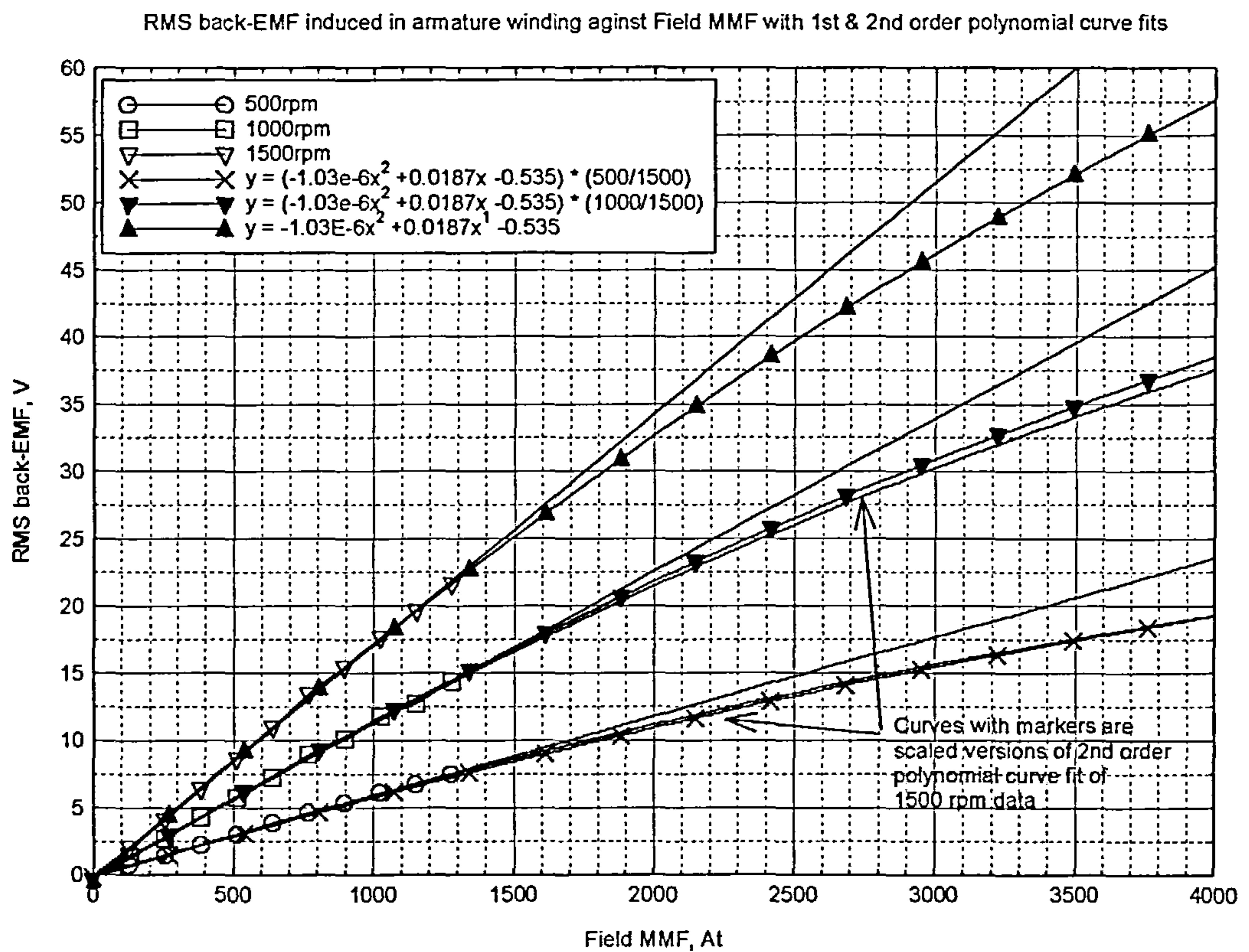


Figure 8.4 RMS back-EMF induced in armature-winding against field-MMF with 1st and 2nd order polynomial curve fits (zoomed out)

8.2.3 Field and armature-current data

Having obtained the back-EMF data for one half of the torque equation the remaining field and armature-current data was recorded during four load tests. A pair of tests was performed with the motor in a series configuration, whilst the remaining two tests were carried out with the series-windings of the motor being separately excited. For each load-point instantaneous values of field and armature-current were recorded over a complete electrical cycle, along with mean and RMS values, respectively. The mean-torque was also measured.

8.2.4 Analysis of instantaneous data

The instantaneous data was analysed and processed via a simple spreadsheet, with the objective of multiplying the components of the torque equation (8.1) together to obtain a calculated value that could be compared to the real value. The process of analysis was as follows:

- i). To multiply the instantaneous $\frac{\left(\frac{dk}{d\theta}\right)}{\Re}$ (rate-of-change of coupling-coefficient divided by the reluctance) data, derived from the back-EMF tests, by the instantaneous field and armature-currents, from the load tests, both sets of data had to be of the same sample-length. The back-EMF data was resampled using a spline function, within MATLAB, to match the current-data sample-length in each case.

- ii). With the data having matching sample-lengths it was then multiplied, as indicated by the torque equation, to give values of instantaneous torque.

- iii). The average value of torque was then calculated.

- iv). This value was then multiplied by a saturation factor that was calculated from the second-order polynomial curve-fits to the back-EMF data obtained previously. This was based on inputting the rotor-speed and the mean field-MMF into the equation for the fitted curve.

- v). The final value of torque was then compared with the real value recorded.

Table 8.1 gives a summary of the results.

Torque			
Calculated	Multiplied by saturation factor	Measured	Difference between Calculated with saturation and measured
Nm	Nm	Nm	Nm
0.96	0.82	0.81	1%
0.92	0.76	0.81	-5%
0.96	0.83	0.81	3%
1.27	1.10	1.12	-1%
1.21	1.03	1.12	-8%
1.26	1.12	1.12	0%
1.50	1.31	1.27	3%
1.44	1.23	1.27	-3%
1.49	1.33	1.27	5%
1.62	1.45	1.40	4%
1.55	1.36	1.40	-3%
1.61	1.48	1.40	6%
		Average difference	0.2%

Table 8.1 A summary of the results of the analysis showing a comparison between the calculated and measured torques

Referring to Table 8.1 it can be seen that the average difference between the calculated and measured values is 0.2 %. The highest difference is -8% but the majority of values fall within ± 5 %. These results demonstrate that this is a valid method of predicting and calculating the torque of these flux-switching motors, thus validating the proposed torque equation (3.33).

The analysis of the instantaneous data can be reinforced with the addition of the comparison of four different differentials of coupling-coefficients. Recalling figure 6.5, where the differential of the real measured coupling-coefficient was compared to the differential of the simulated coupling-coefficient, another curve was added. The calculated values of the differential of the coupling-coefficient, that were derived from the back-EMF tests, were multiplied by the values of measured reluctance to give another set of differential of the coupling-coefficient values. These values were plotted to give figure 8.5. The difference between the previous values and these new values, derived from the back-EMF, is that the back-EMF values already contain a saturation factor. This explains the obvious difference in magnitude of this and the previous curves. Dividing the saturated data by the saturation factor, derived earlier, results in a non-saturated curve that is very similar in magnitude and shape to the original two curves. This result gives further credence to the equations used to model this motor and the use of the saturation factor.

8.3 Conclusions

An additional series of tests to the performance tests were carried out to validate the proposed torque equation (3.33). The tests consisted of recording the instantaneous variables that the torque equation (3.33) was comprised of such that they could be processed to obtain a calculated torque value. The resulting value was then multiplied by a saturation factor to give a final value. In summary, comparing the calculated value with the measured value

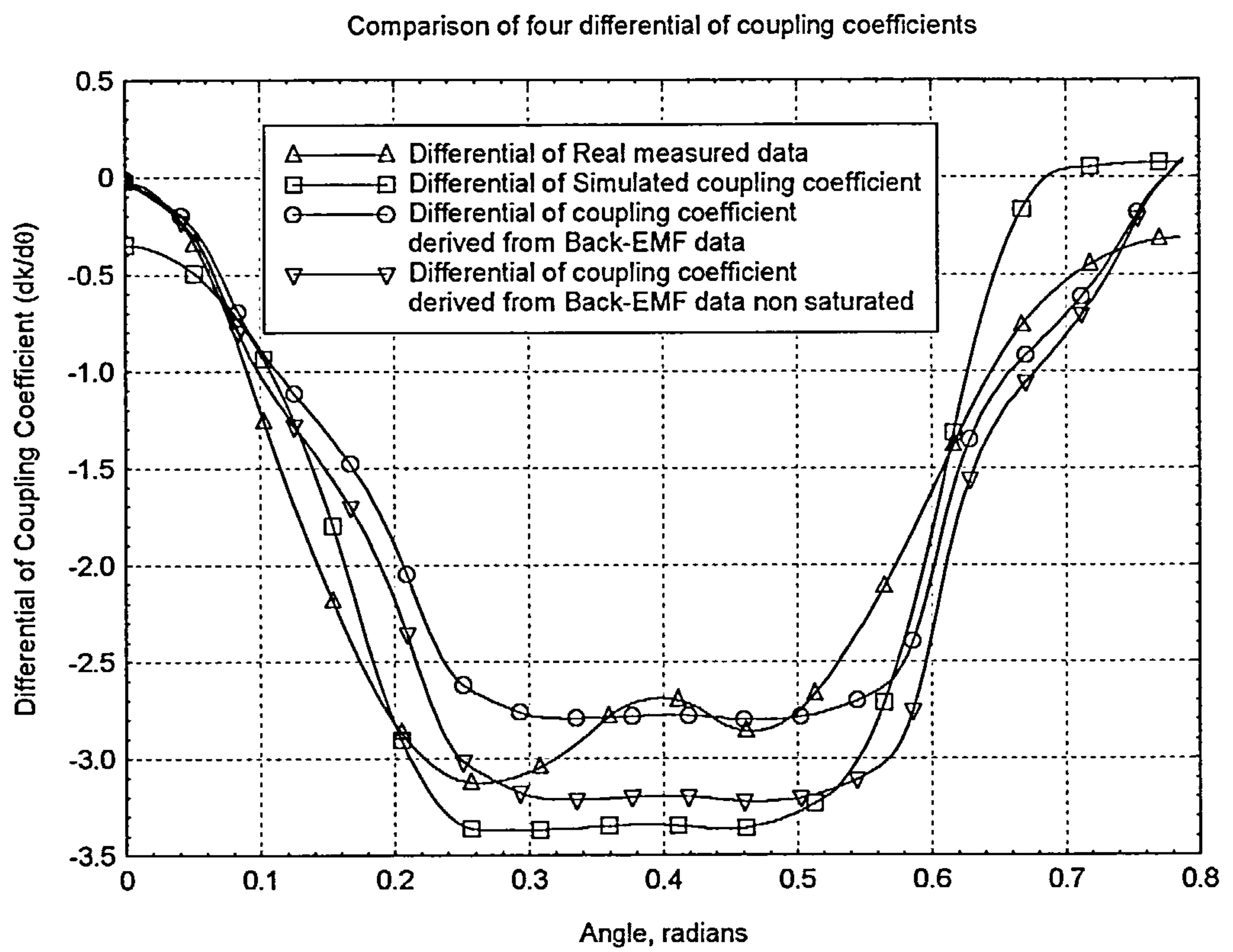


Figure 8.5 Comparison of four differential of coupling-coefficients

demonstrated that the equation was valid in predicting the torque of the flux-switching motor. A further comparison of different values of the differential of coupling-coefficient also gave credence to the use of a saturation factor, and therefore the equation. The implication of validating the torque equation (3.33) is that the simple DC-motor theory used to formulate it defines that the flux-switching motor can be considered to be a DC-motor, given that the appropriate saturation factor is applied. A further implication for the design of future motors is that they can be more rapidly prototyped using this simple theory.

CHAPTER 9 CONCLUSIONS

9.1 General conclusions

This thesis has described features of the operation, modelling, design, manufacture, performance and development of a new type of electronically-commutated doubly-salient wound-field brushless DC-motor. The evolution of the flux-switching motor (as it has been named) from a switched-reluctance motor, with fully-pitched windings, was initially presented, in conjunction with other electrical-machines, with fully-pitched windings. The characteristics that the flux-switching motor exhibits were identified, and comparisons were drawn with the operation of the conventional DC-motor. These characteristics were then developed from first-principles in the form of mathematical equations used to model the flux-switching motor. A more comprehensive coupling-coefficient model was formulated, and the equations derived were incorporated into a MATLAB SIMULINK time stepping model, which was used to produce a winding specification.

Prior to the completion of the MATLAB SIMULINK model a proof-of-principle flux-switching motor was built to test the concept. Tests showed that the motor worked in line with the principle of the generation of a back-EMF across the armature windings by the rotation of the rotor within a field-flux. Thus, confirming the expected DC-motor operating characteristics. Despite the performance capabilities of the motor being lower than expected, the most important result demonstrated was that, the drive-system showed potential to

be developed further. This led to the design and manufacture of a prototype flux-switching motor based upon the parameters given in a commercial specification provided. The design stage incorporated the development of the drive and its control. This demonstrated that the motor was capable of being controlled with a closed-loop speed-control system, that interpreted current in proportion to speed under the different operating conditions without the need for current-feedback.

Upon testing the prototype motor it was found that it had reached the limits of its operation, as defined by its natural torque-speed curve, prior to reaching the desired operating point at a power of 1864 W, and at a speed of 9000 rpm.

The torque-speed curve described gave constant power-out so that changing the target speed had no effect on output-power. No further testing could be carried out without increasing the power-input. A simple calculation suggested that raising the supply-voltage to the armature-winding to 280 V would allow the desired torque and power to be reached. Testing the motor again at a higher speed, to restrict the temperature rise of the armature windings, gave the required power as speculated. In conclusion, testing of the first prototype motor showed that it was capable of starting, delivering the power-out required, and braking as required. A further second prototype with a rewound armature-winding with less turns and the same shunt field-winding was manufactured.

Another fourth prototype motor with a series-field winding was also manufactured. The results from testing these further prototypes showed that the majority of the specification was achieved and it can be confidently stated

that with refinement in some areas there is no reason why the specification cannot be exceeded.

Based upon the delivery of power the series-motor promises the most potential. When pushed to its limit, the series-motor delivered nearly 3.8 kW, twice the specified output-power. Another factor in choosing between a shunt and series-field-winding was the cost of the solution. The shunt-wound-field motor used a low-powered MOSFET, a relatively small power diode and the corresponding gate-drive circuitry to operate the field-winding. The series-wound-field motor used a 15 μ F polypropylene capacitor and a power-diode. The series-motor can deliver the power in a more controlled manner with an economic power-converter that is altogether a more robust solution.

An additional series of tests were performed to prove the proposed torque equation (3.33). It was shown that when the calculated value of torque was compared with the measured value the equation was valid in predicting the torque of the flux-switching motor. Validating the torque equation (3.33) provides further evidence that the simple DC-motor theory used to derive it is well founded and that the flux-switching motor can be considered to be a DC-motor, given that the appropriate saturation factor is applied.

In summary this drive-system is a complete package. A very simple drive and control is combined with a simple motor to provide an innovative, inexpensive solution. Not only that, but the modelling, although not entirely accurate, shows

promise for rapid-prototyping using the simple mathematical theory presented. This solution has shown that the motor and drive can perform to a very stringent commercial specification, and shows what brushless doubly-salient motors can achieve.

9.2 Author's contribution to knowledge

The drive-system that was designed, and developed, was specifically intended to be used in a low-power application (2.5 horsepower, less than 2 kW output-power), according to a given specification. However, this does not imply that the motor is restricted to use in this output-power range. A wide-ranging variety of designs at different power levels for different applications are possible. It is believed that all of the design principles discussed are scaleable with power. Confirmation of this can only be given with the appropriate testing of such motors. The thesis has concentrated on the aforementioned motor, and it does not contain results for any larger motors.

The research carried out has been responsible for the introduction of a new type of motor, the flux-switching motor. Extensive testing using four prototype motors has been carried out in attempting to satisfy the specification. From this testing empirical modelling techniques have been demonstrated to be of use in the design of such motors. The motor is showing excellent promise for the future, when it should become a realistic alternative to the universal motor used in the majority of appliances today. How soon in the future depends on how

rapidly the cost of the power electronics will fall, and the development effort forthcoming.

9.3 Further work

The flux-switching motor has been shown to work very successfully. However, the area with the greatest need for further work is the modelling of the motor, which translates the mathematical equations, and the predicted magnetic characteristics, of a lamination design into a winding specification. The simulation used, was a fair model of the real motor characteristics, although it became apparent whilst testing that the simulation needed to be developed to include the complex mutual effects that were present.

REFERENCES

- [1] W.H. Taylor, "Obtaining Motive Power", GB patent number 8255, May 2nd 1840.
- [2] V. Ostovic, "Computer Aided Analysis of Electrical Machines", Prentice Hall, 1994.
- [3] United Kingdom Patent Specification 132110, 1973.
- [4] J.V. Byrne, J.G. Lacy, "Characteristics of Saturable Stepper and Reluctance Motors", IEE Conference Publication on "Small Electric Machines", 136, 1976, pp. 93 - 96.
- [5] L.E. Unnewehr, H.W. Koch, "An Axial Air-gap Reluctance Motor for Variable Speed Applications", IEEE Transactions on Power Apparatus and Systems, Vol. PAS-93, No. 1, January 1974, pp. 367 - 376.
- [6] S.A. Nasar, "DC Switched Reluctance Motor", Proceedings of the IEE, Vol. 116, No. 6, June 1969, pp. 1048 - 1049.
- [7] B.D. Bedford, United States Patent 3,678,352.
- [8] B.D. Bedford, United States Patent 3,679,953.
- [9] P.J. Lawrenson, J.M. Stephenson, P.T. Blenkinsop, J. Corda, N.N. Fulton, "Variable-speed Switched Reluctance Motors", IEE proceedings, part B : Electric Power Applications, Jul 1980, Vol. 127, No. 4, pp. 253 - 265.

- [10] N.N. Fulton, P.J. Lawrenson, J.M. Stephenson, R.J. Blake, R.M. Davis, W.F. Ray, "Recent Developments in High-performance Switched Reluctance Drives", IEE Conference Publication, 17 - 19 Sep 1985, No.254, pp.130 - 133.
- [11] W.F. Ray, P.J. Lawrenson, R.M. Davis, J.M. Stephenson, N.N. Fulton, R.J. Blake, "High Performance Switched Reluctance Brushless Drives", IEEE Transactions on Industry Applications, July-Aug 1986, Vol. IA-22, No. 4, pp. 722 - 730.
- [12] T.J.E. Miller, "Switched Reluctance Motors and their Control", Oxford University Press, 1993.
- [13] D.C. White, H.H. Woodson, "Electromagnetic Energy Conversion", Wiley, UK, 1959.
- [14] J.M. Stephenson, J. Corda, "Computation of Torque and Current in Doubly Salient Reluctance Motors from Non-Linear Magnetisation Data", IEE Proceedings, Vol. 126, no. 5, May 1979.
- [15] H.R. Bolton, D.A.G. Pedder, "Low-Cost Reluctance Drive System for Low Power, Low Speed Application", Proceedings of 2nd International Conference on Electrical Variable-Speed Drives, pp. 88 - 92.
- [16] S. Chatratana, H.R. Bolton, D.A.G. Pedder, "Investigations Into Small Single Phase Switched Reluctance Motors", Power Division of the IEE, 2nd International Conference on Small and Special Electrical Machines, September 1981.

- [17] J.V. Byrne, J.G. Lacy, "Electrodynamic System Comprising a Variable Reluctance Machine", UK patent number 1321110, 1973.
- [18] F.L. Rohdin, "Two Pole Reluctance Motor with Non-Uniform Pole shape for Better Starting", US patent number 4,506,182, 1985.
- [19] M.A. El-Khazendar, J. Stephenson, "Analysis and Optimisation of a 2-Phase Self-starting Switched Reluctance Motor", Proceedings International Conference on Electric Machines, 1986, pp. 1031 - 1034.
- [20] M. Barnes, A.M. Michaelides, C. Pollock, "The Design and Performance of a Self-Starting Switched Reluctance Drive", IEE Conference on Power Electronics and Variable Speed Drives, September 1996, pp. 419 - 423.
- [21] C.C. Chan, "Single Phase Switched Reluctance Motor", IEE Proceedings, Part-B, Vol. 134, No. 1, 1987, pp. 53 - 56.
- [22] S. Chan, H.R. Bolton, "Development of Sub-kW Single-Phase Switched-Reluctance Drives", Conference Proceedings of International Conference on Electric Machines, Vol. 2, 1992, pp. 527 - 531.
- [23] M. Barnes, C. Pollock, "Two Phase Switched Reluctance Drive with New Power Electronic Converter for Low Cost Applications", Proceedings of 6th European Conference on Power Electronics and Applications, Vol. 1, 1995, pp. 427 - 430.
- [24] R. Krishnan, P.N. Materu, "Design of a Single-Switch-per-Phase Converter for Switched Reluctance Motor Drives", IEEE Transactions on Industrial Electronics, Vol. 37, No. 6, 1990, pp. 469 - 476.

- [25] N. Mohan, T.M. Undeland, W.P. Robbins, "Power Electronics: Converters, Applications, and Design", John Wiley and Sons, 1st edition, 1989.
- [26] C. Pollock, B.W. Williams, "Power Converter Circuits for Switched Reluctance Motors with the Minimum Number of Switches", IEE Proceedings, Part-B, Vol. 137, No. 6, 1990, pp. 373 - 384.
- [27] M. Ehsani, J.T. Bass, T.J.E. Miller, R.L. Steigerwald, "Development of a Unipolar Converter for Switched Reluctance Motor Drives", IEEE Transactions on Industrial Applications, Vol. IA-23, No. 3, 1987, pp. 545 - 583.
- [28] R.J. Blake, P.D. Webster, D.M. Sugden, "The Application of GTOs to Switched Reluctance Drives", 2nd International Conference on Power Electronics and Variable Speed Drives, 1988, pp. 24 - 28.
- [29] V.R. Stefanovic, S. Vukosavic, "SRM Inverter Topologies: A Comparative Evaluation", IEEE Transactions on Industry Applications, Vol. 27, No. 6, 1991, pp. 1034 - 1047.
- [30] Y. Li, Y. Tang, "Switched Reluctance Motor Drives with Fractionally-Pitched Winding Design", PESC Record - IEEE Annual Power Electronics Specialists Conference, 1997, Vol. 2, pp.875 - 880.
- [31] B.C. Mecrow, "Fully Pitched -Winding Switched Reluctance and Stepping-Motor Arrangements", IEE proceedings, part B : Electric Power Applications, Jan 1993, Vol. 140, No. 1, pp. 61 - 70.

- [32] H.Y. Li, F. Liang, Y. Zhao, T.A. Lipo, "Doubly Salient Doubly Excited Variable Reluctance Motor", Conference record - IAS Annual Meeting, IEEE, 1993, Vol. 1, pp. 137 - 143.
- [33] F. Liang, T.A. Lipo, "New Variable Reluctance Motor Utilizing an Auxiliary Commutation Winding", IEEE Transactions on Industry Applications, Mar-Apr 1994, Vol. 30, No. 2, pp. 423 - 432.
- [34] Y. Li, J.D. Lloyd, G.E. Horst, "Switched Reluctance Motor with DC Assisted Excitation", Conference record - IAS Annual Meeting, IEEE, 1996, Vol. 2, pp. 801 - 807.
- [35] W.F. Ray, R.M. Davis, R.J. Blake, N.N. Fulton, J.M. Stephenson, P.J. Lawrenson, "Industrial Switched Reluctance Drives - Concepts and Performance", IEE Conference Publication, 1 - 4 May 1984, No.234, pp.357 - 360.
- [36] J.M Stephenson, "Switched Reluctance Motor", Section 2 of Switched Reluctance Drives, IEEE/IAS Tutorial Course, 1990.
- [37] Y. Liao, F. Liang, T.A. Lipo, "Novel Permanent Magnet Motor with Doubly Salient Structure", IEEE Transactions on Industry Applications, Sep-Oct 1995, Vol. 31, No. 5, pp. 1069 - 1078.
- [38] X. Luo, D. Qin, T.A. Lipo, "Novel Two Phase Doubly Salient Permanent Magnet Motor", Conference record - IAS Annual Meeting, IEEE, 1996, Vol. 2, pp. 808 - 815.

- [39] F. Leonardi, T. Matsuo, Y. Li, T.A. Lipo, P. McCleer, "Design Considerations and Test Results for a Doubly Salient PM Motor with Flux Control", Conference record - IAS Annual Meeting, IEEE, 1996, Vol. 1, pp. 458 - 463.
- [40] B.C. Mecrow, "New Winding Configurations for Doubly Salient Reluctance Machines", IEEE Transactions on Industry Applications, Nov-Dec 1996, Vol. 32, No. 6, pp. 1348 - 1356.
- [41] P.G. Barrass, B.C. Mecrow, A.C. Clothier, "Bipolar Operation of Fully-Pitched Winding Switched Reluctance Drives", IEE Conference Publication, No. 412, pp. 252 - 256, Electrical Machines and Drives, Durham, UK, Sep 1995.
- [42] A.C. Clothier, B.C. Mecrow, "Use of Three Phase Bridge Inverters with Switched Reluctance Drives", IEE Conference Publication, No. 444, pp. 351 - 355, Electrical Machines and Drives, Cambridge, UK, Sep 1997.
- [43] B.C. Mecrow, A.C. Clothier, P.G. Barrass, "High Performance Switched Reluctance Drives using Novel Windings", IEE Colloquium (Digest), No.152, p.var paging. Proceedings of the IEE Colloquium on Machines and Drives for Electric and Hybrid Vehicles, London, UK, Jun 1996.
- [44] B.C. Mecrow, A.C. Clothier, P.G. Barrass, C. Weiner, "Drive Configurations for Fully-Pitched Winding Switched Reluctance Machines", Conference record - IAS Annual Meeting (IEEE Industry Applications Society), 1998, Vol. 1, pp. 563 - 570.

- [45] H.R. Bolton, Y. Shakweh, "Performance Prediction of Laws's Relay Actuator", IEE Proceedings, Vol137, Part B, January 1990, pp 1 - 13.
- [46] J.D. Wale, C. Pollock, "Novel Converter Topologies for a Two Phase Switched Reluctance Motor with Fully Pitched Windings", PESC Record - IEEE Annual Power Electronics Specialists Conference, 1996, Vol. 2, pp. 1798 - 1803.
- [47] C. Pollock, M. Wallace, "The Flux Switching Motor, A DC Motor without Magnets or Brushes", IEEE Industrial Applications Society – 34th Annual Meeting and Technical Conference, October 1999.
- [48] G. Guy, "Improvements in Dynamo Electric Machines and Motors", Patent Specification, 1901, No. 18027, Application 9th Sept. 1901, Accepted 16th Jan. 1902.
- [49] The British Thomson-Houston Company Limited, "Improvements in Heteropolar Inductor Alternators", Patent Specification, 1941, No. 554827, Application 15th Nov. 1941, Accepted 21st Jul. 1943.
- [50] J.H. Walker, "The Theory of the Inductor Alternator", IEE Journal, 1942, 89, Part II, pp. 227.
- [51] K.F. Raby, "Inductor Alternators for 10 KC/s", Technical Monograph, Engineering Department, The British Thompson-Houston Company Ltd, April 1950.
- [52] F.W. Walkden, "A Power-Frequency Inductor Alternator", 2nd International Conference on Electrical Machines – Design and Applications, September 1985, No. 254, pp.139 - 141.

- [53] R.P. Deodhar, S. Andersson, I. Boldea, T.J.E. Miller, "The Flux-Reversal Machine: a New Brushless Doubly-Salient Permanent-Magnet Machine", Conference record - IAS Annual Meeting, IEEE, 1996, Vol. 2, pp. 786 - 793.
- [54] J.D. Law, A. Chertok, T.A. Lipo, "Design and Performance of Field Regulated Reluctance Machine", IEEE Transactions on Industry Applications, Sept-Oct 1994, Vol. 30, No. 5, pp. 1185 - 1192.
- [55] S.H.Y. Li, F. Liang, Y. Zhao, T.A. Lipo, "Doubly Salient Doubly Excited Variable Reluctance Motor", IEEE Transactions on Industry Applications, Jan-Feb 1995, Vol. 31, No. 1, pp. 99 - 106.
- [56] E. Hughes, revised by I. McKenzie Smith, "Electrical Technology", 6th Edition, Longman Scientific & Technical, 1987, pp. 486 – 494.
- [57] J.C. Moreira, T.A. Lipo, "Simulation of a Four Phase Switched Reluctance Motor including the effects of Mutual Coupling", Electric Machines and Power Systems, Jul-Aug 1989, Vol. 16, No. 4, pp. 281 - 299.
- [58] J.M. Kokernak, D.A. Torrey, "Magnetic Circuit Model for the Mutually Coupled Switched Reluctance Machine", IEEE Industrial Applications Society – Annual Meeting and Technical Conference, 1997, Vol. 1, pp. 302 – 309.
- [59] T.J.E. Miller, "Converter Volt-Ampere Requirements of the Switched Reluctance Motor Drive", IEEE Transactions on Industry Applications, July-Aug 1985, Vol. IA-21, No. 5, pp. 1136 - 1144.

- [60] S. Huang, J. Luo, F. Leonardi, T.A. Lipo, "General Approach to Sizing and Power Density Equations for Comparison of Electrical Machines", IEEE Transactions on Industry Applications, Jan-Feb 1998, Vol. 34, No. 1, pp. 92 - 97.
- [61] T.J.E. Miller, "Faults and Unbalance Forces in the Switched Reluctance Machine", IEEE Transactions on Industry Applications, Mar-Apr 1995, Vol. 31, No. 2, pp. 319 - 328.

APPENDIX I – Performance specification

Performance:

2.5 HP (1864 Watts) at 2 Nm rotor torque.
14000 rpm Idle rotor speed.
Maximum torque (Reserve torque) 3 Nm for a duration of 5 seconds.
240 Volt 50 Hz input.
1800 Watts input-power rating. (Continuous duty, 85 °C rise on coils).
75 % Efficiency at rated. (excluding gear losses).
4.7 : 1 Gear ratio.

Starting:

Motor must start from full line voltage without excessive current, but without noticeable time delay. Smooth acceleration must be perceived.
Maximum starting current target: 60 Amps from the DC link.
Maximum acceleration time target: 0.5 seconds.

Braking:

Dynamic braking is required.
Stopping time objective: 1.5 seconds from no-load speed.
Target inertia: $\sim 0.008 \text{ Kg m}^2$.

Motor size:

Stator outside diameter & stack length: The D^2L product must not exceed 554470 mm^3

Cooling:

The motor windings will be cooled by a shaft mounted internal fan.
Flow constant: $9.96 \times 10^{-4} \text{ litres / second / rpm}$.
Power consumption constant: $3.2 \times 10^{-11} \text{ Watts / rpm}^3$.